

DRAFT VERSION DECEMBER 14, 2018
 Typeset using **LATEX** **preprint** style in AASTeX62

A Large Catalog of Multiwavelength GRB Afterglows I: Color Evolution And Its Physical Implication

LIANG LI,^{1, 2, 3, 4, 5} **YU WANG**,^{4, 6} **LANG SHAO**,^{7, 8} **XUE-FENG WU**,⁵ **YONG-FENG HUANG**,^{9, 10}
BING ZHANG,¹¹ **FELIX RYDE**,^{1, 2} AND **HOI-FUNG YU**^{1, 2}

¹*Department of Physics, KTH Royal Institute of Technology, SE-106 91 Stockholm, Sweden*

²*The Oskar Klein Centre for Cosmoparticle Physics*

³*Department of Physics, Stockholm University, SE-106 91 Stockholm, Sweden*

⁴*ICRANet, Piazza della Repubblica 10, I-65122 Pescara, Italy*

⁵*Purple Mountain Observatory, Chinese Academy of Sciences, Nanjing 210008, China*

⁶*Dip. di Fisica and ICRA, Sapienza Universit di Roma, Piazzale Aldo Moro 5, I-00185 Rome, Italy*

⁷*Department of Space Sciences and Astronomy, Hebei Normal University, Shijiazhuang 050024, China*

⁸*Key Laboratory of Dark Matter and Space Astronomy, Purple Mountain Observatory, Chinese Academy of Sciences, Nanjing 210008, China*

⁹*Department of Astronomy, Nanjing University, Nanjing 210093, Jiangsu, China*

¹⁰*Key Laboratory of Modern Astronomy and Astrophysics (Nanjing University), Ministry of Education, Nanjing 210093, China*

¹¹*Department of Physics and Astronomy, University of Nevada, Las Vegas, NV 89154, USA*

(Received May 26, 2017; Accepted December 02, 2017; Published February 01, 2018)

ABSTRACT

The spectrum of gamma-ray burst (GRB) afterglows can be studied with color indices. Here we present a large comprehensive catalog of 70 GRBs with multiwavelength optical transient data on which we perform a systematic study to find the temporal evolution of color indices. We categorize them into two samples based on how well the color indices are evaluated. The Golden sample includes 25 bursts mostly observed by GROND, and the Silver sample includes 45 bursts observed by other telescopes. For the Golden sample, we find that 96% of the color indices do not vary over time. However, the color indices do vary during short periods in most bursts. The observed variations are consistent with effects of (i) the cooling frequency crossing the studied energy bands in a wind medium (43%) and in a constant-density medium (30%), (ii) early dust extinction (12%), (iii) transition from reverse-shock to forward-shock emission (5%), or (iv) an emergent SN emission (10%). We also study the evolutionary properties of the mean color indices for different emission episodes. We find that 86% of the color indices in the 70 bursts show constancy between consecutive ones. The color index variations occur mainly during the late GRB-SN bump, the flare, and early reverse-shock emission components. We further perform a statistical analysis of various

Corresponding author: Liang Li

liang.li@fysik.su.se, yu.wang@icranet.org, lshao@hebtu.edu.cn, xfwu@pmo.ac.cn, hyf@nju.edu.cn

observational properties and model parameters (spectral index β_o^{CI} , electron spectral indices p^{CI} , etc.) using color indices. Overall, we conclude that $\sim 90\%$ of colors are constant in time and can be accounted for by the simplest external forward-shock model, while the varying color indices call for more detailed modeling.

Keywords: methods: statistical-(stars:) gamma-ray burst: general -(ISM:) dust, extinction

1. INTRODUCTION

The first observation of gamma-ray burst (GRB) optical afterglow was that of the BeppoSAX-detected GRB 970228 (van Paradijs et al. 1997). Since the launch of the *Swift* satellite more than 10 yr ago (Gehrels et al. 2004), many ground-based optical telescopes with increasing sensitivity have accumulated a rich collection of optical afterglows. In recent years, optical afterglows have been studied extensively either in terms of either their multiband light curves (e.g., Panaiteescu & Kumar 2002; Huang et al. 2006; Zeh et al. 2006; Kann et al. 2010, 2011; Li et al. 2012; Liang et al. 2013; Wang et al. 2015; Roming et al. 2017, and references therein), or their spectral energy distributions (SEDs) derived from simultaneous multiband photometry (e.g., Stratta et al. 2004; Starling et al. 2007; Kann et al. 2006, 2010, 2011; Roming et al. 2017). The latter, if studied in a broad bandpass, provides tight constraints on the radiation mechanism and circumburst environment of GRBs. Given the rapid progress made in the detection of afterglows in the *Swift* era, unforeseen temporal and spectral features were discovered, which challenge our understanding of GRB afterglow physics (Zhang 2007; Gehrels et al. 2009, and references therein).

The temporal and spectral properties of optical transients can be studied by color indices (hereinafter CIs), defined as the magnitude difference between two filters. They can be used to study the SED with a good temporal resolution, even when high-resolution spectra are not available. For instance, CIs can resolve small variations in the spectral profiles of optical transients (Šimon et al. 2001; Šimon et al. 2013). They are also helpful in identifying different radiation mechanisms or progenitors in a single burst. As an example, CIs were used as an indicator of the underlying Type Ib/c supernovae (SNe; Šimon et al. 2004).

Theoretically, the conventional afterglow model has been discussed by many authors (e.g., Mészáros & Rees 1997; Sari et al. 1998; Huang & Cheng 2003), and the relationship between temporal and spectral indices (the so-called closure relation) has been extensively reviewed in Zhang & Mészáros (2004) and Gao et al. (2013). According to this model, which assumes that synchrotron radiation dominates the afterglow emission, the color index should not change with time. Instead, if a change is observed, there may be several possible reasons (Melandri et al. 2017), for instance: (i) the cooling frequency crosses the studied energy bands (e.g., Filgas et al. 2011a). (ii) an additional emission component emerges, e.g., the SN counterpart observed in some GRBs, or the mixture of different emission stages, such as forward and reverse shock (Kobayashi & Zhang 2003) in the context of the fireball model (Piran 2004). (iii) after being destroyed by the initial intense radiation, host extinction could be changed owing to dust photodestruction (Perna & Lazzati 2002; Morgan et al. 2014). Some other possible reasons, such as a structured jet, could also produce the change in the CIs.

In this paper, we have made an extensive effort to collect publicly available optical and near-infrared photometric data. We restricted the study to 70 bursts with high-quality multiband observations,

which were detected during both the pre-*Swift* and *Swift* eras. Our goal is to study the temporal variability of CIs and explore its physical implications. In a following paper, we will present a detailed time-resolved analysis of afterglow spectra using X-ray and optical data, which will be used to study the extinction curve and explore the physics in the circumburst medium in the host galaxy (Li et al, in prep.).

This paper is organized as follows. The sample selection and data analysis are presented in Section 2. The statistical properties of CIs are summarized in Section 3. The evolution of the CIs is presented in Section 4. The theoretical implications are discussed in Section 5. Finally, conclusions are provided in Section 6.

2. SAMPLE SELECTION, CORRECTIONS, AND SCALING

We extensively compiled as many optical/near-IR (NIR) photometric data as possible, detected by ground-based telescopes from both pre-*Swift* and *Swift*-era afterglows. The bursts in our sample were observed before 2016¹. We collected observational data from published papers and the Gamma-ray Burst Coordinates Networks Circular Service (GCN)². We initially selected GRBs with known redshift that have high-quality data in at least three optical bands. We then restricted the study to the GRBs that were observed in optical wavelength for at least 1 hr, facilitating the study of CIs temporal evolution. A total of 70 bursts satisfy these criteria (from 1997 February 28 to 2015 December). To obtain a trustworthy data set, the data sources should be well calibrated. We made corrections to the data as follows.

We studied the temporal properties of the CIs in the rest frame, $t_{\text{rest}} = t_{\text{obs}}/(1+z)$. For some specific cases (GRB 970508, GRB 990510, GRB 990712, GRB 060614, GRB 060908, GRB 090426, GRB 091127, GRB 100621A, GRB 100814A, GRB 110918A, GRB 120422A, GRB 120729A, GRB 130702A, GRB 130925A), we subtracted the flux contribution at very late epochs that we interpret as coming from the host galaxy. This contribution is determined by identifying constant flux values at a late time, $\sim 10^6$ s after the GRB trigger.

We calculated the Galactic extinction correction from the reddening map presented in Schlafly & Finkbeiner (2011) for optical and NIR magnitudes, and we assume³ $R_v=3.1$.

The observed spectra are k -corrected, where k is defined as $m_T = m_O - k$ (e.g., Oke & Sandage 1968; Peterson 1997), with $k = 2.5(\beta_o - 1) \log(1+z)$. Here m_O and m_T are the observed and true magnitudes, respectively. β_o is the spectral index⁴ of the optical afterglow, and z is the redshift.

2.1. Corrections for Host Dust Extinction

The extinction due to dust from the host galaxy can significantly affect the observations. For wavelength λ_i , the dust extinction is defined as

$$A(\lambda_i) = m_O(\lambda_i) - m_T(\lambda_i). \quad (1)$$

The observed SED of the optical afterglow is modeled by an absorbed power law in frequency (Kann et al. 2006)

$$F_\nu = F_0 \nu^{-\beta_o} e^{-\tau(\nu_{\text{host}})}, \quad (2)$$

¹ We note that the last burst satisfying our criteria is GRB 130925A.

² <https://gcn.gsfc.nasa.gov>

³ $R_V \equiv A_V/E_{B-V}$ is the total-to-selective extinction ratio, where the color excess $E_{B-V} \equiv A_B - A_V$, is the difference between the extinction in B and V bands.

⁴ We assume a typical value of 0.75 for those bursts whose spectral indices are not available, which are indicated by ellipsis dots in Table 1.

where

$$\tau(\nu_{\text{host}}) = \frac{1}{1.086} A_V \eta(\nu_{\text{host}}), \quad (3)$$

in which β_o is the intrinsic power-law slope of the SED, F_0 is the normalization constant, $\eta(\nu_{\text{host}}) = A_{\lambda}^{\text{host}} / A_V^{\text{host}}$ is given by the extinction model assumed for the GRB host galaxy, and $A_{\lambda}^{\text{host}}$ is the host galaxy extinction correction (known only with large uncertainties). We do not carry out spectral fitting in this paper. Instead, the host galaxy extinction A_V^{host} , the spectral index β_o , and the redshift z are acquired from the literature, and their values are given in Table 1.

Specifically, A_V^{host} is chosen by the following three steps. First, we selected the values obtained by Kann et al. (2006) and Kann et al. (2010) corresponding to the Small Magellanic Cloud (SMC) dust model. Second, when they are not available in Kann et al. (2006) and Kann et al. (2010), the extinction parameters are retrieved from other papers (given as a reference in Table 1) from the SMC dust model. This model is our first choice since it is shown to best describe dust in GRB environments (Kann et al. 2010). When the information is not available for this model, the value of A_V^{host} is obtained from either from the Milky Way (MW) or the large Magellanic Cloud (LMC) models. Finally, for a few cases, when the value of A_V^{host} is unavailable for any model, we use the value obtained by fitting a Gaussian to the extinction distribution (see Figure 1), $\log_{10}(A_V^{\text{host}}) = -0.82 \pm 0.41$; here -0.82 and 0.41 are the mean value and standard deviation of the Gaussian fit⁵, respectively. After obtaining the value of A_V^{host} , we derived the extinction values in any optical band, $A_{\lambda}^{\text{host}}$, in the GRB host galaxies following Pei (1992). Figure 2 illustrates the spectral behavior of $A_{\lambda}^{\text{host}} / A_V^{\text{host}}$ for the three dust models and displays the position of the filters considered in this paper.

2.2. Light-curve Fitting

In this section, we describe the fits to the GRB light curves in our 70 bursts. The purpose of this procedure is twofold. First, it allows us to identify different emission phases. Second, the results are used to interpolate the magnitude, in order to compute the CIs, when there are no simultaneous multi-wavelength observations available.

The observed magnitude m is obtained from the flux F as

$$m = -2.5 \log_{10} \left(\frac{F}{F_0} \right), \quad (4)$$

where F_0 is the flux of an object with magnitude zero. Note that in this paper we adopt the AB magnitude system.

After taking into account all the correction factors (our Galaxy and the host galaxy extinction corrections, and the spectral k -correction), we fit the light curves in each band separately with a model of multiple components (Li et al. 2012). The basic model is either a single power law (SPL) or a smoothly broken power law (BKPL) for the flux, resulting in⁶:

$$m_T(t) = -2.5 \log_{10}(10^{-0.4m_c} t^{-\alpha} + 10^{-0.4m_G} + 10^{-0.4m_K} + 10^{-0.4m_{\text{host}}} + 10^{-0.4m_{\text{GF}}}), \quad (5)$$

$$m_T(t) = -2.5 \log_{10}\{10^{-0.4m_c}[(t/t_{b,1})^{\alpha_1 \omega_1} + (t/t_{b,1})^{\alpha_2 \omega_1}]^{-1/\omega_1} + 10^{-0.4m_G} + 10^{-0.4m_K} + 10^{-0.4m_{\text{host}}} + 10^{-0.4m_{\text{GF}}}\}, \quad (6)$$

⁵ Hereinafter we adopt the same convention for all Gaussian fits.

⁶ We apply these afterglow models to the light-curve fitting in magnitude (linear)- time (log) space.

here α , α_1 , and α_2 are the temporal slopes, t_{b1} is the break time, and ω_1 describes the sharpness of the break (the smaller the value, the smoother the break). For most GRBs, we fix this last parameter to $\omega_1 = 3$. For a few cases (GRB 030226, GRB 050922C, GRB 061007, GRB 080603A) that have a smoother break, we fix it to $\omega_1 = 1$, which improves the fit. Equation (5) can be used for both for the light curves with a break and those who exhibit an increasing behavior (e.g., afterglow onset indicated by the dashed line in Fig. 3b). In addition, m_c is the magnitude constant value, m_G is the extinction magnitude for our Galaxy, m_K is the spectral k -correction, m_{host} is the extinction magnitude for the host galaxy, and m_{GF} is the possible contribution from the host galaxy at late time (if identified). Note that m_G , m_K , and m_{host} are known before fitting.

We notice that for two bursts (GRB 061126 and GRB 080319B), the optical-afterglow light curves have a steeper decay slope α_1 in the pre-break segment (which might originate from the reverse-shock emission) than the decay slope α_2 in the post-break segment (possibly from the normal decay dominated by the external forward shock). However, due to the limitation of the BKPL model, it is impossible to fit the light curves whose pre-break slope is steeper than the post-break slope. In this case, we adopted the BKPL model function with a negative sharpness of the break $\omega=-3$ (Fig. 3c).

A double-BKPL light curve (Fig. 3d) is also expected in some afterglow models. For example, it is theoretically expected that the afterglow light curves may have a shallow segment owing to energy injection at an early time, which then changes into a normal-decay segment when the energy injection is over, and finally steepens owing to a jet break (Zhang et al. 2006). We therefore consider a smooth triple-power-law function (TPL) to fit the light curves (e.g., Liang et al. 2008; Li et al. 2012):

$$\begin{aligned} m_T(t) = & -2.5 \log_{10} \{ ((10^{-0.4m_c} [(t/t_{b,1})^{\alpha_1 \omega_1} + (t/t_{b,1})^{\alpha_2 \omega_1}]^{-1/\omega_1})^{-1/\omega_2} \\ & + ((10^{-0.4m_c} [(t/t_{b,1})^{\alpha_1 \omega_1} + (t/t_{b,1})^{\alpha_2 \omega_1}]^{-1/\omega_1}) (t_{b,2}) (t/t_{b,2})^{-\alpha_3})^{-1/\omega_2})^{-1/\omega_2} \\ & + 10^{-0.4m_G} + 10^{-0.4m_K} + 10^{-0.4m_{\text{host}}} + 10^{-0.4m_{\text{GF}}}\}. \end{aligned} \quad (7)$$

where ω_2 is the sharpness parameter at the second break time $t_{b,2}$.

The fits are performed with the IDL routine "mpfitfun.pro"⁷ (Markwardt 2009), which uses the Levenberg-Marquardt algorithm to achieve minimization. To select the best model, we compare the reduced χ^2 values and choose the one that has a more reasonable value (close to 1). For example, the χ^2_r of GRB 990510 (R band) is 31/39 (a little less than 1) for the BKPL model and 169/36 (much larger than 1) for the SPL model. Therefore, we adopt the BKPL as the best model for GRB 990510. Second, if both models have a χ^2_r close to 1, our principle is to choose the simpler one (fewer parameters). For instance, for GRB 060908, a χ^2_r is equal to 38/49 (~ 1) for the BKPL model and 52/46 (~ 1) for the SPL model. In this case, we choose the SPL model.

For multicomponent light curves (see §2.3), we introduce the minimum number of components by eye inspection of the temporal features. If the χ^2_r is still much larger than 1, we continue to add more components and redo the fit, until the χ^2_r becomes close to 1 (Li et al. 2012). For instance, the value of the χ^2_r of GRB 071025 (J band) for the BKPL is 474/39 (much larger than 1), while it is 58/34 (close to 1) for the double-BKPL model. As a result, the double-BKPL model is selected as the best model for this burst. Examples of light-curve fitting with various models or their composition are shown in Figure 4.

⁷ <http://purl.com/net/mpfit>

2.3. Component Identification

Optical afterglows have complicated light curves with up to eight emission episodes (Li et al. 2012; Li et al. 2015; Liang et al. 2006; Liang et al. 2013; Nardini et al. 2006; Kann et al. 2006, 2010, 2011; Panaitescu & Vestrand 2008, 2011). A synthetic optical-afterglow light curve is presented in Li et al. (2012). To study the spectral behaviors in these different emission phases, we investigate the temporal evolution of their mean CIs. Here we explain which components are considered and how they are identified based on their temporal and spectral features.

Ia: the prompt optical flares (Prompt-Optical); in the very early time of some bursts when the prompt GRB emission is still going on, a highly variable optical emission component may be observed as in GRB 080319B⁸. They are selected such that the observation time is smaller than T_{90} and the temporal slope⁹ $\alpha > 2.0$.

Ib: the early optical flares (Reverse-Shock); in a few cases, the early light curves have steep slopes, which likely indicate an early reverse-shock emission component, such as the early phase of GRB 061126. They were selected such that their typical temporal index $\alpha \sim 1.7$ and the peak time t_p is a few hundreds seconds.

II: an early shallow-decay component (Energy-Injection); the afterglow light curve might show an initial shallow-decay segment followed by a normal-decay/post-jet-break segment, which is likely due to energy injection from a long-lasting spinning-down central engine or piling up of flare materials into the blast wave (Liang et al. 2007; Li et al. 2012; Li et al. 2015). This component is described as the energy injection phase. They are identified by their temporal index $\alpha^{\text{Shallow}} < \alpha^{\text{Normal}}$ with a typical value $\alpha^{\text{Shallow}} \sim 0.5$ and with a typical value of break time $t_b \sim 10^4$ s. Here α^{Shallow} is the temporal index during the shallow-decay segment and α^{Normal} is the temporal index during the normal-decay phase.

III: the standard afterglow component (Onset/Normal-Decay); the light curves sometimes have an early onset rising segment followed by a normal decay. In most of the cases, a lack of observations in the early time lead to only a single normal decay. Afterglow onsets are identified with an early smooth bump with a typical value of peak time t_p of several hundreds of seconds, coupled to the following normal decay with $\alpha \sim 1.2$.

IV: the jet-break component (Jet-Break); the light curves break into a steeper decay. They are identified with $\alpha \sim p \sim 2.5$ (Zhang et al. 2006) and a break time $\sim 10^5$ s. Here p is the electron index.

V: the late optical flares (Flare); the light curves have prompt-like flares during the afterglow phase when the prompt emission is turned off. They indicate the late-time activities of the central engine. The late optical flares are characterized by a very sharp temporal index $\alpha > 2.0$.

VI: the late re-brightening bumps (Re-Bump); the late bumps would emerge at late times, which is distinguished from the onset bump of the early afterglow. Both are likely involved in the jet component that produces the re-brightening bump, which seems to be on-axis and independent of the prompt emission jet component (Liang et al. 2013). They are described by a smooth bump around $t_p \sim 10^5$ seconds.

⁸ We discard the observations of the early optical-afterglow emission of GRB 080319B since it lacks multiband observations.

⁹ Throughout the paper, the convention $F_\nu \propto \nu^{-\beta} t^{-\alpha}$ is adopted.

VII: the late SN bumps (SN-Bump); in some cases, the optical transient light curves at late time show an SN bump. They form a late smooth bump at $t_p \sim 10^6$ s. In addition, we checked that the GRB-SN associations were confirmed in the literature (see §5.2.3).

All the assigned emission components in our 70 bursts are presented in Table 2 and 3, and are marked with arrows in Figures 5 and 6.

2.4. Definition of Color Index Variation

Once the fits are obtained, one can derive the CIs. They are defined as the magnitude difference between two filters,

$$CI = m(\lambda_2) - m(\lambda_1), \quad (8)$$

where $\lambda_2 < \lambda_1$ is required so that the smaller the CI, the bluer (or hotter) the optical afterglow. In this paper, we uniquely focus on the CI between two adjacent bands¹⁰. CI can be affected by optical extinction, which can be characterised by the color excess (CE), defined by the difference between the observed color index (CI_O) and the intrinsic color index (CI_T)

$$CE = CI_O - CI_T = A(\lambda_2) - A(\lambda_1). \quad (9)$$

2.4.1. Definition of the Golden and Silver Samples

To compute the CIs, simultaneous observations or interpolated values are required. We also note that different telescopes have different photometric systems (i.e., different light filters and spectral response functions), which are either the common Johnson-Cousins UBVRI photometry system¹¹ or the Sloan Digital Sky Survey (SDSS) ugriz photometry system¹². Instead of converting one system into another with empirical correlations (e.g., Jordi et al. 2006), we group the bursts by photometric systems, which are studied separately.

Therefore, we sort all GRBs into two samples based on the photometric system used for the observation. This also naturally separates bursts for which interpolation is required from those for which it is not.

- *Golden sample:*

The 25 bursts have simultaneous observations in multiple filters in the optical/IR bands (g, r, i, z, J, H, Ks) for a wide time window. They are mostly observed by the Gamma-Ray Burst Optical/NIR Detector (GROND; Greiner et al. 2008), with some events contributed from observations of the RAPid Telescopes for Optical Response (RAPTOR; Wren et al. 2010) and the Peters Automated IR Imaging Telescope (PAIRTEL; Bloom et al. 2006). These define our Golden sample. Obtaining the CI¹³ for these bursts is straightforward. The afterglow multicolor light curves and the time evolution of CIs are displayed in Figure 5.

- *Silver sample:*

The 45 remaining bursts in our sample do not have simultaneous observations in multiple filters but have instead multiple observations in different filters from different optical instruments at

¹⁰ u-g, g-r, r-i, i-z for the SDSS photometric system and UVW2-UVM2, UVM2-UVW1, UVW1-U, U-B, B-V, V-R, R-I, I-J, J-H, H-K for the commonly UBVRI photometric system.

¹¹ UVW2(1880 Å), UVM2(2170 Å), UVW1(2510 Å), U(3650 Å), B(4400 Å), V(5500 Å), R(6588 Å), I(8060 Å), J(12350 Å), H(16620 Å), K(22000 Å)

¹² u(3596 Å), g(4586.9 Å), r(6219.8 Å), i(7640.7 Å), z(8989.6 Å)

¹³ We focus on five color indices (g-r, r-i, i-z, J-H and H-Ks) for our Golden sample and 10 color indices (UVW2-UVM2, UVM2-UVW1, UVW1-U, U-B, B-V, V-R, R-I, I-J, J-H and H-K) for our Silver sample.

different times. For those bursts, we use the light-curve fits (§2.3) and interpolate the missing data points to obtain concurrent values in different filters (UVW2, UVM2, UVW1, U, B, V, R, I, J, H and K). This group of bursts defines the Silver sample. It has wider observed energy bands than the Golden sample. We try to include a maximum number of possible multiple data to represent the whole light curve. The multicolor light curves¹⁴ and the time evolution of CIs for each burst are shown in Figure 6.

The most accurate CIs are obtained in cases where there are simultaneous observations in multiple filters. This is the case for the bursts in the Golden sample. For many of these bursts there are additional nonsimultaneous data as well, which are discarded in order to keep the sample pure. Three criteria are applied to consider whether to add the additional data sources into the Golden sample: (i) there is at least an order-of-magnitude extension in the duration of observation; (ii) the number of data points should be greater than (or at least equal to) that in the original data source; (iii) at least three new bands have good observational data. Most cases do not satisfy these criteria. However, in two particular cases, GRB 090426 and GRB 130427A, there is a significant amount of additional data. We therefore use these cases to compare the results from the Golden and Silver samples.

For example, we add the R-band data to the multicolor light curves in the Golden sample for GRB 090426 (Figure 5). It provides a much earlier observation that can be compared to the GROND griz observation.

2.4.2. Methods to Determine the Temporal Behavior of Color Indices

We further define sets of CIs. The first one contains time-resolved data (Data Set I). The second set is made of component-wise averaged CIs (Data Set II). Finally, the mean CIs over the entire burst duration give Data Set III. Hereinafter all the analysis (such as the figures and the tables) will be marked with which sets of data are used.

According to Šimon et al. (2001), CIs should not be derived from fits to the light curve. They claimed that any fits to the data would distort the CIs. The Golden sample gives directly CIs directly while the Silver sample CIs are obtained with a fit to the light curve. Studying the difference between Golden and Silver samples allows us to check the consistency between our results and that of Šimon et al. (2001).

To account for the missing data points, two methods can be employed: (i) interpolation of the light curve from the fits (applied to the Silver sample), and (ii) averaging of existing data points as in Šimon et al. (2001). Interpolating missing data points results in large uncertainties but has the advantage of preserving a maximum number of simultaneous CIs. If the afterglow emission is smooth enough, the uncertainties should not be too large. On the other hand, averaging data results in more accurate estimation of the CIs, but strongly reduces their number. As pointed out by Šimon et al. (2001), averaging is also not reliable when light curves have rapid changes. Interestingly, after comparing both methods, we find that the results are consistent. We note that our Set II, which is obtained by averaging the CIs on each afterglow component, is similar to averages in arbitrary time intervals, as in Šimon et al. (2001), except that, in our paper, the time intervals are imposed by expected physical variations of the light curves.

¹⁴ We uniformly added different numbers to make a fixed set of offsets to different bands. For the Golden sample: g: 6, r: 5, i: 4, z: 3, J: 2, H: 1, K: 0; For the Silver sample: UVW2: 12, UVM2: 9, UVW1: 8, UVM1: 7, U: 7, B: 5, V: 4, R: 3, I: 2, J: 1.5, H: 1, K: 0, u: 14, g: 11, r: 10, i: 9, z: 8.

We investigate the correlation of the CIs from GRB 130427A using these two methods. This burst has a well-observed afterglow with a great number of data points. In Figure 7, we compare the CIs in the same observation duration between the Golden and the Silver samples. The CIs from the Golden sample are derived directly from RAPTOR (Vestrand et al. 2014) with simultaneous observations in multiple filters, while the CIs from the Silver sample are obtained by an interpolation method from the RATIR (Becerra et al. 2017), which in general do not have simultaneous observation, compared with the GROND observation in the corresponding period. We find that the data cluster around the equal line, which indicates that the results of both methods are consistent with each other.

2.4.3. Determination of Time Evolution

To determine whether the CI changes with time, we consider the following quantitative analysis. First, we calculate the mean color index \bar{m} and the standard deviation σ_s for each CI. We do this for Data Set I and II defined in Section §2.4.2. If a significant variation exists for the i th CIs, the criteria $|m_i - \bar{m}| > \sigma_{m_i} + \sigma_s$ should be met; here σ_{m_i} is the error on the i th CI. Note that both σ_{m_i} and σ_s are positive. Therefore, we define two grades for the CI:

- Constant: the CI is consistent with the overall mean value.
- Variable: the CI presents a significant variation.

3. STATISTICAL PROPERTIES OF COLOR INDICES

Table 4 summarizes the statistical properties of the CIs in our sample, which include the total number of data points, the distributed ranges, and their mean values. In Figure 8, we present all CIs as functions of time in one panel to show the global behavior. We find that more than 90% of the CIs distribute within [-1.0, 1.0] in the observed time intervals.

We analyze the distributions of the CIs (Data Set I) for both the Golden and Silver samples. They are all well fitted with Gaussian functions. Figure 9 displays the distributions together with the best Gaussian fits and with the mean CI values, as well as their standard deviations. For the Golden sample (Fig.9a), we have $g-r=0.15\pm0.14$, $r-i=0.09\pm0.10$, $i-z=0.13\pm0.11$, $J-H=0.23\pm0.10$ and $H-Ks=0.25\pm0.17$, respectively. We find that the distributions¹⁵ are consistent with each other with a mean value around 0.2. We note the presence of a tail at large values for the CI $g-r$. For the Silver sample (Fig.9b), we obtained $UVM2-UVW1=0.16\pm0.27$, $UVM2-UVW1=-0.19\pm0.24$, $UVW1-U=0.93\pm0.39$, $U-B=0.09\pm0.23$, $B-V=0.23\pm0.23$, $V-R=0.15\pm0.16$, $R-I=0.22\pm0.07$, $I-J=0.17\pm0.08$, $J-H=0.28\pm0.14$ and $H-K=0.14\pm0.22$, respectively. We find that the distributions are still consistent with each other with a mean value also around 0.2 for most of the CIs. This indicates that most of the CIs could be explained by the standard afterglow model with a single power-law spectral slope.

Note, however, that there are two inconsistent peaks in the Ultraviolet (UV) bands, with the $UVM2-UVW1$ CIs at -0.19 and $UVW1-U$ CIs at 0.93. The difference between the distributions could originate from the method that the CIs are obtained for the Silver sample. Because of the fitting and interpolation procedures, they carry large uncertainties, not taken into account by the histograms. A second reason for this difference could be underestimation of the extinction corrections. This is because the extinction curve in the host galaxy is largely uncertain¹⁶ and therefore the corrected

¹⁵ We note that these results are similar to the ones if only CIs with simultaneous observations for all five CIs are selected.

¹⁶ The uncertainty of the value stems from the method of obtaining the host extinction. If the extinction value of each energy band is constant, then the derived CIs will also be constant.

data could deviate from the actual values. This implies that after making the correction to the data, there could also be an additional reddening. Further investigation of the extinction property for each individual burst will be presented in a following paper (Li et al, in prep.). Stronger deviations are expected in high-energy bands in the Silver sample, tentatively explaining the possible reddening in those bands (Fig. 9b). Also, very few GRB host galaxies show MW/LMC-like 2175 \AA features. However, the redshifts are distributed over a wide range of values, so even if such features exist, they would appear in different observer-frame bands. Therefore, the effect would be completely diluted.

To test whether there exists an additional reddening, we analyze the SED, using the average CIs (Data Set III, regardless GRBs) and assuming a typical magnitude for the r-band (Golden sample)/R band (Silver sample). In Figure 10, we show the SED of the afterglow from a wide-band observations. We note that the difference in the distributions between the Golden and Silver samples are negligible in the SED; thus, it is reasonable to analyze the SED of the Silver sample. However, we find that the SED is still not completely consistent with the theoretical expectations (a single power-law spectral slope). This implies that the traditional extinction models (LMC, SMC, MK, etc.) are not precise in fully describing the extinction character for some GRBs.

We conclude by estimating the influence of redshift on the CI. The redshifts of our bursts lie between $z=0.007$ and 5.2. In Figure 11, we plot the CIs against the redshifts. We obtain a Spearman correlation coefficient $r=0.21$, corresponding to a chance probability $\hat{p} = \leq 10^{-4}$. This indicates that the possible dependence of the CIs on the redshift is very weak.

4. TEMPORAL EVOLUTION OF THE COLOR INDICES

4.1. Time Evolution for Data Set I (Full Resolution Data)

Following the definition of time evolution outlined in Section §2.4.3, we find that there are 20 out of 25 GRBs in the Golden sample that have at least more than two data points that are *variable* CIs. This indicates that the evolution of the CIs in the afterglow is very common. GRB 080413B is taken as an example, and its CIs as functions of time are displayed in Figure 12(a). The *variable* CIs are indicated by arrows. We note that the evolution of CIs tends to appear at a late time. In Figure 12(b), we compare the distributions of *constant* and *variable* CIs. We see that the nonvarying CIs are distributed similarly from one color to the others. Fitting the histograms by a Gaussian function, one has $g-r=0.15\pm0.14$ (mean \pm standard deviations), $r-i=0.08\pm0.09$, $i-z=0.13\pm0.10$, $J-H=0.23\pm0.11$ and $H-Ks=0.25\pm0.17$, respectively.

Instead, the group of varying CIs shows a broad distribution for different colors, possibly indicating different underlying phenomena. Table 5 summarizes the total number of *constant/variable* CIs. In the 25 GRBs of the Golden sample, 4039 out of 4212 (95.9%) values for all the five CIs in all the time bins are *constant* while only 173 (4.1%) are *variable*. This indicates that during most of the observed intervals, the CIs are constant, even for the 20 bursts that have a change (a small number of data points) in them.

4.2. Time Evolution for Data Set II (Component-wise Average)

We investigate the connection between the values of CIs and the afterglow light-curve components to determine their temporal evolution from one component to another. The components were identified

in §2.4. We calculate the mean value of CIs for each emission component¹⁷. The results are presented in Table 2 for the Golden sample and in Table 3 for the Silver sample.

In Figure 13(a), we show the distribution of CIs among various optical emission components (Data Set II, regardless of the bursts and CIs) and the distribution of ΔCI (results from Gaussian fits are summarized in Table 6) between one component and the following one (Figs. 13b). ΔCI is defined by

$$\Delta\text{CI} = \text{CI}(t_2) - \text{CI}(t_1), \quad (10)$$

where $t_2 > t_1$. This means that an increasing CI, with a red-to-blue color change, corresponds to $\Delta\text{CI} > 0$; in contrast, $\Delta\text{CI} < 0$ represents a decrease in CI with a blue-to-red color change.

We defined the global sample as the set of all CIs from both the Golden and Silver samples. We find that various emission components generally have similar distributions, with typical values ~ 0.2 , except the SN component, which presents a different ΔCI distribution. Comparing the CIs, we find that the distributions are consistent, though the number of data points is small. Note, however, that the distribution is very broad.

We present in Figure 14 the CI-CI correlations between consecutive components, regardless of the CIs. We compute the correlation index r in all cases and find that it is systematically close to 1. The two smallest values are the transition to an SN component with $r=0.57$ and a flare component with $r=0.60$. In addition, a linear fit to the slope for most correlations is also close to 1. This indicates that the CIs do not have a significant change between consecutive components. The fit results, along with the Spearman correlation coefficient r and the chance probability \hat{p} are reported in Table 6. This table also gives the number of CIs per emission component and the distribution range of ΔCI .

We find that 263 of 306 (85.9%) pair components satisfy the criterion that the CI does not change. The large fraction of CI without significant time variation for both the Golden and Silver samples suggests that the emission mechanism of the various components in the optical transient may stay the same. This is consistent with the prediction of the external shock afterglow model, for which the emission is dominated by synchrotron radiation, provided that the observation bands do not cover the spectral breaks.

Only 43 of the 306 (14.1%) pair components have a significant difference. For these pairs, we found that 18 include SN components, 5 include reverse-shock components, and 5 include flares (see Table 5). The Golden and the Silver samples show similar results. In those pair components that include an SN, 36% show variation. Likewise, 20% of the pair components including flares show variation. This makes the SN and flare components the ones that exhibit most common variations. This is consistent with the observational evidence that the optical transient spectrum typically changes during the associated SN and flares (e.g., Šimon et al. 2001, 2004; Zhang et al. 2006; Mu et al. 2016; Geng et al. 2016, 2017, and references therein). We also found a few cases of CI variation for the jet break components. This is note-worthy since a jet-break is believed to be purely dynamical. Therefore, CI evolution is not expected. Here, one should bear in mind the possibility that we could have identified the wrong component. For example, we could have identified a flare as a re-brightening bump if the flare is weak (GRB 021004, GRB 000301C, GRB 060707A). This is because they have similar light curves. Another possibility is that the interpolation procedure for the Silver sample introduces uncertainties affecting the determination of the CI.

¹⁷ Note that if several similar emission phases exist at different times in a single burst, we merge them together and calculate the mean value. This is applied for GRB 021004 and GRB 071031 (with two late flares).

5. PHYSICAL IMPLICATION

5.1. Constant Color Indices in the External Shock Model

There is a natural connection between the CIs and the spectral indices. Assuming that the SED of the afterglow in the considered bands is well described by an intrinsically single power law, the spectral flux density ($\text{erg cm}^{-2}\text{s}^{-1}\text{Hz}^{-1}$) for the afterglow is described by Equation (2). The relation between the flux and the observed magnitude is given by Equation (4), so we can write the CI, which is expressed from the flux density as

$$\text{CI} = -2.5\log_{10}\left(\frac{F_{\nu_2}}{F_{\nu_1}}\right) + C, \quad (11)$$

where $C = \text{ZP}_2 - \text{ZP}_1$, and $\text{ZP}_i = 2.5\log_{10}(F_{\nu_i,0})$ is the zero-point of various bands i . Therefore, the spectral index β_o can be connected to the CI as

$$\text{CI} = 2.5\beta_o\log_{10}\left(\frac{\nu_2}{\nu_1}\right) \quad (12)$$

According to Equation (12), there exists a linear relation between CIs and spectral indices. Therefore, CIs provide a probe to investigate the spectral properties of the optical afterglow.

Using Equation (12), we derive the index β_o^{CI} using *constant* CIs of Data Set I of the Golden sample (see Appendix Table 7) and the Data Set II of both the Golden and Silver samples during the normal-decay phase. We show the distribution of β_o^{CI} in Figure 15. The distribution is well fitted by a Gaussian function, and $\beta_o^{\text{CI}} = 0.68 \pm 0.60$ for *constant* CIs of Data Set I and $\beta_o^{\text{CI}} = 0.68 \pm 0.68$ for the Data Set II during the normal decay phase, which are consistent with each other.

The distributions are consistent with the predictions of the external shock model, with typical β_o around 0.75 (Mészáros & Rees 1997; Sari et al. 1998; Zhang et al. 2006). The spectral indices inconsistent with the external shock model are obtained from the high-energy bands, which could point toward a stronger reddening. We note that according to the external shock model, β_o^{CI} should cluster between 0.5 and 1.0. However, we found that a small fraction of data deviate from this range, which have large error bars, and thus they cannot accurately constrain the calculation of CI. Then this uncertainty propagates to the calculation of spectral index.

According to the standard synchrotron afterglow model, radiation is produced by electrons distributed with a power-law index p . Therefore, the CIs can be derived from the following equations for both a constant-density interstellar medium (ISM) and a wind-like medium (wind):

(i) Fast cooling:

$$\text{CI} = \begin{cases} -2.5\log_{10}\left(\frac{\nu_2}{\nu_1}\right)^{-\frac{1}{2}}, & (\nu_m > \nu_2 > \nu_1 > \nu_c) \\ -2.5\log_{10}\left(\frac{\nu_2}{\nu_1}\right)^{-\frac{1}{2}} - 2.5\log_{10}\left(\frac{\nu_2}{\nu_m}\right)^{-\frac{(p-1)}{2}}, & (\nu_2 > \nu_m > \nu_1 > \nu_c) \\ -2.5\log_{10}\left(\frac{\nu_2}{\nu_1}\right)^{-\frac{p}{2}}, & (\nu_2 > \nu_1 > \nu_m > \nu_c) \end{cases} \quad (13)$$

(ii) Slow cooling:

$$\text{CI} = \begin{cases} -2.5\log_{10}\left(\frac{\nu_2}{\nu_1}\right)^{-\frac{(p-1)}{2}}, & (\nu_c > \nu_2 > \nu_1 > \nu_m) \\ -2.5\log_{10}\left(\frac{\nu_2}{\nu_1}\right)^{-\frac{(p-1)}{2}} - 2.5\log_{10}\left(\frac{\nu_2}{\nu_c}\right)^{-\frac{1}{2}}, & (\nu_2 > \nu_c > \nu_1 > \nu_m) \\ -2.5\log_{10}\left(\frac{\nu_2}{\nu_1}\right)^{-\frac{p}{2}}, & (\nu_2 > \nu_1 > \nu_c > \nu_m) \end{cases} \quad (14)$$

Here ν_c is the cooling frequency, ν_m is the minimum frequency, and ν_2 and ν_1 are the frequencies of adjacent bands. In the fast cooling regime, electrons at the injection Lorentz factor have time to lose their energy by emitting synchrotron radiation, while they do not in the slow cooling regime.

Next, we use the observed CIs (Data Set I of the Golden sample) to derive the electron power-law indices p^{CI} using the Equations (13-14). In Figure 16, we present the distribution of p^{CI} , fit by a Gaussian. The mean values with their standard deviations are $p^{\text{CI}}=2.43\pm1.06$ for slow cooling ($\nu_c > \nu_2 > \nu_1 > \nu_m$) and $p^{\text{CI}}=1.43\pm1.06$ for fast/slow cooling ($\nu_2 > \nu_1 > \max(\nu_c, \nu_m)$). We find that the slow cooling scenario is consistent with the theoretical predictions for relativistic shocks, $p \sim 2.5$. A wide range of the electron index is obtained, which is consistent with previous studies (Shen et al. 2006; Liang et al. 2008).

Next, we use the closure relations to compute the electron index p from the temporal index α of the normal decay, which was obtained by fitting the light curve, or the spectral index β_o . We then further estimate the expected value of the color indices CI_{th} (Data Set III of the Golden sample) using Eq.(13-14). Figure 17 displays the correlation between the CI and CI_{th} for these spectral regimes. Their distributions are also shown with the best Gaussian fits $\text{CI}_{\text{obs}}=0.16\pm0.14$ for observed CI and $\text{CI}_{\text{th}}=0.13\pm0.07$ for theoretical CI.

We find that the data smoothly cluster around the equal line, and both observed CI and theoretical CI_{th} have a similar distributions, consistent with the afterglow synchrotron radiation model with an intrinsic power-law decay.

We also find that a small part of CIs are far away from the equal line, which implies that these data are inconsistent with the model. These CIs are mainly derived from GRB 081029 and 100621A (Fig.17). It is interesting that both GRB 081029 and GRB 100621A present a light curve with re-brightening bumps (see Figure 5). The late re-brightening bumps could come from different emission components. Overlapping bumps could alter the CIs estimation. However, we also find that CIs preceding the bump are still inconsistent with the model. To investigate this further, we searched all the bursts in the Golden sample to find more cases presenting a clear late re-brightening bumps in the light curves. We find that, GRB 071025, GRB 091029, and GRB 100814A are consistent with the theoretical values and present a late re-brightening. The results show that the afterglow emission for both GRB 081029 and GRB 100621A is likely different from other bursts.

In Figure 18, we show color-color diagrams using the Golden sample (Data Set I) to investigate the evolution of CI shift. We calculate the distance of data points to the equal line and the difference value between the two CIs. We find that most of the CIs cluster around the equal line and the typical difference value between two CIs is close to 0. For the distances, one has $(g-r)-(r-i)=-0.03\pm0.07$, $(r-i)-(i-z)=0.00\pm0.06$ and $(J-H)-(H-K_s)=0.00\pm0.14$, respectively. For their differences, one has $(g-r)-(r-i)=-0.04\pm0.10$, $(r-i)-(i-z)=0.01\pm0.09$, and $(J-H)-(H-K_s)=0.00\pm0.20$, respectively.

This result indicates that the CI shift is not significant, and the intrinsic reddening inside their host galaxies must be quite similar and relatively small for these events. This is also expected from the narrow distributions in wavelength of the ugriz filters. This result also implies that the afterglow spectral shapes are similar from one to another and can be described by a smooth power-law spectral decay, with no bumps or strong lines for these bands. These results are consistent with the finding of Šimon et al. (2004).

5.2. Possible Explanations For The Color Indices Variation

Below we outline three possible explanations for the CI variation, and in §5.2.4 we compare the prediction to the data.

5.2.1. The Cooling Frequency Crosses the Studied Energy Bands

In the external shock synchrotron model, the cooling frequency, ν_c , is likely to cross the optical bands at a time later than approximately 1 hr (Uhm & Zhang 2014). This will cause a change in the spectral indices and thereby in the observed CIs.

According to Eqs. (13)-(14), if the cooling frequency crosses all the optical bands and the spectral regime from a stable phase transition to another stable phase, then the change in the CIs, ΔCI , is given by

(i) Fast cooling:

$$\Delta\text{CI} = \begin{cases} -2.5\log_{10}\left(\frac{\nu_2}{\nu_m}\right)^{-\frac{(p-1)}{2}}, & (\text{from } \nu_2 > \nu_m > \nu_1 > \nu_c \text{ to } \nu_m > \nu_2 > \nu_1 > \nu_c) \\ -2.5\log_{10}\left(\frac{\nu_1}{\nu_m}\right)^{-\frac{(p-1)}{2}}, & (\text{from } \nu_2 > \nu_1 > \nu_m > \nu_c \text{ to } \nu_2 > \nu_m > \nu_1 > \nu_c) \\ -2.5\log_{10}\left(\frac{\nu_2}{\nu_1}\right)^{-\frac{(p-1)}{2}}, & (\text{from } \nu_2 > \nu_1 > \nu_m > \nu_c \text{ to } \nu_m > \nu_2 > \nu_1 > \nu_c) \end{cases} \quad (15)$$

(ii) Slow cooling:

$$\Delta\text{CI} = \begin{cases} -2.5\log_{10}\left(\frac{\nu_2}{\nu_c}\right)^{-\frac{1}{2}}, & (\text{from } \nu_2 > \nu_c > \nu_1 > \nu_m \text{ to } \nu_c > \nu_2 > \nu_1 > \nu_m) \\ -2.5\log_{10}\left(\frac{\nu_1}{\nu_c}\right)^{-\frac{1}{2}}, & (\text{from } \nu_2 > \nu_1 > \nu_c > \nu_m \text{ to } \nu_2 > \nu_c > \nu_1 > \nu_m) \\ -2.5\log_{10}\left(\frac{\nu_2}{\nu_1}\right)^{-\frac{1}{2}}, & (\text{from } \nu_2 > \nu_1 > \nu_c > \nu_m \text{ to } \nu_c > \nu_2 > \nu_1 > \nu_m) \end{cases} \quad (16)$$

In the constant environment model (the ISM model), the ν_c decreases with time (Sari et al. 1998). The optical band is initially below ν_c (bluer spectrum). As ν_c decreases in time, the optical band becomes above ν_c , and the spectrum becomes redder. This gives rise to a negative ΔCI . On the other hand, in the wind model, ν_c increases with time (Chevalier & Li 1999). The optical band is initially above ν_c (redder spectrum). As ν_c increases in time, the optical band becomes below ν_c (the spectrum becomes bluer). This gives a positive ΔCI .

We note that the cooling break in the afterglow spectra may not be sharp (Uhm & Zhang 2014). The transition from one regime to another is rather smooth and requires a very long time, especially in the optical bands. For most of the cases analyzed in this paper the transition has not finished during the period investigated, so what we have tested is an upper limit of ΔCI .

5.2.2. Effects of Host Extinction

The host extinction may also cause the CI change (e.g., Waxman & Draine 2000; Morgan et al. 2014). After being eventually destroyed by the initial intense radiation, dust could reform at an early time near the burst region, changing the host extinction (Perna & Lazzati 2002). This leads to two temporal changes in the CI. During the early afterglow phase (Phase I), dust might be destroyed, and the CI can be described by a red-to-blue change, implying an increase in the CI with $\Delta\text{CI} > 0$. On the contrary, at a late time (Phase II), dust could reform and reddening will reappear, and the CI presents a blue-to-red change, which provides a decrease in the CI with $\Delta\text{CI} < 0$. We note that Phase II might not occur, since the photodestruction could be irreversible (Perna & Lazzati 2002; Perna et al. 2003; Lazzati & Perna 2003).

The true magnitudes in the optical bands are estimated through considerations of extinctions (in both in our Galaxy and the host galaxy) and the spectral k -correction. We display the distributions of all correction factors in Figure 19. The factor that affects the achromatic energy band is given by $(-\text{A}^G - \text{K} - \text{A}^H)$. This quantity is distributed in $[-4.29, 0.22]$, and, as seen in Fig. 19b, it is negligible compared to the brightness (Data Set III).

The factor affecting the CIs can be characterised by the color excess, CE, such that

$$\begin{aligned}\text{CI}_T &= m_O(\lambda_1) - A^G(\lambda_1) - K - A^H(\lambda_1) - \{m_O(\lambda_2) - A^G(\lambda_2) - K - A^H(\lambda_2)\} \\ &= \text{CI}_O - \{A^G(\lambda_1) - A^G(\lambda_2) + A^H(\lambda_1) - A^H(\lambda_2)\} \\ &= \text{CI}_O - \text{CE},\end{aligned}\quad (17)$$

where A^H is the magnitude of the host dust extinction and A^G is the magnitude of our Galaxy dust extinction. Here the CE includes contributions from our Galaxy and the host galaxy, while the k -correction factor is the same for both bands. Therefore $\text{CE} = \{A^G(\lambda_1) - A^G(\lambda_2) + A^H(\lambda_1) - A^H(\lambda_2)\}$ is the total correction, ranging from 0.00 to 0.99. Figure 19(c) presents the CE as a function of CI. Since both the CI and CE have similar magnitudes, uncertainties on the corrections have large effects on the value of the CIs.

5.2.3. Effects of the Supernova Emission Component

GRB-associated SNe in some long bursts (Woosley & Bloom 2006; Hjorth et al. 2003; Cano et al. 2017) could produce an additional emission component embedded in the late afterglow synchrotron emission. This results in a CI variation (e.g., Šimon et al. 2004; Gal-Yam et al. 2004), described as a red afterglow bump. From the literature, 13 cases¹⁸ of GRB-SN associations in our sample were reported. We compare the CIs between the GRB-SN emission and their previous components, regardless of the nature of this previous component. We are only concerned here with the variation of the CI (Data Set II). The results displayed by Figure 14 show that a very high fraction (see Table 5) of CIs exhibit a significant variation, indicating a spectral change as expected.

5.2.4. Statistical Analysis

¹⁸ GRB 980425/SN 1998bw (Galama et al. 1998), GRB 030329/SN 2003dh (Resmi et al. 2005), GRB 050525A/SN 2005nc (Della Valle et al. 2006a), GRB 060218/SN 2006aj (Campana et al. 2006), GRB 081007/SN 2008hw (Olivares E. et al. 2015), GRB 091127/SN 2009nz (Cobb et al. 2010), GRB 100316D/SN 2010bh (Cano et al. 2011a), GRB 101219B/SN 2010ma (Olivares E. et al. 2015), GRB 120422A/SN 2012bz (Melandri et al. 2012), GRB 130215A/SN 2013ez (Cano et al. 2014), GRB 130427A/SN 2013cq (Xu et al. 2013), 130702A/SN 2013dx (D'Elia et al. 2015), GRB 130831A/SN 2013fu (Cano et al. 2014).

We perform a statistical analysis considering only *variable* CIs to explore possible physical origins. Figure 20(a) shows the distribution of variable CIs. If the observed variation is due to the crossing of the cooling spectral break, then either positive or negative values of Δ CIs are expected, depending on the density profile of the circumburst medium. As discussed above, a positive value of Δ CIs is expected in the early afterglow phase (earlier than 1 hr) owing to dust destruction. Variable CIs for the SN are defined as the identification of a GRB-SN bump at a later time, which is confirmed in published papers (see §5.2.3).

Figure 20(b) presents the temporal evolution of the ratio of varying CIs to the total number of varying CIs in a given time interval. We group the ratios depending, in turn, on (i) the identification of the SN component and whether the Δ CIs are part of it and (ii) the sign of the Δ CIs.

Among the positive Δ CIs (64 % of all cases, labeled II in Figure 20(a)) we find two peaks, at around 500s and $\sim 10^6$ s. The early peak is consistent with being due to dust extinction, corresponding to 12% of the Δ CIs. These cases are marked by the red line in the figure. The peak at 10^6 s is consistent with effects of ν_c crossing the observed band in a wind environment, causing a red-to-blue change, i.e., a shallowing of the spectrum (yellow line in the figure), including 43% of the variable CIs.

Likewise, among the negative Δ CIs (36 % of all cases, labelled I in Figure 20(a)), there are two peaks, one at around 100 s, and one at $\sim 10^5 - 10^6$ s. The latter peak contains Δ CIs that are consistent with effects of ν_c crossing the observed band in an ISM environment, causing a blue-to-red change, i.e., a steepening of the spectrum (green line in the figure), corresponding to 30% of the cases. For the bursts that exhibit a color change at around 100s (blue curve in the figure), the most natural explanation is the transition from reverse-shock (RS) emission to forward-shock (FS) emission. Early on, the emission is likely dominated by the RS component and the optical band is below $\nu_{c,r}$ (bluer spectrum). At around 100 s, there is likely a transition from the RS to the FS emission (Type II light curve reported in Zhang et al. 2003). At this time, the FS may be already above $\nu_{c,f}$. This gives a redder color. For the wind model (Wu et al. 2003; Kobayashi & Zhang 2003), a similar situation is expected. This case includes $\sim 5\%$ of Δ CIs.

Finally, the SN cases dominate the late-time variations (purple curve in the figure), the last one corresponding to 10% of the variable CIs.

6. CONCLUSION

We studied the multiband optical afterglows of 70 bursts with their CIs. The optical/NIR photometric data are not only based on *Swift*/UVOT but are also obtained from ground-based instruments, especially the GROND. This catalog of multiwavelength GRB afterglow data provides an opportunity for a statistical study. We corrected the data with the Galactic and host galaxy extinctions. After performing a spectral k -correction, we divided the bursts into two samples depending on whether the different optical bands have a simultaneous observation. Our main results are summarized as follows:

- A Golden sample includes 25 out of 70 GRBs with five CIs. The distributions of these CIs are approximately the same. There is no color shift between CIs, and in general they satisfy the afterglow model prediction of a single power-law spectral slope.
- A Silver sample includes 45 out of 70 GRBs with 10 CIs with wider energy ranges. The distributions of these CIs are consistent with the Golden sample in the corresponding energy bands. For most of these CIs, the typical value is around 0.2, and they also, in general, satisfy the afterglow model prediction of a single power-law spectral slope. There are two significantly

inconsistent peaks, mainly distributed in the UV bands, with UVM2-UVW1=-0.19 and UVW1-U=0.93. This is consistent with the theoretical prediction that the intrinsic reddening is more significant in the high-energy bands.

- After performing all the corrections for the data, the SED of the optical transient, which is derived from the average CI, presents a deviated single power-law spectral slope. This implies that the traditional extinction models could be not accurate enough to describe the extinction characteristics for some GRBs.
- Most CIs (95.9%) are constant in the Golden sample (Data Set I). They are tightly distributed with standard deviations of ~ 0.2 . The variable CIs (4.1%) are widely distributed, presenting evidence for several different emission mechanisms. We determined that around 30% are due to the crossing of the cooling spectral break in an ISM medium, while 43% are due to a wind-like medium, 10% due to the SN emission, 12% due to early dust extinction, and 5% due to the transition from RS to FS emissions.
- Component-wise, we found that most cases of the varying CIs (Data Set II) are in the transition during the SNe, the Reversed-Shock, or the Flare components.
- We derived the correlations between CIs and spectral indices based on the standard afterglow synchrotron model and obtained β_o^{CI} (using the *constant* CI of data Set I and Data Set II during the normal-decay phase) and p^{CI} (using the *constant* CI of Data Set I). The typical values are $\beta_o^{\text{CI}}=0.68\pm0.60$ (Data Set I) and $\beta_o^{\text{CI}}=0.68\pm0.68$ (Data Set II). We found that these two distributions are consistent with each other. Moreover, $p^{\text{CI}}=2.43\pm1.06$ for Slow cooling ($\nu_c > \nu_2 > \nu_1 > \nu_m$) and $p^{\text{CI}}=1.43\pm1.06$ for Fast/Slow cooling ($\nu_2 > \nu_1 > \max(\nu_c, \nu_m)$), which are consistent with the theoretical predictions for relativistic shocks. A wide range of p values is obtained, which is consistent with previous findings. In turn, we derived the theoretical CIs using the p values derive from the closure relation and compared them to the observed CIs. We found that they still clustered around the equal line.
- We also investigated the overall behavior of the CIs:
 - (i) The CIs are independent of the redshift.
 - (ii) More than 90% of CIs are distributed between -1.0 and 1.0. They have negligible variations compared to the decline of the brightness with time.
 - (iii) The dust extinction correction and the spectral k -correction can significantly affect the values of CIs and spectral indices.

We compiled a sample of multiband observations of optical transients to investigate the temporal evolution of the CIs. The variable CIs are clues to unveiling the origin and details of the optical transient and of GRBs in general, prompting for more prolonged and simultaneous observations.

We thank Damien Bégué, Yun-Feng Liang, Jin-Jun Geng, Hüsne Dereli, and Remo Ruffini for helpful discussions, and we are greatly indebted to the referee for an extremely careful reading of the manuscript and for helpful and valuable comments that greatly improved this paper. This work is supported by the Swedish National Space Board, the Swedish Research Council, the National Basic

Research Program of China (973 Program, grant no. 2014CB845800), and the National Natural Science Foundation of China (grant nos. 11725314, 11673068, 11473012, 11673068 and No. 11103083), and the Key Research Program of Frontier Sciences (QYZDB-SSW-SYS005), the Strategic Priority Research Program "Multi-waveband gravitational wave Universe" (grant no. XDB23000000). L.L. acknowledges the support by the Erasmus Mundus Joint Doctorate Program via grant no. 2013-1471 from the EACEA of the European Commission. L.S. acknowledges the supported by the Joint NSFC-ISF Research Program (no. 11361140349), jointly funded by the National Natural Science Foundation of China and the Israel Science Foundation. B.Z. acknowledges NASA NNX14AF85G for support. F.R. is supported by the Göran Gustafsson Foundation for Research in Natural Sciences and Medicine. Part of this work made use of our private Python library.

Table 1. Properties of the GRB Sample with Multicolor Light Curves

GRB	Filters	E_{B-V}^G	β_o	A_v^{host}	z	References (for Data Sources)
		(Galaxy)	(Spectral Index)	(Host Galaxy)	(Redshift)	
970508	<i>UBVRcIc</i>	0.034	1.11	0.38 ± 0.11	0.8349	1,2,3,4,5,6
980425	<i>UBVRcIc</i>	0.059	...	0.17 ± 0.02	0.0085	7,8,9,10
990510	<i>BVRIJHKs</i>	0.226	0.55	0.22 ± 0.07	1.6187	11,12,13,14
990712	<i>VRI</i>	0.035	0.99 ± 0.02	0	0.4331	15,16,17
000301C	<i>UBVRIJK</i>	0.053	0.70	0.12 ± 0.06	2.0404	18,19,20,21,22,23
000926	<i>UBVRI</i>	0.025	1.00 ± 0.18	0.15 ± 0.07	2.0387	24,25,26
021004	<i>UBVRIJHK</i>	0.074	0.14	0.05	2.3304	27,28,29,30,31
030226	<i>UBVRIJHK</i>	0.023	0.70 ± 0.03	0.06 ± 0.06	1.98691	32,33,34
030328	<i>UBVRI</i>	0.075	0.36 ± 0.45	0.05 ± 0.15	1.5216	35
030329	<i>UBVRIJH</i>	0.029	0.54 ± 0.02	0.39 ± 0.15	0.16867	36,37,38,39
050525A	<i>UVW2UVM2UVW1UBVRIJH</i>	0.117	0.97 ± 0.10	0.36 ± 0.05	0.606	40,41,42,43,44
050801	<i>UVW2UVM2UVW1UBVRICJK</i>	0.081	1.00 ± 0.16	0.30 ± 0.18	1.56	43,45,46
050820A	<i>UBVRIJHKg'z'</i>	0.054	0.72 ± 0.03	0.07 ± 0.01	2.61469	43,47
050922C	<i>UBVRI</i>	0.093	0.51 ± 0.05	0.01 ± 0.01	2.198	43,48
051111	<i>BVRI</i>	0.146	0.76 ± 0.07	0.20 ± 0.10	1.54948	49,50,51,52
060218	<i>UVW2UVM2UVW1UBVRIJHK</i>	0.124	...	0.13 ± 0.01	0.03342	53,54,55,56
060418	<i>BVRIJHKz'</i>	0.319	0.78 ± 0.09	0.20 ± 0.06	1.49000	43,57,58
060526	<i>whiteBVRIJHKs</i>	0.078	0.51 ± 0.32	0.05 ± 0.11	3.221	59,60
060607A	<i>whiteUBVgrizH</i>	0.027	0.72 ± 0.27	0.08 ± 0.08	3.0749	58,61,62,63
060614	<i>whiteUVW2UVM2UVW1UBVRIJK</i>	0.017	0.47 ± 0.04	0.28 ± 0.07	0.1254	64,65,66,67,68
060729	<i>whiteUVW2UVM2UVW1UBVCR</i>	0.05	0.78 ± 0.03	0	0.5428	69,70
060906	<i>g'Rci'z'</i>	0.087	0.56 ± 0.02	<0.09	3.6856	71
060908	<i>whiteUBVRIJHKgriz</i>	0.027	0.30	0.05 ± 0.03	1.8836	72
061007	<i>BVRi</i>	0.019	0.78 ± 0.02	0.48 ± 0.10	1.2622	73
061126	<i>UVM2UVW1UBVRIJHKHgri</i>	0.187	0.95	0.10 ± 0.06	1.1588	74,75
070125	<i>UVW2UVM2UVW1UBVRIJHKsgriz</i>	0.052	0.55 ± 0.04	0.11 ± 0.04	1.54705	76,77
071010A	<i>clearUBVRIJHK</i>	0.114	0.68	0.64 ± 0.09	0.985	78
071025	<i>JHKs</i>	0.059	0.42 ± 0.08	0.12 ± 20.6	5.2	79
071031	<i>g'r'i'z'JHKs</i>	0.008	0.64 ± 0.01	0.14 ± 0.13	2.692	80
080109	<i>uvw2uvvm2uvw1UBVRIJHKri</i>	0.02	0.007	81
080310	<i>clearBVRIJHKwhiteubv</i>	0.043	0.42 ± 0.12	0.19 ± 0.05	2.42743	43,82,83
080319B	<i>whiteclearUVW2UVM2UVW1UBVRIJHKsgriz</i>	0.011	0.66	0.06 ± 0.03	0.9371	84,85,86
080330	<i>UVW1UBVRIJHKgrizwhiteclear</i>	0.016	0.49	0.19 ± 0.08	1.5115	43,87
080413B	<i>g'r'i'z'</i>	0.032	0.25 ± 0.07	0	1.1014	88
080603A	<i>clearg'r'i'BVRIJHK</i>	0.044	0.98 ± 0.04	0.90 ± 0.19	1.67842	89
080607	<i>g'r'i'z'clearVRIJHKs</i>	0.023	1.32 ± 0.07	3.3 ± 0.4	3.306	90
080710	<i>g'r'i'z'JHKs</i>	0.046	0.80 ± 0.09	0.11 ± 0.04	0.845	91
080810	<i>whiteBVRIfunfitbvir</i>	0.031	0.44±0	0.16 ± 0.02	3.35104	43,92
081007	<i>g'r'i'z'JHK</i>	0.015	0.47 ± 0.09	0.31 ± 0.25	0.5295	93
081008	<i>UVW1UBVwhiteRcCRIcJHKg'r'i'z'</i>	0.095	1.10 ± 0.04	0.17 ± 0.11	1.9683	43,94
081029	<i>g'r'i'z'JHKs</i>	0.028	1.00 ± 0.01	0.03 ± 0.02	3.8479	95
090102	<i>g'i'z'RJHKs</i>	0.045	0.74	0.12 ± 0.11	1.548	96
090426	<i>g'r'i'z'R</i>	0.015	0.76 ± 0.14	0	2.609	97,98,99

Table 1 continued on next page

Table 1 (*continued*)

GRB	Filters	E_{B-V}^G	β_o	A_v^{host}	z	References
		(Galaxy)	(Spectral Index)	(Host Galaxy)	(Redshift)	
090510	$g'r'i'z'$	0.02	0.85 ± 0.05	0.17 ± 0.21	0.903	100
090618	$uvw2uvm2uvw1uBVwhiteRc$	0.085	0.5	0.3 ± 0.1	0.54	101,102
090926A	$g'r'i'z'$	0.023	0.72 ± 0.17	0.13 ± 0.06	2.1071	103,104
091018	$g'r'i'z'JHKs$	0.034	0.57 ± 0.01	0.09	0.9710	105
091024	$BVRI$	0.98	1.0924	106
091029	$g'r'i'z'$	0.013	0.49 ± 0.12	0	2.752	107
091127	$g'r'i'z'$	0.037	0.43 ± 0.10	0.17 ± 0.15	0.49044	108
100316D	$BVRIg'r'i'z'JH$	0.117	0.94 ± 0.05	0.43 ± 0.03	0.0592	109
100621A	$g'r'i'z'JHKs$	0.028	0.80 ± 0.10	3.65 ± 0.06	0.542	110
100814A	$g'r'i'z'JHKs$	0.02	0.47 ± 0.05	<0.04	1.44	111
101219B	$g'r'i'z'JHK$	0.02	0.62 ± 0.01	<0.1	0.55185	112
110205A	$whiteubvgrizRJHK$	0.098	...	0.35 ± 0.03	2.21442	113
110213A	$whiteclearubvgrizBVR$	0.432	1.22 ± 0.18	...	1.4607	110,114,115,116,117
110918A	$g'r'i'z'JHKs$	0.015	0.70 ± 0.02	0.16 ± 0.06	0.984	118
111209A	$UVW2UVM2UVW1UBVWhiteg'r'i'z'JHK$	0.02	1.07 ± 0.15	0.3-1.5	0.677	119,120,121
120119A	$clearBVRJHK$	0.109	0.92 ± 0.02	0.62 ± 0.06	1.728	122
120404A	$g'r'i'z'UBVRJH$	0.052	1.04 ± 0.02	0.07 ± 0.02	2.8767	123
120422A	$g'r'i'BVRI$	0.068	0.50	0	0.28253	124,125
120711A	$g'r'i'z'JHKs$	0.075	0.53 ± 0.02	0.85 ± 0.06	1.405	126
120729A	$g'r'i'z'VR$	0.162	1.00 ± 0.10	0.15	0.80	127
120815A	$g'r'i'z'$	0.096	0.78 ± 0.01	0.15 ± 0.02	2.3586	128
121024A	$g'r'i'z'JHKs$	0.128	0.86 ± 0.01	0.18 ± 0.04	2.3010	129
121217A	$g'r'i'z'$	0.392	0.87 ± 0.04	0 ± 0.03	3.08	130
130215A	$g'r'i'z'JHK$	0.137	0.90 ± 0.20	0	0.597	127
130427A	$g'r'i'z'$	0.022	0.92 ± 0.10	0.13 ± 0.06	0.3399	131,132
130702A	$clearu'g'r'i'z'UBVRJH$	0.031	0.52 ± 0.19	0.30 ± 0.07	...	133,134,135
130831A	$g'r'i'z'BRcIc$	0.054	0.85 ± 0.01	0.06 ± 0.04	0.4791	123,136, 137
130925A	$g'r'i'z'JHK$	0.018	0.32 ± 0.03	5.00 ± 0.70	0.3479	138

Table 1 continued on next page

Table 1 (*continued*)

Table 2. Color Indices of the Golden Sample

GRB	Component ^a	Epoch ^b (ks)	Model ^c	g - r	r - i	i - z	J - H	H - Ks
				mag	mag	mag	mag	mag
071025(0) ^d	Global	0.17-14.9	0.19±0.14	0.51±0.15
071025(1)	Onset	0.17-0.6	BKPL	0.19±0.25	0.64±0.24
071025(2)	Normal-Decay	0.55-1.0	BKPL	0.22±0.10	0.49±0.11
071025(3)	Re-Bump	0.99-14.9	BKPL	0.18±0.11	0.45±0.13
071031(0)	Global	0.29-25.7	...	0.56±0.03	0.13±0.03	0.09±0.04	0.2±0.06	0.28±0.07
071031(1)	Onset	0.29-1.2	BKPL	0.63±0.02	0.17±0.02	0.09±0.03	0.21±0.05	0.33±0.06
071031(2)	Normal-Decay	1.23-4.0	BKPL	0.58±0.04	0.14±0.03	0.08±0.04	0.21±0.05	0.27±0.07
071031(3)	Re-Bump	4.05-25.7	BKPL	0.55±0.03	0.12±0.03	0.09±0.04	0.19±0.07	0.22±0.08
080413B(0)	Global	0.34-780.5	...	0.14±0.06	0.02±0.06	0.14±0.07
080413B(1)	Normal-Decay	0.34-90.3	BKPL	0.12±0.06	0.00±0.06	0.15±0.06
080413B(2)	Jet-Break	90.3-780.5	BKPL	0.30±0.12	0.19±0.10	0.06±0.12
080710(0)	Global	0.42-353.1	...	0.33±0.01	0.18±0.01	0.19±0.02	0.28±0.02	0.28±0.02
080710(1)	Onset	0.41-2.8	TPL	0.34±0.01	0.19±0.01	0.20±0.01
080710(2)	Normal-Decay	2.83-7.6	TPL	0.32±0.01	0.17±0.01	0.19±0.01	0.26±0.02	0.31±0.03
080710(3)	Jet-Break	7.63-353.1	TPL	0.32±0.01	0.17±0.02	0.18±0.02	0.28±0.02	0.28±0.02
081007(0)	Global	1.12-2500.0	...	-0.09±0.22	0.05±0.24	0.02±0.22	0.46±0.07	0.17±0.07
081007(1)	Jet-Break	1.12-500.0	BKPL	-0.09±0.22	0.03±0.17	0.02±0.15	0.46±0.07	0.17±0.07
081007(2)	SN-Bump	500.0-2500.0	BKPL	...	0.08±0.39	0.02±0.44
081008(0)	Global	13.65-187.8	BKPL	0.19±0.03	0.32±0.04	0.20±0.04	0.15±0.04	0.00±0.05
081008(1)	Normal-Decay	13.65-187.8	BKPL	0.19±0.03	0.32±0.04	0.20±0.04	0.15±0.04	0.00±0.05
081029(0)	Global	0.52-438.7	...	1.03±0.03	0.30±0.04	0.19±0.04	0.26±0.09	0.16±0.09
081029(1)	Energy-Break	0.52-0.9	BKPL	1.02±0.02	0.28±0.03	0.18±0.03	0.19±0.09	0.11±0.10
081029(2)	Normal-Decay	0.94-3.5	BKPL	1.00±0.02	0.27±0.03	0.18±0.03	0.22±0.09	0.14±0.10
081029(3)	Re-Bump	3.55-16.3	BKPL	1.04±0.03	0.32±0.03	0.20±0.03	0.29±0.07	0.16±0.09
081029(4)	Jet-Break	16.26-438.7	BKPL	1.04±0.06	0.28±0.07	0.17±0.05	0.22±0.11	0.18±0.07
090426(0)	Global	44.73-139.8	...	0.35±0.06	0.05±0.08	0.09±0.12	0.08±0.18	...
090426(1)	Energy-Break	0.1-0.5	BKPL
090426(2)	Normal-Decay	0.5-10.0	BKPL
090426(3)	Jet-Break	10.0-139.8	BKPL	0.36±0.06	0.04±0.09	0.09±0.12	0.08±0.18	...
090510(0)	Global	23.13-34.4	...	0.33±0.49	0.19±0.41	0.05±0.46
090510(1)	Normal-Decay	23.13-34.4	PL	0.33±0.49	0.19±0.41	0.05±0.46
090926A(0)	Global	73.16-2070.8	...	0.19±0.04	0.13±0.04	0.13±0.05
090926A(1)	Normal-Decay	73.16-200.0	BKPL	0.18±0.04	0.12±0.04	0.13±0.04
090926A(2)	Re-Bump	200.0-2070.8	BKPL	0.23±0.08	0.18±0.05	0.17±0.07
091018(0)	Global	10.97-272.8	...	0.12±0.03	0.11±0.04	0.10±0.05	0.09±0.05	0.12±0.08
091018(1)	Energy-Break	10.97-19.9	BKPL	0.12±0.03	0.10±0.03	0.10±0.04	0.10±0.05	0.12±0.07
091018(2)	Normal-Decay	19.95-272.8	BKPL	0.11±0.05	0.13±0.06	0.08±0.08	0.07±0.08	0.11±0.10
091029(0)	Global	0.31-344.9	...	0.25±0.03	0.02±0.03	0.14±0.06
091029(1)	Onset	0.31-0.5	BKPL	0.30±0.04	0.09±0.03	0.19±0.05
091029(2)	Normal-Decay	0.52-4.7	BKPL	0.26±0.03	0.03±0.03	0.15±0.05
091029(3)	Re-Bump	4.66-344.9	BKPL	0.23±0.03	0.01±0.04	0.13±0.06
091127(0)	Global	3.3-4673.7	...	0.03±0.02	0.04±0.02	0.02±0.02
091127(1)	Energy-Break	3.3-27.5	BKPL	0.01±0.01	0.02±0.01	0.01±0.01

Table 2 continued on next page

Table 2 (*continued*)

GRB	Component ^a	Epoch ^b (ks)	Model ^c	g - r		r - i		i - z		J - H		H - Ks	
				mag	mag	mag	mag	mag	mag	mag	mag	mag	mag
091127(2)	Normal-Decay	27.47-959.0	BKPL	0.19±0.05	0.10±0.05	0.00±0.07
091127(3)	SN-Bump	959.04-4673.7	BKPL	0.67±0.11	0.43±0.10	0.29±0.16
100316D(0)	Global	42.55-7000.0	...	0.31±0.06	-0.05±0.06	0.40±0.06	-0.35±0.28
100316D(1)	Late-Bump	42.55-300.0	BKPL	-0.16±0.05	-0.01±0.06	0.03±0.07	-0.27±0.40
100316D(2)	SN-Bump	300.0-7000.0	BKPL	0.51±0.06	-0.07±0.06	0.54±0.06	-0.36±0.27
100621A(0)	Global	0.26-100.9	...	0.98±0.24	0.32±0.17	-0.20±0.15	0.52±0.15	0.67±0.14
100621A(1)	Onset	0.22-0.6	BKPL	...	0.15±0.17	0.07±0.13	0.65±0.14	0.49±0.13
100621A(2)	Normal-Decay	0.62-2.1	BKPL	0.24±0.25	0.39±0.24	0.11±0.13	0.51±0.16	0.48±0.16
100621A(3)	Re-Bump	2.13-100.9	BKPL	1.35±0.24	0.33±0.17	-0.28±0.16	0.48±0.15	0.83±0.13
100814A(0)	Global	0.67-2264.3	...	0.08±0.03	0.12±0.04	0.29±0.06	0.15±0.10	0.02±0.16
100814A(1)	Normal-Decay	0.67-23.2	BKPL	0.00±0.02	0.07±0.03	0.25±0.05	0.13±0.10	-0.04±0.14
100814A(2)	Re-Bump	23.21-2264.3	BKPL	0.19±0.04	0.20±0.05	0.34±0.07	0.22±0.12	0.13±0.20
101219B(0)	Global	29.55-3070.0	...	0.29±0.11	0.13±0.12	-0.27±0.19	0.26±0.23	0.34±0.28
101219B(1)	Normal-Decay	29.55-500.0	BKPL	0.05±0.09	0.01±0.07	-0.10±0.10	0.24±0.16	0.34±0.28
101219B(2)	SN-Bump	500.0-3070.0	BKPL	0.61±0.14	0.25±0.16	-0.41±0.26	0.35±0.59
110918A(0)	Global	126.39-553.4	...	0.18±0.04	0.04±0.04	0.09±0.07	0.33±0.15	0.00±0.20
110918A(1)	Normal-Decay	126.39-553.4	BKPL	0.18±0.04	0.04±0.04	0.09±0.07	0.33±0.15	0.00±0.20
111209A(0)	Global	64.49-6241.9	BKPL	-0.03±0.08	-0.04±0.05	-0.10±0.06	0.24±0.21	0.30±0.28
111209A(1)	Late-Bump	64.49-1000.0	BKPL	-0.05±0.06	-0.05±0.04	-0.09±0.06	0.22±0.20	0.28±0.26
111209A(2)	SN-Bump	1000.0-6241.9	BKPL	0.12±0.20	0.13±0.10	-0.22±0.13	0.48±0.40	0.59±0.68
120711A(0)	Global	21.16-370.1	...	0.33±0.15	0.33±0.10	0.08±0.11	0.40±0.19	0.32±0.23
120711A(1)	Normal-Decay	21.16-370.1	BKPL	0.33±0.15	0.33±0.10	0.08±0.11	0.40±0.19	0.32±0.23
120815A(0)	Global	0.17-11.1	...	0.71±0.03	0.33±0.03	0.17±0.04
120815A(1)	Onset	0.17-0.5	BKPL	0.73±0.03	0.32±0.02	0.19±0.03
120815A(2)	Normal-Decay	0.48-11.1	BKPL	0.71±0.03	0.33±0.03	0.17±0.04
121024A(0)	Global	11.09-107.0	...	0.72±0.15	0.23±0.09	0.15±0.11	0.34±0.24	0.28±0.26
121024A(1)	Normal-Decay	11.09-30.0	BKPL	0.74±0.13	0.22±0.08	0.15±0.08	0.37±0.15	0.21±0.17
121024A(2)	Jet-Break	30.0-107.0	BKPL	0.68±0.20	0.23±0.13	0.16±0.16	0.29±0.43	0.43±0.46
121217A(0)	Global	1.12-347.2	...	0.54±0.07	0.11±0.06	0.02±0.08
121217A(1)	Onset	1.12-1.6	BKPL	0.53±0.06	0.13±0.06	0.09±0.06
121217A(2)	Normal-Decay	1.59-347.2	BKPL	0.54±0.07	0.11±0.06	0.01±0.08
130427A(0)	Global	0.14-3480.0	0.15±0.02
130427A(1)	Normal-Decay	0.14-500.0	BKPL	0.14±0.01
130427A(2)	SN-Bump	500.0-3480.0	BKPL	0.17±0.14
130925A(0)	Global	0.94-284.4	BKPL	...	-0.48±2.17	-0.06±0.78	0.62±0.34	0.40±0.26
130925A(1)	Flare	0.94-10.0	BKPL	...	0.06±2.29	0.13±0.51	0.62±0.26	0.44±0.18
130925A(2)	Normal-Decay	10.0-284.4	BKPL	...	-1.01±2.05	-0.80±1.82	0.60±1.98	0.18±0.72

^aThe identifications of various optical-afterglow emission components.^bThe time intervals for each component in the observer frame.^cThe models of the light-curve fits for each component.^dThe serial number, 0, is denoted as global, and other numbers are the components with time sequence.

Table 3. Color Indices of the Silver Sample

GRB	Component	Epoch	Model	Color Indices									
				(ks)	UVW2 – UVM2	UVM2 – UVW1	UVW1 – U	U – B	B – V	V – R	R – I	I – J	
970508(0)	Global	25.57-40594.2	-0.23±0.38	0.32±0.28	0.02±0.23	0.34±0.23	
970508(1)	Late-Bump	25.57-400.0	BKPL	...	-0.33±0.38	0.17±0.28	0.05±0.23	0.21±0.23	
970508(2)	Jet-Break	400.0-1030.0	BKPL	...	-0.24±0.38	0.19±0.28	0.04±0.23	0.22±0.23	
970508(3)	Re-Bump	1030.0-040594.2	BKPL	...	-0.14±0.38	0.48±0.28	-0.01±0.23	0.48±0.23	
980425(0)	Global	94.85-46400.0	2.35±0.21	0.87±0.23	1.25±0.23	0.75±0.21	
980425(1)	Late-Bump	94.85-1530.0	BKPL	...	2.15±0.21	0.54±0.23	0.99±0.23	0.73±0.21	
980425(2)	SN-Bump	1330.0-46400.0	BKPL	...	2.40±0.21	0.96±0.23	1.32±0.23	0.75±0.21	
990510(0)	Global	12.44-2000.0	0.09±0.09	0.64±0.17	-0.02±0.31	...	
990510(1)	Normal-Decay	12.44-92.6	BKPL	...	0.14±0.09	0.71±0.17	-0.02±0.31	...	
990510(2)	Jet-Break	92.64-2000.0	BKPL	...	0.03±0.09	0.56±0.17	-0.01±0.31	...	
990712(0)	Global	15.25-2990.0	BKPL	0.09±0.11	0.63±0.18
990712(1)	Normal-Decay	15.25-410.3	BKPL	0.07±0.11	0.59±0.18
990712(2)	SN-Bump	410.3-2990.0	BKPL	0.21±0.11	0.81±0.18
000301C(0)	Global	116.76-392.5	0.28±0.19	0.11±0.17	0.23±0.15	0.27±0.18	0.41±0.15
000301C(1)	Energy-Break	116.76-170.1	BKPL	...	0.33±0.19	0.11±0.17	0.21±0.15	0.29±0.18	0.40±0.15
000301C(2)	Flare	170.12-239.7	BKPL	...	0.26±0.19	0.11±0.17	0.23±0.15	0.21±0.18	0.43±0.15
000301C(3)	Normal-Decay	239.7-992.5	BKPL	...	0.27±0.19	0.11±0.17	0.24±0.15	0.31±0.18	0.40±0.15
000926(0)	Global	74.48-505.2	0.70±0.17	0.36±0.15	2.90±0.39	...	1.10±0.17
000926(1)	Normal-Decay	74.48-179.3	BKPL	...	0.64±0.17	0.38±0.15	3.06±0.39	...	1.10±0.17
000926(2)	Jet-Break	179.28-505.2	BKPL	...	0.78±0.17	0.34±0.15	2.68±0.39	...	1.10±0.17
021004(0)	Global	2.09-4550.0	0.20±0.08	0.17±0.12	...	0.04±0.19
021004(1)	Energy-Break	2.09-10.6	BKPL	0.15±0.08	0.14±0.12	...	0.25±0.19
021004(2)	Flare	10.64-350.0	BKPL	0.20±0.08	0.16±0.12	...	0.03±0.19
021004(3)	Normal-Decay	350.0-4550.0	BKPL	0.21±0.08	0.25±0.12	...	0.06±0.19
030226(0)	Global	16.14-353.7	0.74±0.12	0.02±0.12	0.41±0.17	...	0.13±0.11
030226(1)	Normal-Decay	16.14-87.5	BKPL	...	0.78±0.12	0.02±0.12	0.44±0.17	...	0.16±0.11
030226(2)	Jet-Break	87.53-353.7	BKPL	...	0.68±0.12	0.03±0.12	0.38±0.17	...	0.10±0.11
030328(0)	Global	4.9-227.5	0.30±0.13	0.09±0.19	0.03±0.18	0.16±0.25
030328(1)	Energy-Break	4.9-21.1	BKPL	...	0.29±0.13	0.09±0.19	-0.04±0.18	0.34±0.25
030328(2)	Normal-Decay	21.05-227.5	BKPL	...	0.30±0.13	0.10±0.19	0.04±0.18	0.14±0.25
030329(0)	Global	11.17-2286.0	0.08±0.07	0.10±0.06	0.25±0.19
030329(1)	Energy-Break	4.52-28.6	BKPL	...	0.23±0.07	-0.04±0.06	0.19±0.19
030329(2)	Normal-Decay	28.55-106.8	BKPL	...	0.13±0.07	0.00±0.06	0.23±0.19
030329(3)	Re-Bump	106.8-2860.0	BKPL	...	0.02±0.07	0.18±0.06	0.27±0.19
050525A(0)	Global	0.07-200.0	...	0.24±0.31	-0.41±0.31	0.69±0.31	-0.22±0.34	-0.24±0.29	0.19±0.10
050525A(1)	Normal-Decay	0.07-3.0	BKPL	0.15±0.31	-0.37±0.31	0.62±0.31	-0.27±0.34	-0.05±0.29	0.19±0.10
050525A(2)	Jet-Break	3.0-200.0	BKPL	0.33±0.31	-0.45±0.31	0.78±0.31	-0.15±0.34	-0.47±0.29	0.19±0.10
050801(0)	Global	0.03-107.3	...	1.42±0.46	-0.42±0.36	0.69±0.21	-0.14±0.13	-0.02±0.13	-0.32±0.23	-0.27±0.22	0.85±0.14
050801(1)	Energy-Break	0.03-0.4	BKPL	1.29±0.46	-0.49±0.36	0.82±0.21	-0.21±0.13	-0.09±0.13	-0.25±0.23	-0.34±0.22	0.85±0.14
050801(2)	Normal-Decay	0.4-107.3	BKPL	1.49±0.46	-0.38±0.36	0.60±0.21	-0.10±0.13	0.02±0.13	-0.36±0.23	-0.23±0.22	0.85±0.14
050820A(0)	Global	0.08-663.3	0.42±0.18	0.58±0.20	0.17±0.13	...	0.10±0.15

Table 3 continued on next page

COLOR EVOLUTION AND ITS PHYSICAL IMPLICATION

Table 3 (continued)

GRB	Component	Epoch	Model	Color Indices										
				(ks)	UVW2 – UVW1	UVM2 – UVM1	UVW1 – U	U – B	B – V	V – R	R – I	I – J		
050820A(1)	Onset	0.08-1.0	BKPL	0.59±0.18	0.98±0.20	0.08±0.13	...	0.15±0.15	
050820A(2)	Normal-Decay	1.0-8.9	BKPL	0.61±0.18	0.75±0.20	0.20±0.13	...	0.14±0.15	
050820A(3)	Re-Bump	8.9-663.3	BKPL	0.39±0.18	0.53±0.20	0.17±0.13	...	0.10±0.15	
050922C(0)	Global	0.14-606.0	0.08±0.23	0.15±0.25	0.14±0.25	0.21±0.17	
050922C(1)	Energy-Break	0.14-8.5	BKPL	0.14±0.23	0.18±0.25	0.12±0.25	0.19±0.17	
050922C(2)	Normal-Decay	8.51-606.0	BKPL	-0.14±0.23	0.04±0.25	0.21±0.25	0.27±0.17	
051111(0)	Global	0.03-89.7	0.30±0.13	0.21±0.23	0.20±0.23	0.23±0.23	
051111(1)	Normal-Decay	0.03-2.69	BKPL	0.30±0.13	0.22±0.23	0.18±0.23	0.25±0.23	
051111(2)	Jet-Break	2.69-89.7	BKPL	0.30±0.13	0.18±0.23	0.25±0.23	0.27±0.23	
060218(0)	Global	0.26-287.0	...	-0.49±0.11	0.00±0.13	1.21±0.13	0.49±0.12	-0.21±0.16	...	-0.78±0.10	...	0.06±0.30	...	
060218(1)	Late-Bump	0.26-171.9	BKPL	-0.26±0.11	-1.10±0.13	0.17±0.13	-0.28±0.12	-0.73±0.16	...	-0.84±0.10	...	-0.31±0.30	...	
060218(2)	SN-Bump	171.9-7870.0	BKPL	-0.51±0.11	0.02±0.13	1.22±0.13	0.51±0.12	-0.14±0.16	...	-0.78±0.10	...	0.06±0.30	...	
060418(0)	Global	0.08-101.4	-0.07±0.21	...	-0.05±0.16	...	0.34±0.14	...	
060418(1)	Onset	0.08-1.0	BKPL	-0.07±0.21	...	-0.14±0.16	...	0.38±0.14	...	
060418(2)	Normal-Decay	0.2-101.4	BKPL	-0.07±0.21	...	0.00±0.16	...	0.32±0.14	...	
060526(0)	Global	0.06-893.5	0.66±0.15	...	0.14±0.13	...	0.27±0.27	...	
060526(1)	Normal-Decay	0.06-96.6	BKPL	0.64±0.15	...	0.17±0.13	...	0.24±0.27	...	
060526(2)	Jet-Break	96.63-893.5	BKPL	0.70±0.15	...	0.09±0.13	...	0.34±0.27	...	
060607A(0)	Global	0.07-25.5	0.62±0.26	
060607A(1)	Onset	0.07-0.3	BKPL	0.67±0.26	
060607A(2)	Normal-Decay	0.3-2.8	BKPL	0.62±0.26	
060607A(3)	Flare	1.42-25.5	BKPL	...	-0.50±0.57	0.87±0.33	0.09±0.28	0.03±0.28	-0.17±0.32	-0.04±0.26	0.32±0.17	
060614(0)	Global	1.55-1280.0	...	0.39±0.64	-0.50±0.57	0.87±0.33	0.09±0.28	0.03±0.28	-0.17±0.32	-0.04±0.26	0.32±0.17	
060614(1)	Late-Bump	1.55-1280.0	BKPL	0.39±0.64	-0.50±0.57	0.87±0.33	0.09±0.28	0.03±0.28	-0.17±0.32	-0.04±0.26	0.32±0.17	
060729(0)	Global	0.12-2576.8	BKPL	0.26±0.22	-0.05±0.24	0.50±0.31	
060729(1)	Energy-Break	0.12-60.0	BKPL	0.19±0.22	-0.25±0.24	0.40±0.31	
060729(2)	Normal-Decay	50.04-2576.8	BKPL	0.29±0.22	0.06±0.24	0.55±0.31	
060908(0)	Global	0.06-34343.9	0.22±0.27	0.10±0.33	0.19±0.31	...	0.01±0.09	
060908(1)	Normal-Decay	0.06-34343.9	PL	0.22±0.27	0.10±0.33	0.19±0.31	...	0.01±0.09	
061007(0)	Global	0.03-149.7	0.14±0.26	0.67±0.26	
061007(1)	Onset	0.03-0.1	BKPL	0.15±0.26	0.69±0.26	
061007(2)	Normal-Decay	0.14-149.7	BKPL	0.14±0.26	0.67±0.26	
061126(0)	Global	0.04-1300.0	...	-0.13±0.87	0.47±0.64	0.18±0.19	-0.04±0.16	0.46±0.18	...	0.48±0.12	...	
061126(1)	Revere-Shock	0.04-1.0	BKPL	-0.13±0.87	0.47±0.64	0.33±0.19	0.03±0.16	0.32±0.18	...	0.30±0.12	...	
061126(2)	Normal-Decay	1.06-1300.0	BKPL	-0.13±0.87	0.47±0.64	0.16±0.19	-0.05±0.16	0.47±0.18	...	0.50±0.12	...	
070125(0)	Global	2.06-106.7	...	0.30±0.29	-0.40±0.29	0.77±0.20	-0.09±0.14	0.40±0.10	0.11±0.21	-0.09±0.35	...	
070125(1)	Normal-Decay	2.06-5.2	PL	0.33±0.29	-0.44±0.29	0.76±0.20	-0.09±0.14	0.40±0.10	0.11±0.21	-0.09±0.35	...	
070125(2)	Re-Bump	5.2-106.7	BKPL	0.11±0.29	-0.21±0.29	0.86±0.20	-0.06±0.14	0.40±0.10	0.11±0.21	-0.07±0.35	...	
071010A(0)	Global	0.12-3523.2	0.12±0.11	0.42±0.06	0.65±0.19	...	0.30±0.14	...
071010A(1)	Onset	0.12-1.0	BKPL	0.14±0.11	0.65±0.06	0.65±0.19	...	0.23±0.14	...
071010A(2)	Normal-Decay	1.0-36.9	BKPL	0.18±0.11	0.47±0.06	0.65±0.19	...	0.43±0.14	...
071010A(3)	Flare	36.91-3523.2	BKPL	0.05±0.11	0.30±0.06	0.65±0.19	...	0.16±0.14	...
080109(0)	Global	70.0-2780.0	1.12±0.15	0.80±0.09	0.37±0.15	...	-0.08±0.19	...

Table 3 continued on next page

Table 3 (continued)

GRB	Component	Epoch	Model	Color Indices								
				(ks)	UVW2 – UVW1	UVM2 – UVM1	UVW1 – U	U – B	B – V	V – R	R – I	I – J
080109(1)	Late-Bump	70.0-541.1	BKPL	0.71±0.15	0.63±0.09	0.26±0.15	...
080109(2)	SN-Bump	541.09-2780.0	BKPL	1.34±0.15	0.90±0.09	0.43±0.15	...
080310(0)	Global	0.08-300.0	0.34±0.11	0.23±0.10	...	-0.07±0.19
080310(1)	Onset	0.08-0.8	BKPL	0.26±0.11	0.15±0.10	...	0.24±0.15
080310(2)	Normal-Decay	0.74-2.0	BKPL	0.36±0.11	0.11±0.10	...	0.29±0.15
080310(3)	Re-Bump	2.0-300.0	BKPL	0.35±0.11	0.29±0.10	...	0.21±0.15
080319B(0)	Global	0.71-209.8	...	0.50±0.15	-0.63±0.15	0.78±0.14	-0.01±0.11	-0.05±0.12	0.97±0.15	0.13±0.13	0.07±0.05	0.09±0.09
080319B(1)	Revere-Shock	0.01-1.7	BKPL	0.59±0.15	-0.92±0.15	1.05±0.14	0.02±0.11	0.09±0.12	0.43±0.15	-0.12±0.13	-0.02±0.05	0.13±0.09
080319B(2)	Normal-Decay	1.68-209.8	BKPL	0.48±0.15	-0.55±0.15	0.73±0.14	0.01±0.11	-0.09±0.12	-0.05±0.15	0.22±0.13	0.12±0.05	0.06±0.09
080330(0)	Global	0.09-116.6	1.65±0.34	-0.28±0.26	-0.04±0.29	0.17±0.28	-0.34±0.14
080330(1)	Onset	0.09-0.46	BKPL	...	1.64±0.34	-0.25±0.26	-0.11±0.29	0.29±0.28	-0.34±0.14
080330(2)	Normal-Decay	0.46-116.6	BKPL	...	1.66±0.34	-0.29±0.26	-0.01±0.29	0.12±0.28	-0.34±0.14
080603A(0)	Global	0.11-350.4	0.39±0.45	1.50±0.42	...	0.30±0.23
080603A(1)	Onset	0.11-2.0	BKPL	0.91±0.45	1.53±0.42	...	0.17±0.23
080603A(2)	Normal-Decay	2.0-350.4	BKPL	0.25±0.45	1.50±0.42	...	0.34±0.23
080607(0)	Global	0.04-7.5	1.82±0.29	...	1.32±0.14
080607(1)	Onset	0.04-0.2	BKPL	1.56±0.29	...	1.04±0.14
080607(2)	Normal-Decay	0.2-1.0	BKPL	1.95±0.29	...	1.53±0.14
080607(3)	Re-Bump	1.0-7.5	BKPL	1.92±0.29	...	1.28±0.14
080810(0)	Global	0.04-497.9	0.38±0.29	0.45±0.19	0.45±0.19	0.19±0.14
080810(1)	Onset	0.04-0.3	BKPL	0.32±0.29	0.54±0.19	0.21±0.14
080810(2)	Normal-Decay	0.3-497.9	BKPL	0.39±0.29	0.45±0.19	0.19±0.14
090102(0)	Global	0.04-264.6	0.66±0.09
090102(1)	Onset	0.04-0.1	BKPL	0.48±0.09
090102(2)	Normal-Decay	0.1-2.3	BKPL	0.75±0.09
090102(3)	Re-Bump	2.28-264.6	BKPL	0.71±0.09
090618(0)	Global	0.12-185.5	BKPL	0.00±0.40	-0.17±0.45	1.28±0.37	-0.34±0.14	0.21±0.20	-0.20±0.17
090618(1)	Energy-Break	0.12-10.0	BKPL	0.12±0.40	-0.17±0.45	1.16±0.37	-0.46±0.14	0.31±0.20	-0.10±0.17
090618(2)	Normal-Decay	10.0-155.5	BKPL	-0.01±0.40	-0.17±0.45	1.29±0.37	-0.32±0.14	0.20±0.20	-0.21±0.17
091024(0)	Global	0.1-246.0	-0.44±0.26	-0.40±0.22	-0.43±0.13	...
091024(1)	Onset	0.1-1.2	BKPL	-0.38±0.26	-0.43±0.22	-0.40±0.13	...
091024(2)	Normal-Decay	1.41-5.0	BKPL	-0.78±0.26	-0.14±0.22	-0.45±0.13	...
091024(3)	Re-Bump	5.0-246.0	BKPL	-0.19±0.26	-0.07±0.22	-0.51±0.13
110205A(0)	Global	0.54-384.2	0.19±0.23
110205A(1)	Onset	0.54-2.0	BKPL	0.19±0.23
110205A(2)	Normal-Decay	2.0-384.2	BKPL	0.19±0.23
110213A(0)	Global	0.16-384.2	-0.37±0.08	-0.18±0.08
110213A(1)	Onset	0.16-0.7	BKPL
110213A(2)	Normal-Decay	0.3-2.0	BKPL	-0.51±0.08	-0.55±0.08
110213A(3)	Re-Bump	2.0-384.2	BKPL	-0.30±0.08	0.00±0.08	0.47±0.14
120119A(0)	Global	0.04-26.9	BKPL	0.37±0.27	0.55±0.14	...	0.11±0.12
120119A(1)	Normal-Decay	0.04-0.3	BKPL	0.31±0.27	0.44±0.14	...	0.15±0.12
120119A(2)	Re-Bump	0.3-26.9	BKPL	0.39±0.27	0.44±0.12	...	0.10±0.12

Table 3 continued on next page

Table 3 (*continued*)

GRB	Component	Epoch	Model	Color Indices								
				UVW2 – UVW1	UVM2 – UVM1	UVW2 – UVW1	U – B	B – V	V – R	R – I	I – J	J – H
120404A(0)	Global	0.25-257.3	1.10±0.31	0.54±0.28	0.61±0.22	...
120404A(1)	Onset	0.25-2.9	BKPL	1.46±0.31	0.18±0.28	0.61±0.22	...
120404A(2)	Normal-Decay	2.87-257.3	BKPL	0.93±0.31	0.70±0.28	0.61±0.22	...
120422A(0)	Global	407.1-2650.0	BKPL	-1.26±0.26	1.46±0.20
120422A(1)	Onset	0.35-2.0	BKPL	-1.24±0.26	1.45±0.20
120422A(2)	Normal-Decay	2.0-407.1	BKPL	-1.55±0.26	1.39±0.20
120422A(3)	SN-Bump	407.1-2650.0	BKPL	-1.26±0.26	1.46±0.20
120729A(0)	Global	0.29-65.5	0.24±0.37
120729A(1)	Energy-Break	0.29-2.0	BKPL	0.14±0.37
120729A(2)	Normal-Decay	2.0-65.5	BKPL	0.29±0.37
130215A(0)	Global	0.7-1517.9
130215A(1)	Normal-Decay	0.7-500.0	PL	-0.02±0.29
130215A(2)	SN-Bump	499.96-1517.9	BKPL	-0.06±0.29
130702A(0)	Global	15.11-54600.0	1.20±0.17	-0.62±0.12	0.93±0.29
130702A(1)	Normal-Decay	15.11-362.0	PL	0.54±0.17	-0.54±0.12
130702A(2)	SN-Bump	362.02-54600.0	BKPL	1.30±0.17	-0.63±0.12	-0.40±0.18
130831A(0)	Global	33.76-13500.0	BKPL	-0.18±1.13	0.27±2.82	1.31±2.92	-0.42±1.04	0.25±0.57	-0.21±0.41	0.74±0.79
130831A(1)	Onset	0.13-1.0	BKPL	0.40±1.13	-0.15±2.82	1.97±2.92	-0.71±1.04	0.34±0.57	1.35±0.41	0.24±0.79
130831A(2)	Normal-Decay	1.0-800.0	BKPL	0.09±1.13	0.01±2.82	1.05±2.92	0.13±1.04	0.23±0.57	0.17±0.41	0.25±0.79
130831A(3)	SN-Bump	800.0-13500.0	BKPL	-0.31±1.13	0.60±2.82	1.29±2.92	-0.77±1.04	0.33±0.57	-0.52±0.41	1.39±0.79

Table 4. Statistics of Color Indices

Color	Range (Total)	Mean	Correlation	β_o^{CI}	β_o^{CI}
		(Gaussian Fitting)	(CI- β_o)	(CI=Mean)	(CI=0.2)
Data Set I/Golden/Color Indices ^a					
g-r	(-0.29,2.51)	0.15±0.14	0.30 β_o	0.50±0.47	0.67
r-i	(-1.01,1.04)	0.09±0.10	0.21 β_o	0.43±0.48	0.95
i-z	(-2.10,1.44)	0.13±0.11	0.19 β_o	0.68±0.58	1.05
J-H	(-0.68,1.03)	0.23±0.10	0.30 β_o	0.77±0.33	0.67
H-Ks	(-0.42,3.00)	0.25±0.17	0.32 β_o	0.78±0.53	0.63
Data Set I/Silver/Color Indices ^a					
UVW2-UVM2	(-0.88,1.65)	0.16±0.27	0.16 β_o	1.00±1.69	1.25
UVM2-UVW1	(-1.26,0.72)	-0.19±0.24	0.16 β_o	-1.19±1.50	1.25
UVW1-U	(-0.11,3.02)	0.93±0.39	0.41 β_o	2.27±0.95	0.49
U-B	(-1.83,2.65)	0.09±0.23	0.20 β_o	0.45±1.15	1.00
B-V	(-1.50,2.14)	0.23±0.23	0.24 β_o	0.96±0.96	0.83
V-R	(-1.23,2.9)	0.15±0.16	0.26 β_o	0.58±0.62	0.77
R-I	(-0.82,2.85)	0.22±0.07	0.28 β_o	0.79±0.25	0.71
I-J	(-1.86,3.15)	0.17±0.08	0.36 β_o	0.47±0.22	0.56
J-H	(-0.63,2.11)	0.28±0.14	0.30 β_o	0.93±0.47	0.67
H-K	(-0.47,1.61)	0.13±0.22	0.32 β_o	0.41±0.69	0.63

^aStatistics of color indices regardless of GRBs and components.

Table 5. Constant versus Variable Color Indices

GRB/Color/Component	Number/Fraction	Number/Fraction	Number (Total)
	(Constant)	(Variation)	
Data Set I/Golden/Color Indices ^a			
g-r	1135/94.9%	61/5.1%	1196
r-i	1135/95.9%	48/4.1%	1183
i-z	984/96.3%	38/3.7%	1022
J-H	408/96.7%	14/3.3%	422
H-K	377/96.9%	12/3.1%	389
Total Colors	4039/95.9%	173/4.1%	4212
Data Set I/Golden/Components ^b			
Onset	172/92.5%	14/7.5%	186
Normal-Decay	1924/97.8%	43/2.2%	1967
Flare	36/87.8%	5/12.2%	41
Energy-Break	613/99.5%	3/0.5%	616
Jet-Break	319/91.9%	28/8.1%	347
Late-Bump	204/96.7%	7/3.3%	211
Re-Bump	668/93.0%	50/7.0%	718
SN-Bump	103/81.7%	23/18.3%	126
Total Components	4039/95.9%	173/4.1%	4212
Data Set I/Golden/GRBs ^c			
071025	78/100.0%	0/0.0%	78
071031	268/94.0%	17/6.0%	285
080413B	147/96.1%	6/3.9%	153
080710	249/91.9%	22/8.1%	271
081007	50/100.0%	0/0.0%	50
081008	95/96.9%	3/3.1%	98
081029	357/98.3%	6/1.7%	363
090426	44/95.7%	2/4.3%	46
090510	49/100.0%	0/0.0%	49
090926A	244/97.2%	7/2.8%	251
091018	205/99.0%	2/1.0%	207
091029	125/96.9%	4/3.1%	129
091127	450/96.8%	15/3.2%	465
100316D	52/81.3%	12/18.8%	64
100621A	56/93.3%	4/6.7%	60
100814A	505/92.0%	44/8.0%	549
101219B	54/91.5%	5/8.5%	59
110918A	50/94.3%	3/5.7%	53
111209A	208/98.1%	4/1.9%	212
120711A	117/97.5%	3/2.5%	120
120815A	93/96.9%	3/3.1%	96
121024A	30/100.0%	0/0.0%	30
121217A	86/97.7%	2/2.3%	88
130427A	380/97.7%	9/2.3%	389
130925A	47/100.0%	0/0.0%	47

Table 5 continued on next page

Table 5 (*continued*)

GRB/Color/Component	Number/Fraction	Number/Fraction	Number (Total)
	(Constant)	(Variation)	
Total GRBs	4039/95.9%	173/4.1%	4212
Data Set II/Golden+Silver+Pair Components ^b			
Onset-to-Normal	63/92.6%	5/7.4%	68
Reverse-to-Normal	11/68.8%	5/31.3%	16
Energy-to-Normal	40/95.2%	2/4.8%	42
Flare-to-Normal	10/83.3%	2/16.7%	12
Normal-to-Flare	4/80.0%	1/20.0%	5
Energy-to-Flare	6/75.0%	2/25.0%	8
Normal-to-Re	49/87.5%	7/12.5%	56
Normal-to-Jet	35/97.2%	1/2.8%	36
Late-to-Jet	4/100.0%	0/0.0%	4
Re-to-Jet	5/100.0%	0/0.0%	5
Jet-to-Re	4/100.0%	0/0.0%	4
Normal-to-SN	16/66.7%	8/33.3%	24
Late-to-SN	14/58.3%	10/41.7%	24
Jet-to-SN	2/100.0%	0/0.0%	2
Total Pari Components	263/85.9%	43/14.1%	306

^a Statistics regardless GRBs and components.

^b Statistics regardless GRBs and colors.

^c Statistics regardless colors and components.

Table 6. Results of Linear Correlation Analysis for Data Set II

Component-to-Component (Previous-to-Following)	Number (Total)	ΔCI (range)	ΔCI (Gaussian fits)	r (Spearman)	p (Spearman)
Onset-to-Normal	68	[-1.18,0.84]	-0.02±0.06	0.85	$< 10^{-4}$
Reverse-to-Normal	16	[-0.48,0.37]	-0.04±0.22	0.68	3.9×10^{-3}
Energy-to-Normal	42	[-0.28,0.31]	0.03±0.10	0.87	$< 10^{-4}$
Flare-to-Normal	12	[-1.07,0.14]	0.03±0.12	0.77	3.6×10^{-3}
Normal-to-Flare	5	[-0.27,0.00]	... ^a	0.80	$< 10^{-4}$
Energy-to-Flare	8	[-0.22,0.05]	...	0.60	0.12
Late-to-Jet	4	[-0.01,0.09]	...	1.00	$< 10^{-4}$
Normal-to-Re	56	[-0.39,1.11]	0.00±0.06	0.88	$< 10^{-4}$
Normal-to-Jet	36	[-0.42,0.22]	-0.02±0.08	0.89	$< 10^{-4}$
Re-to-Jet	5	[-0.07,0.02]	...	0.90	0.04
Jet-to-Re	4	[-0.05,0.29]	...	0.95	0.05
Normal-to-SN	24	[-0.90,1.14]	0.13±0.33	0.57	3.7×10^{-3}
Late-to-SN	24	[-0.24,1.13]	0.25±0.48	0.82	$< 10^{-4}$
Jet-to-SN	2	[0.00,0.05]
Total	306	[-1.18,1.14]	-0.01±0.04	0.86	$< 10^{-4}$

^a Small number of data points leading to unreliable fits.

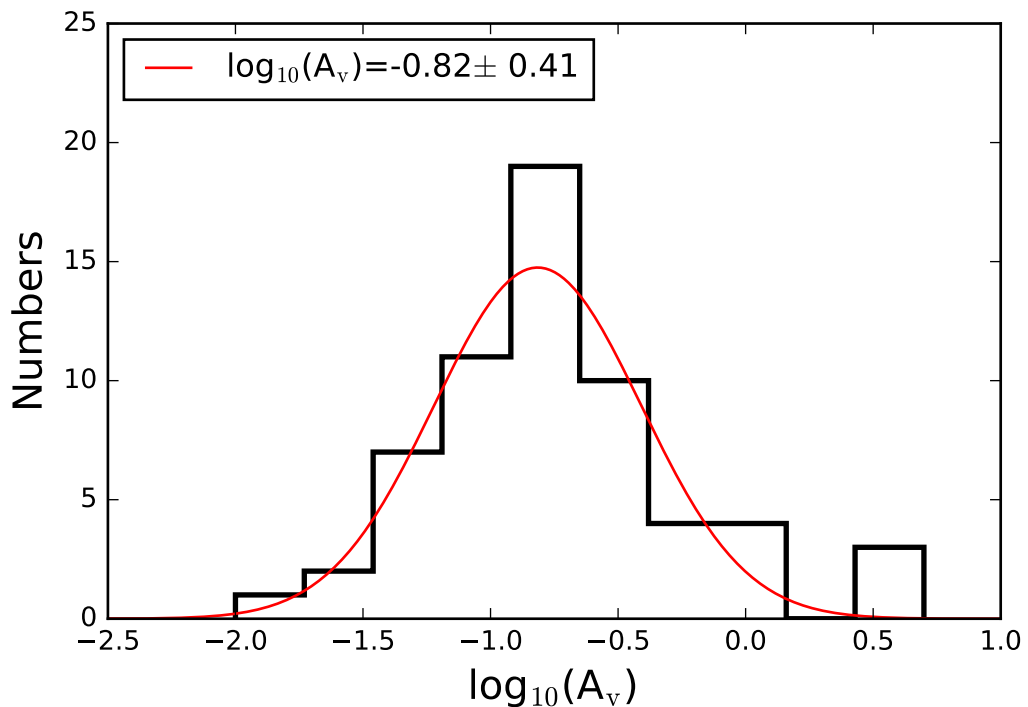


Figure 1. Distribution of the host galaxy extinction in the V band, A_v^{host} , obtained from published papers. The best Gaussian fit gives the mean A_v^{host} and the standard deviation such that $\log_{10}(A_v^{\text{host}}) = -0.82 \pm 0.41$.

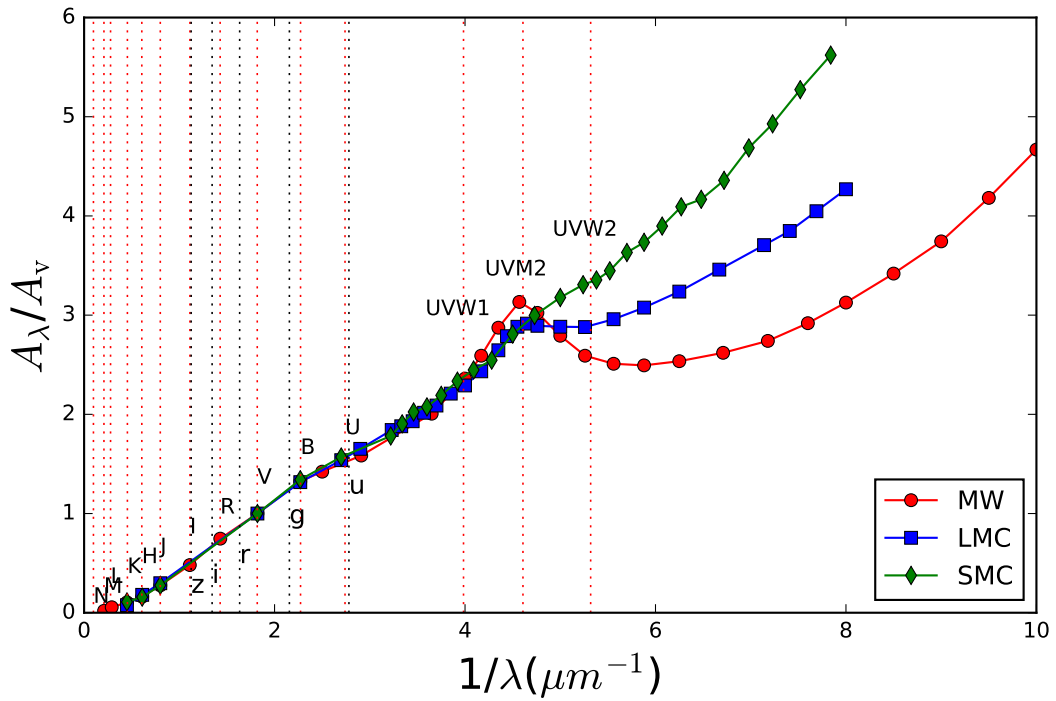


Figure 2. Dust models for the host extinction reproduced from Pei (1992). The solid lines of different colors are for different models, while the black and red dashed lines correspond to the energy bands considered in this work.

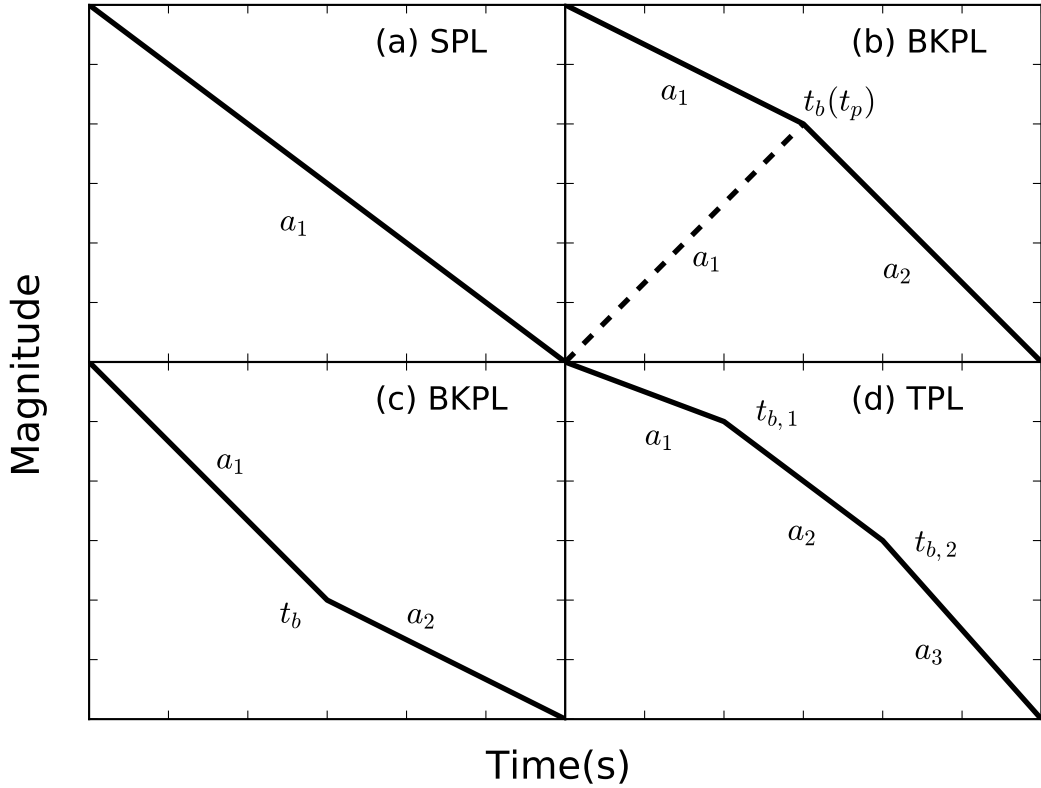


Figure 3. Cartoons of the light-curve models. From top left to bottom right, the figure presents in turn (a) a single power-law model, a smoothly broken power-law with positive ω , which can be adopted to fit (b) a break (solid line)/bump (dash line), and (c) negative ω , and (d) finally a triple power-law.

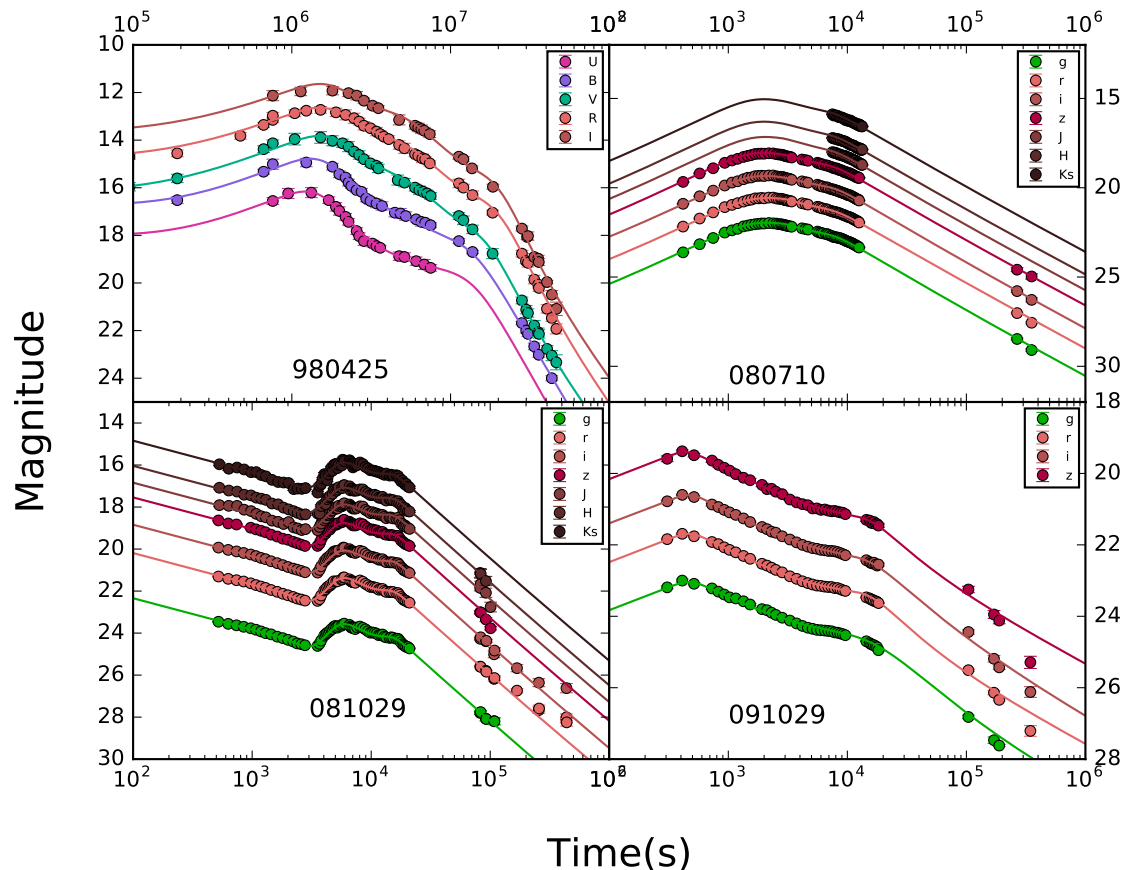


Figure 4. Some examples of the best fitting of the multiband data for the optical-afterglow light curves.

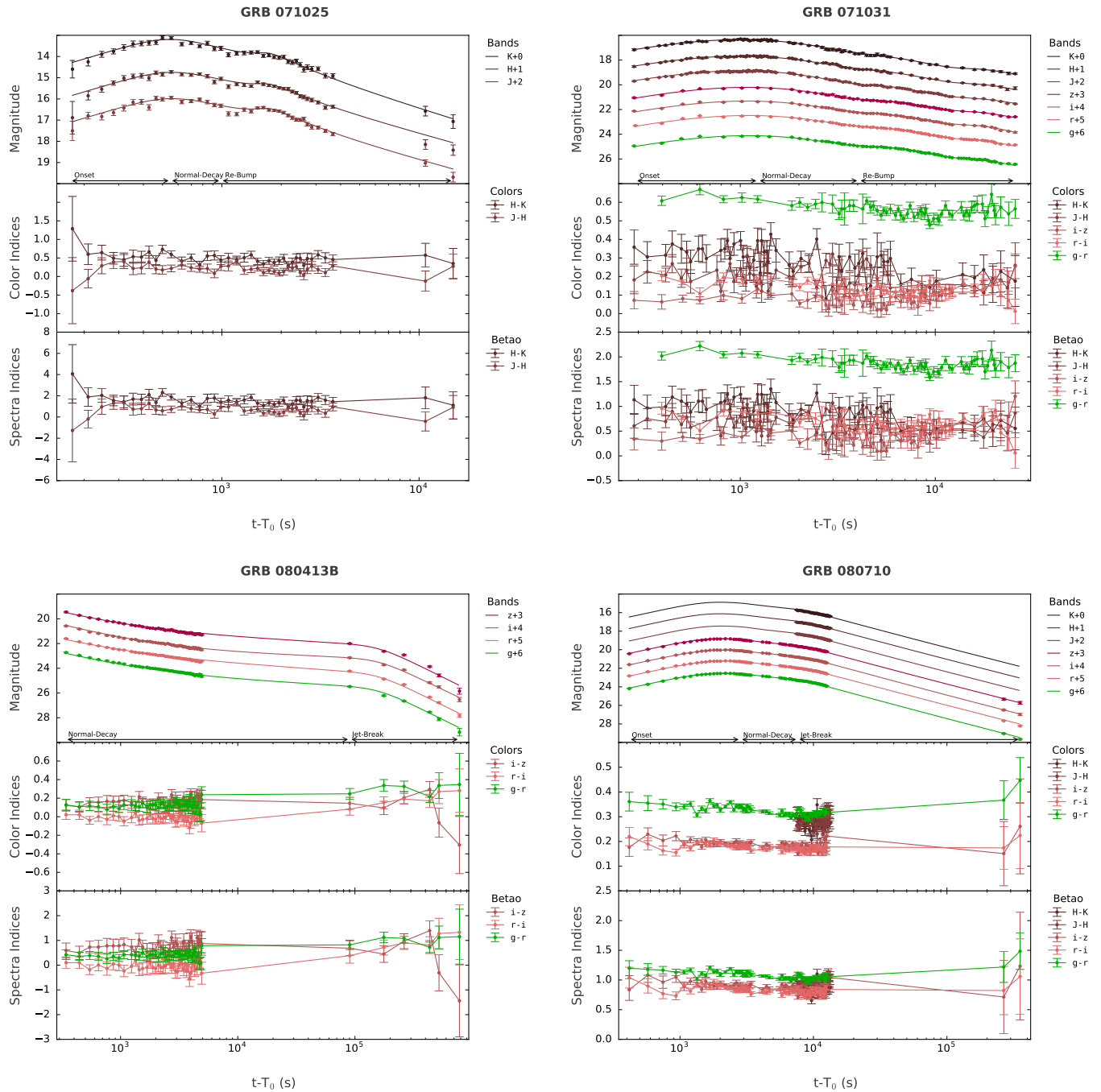


Figure 5. Best multiband optical-afterglow light-curve fits and the time evolution of color indices and spectral indices for each burst for the Golden sample, in magnitude (linear)-time (logarithmic) scale space. The spectral indices are derived from the CI- β_o correlation assuming a power-law spectral decay.

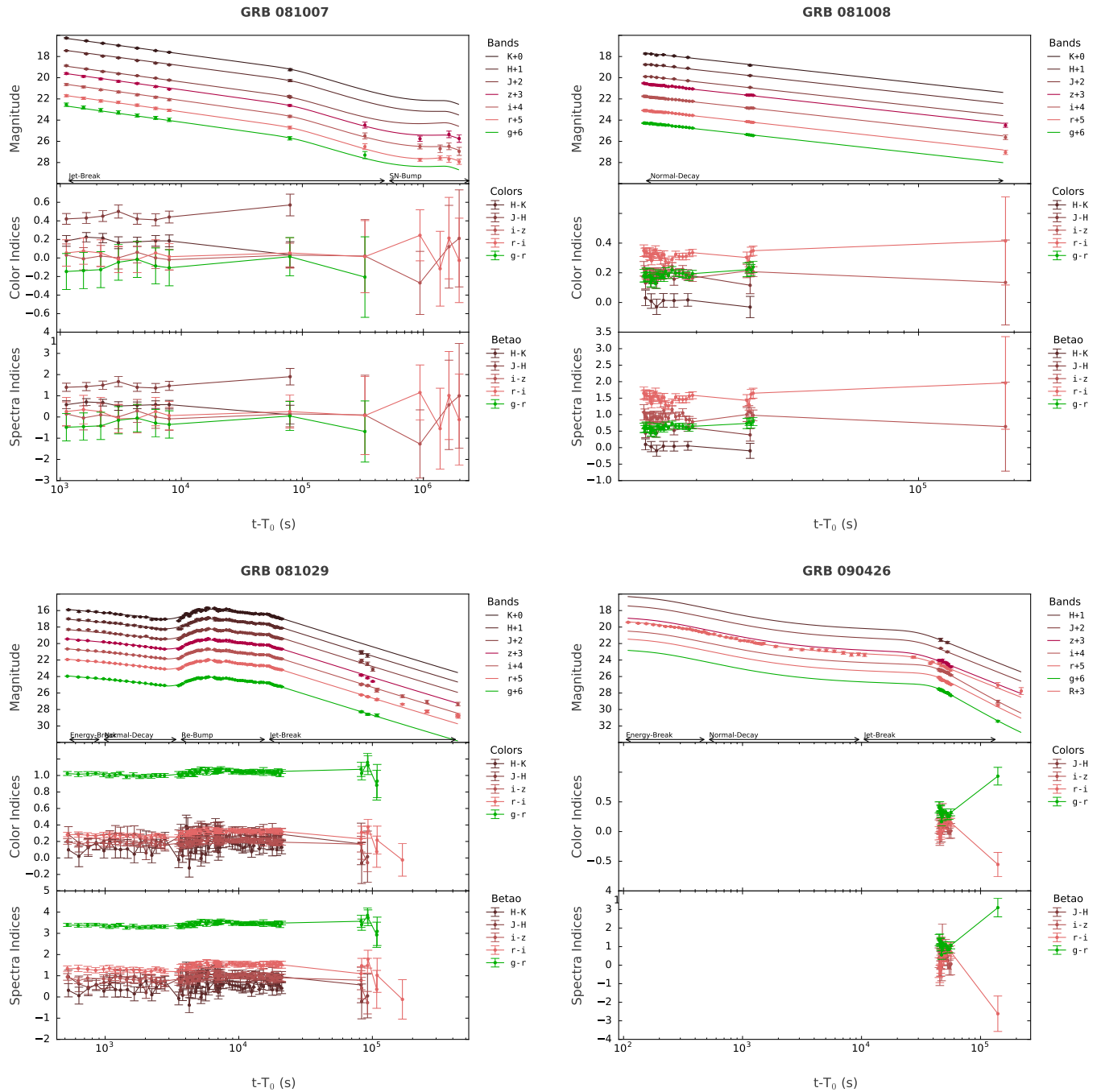


Fig. 5— Continued

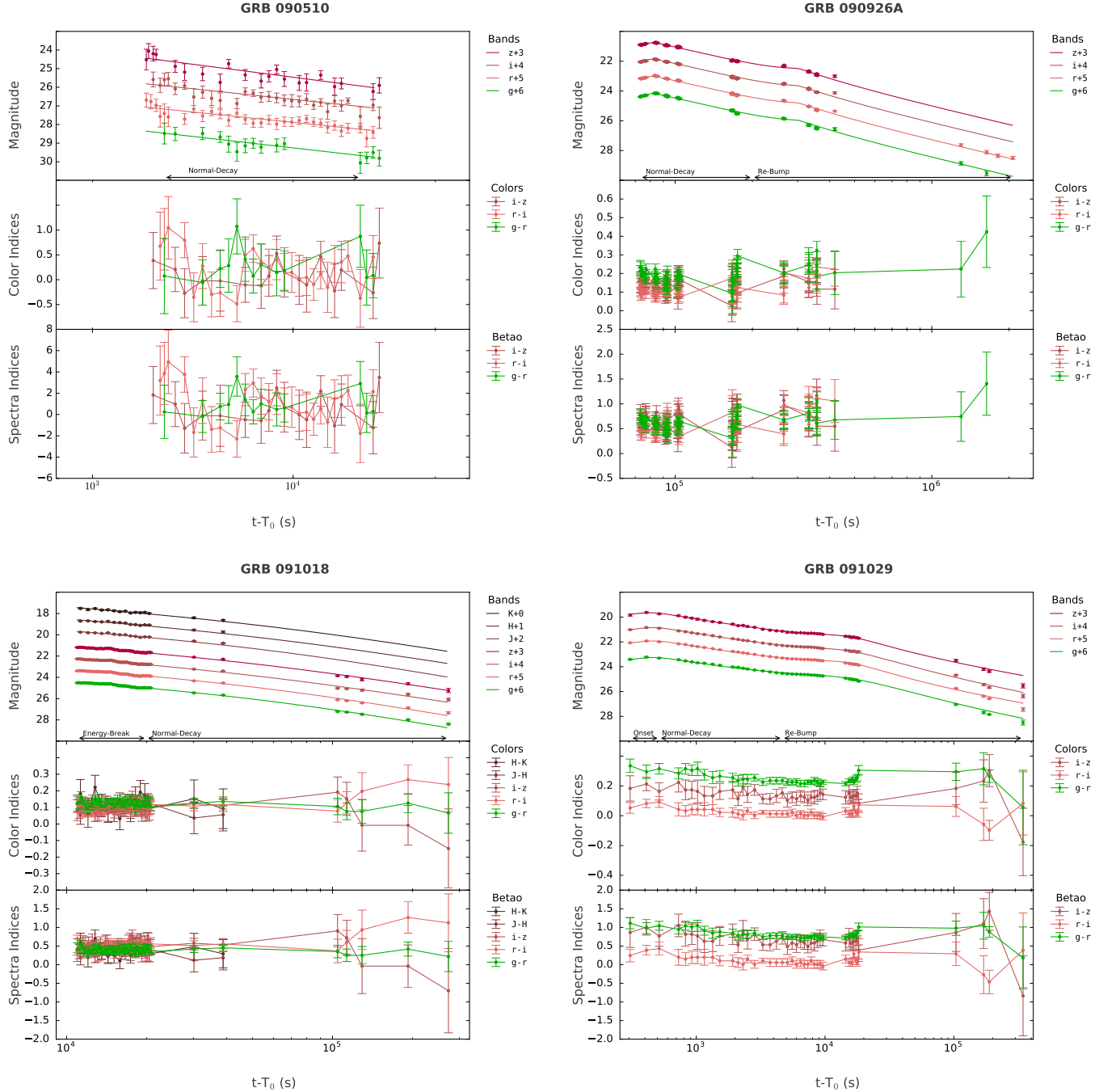


Fig. 5— Continued

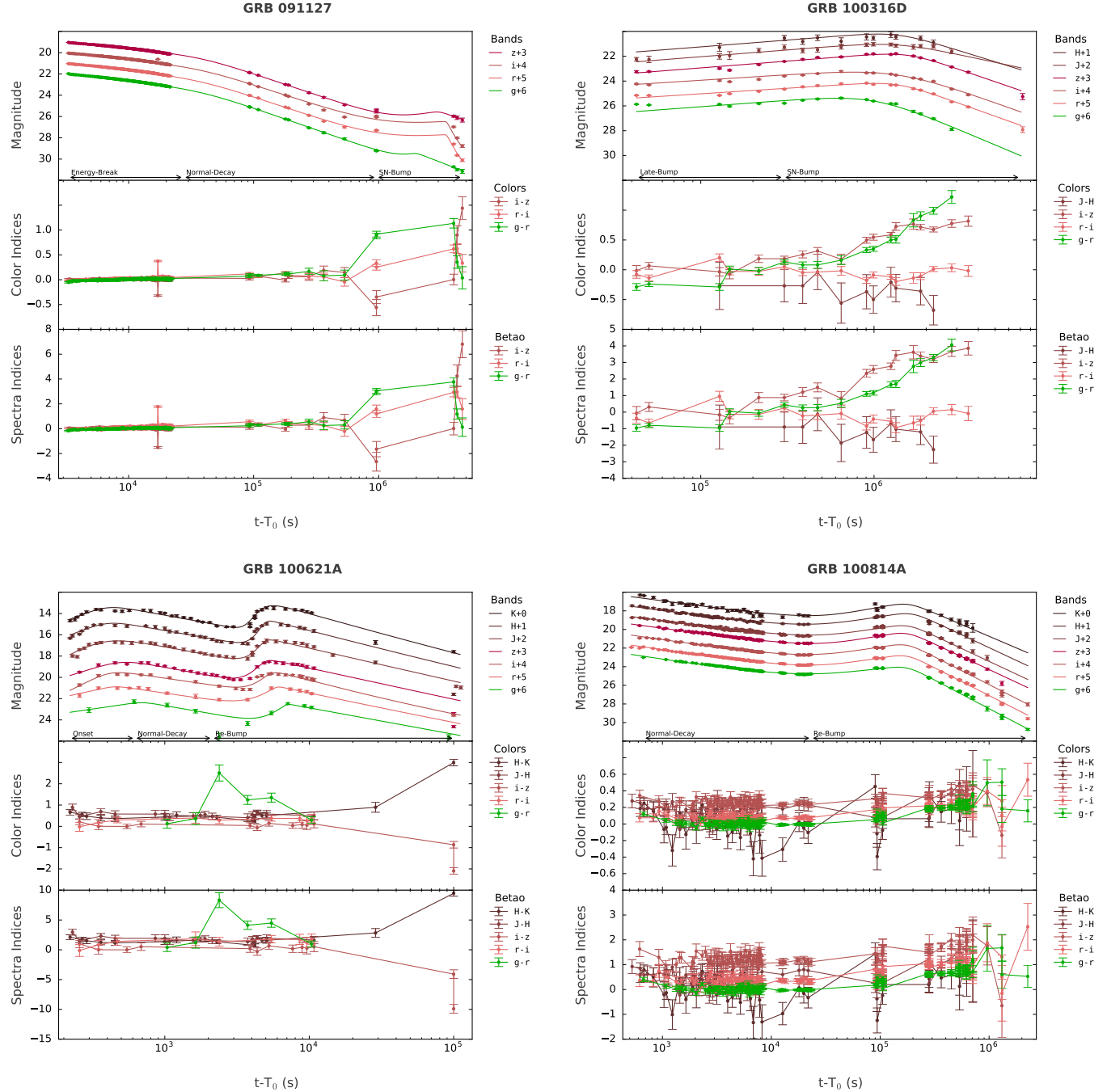


Fig. 5— Continued

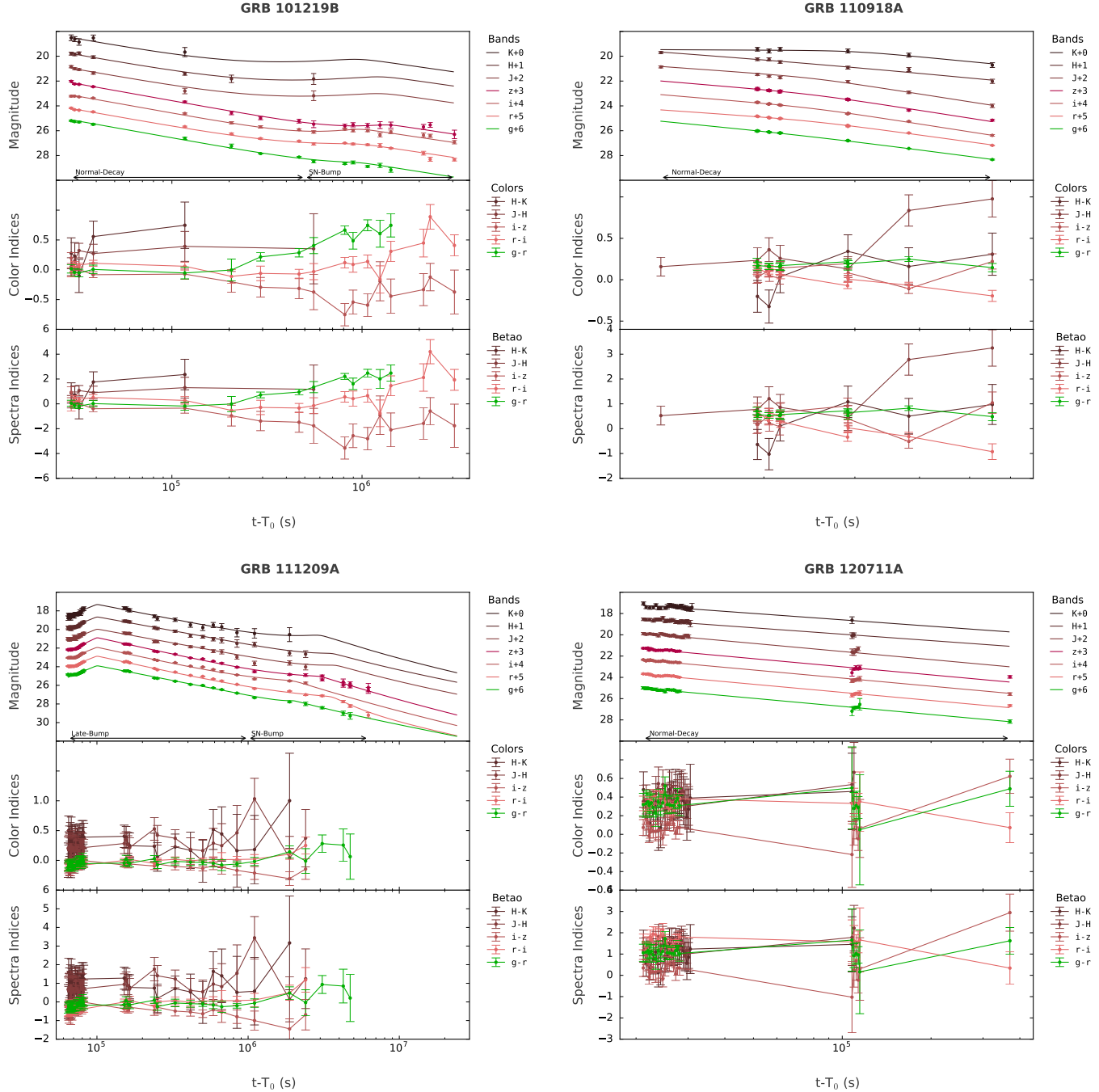


Fig. 5— Continued

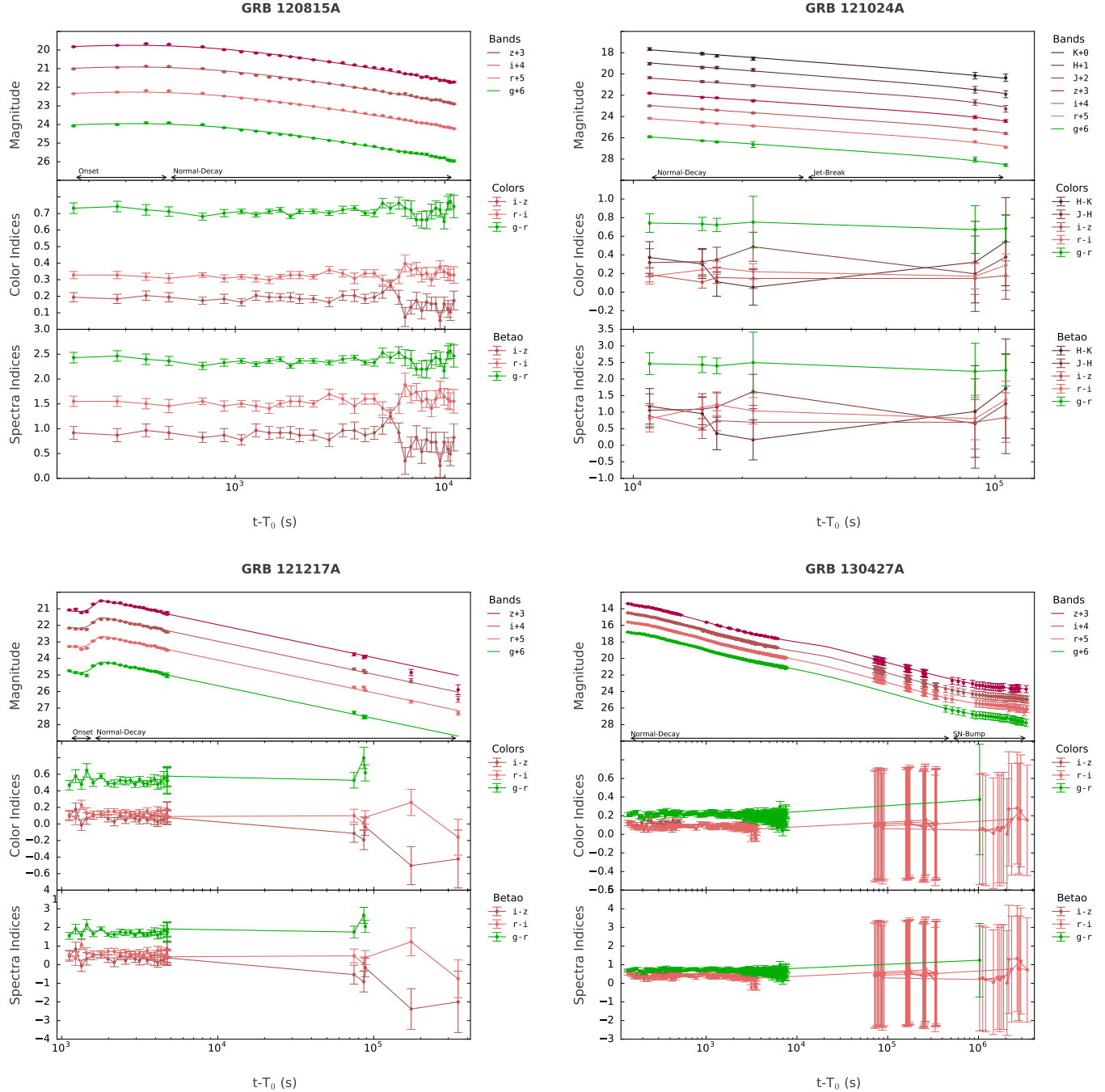


Fig. 5— Continued

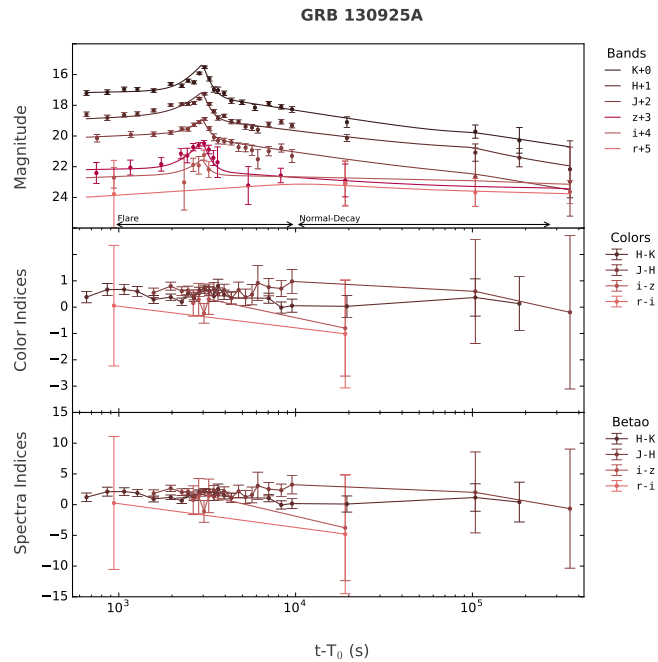


Fig. 5—Continued

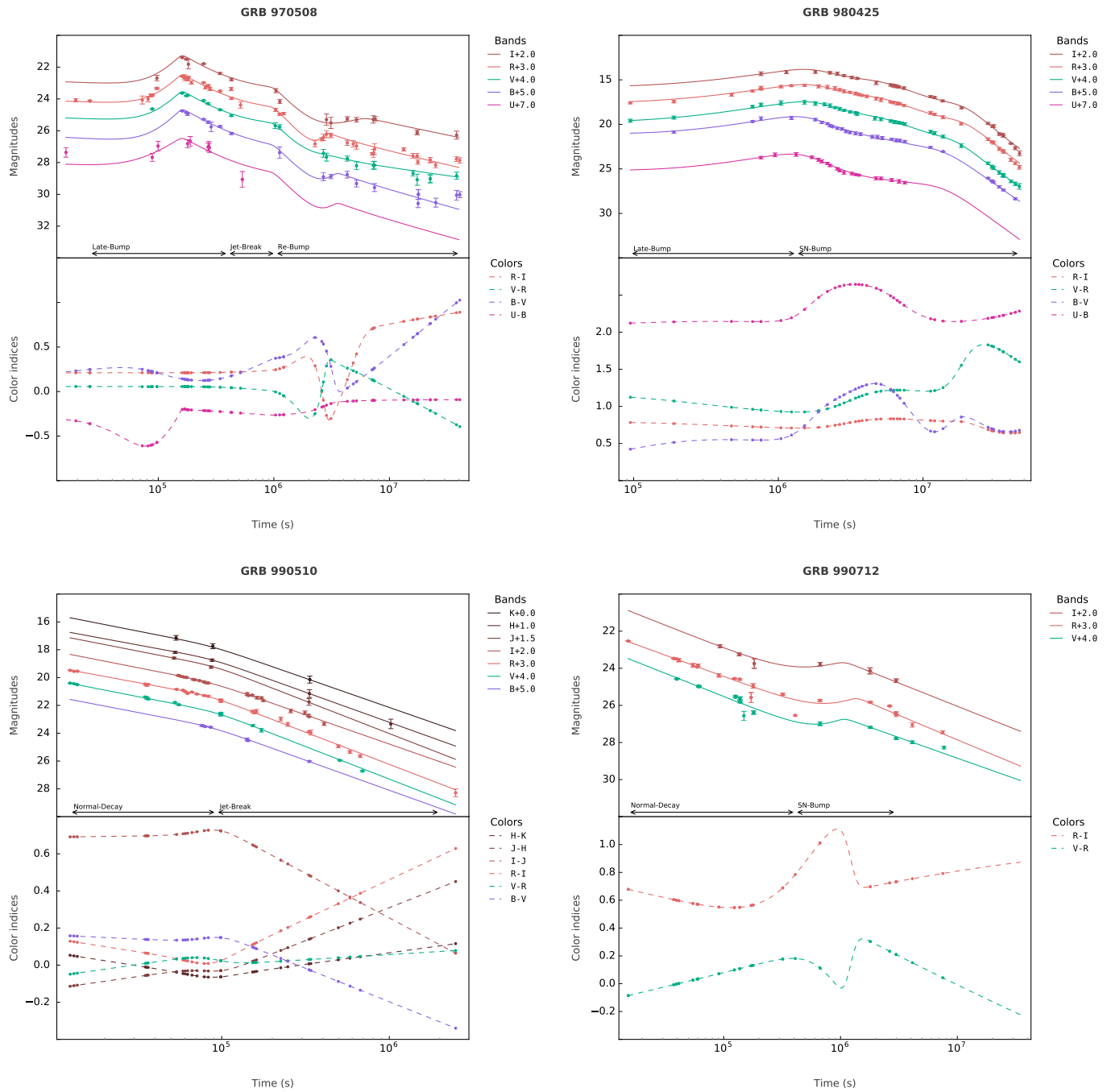


Figure 6. The symbols are the same as Figure 5, but for the Silver sample.

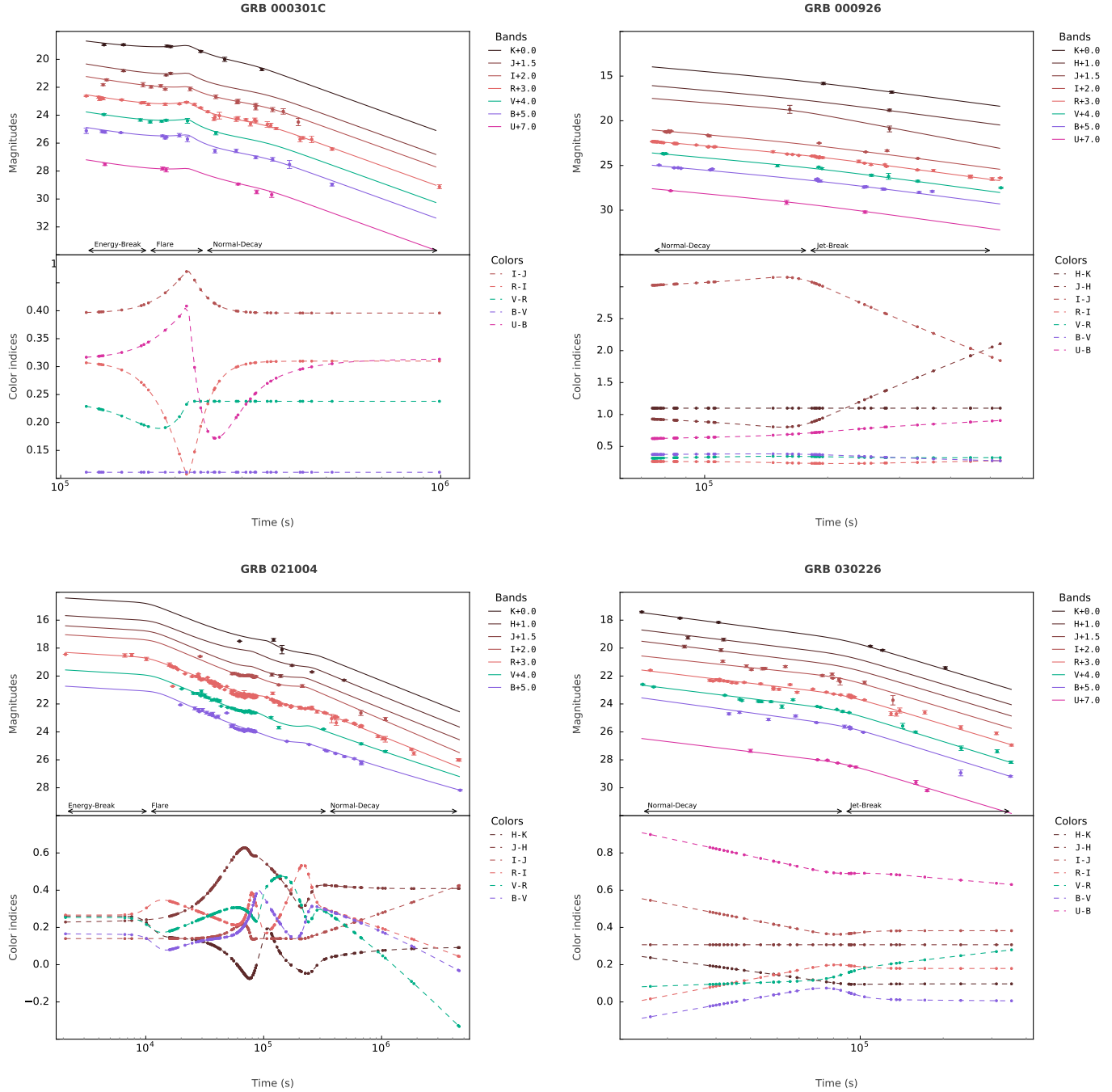


Fig. 6—Continued

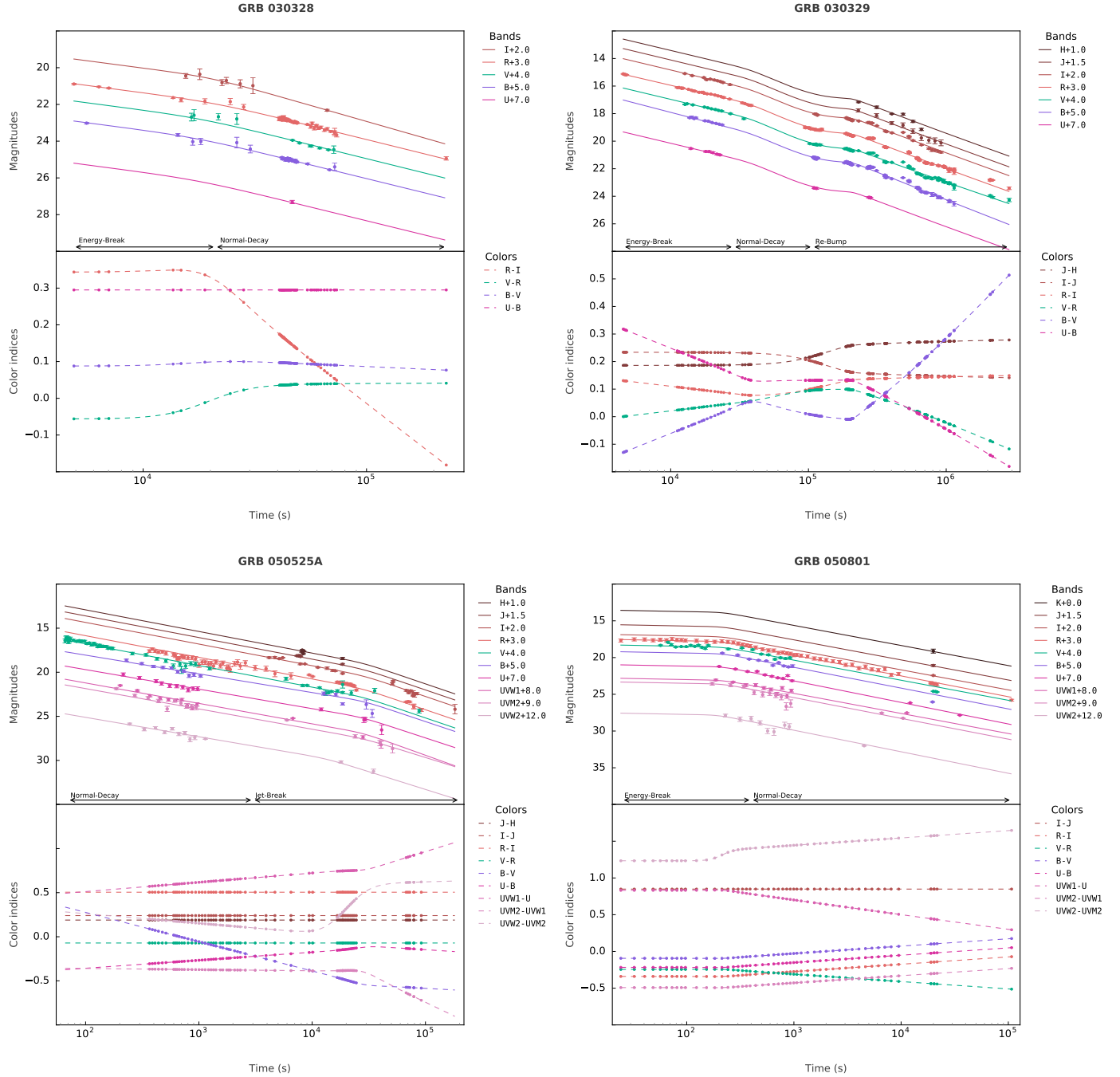


Fig. 6—Continued

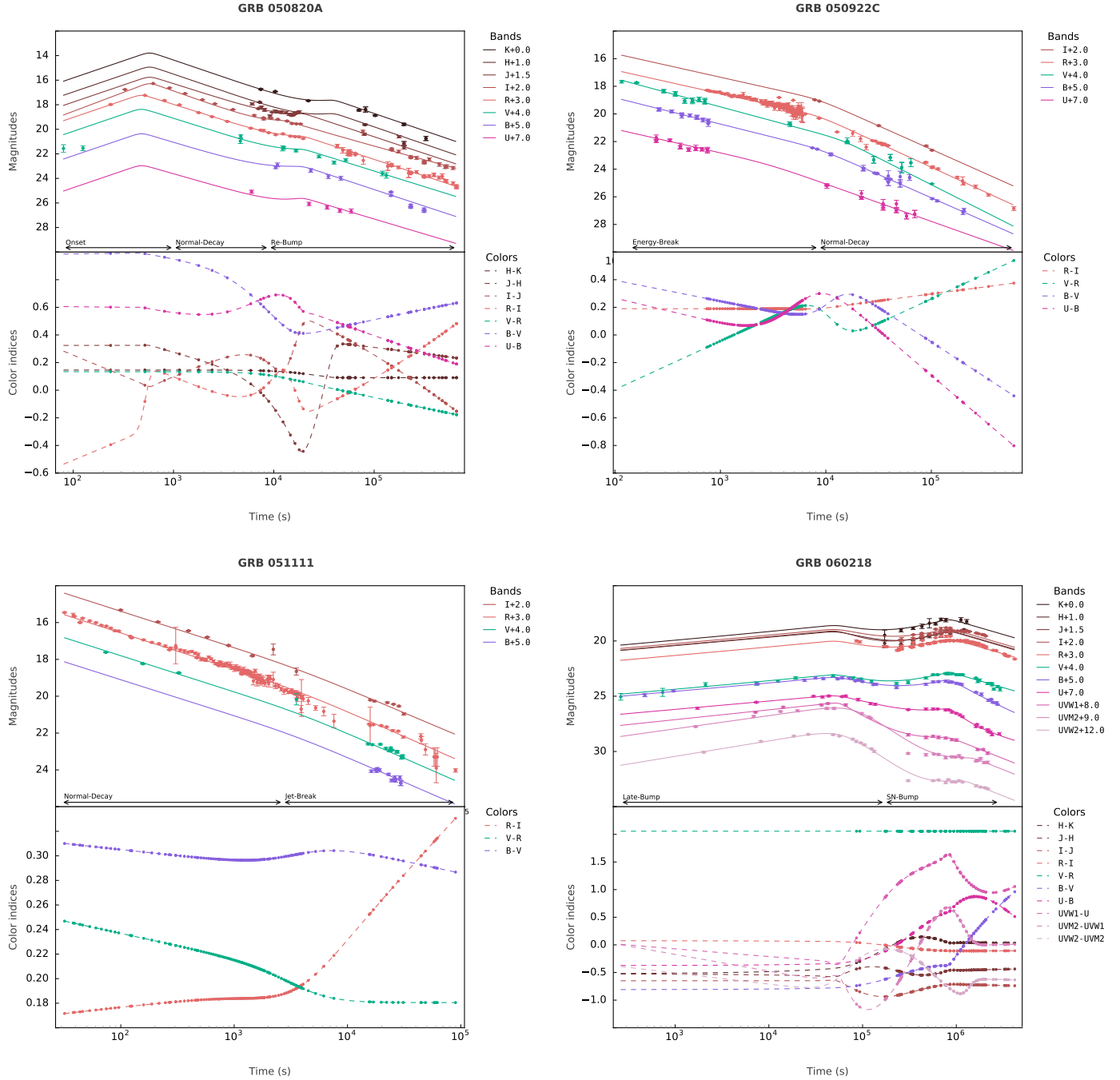


Fig. 6— Continued

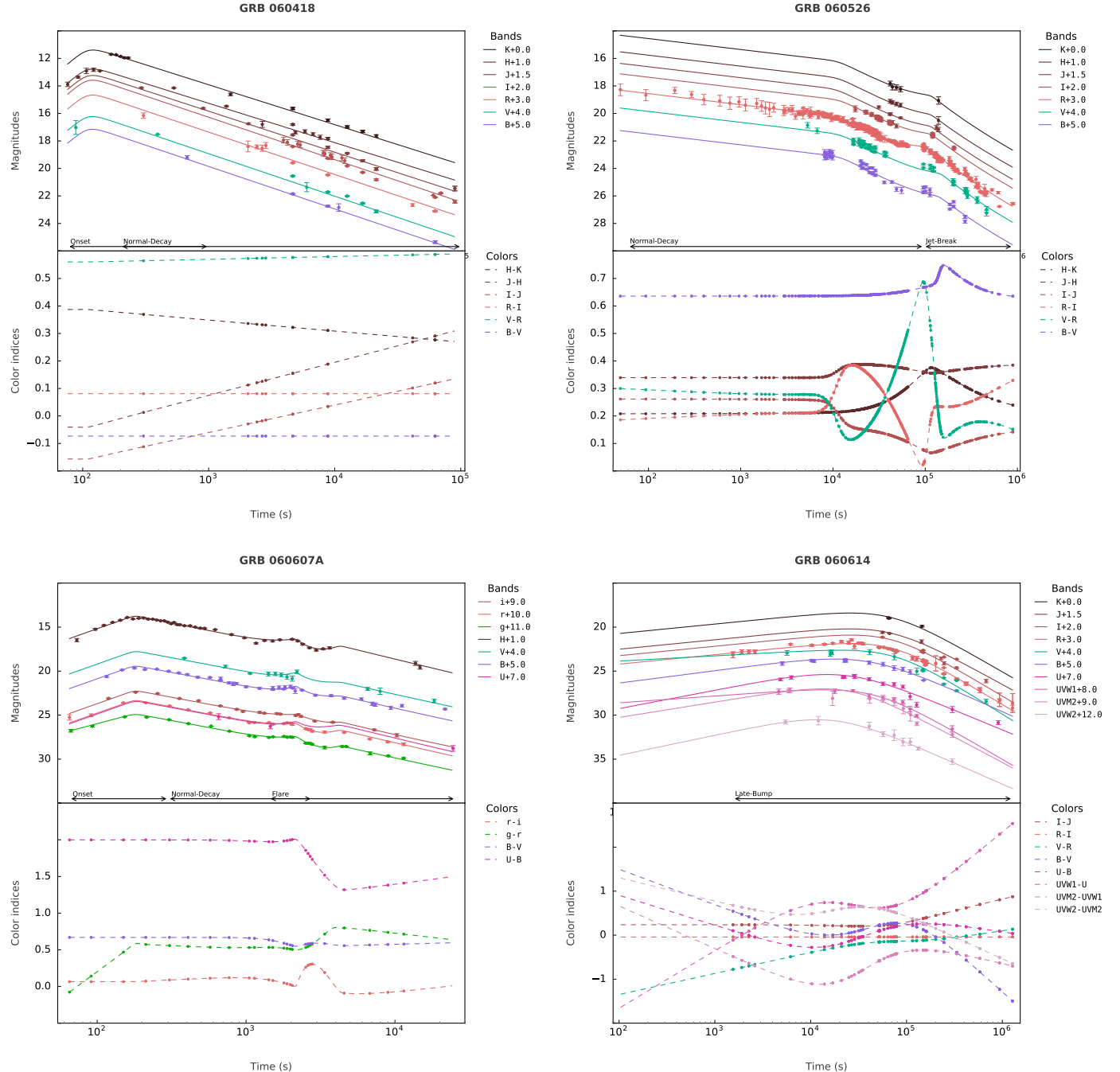


Fig. 6— Continued

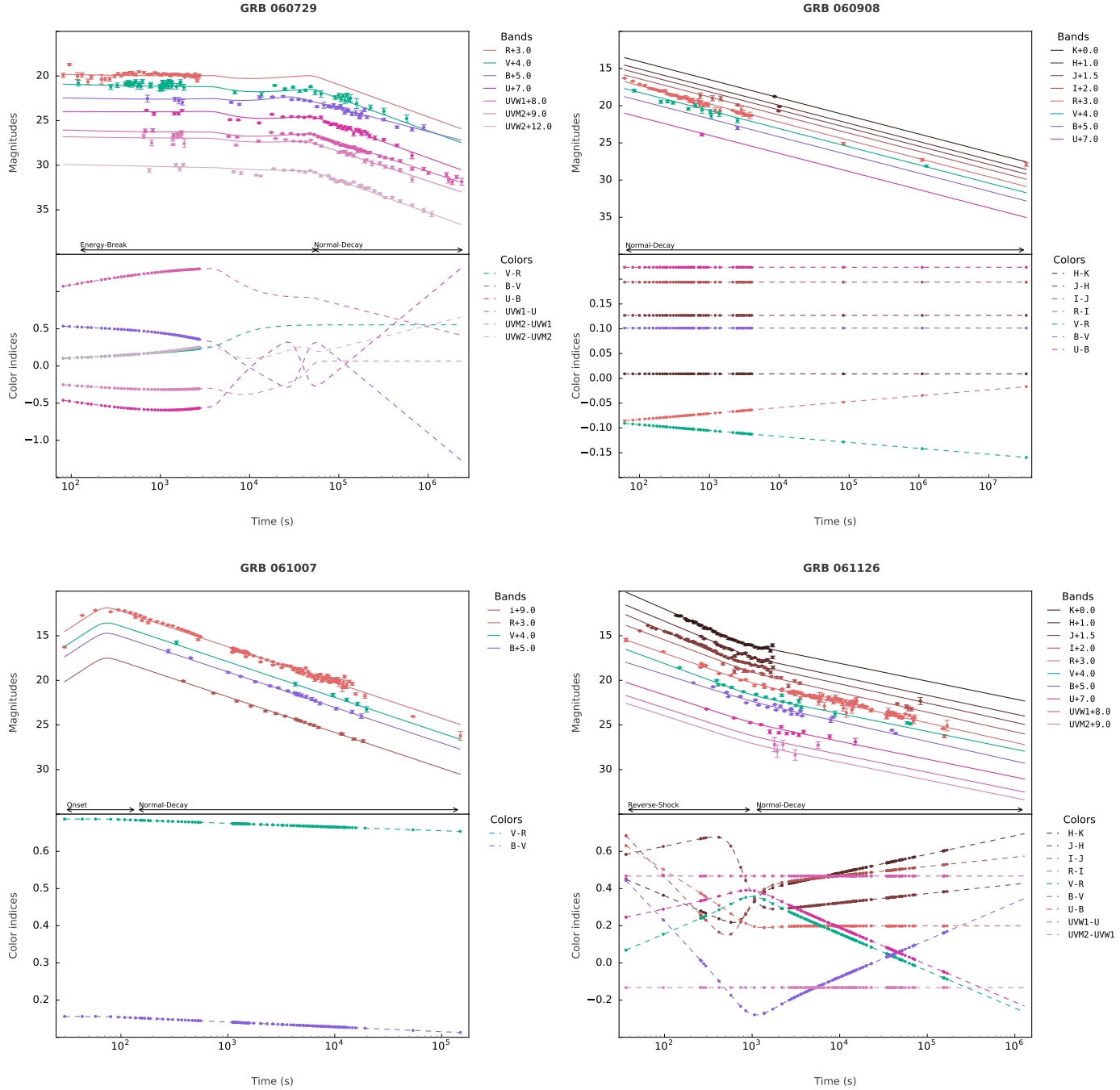


Fig. 6—Continued

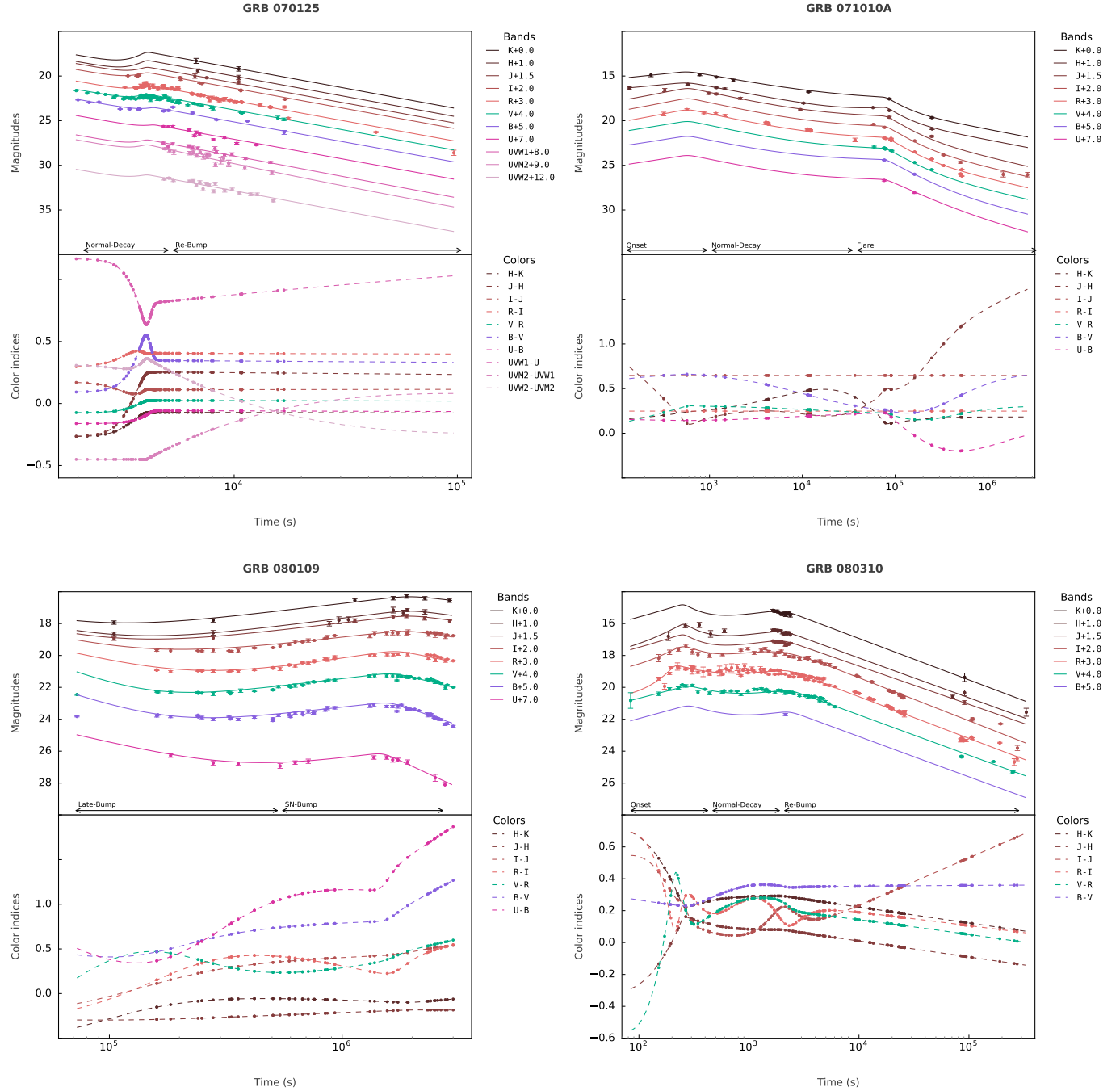


Fig. 6—Continued

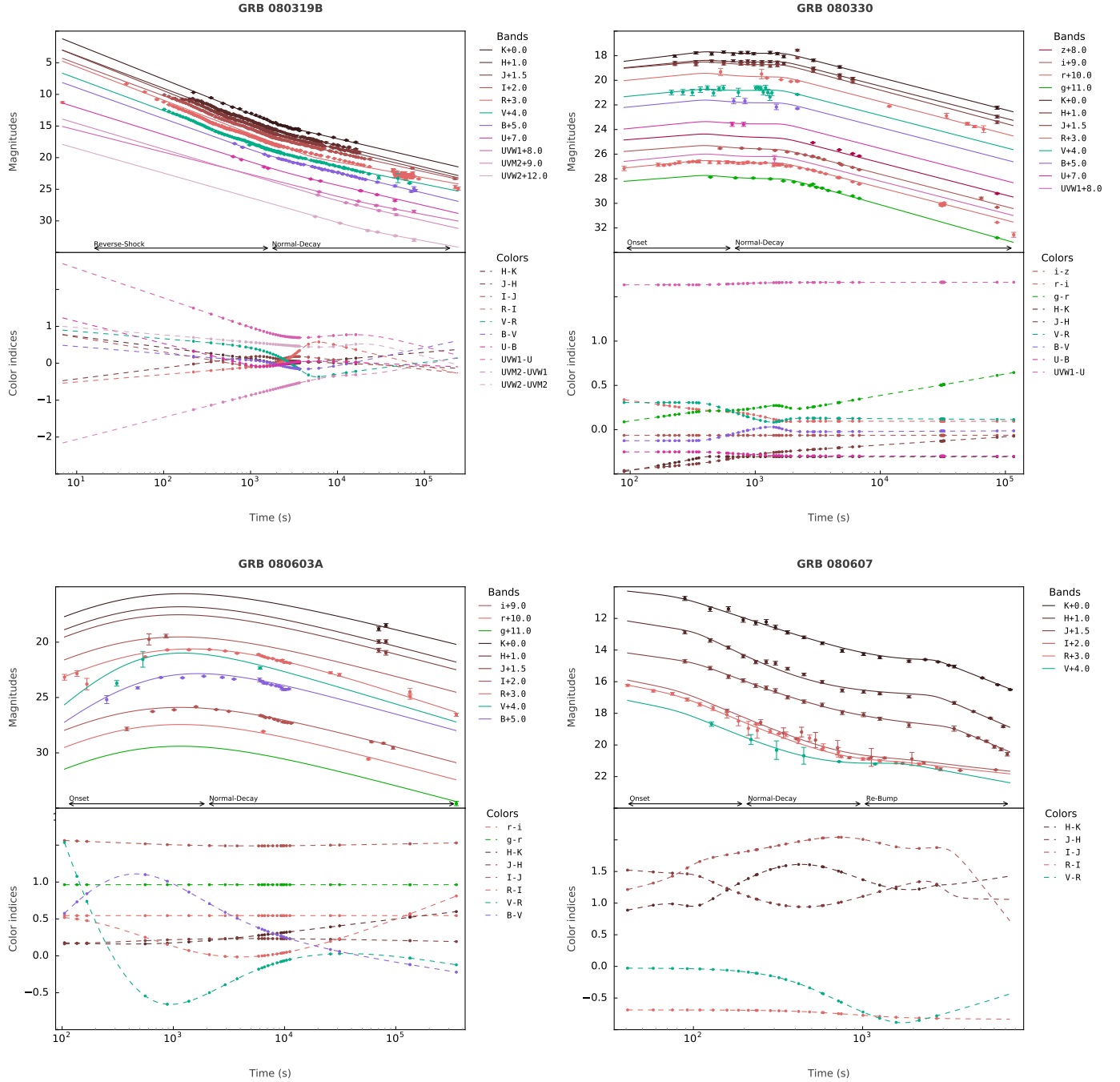


Fig. 6—Continued

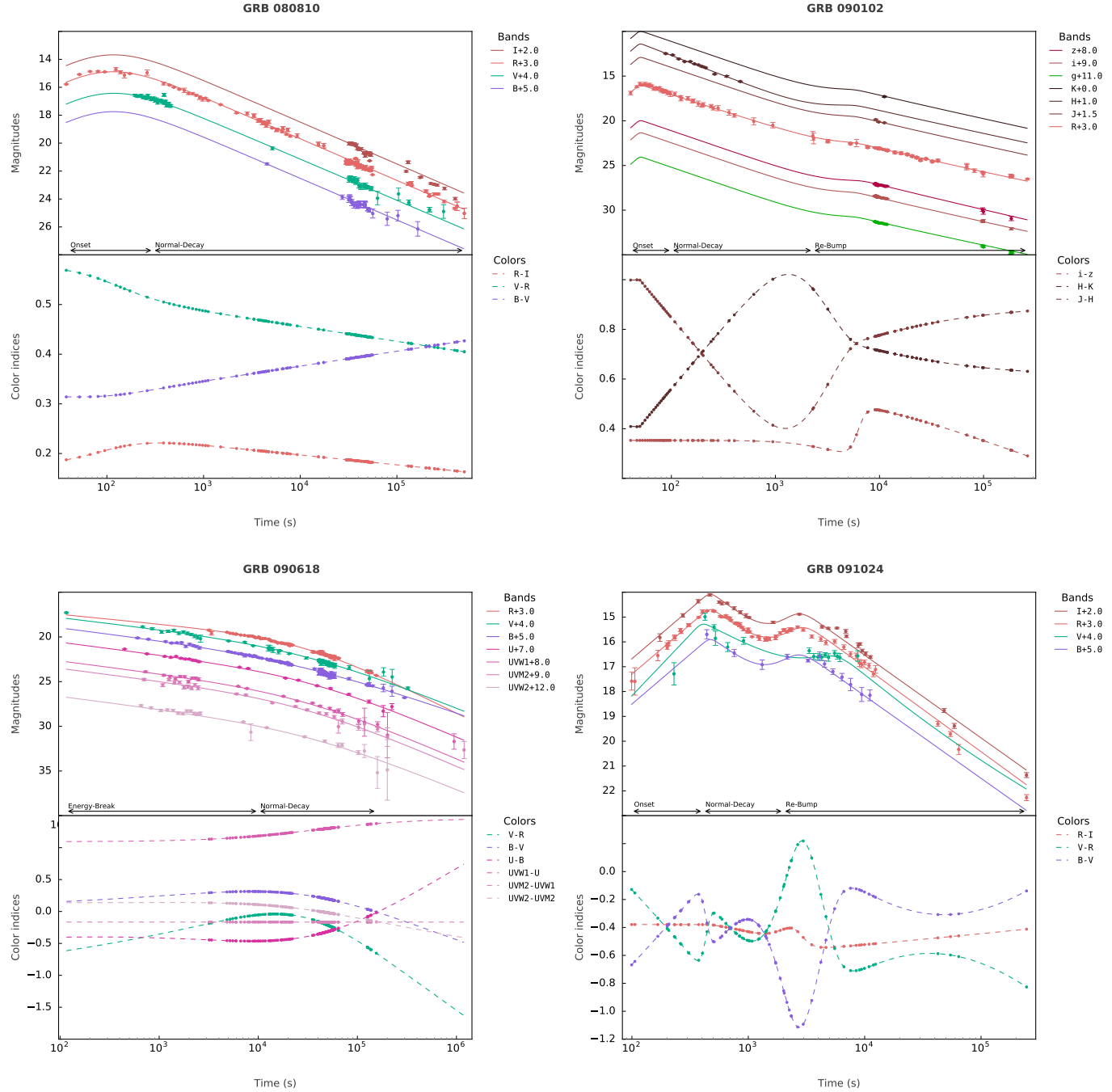


Fig. 6—Continued

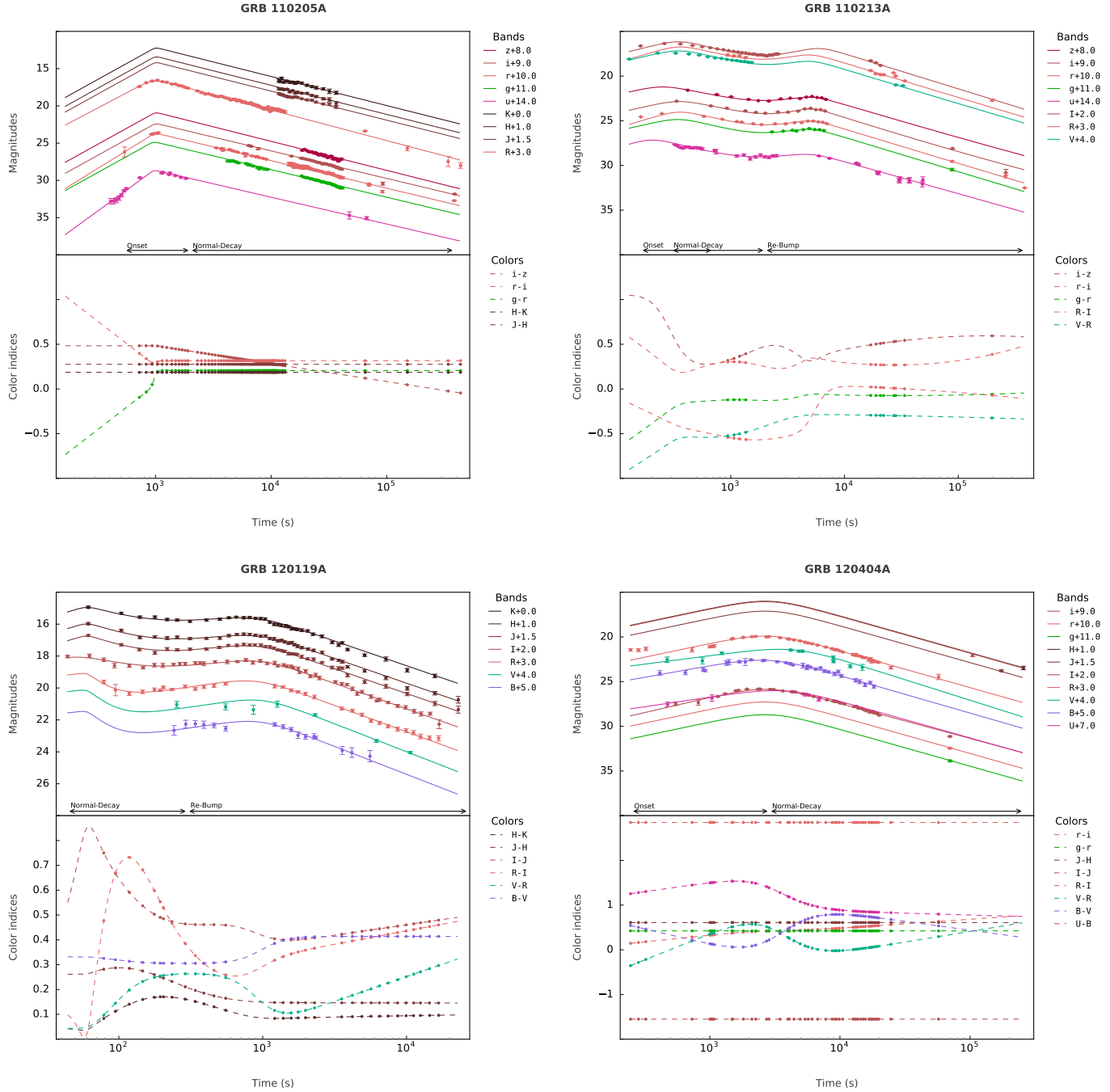


Fig. 6—Continued

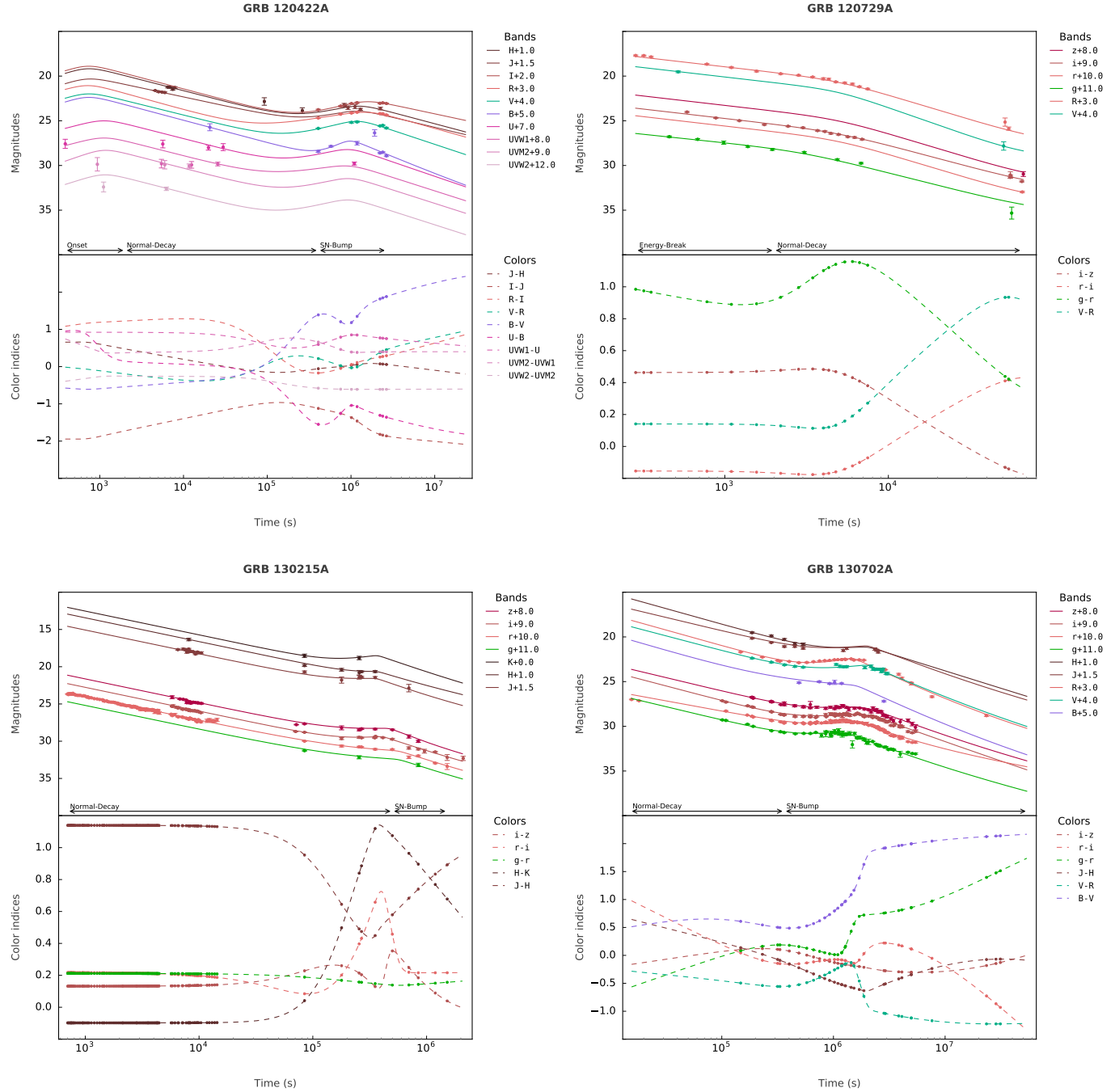


Fig. 6— Continued

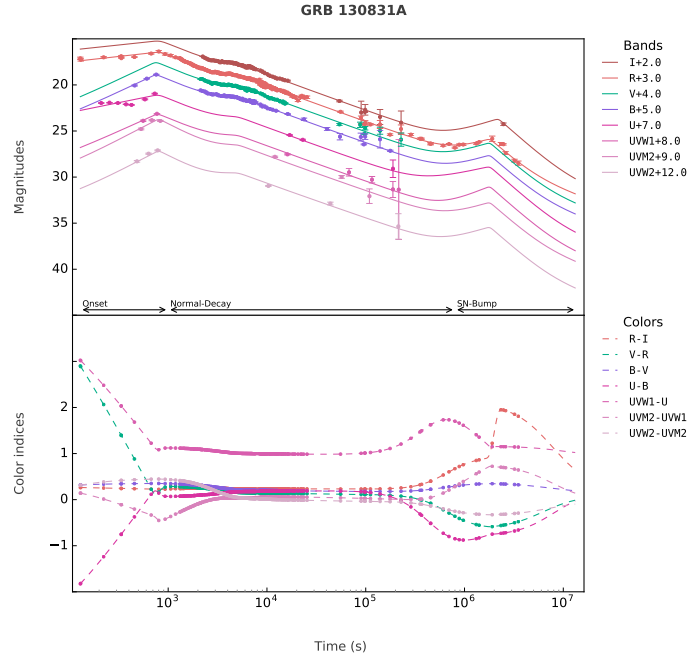


Fig. 6— Continued

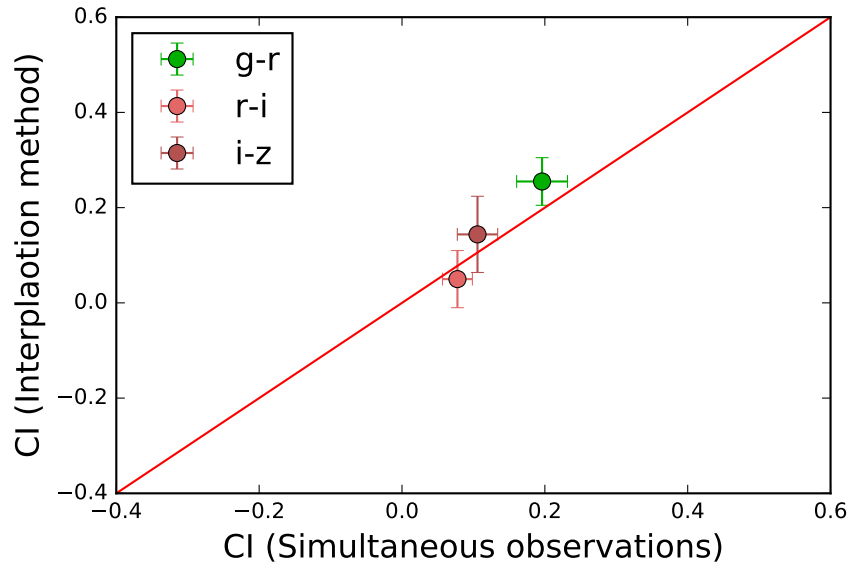


Figure 7. Correlation of the CI between two different methods: Golden (CI is derived directly by simultaneous multiband observations) and Silver (interpolation method); data are derived from GRB 130427A. The equal line is represented by the solid curve.

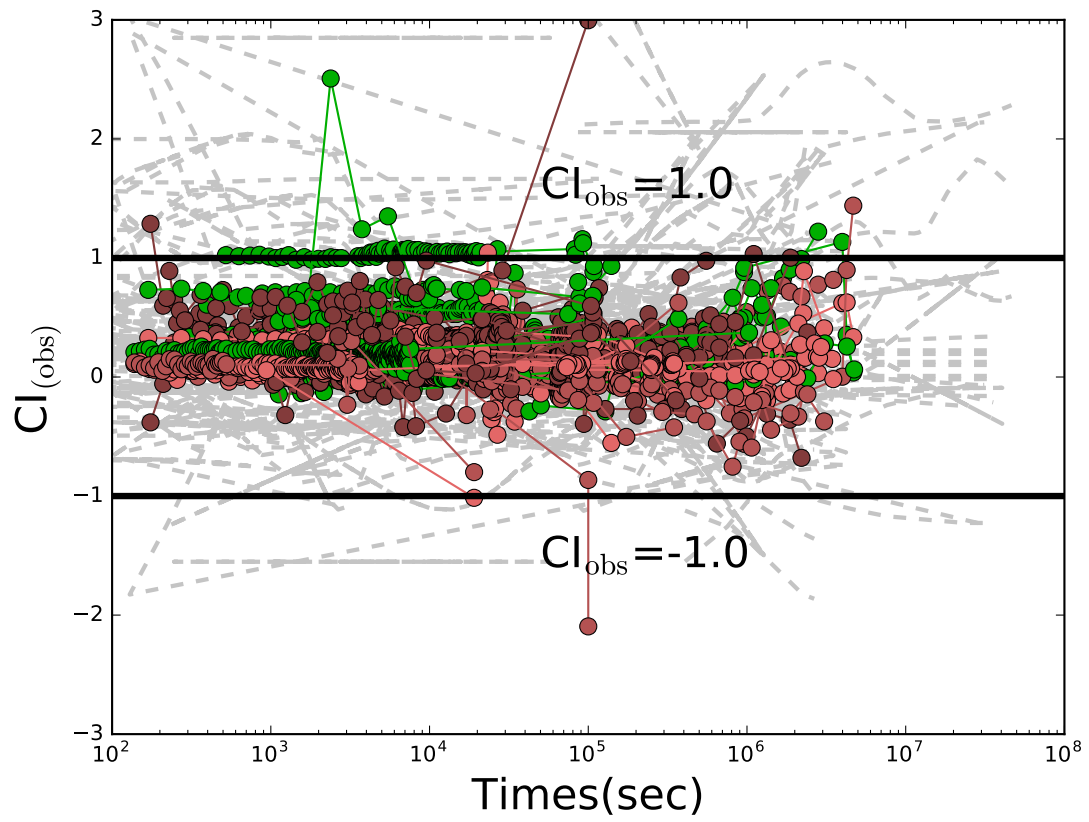


Figure 8. Temporal evolution of all CIs for all bursts (Data Set I). The Silver sample is in grey, while each color represents a different combination of bands for the Golden sample. Two horizontal black lines show $\text{CI} = -1$ and 1.

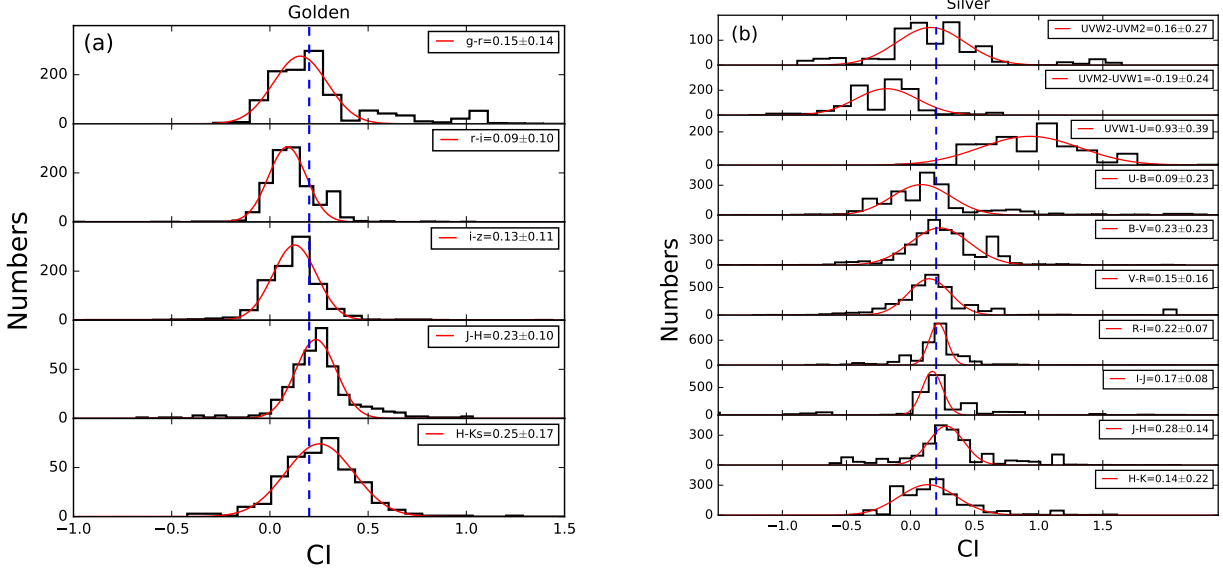


Figure 9. Distributions of the color indices (Data Set I) for the (a) Golden and the (b) Silver sample. The red lines are the best Gaussian fits, whose results can be found in Table 4. The vertical blue dashed lines represent CIs equal to 0.2.

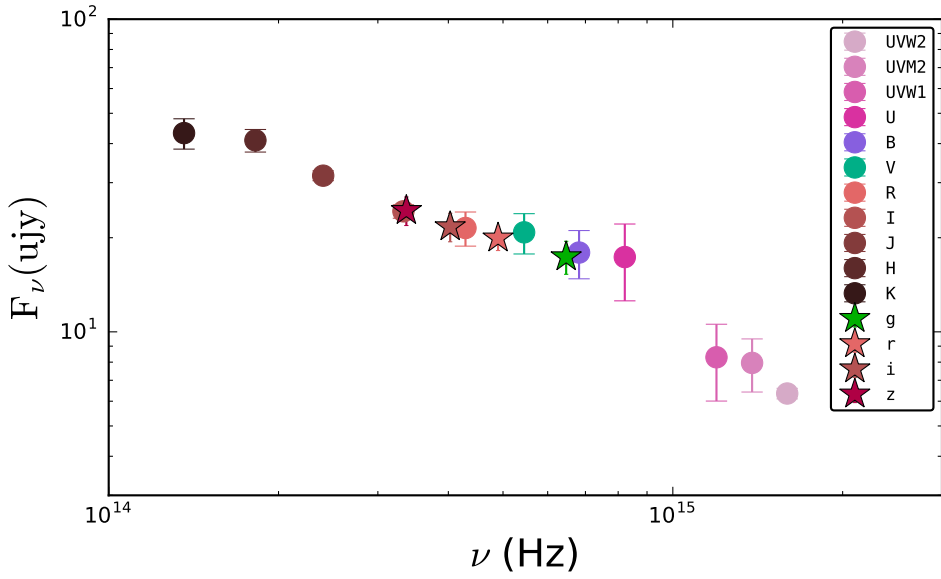


Figure 10. SED of the afterglow, which derives from average values of CIs (Data Set III) and assumes a typical observation magnitudes for r band (Golden sample)/R band (Silver sample). Different colors represents different energy bands. The stars represent the Golden sample (SDSS griz system), while the circles represent the Silver sample (common UBVRI photometry system).

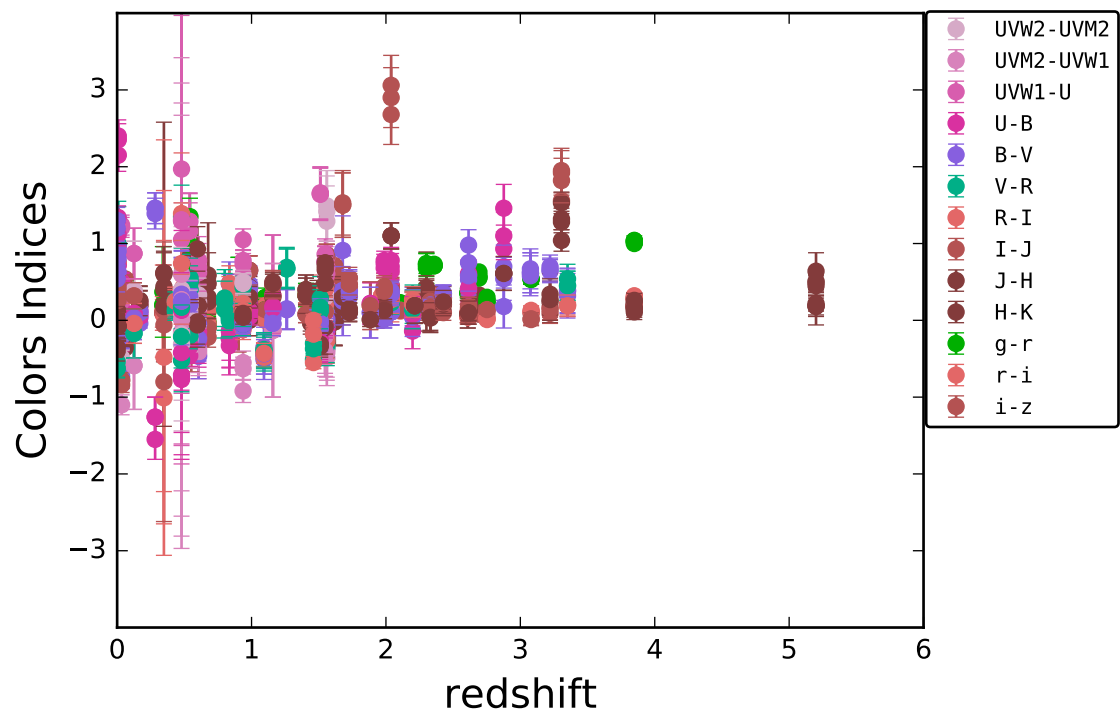


Figure 11. Color indices (based on Data Set III) as a function of redshift. Different colors represent different bands.

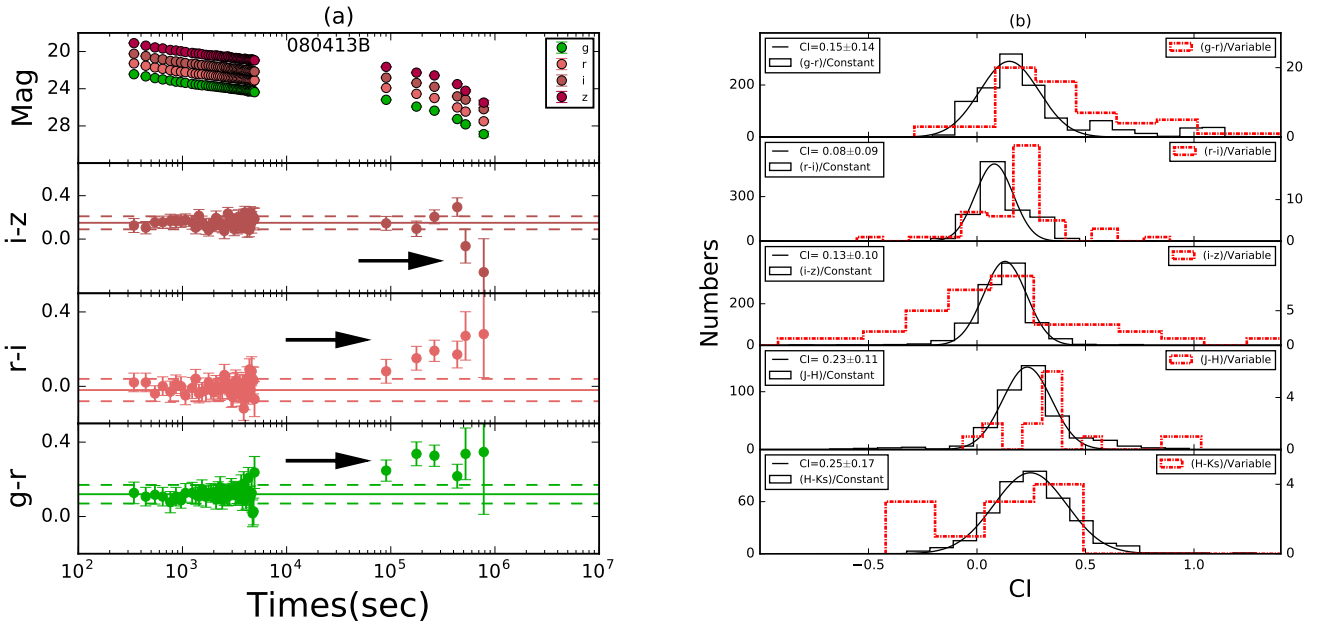


Figure 12. Left: multiband light curves together with the color indices of GRB 080413B. Variable CIs are labeled with the arrow. Right: distribution of *variable* (in red) and *constant* (in gray) CIs. The best Gaussian fit of the *constant* CI is represented by the gray curve, one has $g-r = 0.15 \pm 0.14$, $r-i = 0.08 \pm 0.09$, $i-z = 0.13 \pm 0.10$, $J - H = 0.23 \pm 0.11$ and $H - Ks = 0.25 \pm 0.17$, respectively.

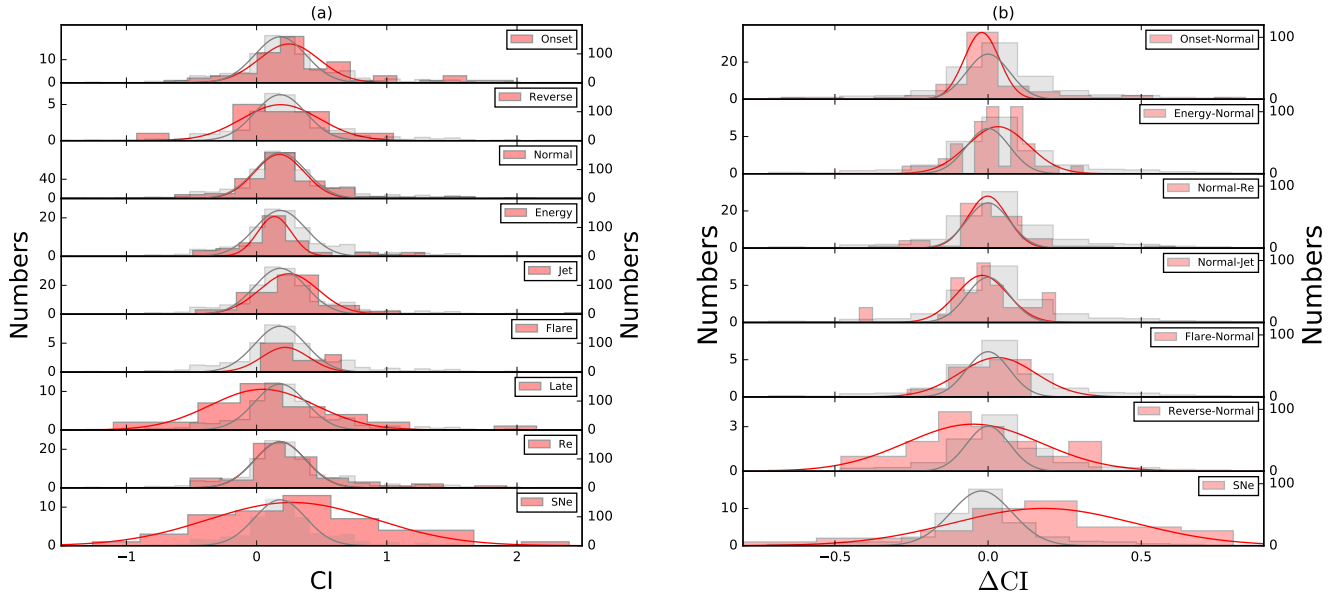


Figure 13. Distributions of CI and Δ CI for various emission components (in red), while the total distribution of CI or Δ CI appears in grey. (a) Distributions of CI (Data Set II, regardless of the color and GRBs), together with the best Gaussian fits with Onset=0.25±0.23, Reverse=0.18±0.30, Normal=0.17±0.19, Energy=0.14±0.13, Jet=0.25±0.23, Flare=0.22±0.18, Late=0.05±0.40, Re=0.18±0.20, SNe=0.27±0.64, while the gray histograms are comparing with their global behaviors, and the gray lines are the best Guassian fits with Global=0.18±0.20. (b) Distributions of Δ CI (Data Set II, regardless of the color and of GRBs) between one component and its following one, together with the best Gaussian fit, whose results are given by Table 6.

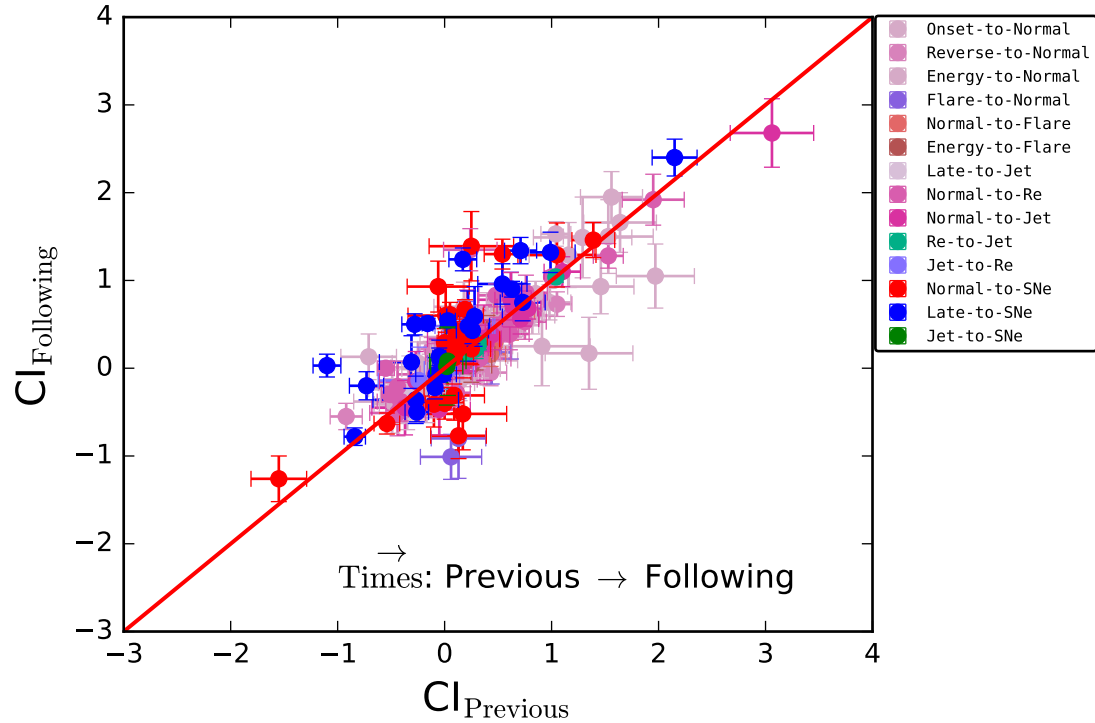


Figure 14. CI correlation between one component and its following one (Data Set II for both the Golden and Silver samples). The equal line is represented by the continuous curve.

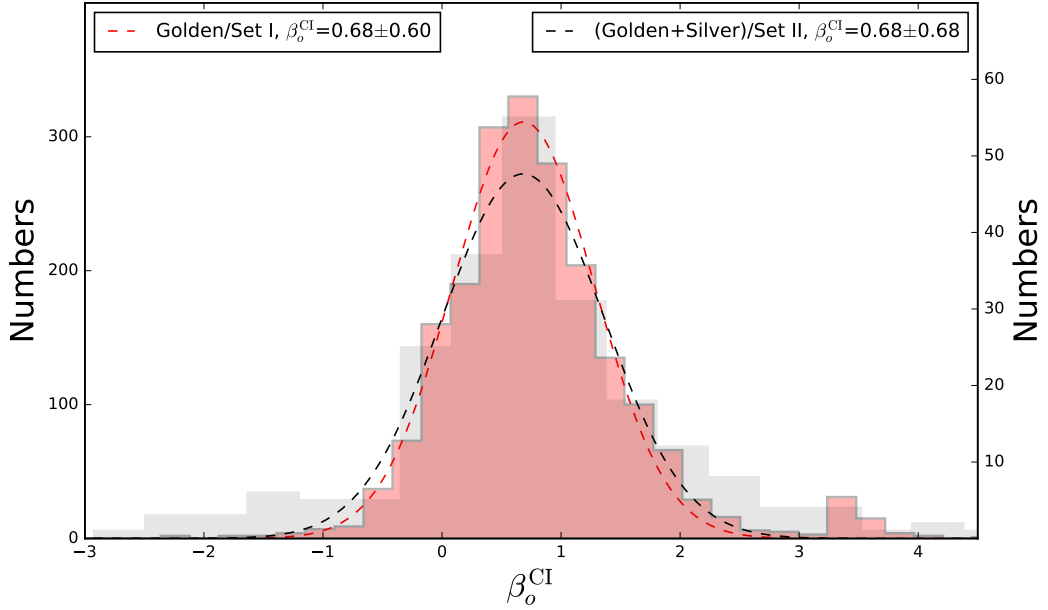


Figure 15. Distributions of spectral indices β_o^{CI} and their best Gaussian fits (dashed line), β_o^{CI} are derived from the CI- β_o relation (Eq 12) using the *constant* color indices of data Set I for the Golden sample and the Data Set II during the normal-decay phase for both the Golden and the Silver samples. We find $\beta_o^{\text{CI}}=0.68\pm 0.60$ for Data Set I and $\beta_o^{\text{CI}}=0.68\pm 0.68$ for Data Set II.

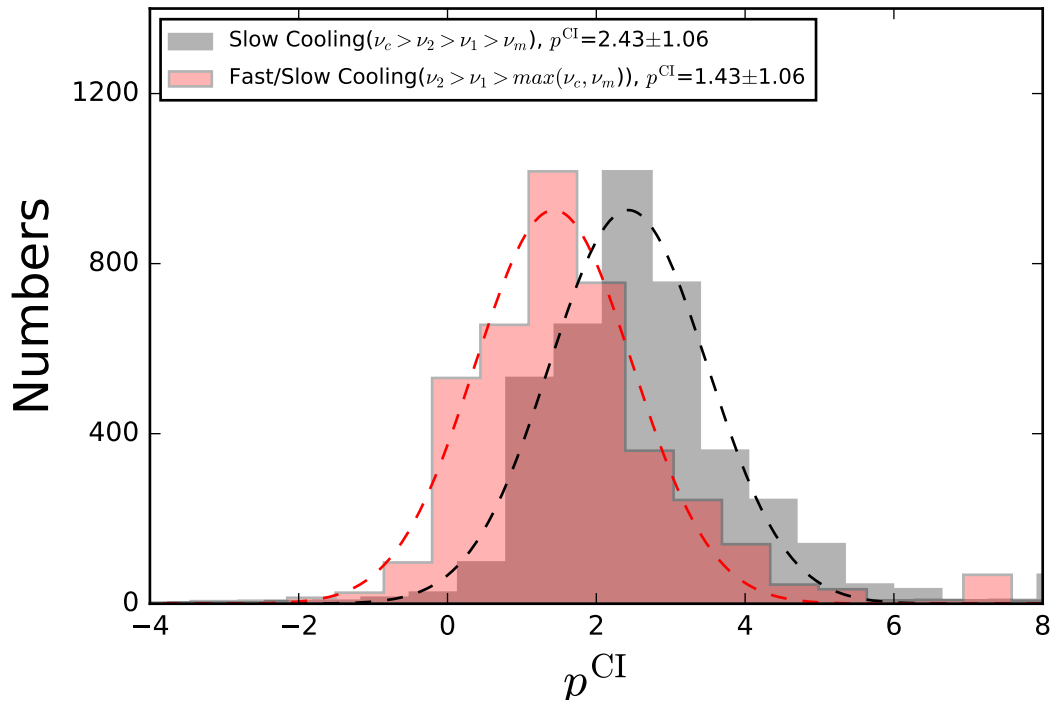


Figure 16. Distributions of observed electron spectral indices p^{CI} , derived from the *constant* CI of the Golden sample (Data Set I). The dashed lines are the best Gaussian fits giving $p^{\text{CI}}=2.43\pm 1.06$ for the slow cooling case ($\nu_c > \nu_2 > \nu_1 > \nu_m$) and $p^{\text{CI}}=1.43\pm 1.06$ for the fast/slow cooling case ($\nu_2 > \nu_1 > \max(\nu_c, \nu_m)$).

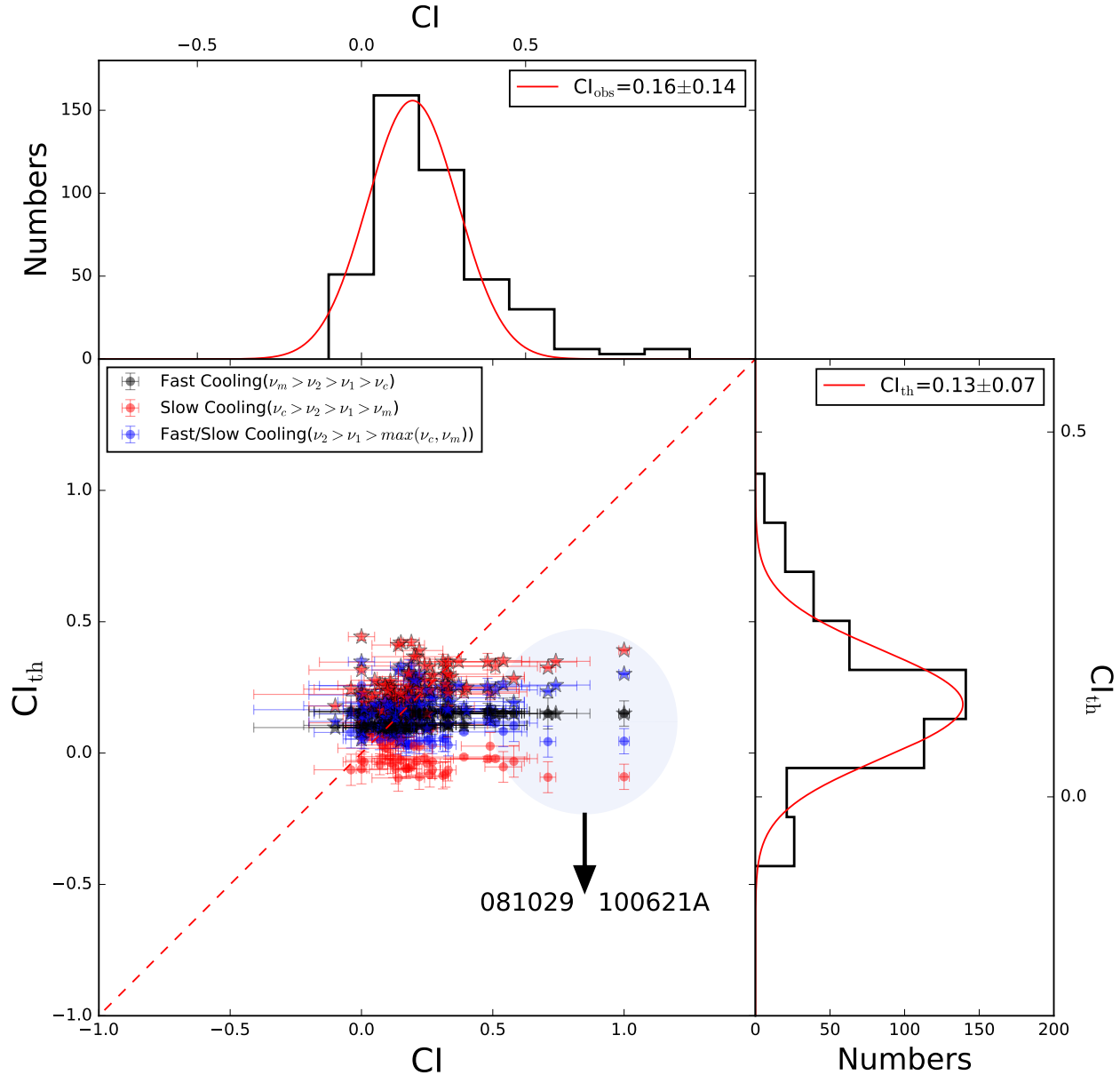


Figure 17. Correlation with their distributions between theoretical and observed CI for all GRBs in the three different spectral regimes (Data Set III). The red dashed line is the equal line, and the red solid lines are the best Gaussian fits giving $CI_{\text{obs}}=0.16\pm0.14$ for observed CI and $CI_{\text{th}}=0.13\pm0.07$ and for theoretical CI.

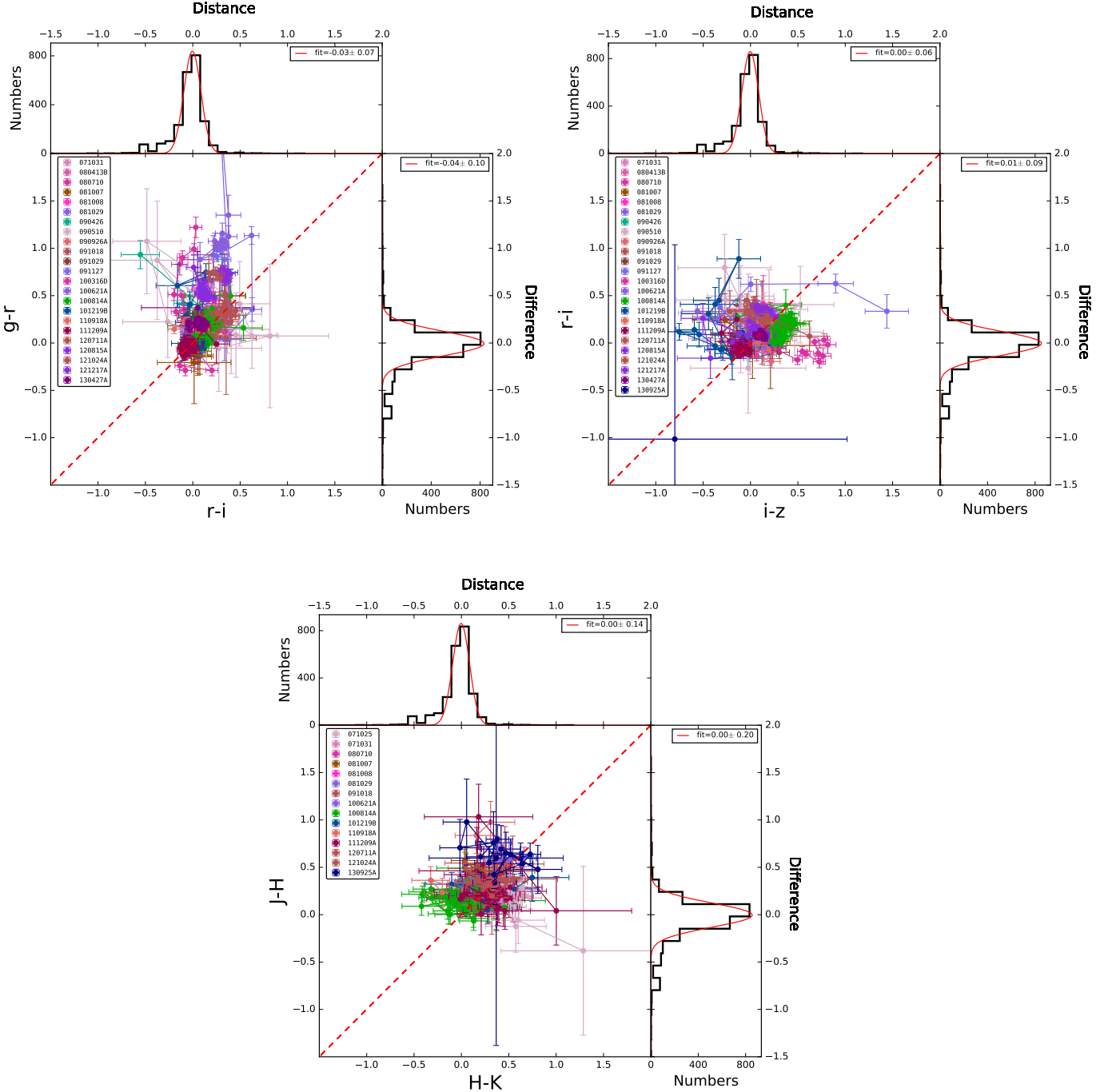


Figure 18. Color-color diagrams with the distributions of distances between the data points to the equal line and the distributions of differences between two colors (Data Set I of the Golden sample). The red dashed lines are the equal lines, and the red solid lines are the best Gaussian fits.

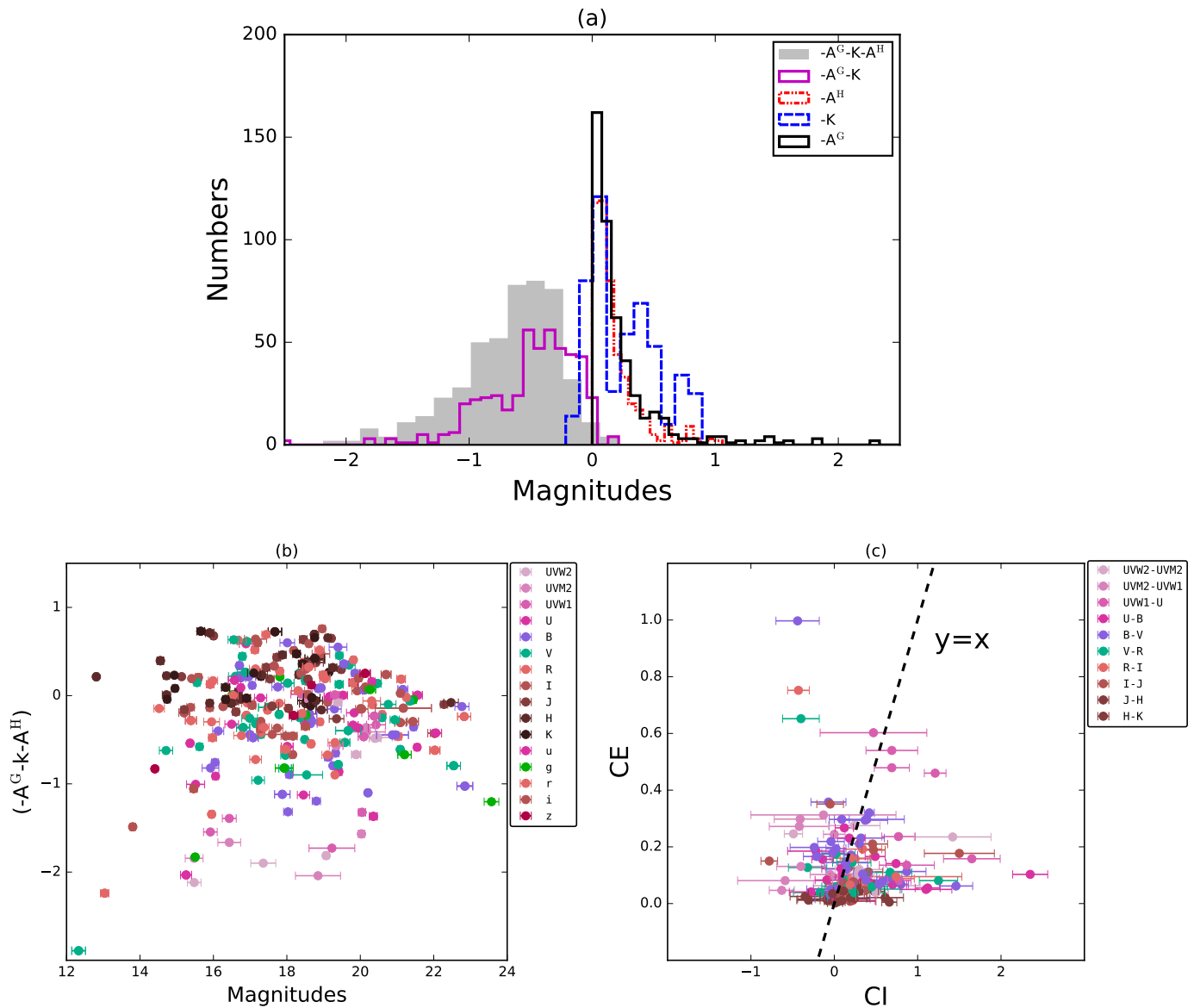


Figure 19. Top: distributions of extinction and spectral k -correction factors (Data Set III). Bottom left: total correction factors compared against the magnitude in a given band. Bottom right: comparison between CI and CE. The dashed line is the equal line.

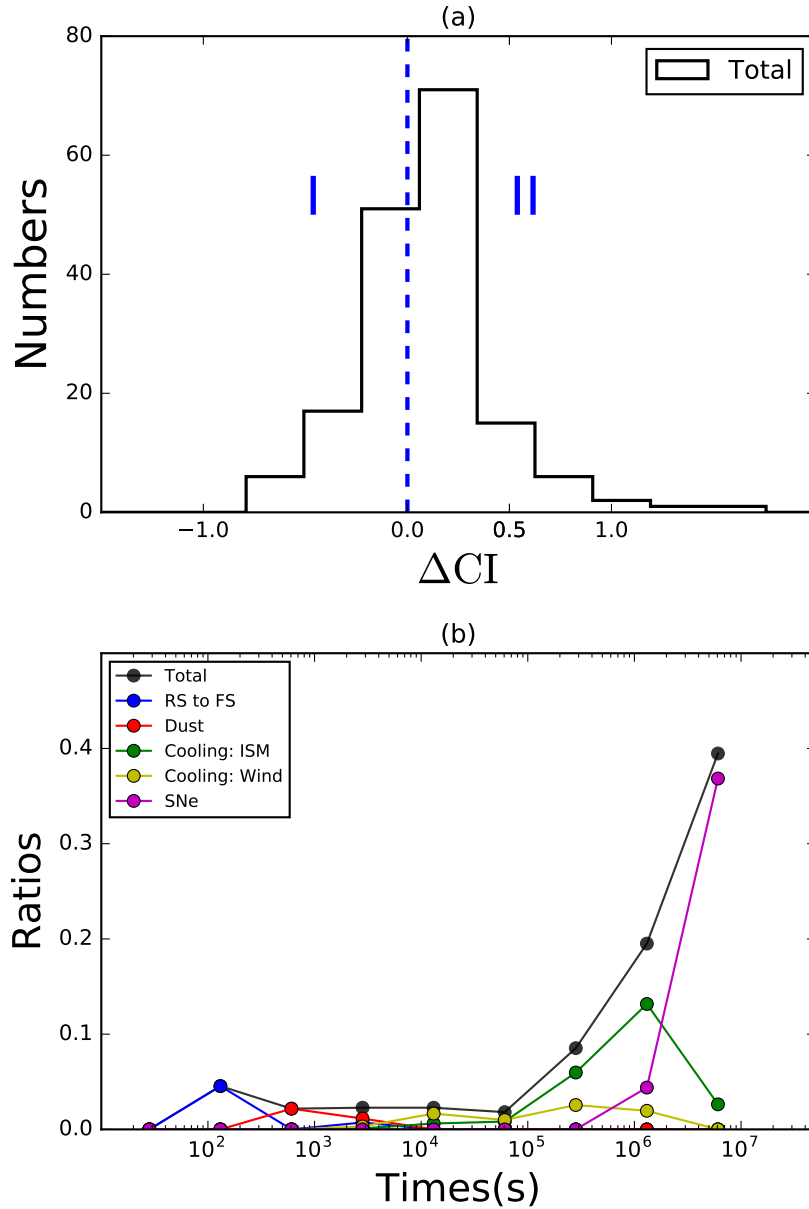


Figure 20. (a) Distribution of ΔCI for the Golden sample (Data Set I). The blue line separates positive and negative ΔCI . (b) Ratios of *variable* CIs associated with a given phenomenon to the total number of *variable* CIs in each time interval (see text for detailed explanations). Different colors represent different phenomena.

Facilities: *Swift*/UVOT

Software: Python

REFERENCES

- Becerra, R. L., Watson, A. M., Lee, W. H., et al. 2017, ApJ, 837, 116, doi: [10.3847/1538-4357/aa610f](https://doi.org/10.3847/1538-4357/aa610f)
- Berger, E., Fox, D. B., Cucchiara, A., & Cenko, S. B. 2008, GRB Coordinates Network, 8335, 1
- Bernardini, M. G., Dainotti, M. G., Bianco, C. L., et al. 2009, PROBING STELLAR POPULATIONS OUT TO THE DISTANT UNIVERSE: CEFALU 2008, 1111, 383
- Beuermann, K., Hessman, F. V., Reinsch, K., et al. 1999, A&A, 352, L26
- Bhargavi, S. G., & Cowsik, R. 2000, ApJL, 545, L77, doi: [10.1086/317878](https://doi.org/10.1086/317878)
- Björnsson, G., Hjorth, J., Jakobsson, P., Christensen, L., & Holland, S. 2001, ApJL, 552, L121, doi: [10.1086/320328](https://doi.org/10.1086/320328)
- Bloom, J. S., Djorgovski, S. G., Kulkarni, S. R., & Frail, D. A. 1998, ApJL, 507, L25, doi: [10.1086/311682](https://doi.org/10.1086/311682)
- Bloom, J. S., Starr, D. L., Blake, C. H., Skrutskie, M. F., & Falco, E. E. 2006, in Astronomical Society of the Pacific Conference Series, Vol. 351, Astronomical Data Analysis Software and Systems XV, ed. C. Gabriel, C. Arviset, D. Ponz, & S. Enrique, 751
- Bloom, J. S., van Dokkum, P. G., Bailyn, C. D., et al. 2004, AJ, 127, 252, doi: [10.1086/380229](https://doi.org/10.1086/380229)
- Bloom, J. S., Perley, D. A., Li, W., et al. 2009, ApJ, 691, 723, doi: [10.1088/0004-637X/691/1/723](https://doi.org/10.1088/0004-637X/691/1/723)
- Blustin, A. J., Band, D., Barthelmy, S., et al. 2006, ApJ, 637, 901, doi: [10.1086/498425](https://doi.org/10.1086/498425)
- Brown, P. J., Holland, S. T., Immel, S., et al. 2009, AJ, 137, 4517, doi: [10.1088/0004-6256/137/5/4517](https://doi.org/10.1088/0004-6256/137/5/4517)
- Bufano, F., Pian, E., Sollerman, J., et al. 2012, The Astrophysical Journal, 753, 67
- Butler, N. R., Li, W., Perley, D., et al. 2006, ApJ, 652, 1390, doi: [10.1086/508624](https://doi.org/10.1086/508624)
- Campana, S., Mangano, V., Blustin, A. J., et al. 2006, Nature, 442, 1008, doi: [10.1038/nature04892](https://doi.org/10.1038/nature04892)
- Cano, Z., Wang, S.-Q., Dai, Z.-G., & Wu, X.-F. 2017, Advances in Astronomy, 2017, 8929054, doi: [10.1155/2017/8929054](https://doi.org/10.1155/2017/8929054)
- Cano, Z., Bersier, D., Guidorzi, C., et al. 2011a, ApJ, 740, 41, doi: [10.1088/0004-637X/740/1/41](https://doi.org/10.1088/0004-637X/740/1/41)
- . 2011b, MNRAS, 413, 669, doi: [10.1111/j.1365-2966.2010.18164.x](https://doi.org/10.1111/j.1365-2966.2010.18164.x)
- Cano, Z., de Ugarte Postigo, A., Pozanenko, A., et al. 2014, Astronomy & Astrophysics, 568, A19
- Castro, S., Galama, T. J., Harrison, F. A., et al. 2003, The Astrophysical Journal, 586, 128
- Castro-Tirado, A. J., Gorosabel, J., Benítez, N., et al. 1998, Science, 279, 1011, doi: [10.1126/science.279.5353.1011](https://doi.org/10.1126/science.279.5353.1011)
- Castro-Tirado, A. J., Møller, P., García-Segura, G., et al. 2010, Astronomy and Astrophysics, 517, A61
- Cenko, S. B., Kasliwal, M., Harrison, F. A., et al. 2006, ApJ, 652, 490, doi: [10.1086/508149](https://doi.org/10.1086/508149)
- Cenko, S. B., Kelemen, J., Harrison, F. A., et al. 2009, ApJ, 693, 1484, doi: [10.1088/0004-637X/693/2/1484](https://doi.org/10.1088/0004-637X/693/2/1484)
- Cenko, S. B., Frail, D. A., Harrison, F. A., et al. 2011, ApJ, 732, 29, doi: [10.1088/0004-637X/732/1/29](https://doi.org/10.1088/0004-637X/732/1/29)
- Chandra, P., Cenko, S. B., Frail, D. A., et al. 2008, ApJ, 683, 924, doi: [10.1086/589807](https://doi.org/10.1086/589807)
- Chevalier, R. A., & Li, Z.-Y. 1999, The Astrophysical Journal, 520, L29
- Christensen, L., Hjorth, J., Gorosabel, J., et al. 2004, A&A, 413, 121, doi: [10.1051/0004-6361:20031517](https://doi.org/10.1051/0004-6361:20031517)
- Clocchiatti, A., Suntzeff, N. B., Covarrubias, R., & Candia, P. 2011, AJ, 141, 163, doi: [10.1088/0004-6256/141/5/163](https://doi.org/10.1088/0004-6256/141/5/163)
- Cobb, B. E. 2006, GRB Coordinates Network, 4972, 1
- Cobb, B. E., Bailyn, C. D., van Dokkum, P. G., & Natarajan, P. 2006, ApJL, 651, L85, doi: [10.1086/509724](https://doi.org/10.1086/509724)
- Cobb, B. E., Bloom, J. S., Perley, D. A., et al. 2010, ApJL, 718, L150, doi: [10.1088/2041-8205/718/2/L150](https://doi.org/10.1088/2041-8205/718/2/L150)

- Covino, S., D'Avanzo, P., Klotz, A., et al. 2008, MNRAS, 388, 347, doi: [10.1111/j.1365-2966.2008.13393.x](https://doi.org/10.1111/j.1365-2966.2008.13393.x)
- Covino, S., Campana, S., Conciatore, M. L., et al. 2010, A&A, 521, A53, doi: [10.1051/0004-6361/201014994](https://doi.org/10.1051/0004-6361/201014994)
- Covino, S., Melandri, A., Salvaterra, R., et al. 2013, MNRAS, 432, 1231, doi: [10.1093/mnras/stt540](https://doi.org/10.1093/mnras/stt540)
- Cucchiara, A., & Fumagalli, M. 2013, GRB Coordinates Network, 4207, 1
- Cucchiara, A., & Perley, D. 2013, GRB Coordinates Network, 5144, 1
- Cucchiara, A., & Prochaska, J. X. 2012, GRB Coordinates Network, 1286, 1
- Cucchiara, A., Cenko, S. B., Bloom, J. S., et al. 2011, ApJ, 743, 154, doi: [10.1088/0004-637X/743/2/154](https://doi.org/10.1088/0004-637X/743/2/154)
- Curran, P. A., Wijers, R. A. M. J., Heemskerk, M. H. M., et al. 2008, A&A, 490, 1047, doi: [10.1051/0004-6361:200810545](https://doi.org/10.1051/0004-6361:200810545)
- Dai, X., Halpern, J. P., Morgan, N. D., et al. 2007, ApJ, 658, 509, doi: [10.1086/510774](https://doi.org/10.1086/510774)
- D'Avanzo, P., D'Elia, V., & Covino, S. 2008, GRB Coordinates Network, 8350, 1
- De Cia, A., Starling, R. L. C., Wiersema, K., et al. 2011, MNRAS, 418, 129, doi: [10.1111/j.1365-2966.2011.19471.x](https://doi.org/10.1111/j.1365-2966.2011.19471.x)
- de Pasquale, M., Oates, S. R., Page, M. J., et al. 2007, MNRAS, 377, 1638, doi: [10.1111/j.1365-2966.2007.11724.x](https://doi.org/10.1111/j.1365-2966.2007.11724.x)
- De Pasquale, M., Oates, S. R., Racusin, J. L., et al. 2016, MNRAS, 455, 1027, doi: [10.1093/mnras/stv2280](https://doi.org/10.1093/mnras/stv2280)
- de Ugarte Postigo, A., Castro-Tirado, A. J., Gorosabel, J., et al. 2005, A&A, 443, 841, doi: [10.1051/0004-6361:20052898](https://doi.org/10.1051/0004-6361:20052898)
- de Ugarte Postigo, A., Horváth, I., Veres, P., et al. 2011, A&A, 525, A109, doi: [10.1051/0004-6361/201015261](https://doi.org/10.1051/0004-6361/201015261)
- de Ugarte Postigo, A., Fynbo, J. P. U., Thöne, C. C., et al. 2012, Astronomy & Astrophysics, 548, A11
- D'Elia, V., Fiore, F., Perna, R., et al. 2009a, The Astrophysical Journal, 694, 332
- . 2009b, Astronomy & Astrophysics, 503, 437
- D'Elia, V., Fynbo, J. P. U., Covino, S., et al. 2010, Astronomy and Astrophysics, 523, A36
- D'Elia, V., Pian, E., Melandri, A., et al. 2015, A&A, 577, A116, doi: [10.1051/0004-6361/201425381](https://doi.org/10.1051/0004-6361/201425381)
- Della Valle, M., Malesani, D., Bloom, J. S., et al. 2006a, ApJL, 642, L103, doi: [10.1086/504636](https://doi.org/10.1086/504636)
- Della Valle, M., Chincarini, G., Panagia, N., et al. 2006b, Nature, 444, 1050, doi: [10.1038/nature05374](https://doi.org/10.1038/nature05374)
- Elliott, J., Krühler, T., Greiner, J., et al. 2013, Astronomy & Astrophysics, 556, A23
- Elliott, J., Yu, H.-F., Schmidl, S., et al. 2014, A&A, 562, A100, doi: [10.1051/0004-6361/201322600](https://doi.org/10.1051/0004-6361/201322600)
- Fatkullin, T., Komarova, V., Sokolov, V., Cherepashchuk, A., & Postnov, K. 2003, GRB Coordinates Network, 1925, 1
- Ferrero, P., Kann, D. A., Zeh, A., et al. 2006, A&A, 457, 857, doi: [10.1051/0004-6361:20065530](https://doi.org/10.1051/0004-6361:20065530)
- Filgas, R., Greiner, J., Schady, P., et al. 2011a, A&A, 535, A57, doi: [10.1051/0004-6361/201117695](https://doi.org/10.1051/0004-6361/201117695)
- Filgas, R., Krühler, T., Greiner, J., et al. 2011b, A&A, 526, A113, doi: [10.1051/0004-6361/201015320](https://doi.org/10.1051/0004-6361/201015320)
- Filgas, R., Greiner, J., Schady, P., et al. 2012, Astronomy & Astrophysics, 546, A101
- Flores, H., Covino, S., Xu, D., et al. 2013, GRB Coordinates Network, 14491
- Friis, M., De Cia, A., Krühler, T., et al. 2015, MNRAS, 451, 167, doi: [10.1093/mnras/stv960](https://doi.org/10.1093/mnras/stv960)
- Fynbo, J. P. U., Gorosabel, J., Møller, P., et al. 2002, in Lighthouses of the Universe: The Most Luminous Celestial Objects and Their Use for Cosmology: Proceedings of the MPA/ESO/MPE/USM Joint Astronomy Conference Held in Garching, ESO, Garching bei München, Germany (Berlin/Heidelberg: Springer-Verlag), 187–
- Fynbo, J. P. U., Jakobsson, P., Prochaska, J. X., et al. 2009, The Astrophysical Journal Supplement, 185, 526
- Fynbo, J. U., Gorosabel, J., Dall, T. H., et al. 2001, A&A, 373, 796, doi: [10.1051/0004-6361:20010531](https://doi.org/10.1051/0004-6361:20010531)
- Gal-Yam, A., Moon, D.-S., Fox, D. B., et al. 2004, ApJL, 609, L59, doi: [10.1086/422841](https://doi.org/10.1086/422841)
- Galama, T. J., Vreeswijk, P. M., van Paradijs, J., et al. 1998, Nature, 395, 670

- Galama, T. J., Groot, P. J., van Paradijs, J., et al. 1998, ApJL, 497, L13, doi: [10.1086/311268](https://doi.org/10.1086/311268)
- Galama, T. J., Vreeswijk, P. M., van Paradijs, J., et al. 1999, A&AS, 138, 465, doi: [10.1051/aas:1999311](https://doi.org/10.1051/aas:1999311)
- Gao, H., Lei, W.-H., Zou, Y.-C., Wu, X.-F., & Zhang, B. 2013, arXiv.org, 141
- Gaudi, B Scott, Granot, Jonathan, & Loeb, Abraham. 2001, The Astrophysical Journal, 561, 178
- Gehrels, N., Ramirez-Ruiz, E., & Fox, D. B. 2009, ARA&A, 47, 567, doi: [10.1146/annurev.astro.46.060407.145147](https://doi.org/10.1146/annurev.astro.46.060407.145147)
- Gehrels, N., Chincarini, G., Giommi, P., et al. 2004, The Astrophysical Journal, 611, 1005
- Gendre, B., Klotz, A., Palazzi, E., et al. 2010, MNRAS, 405, 2372, doi: [10.1111/j.1365-2966.2010.16601.x](https://doi.org/10.1111/j.1365-2966.2010.16601.x)
- Geng, J.-J., Huang, Y.-F., & Dai, Z.-G. 2017, The Astrophysical Journal Letters, 841, L15
- Geng, J. J., Wu, X. F., Huang, Y. F., Li, L., & Dai, Z. G. 2016, The Astrophysical Journal, 825, 107
- Gomboc, A., Kobayashi, S., Guidorzi, C., et al. 2008, ApJ, 687, 443, doi: [10.1086/592062](https://doi.org/10.1086/592062)
- Gorbovskoy, E., Lipunov, V., Tyurina, N., et al. 2015, GRB Coordinates Network, 8673, 1
- Greiner, J., Bornemann, W., Clemens, C., et al. 2008, PASP, 120, 405, doi: [10.1086/587032](https://doi.org/10.1086/587032)
- Greiner, J., Krühler, T., Nardini, M., et al. 2013, Astronomy & Astrophysics, 560, A70
- Greiner, J., Yu, H. F., Krühler, T., et al. 2014, Astronomy & Astrophysics, 568, A75
- Grupe, D., Gronwall, C., Wang, X.-Y., et al. 2007, ApJ, 662, 443, doi: [10.1086/517868](https://doi.org/10.1086/517868)
- Guenther, E. W., Klose, S., Vreeswijk, P., Pian, E., & Greiner, J. 2006, GRB Coordinates Network, 4863, 1
- Guidorzi, C., Gomboc, A., Kobayashi, S., et al. 2006, Astronomy & Astrophysics, 463, 539
- Guidorzi, C., Gomboc, A., Kobayashi, S., et al. 2007, A&A, 463, 539, doi: [10.1051/0004-6361:20065974](https://doi.org/10.1051/0004-6361:20065974)
- Guidorzi, C., Clemens, C., Kobayashi, S., et al. 2009, A&A, 499, 439, doi: [10.1051/0004-6361/200911719](https://doi.org/10.1051/0004-6361/200911719)
- Guidorzi, C., Kobayashi, S., Perley, D. A., et al. 2011, Monthly Notices of the Royal Astronomical Society, 417, 2124
- Guidorzi, C., Mundell, C. G., Harrison, R., et al. 2014, MNRAS, 438, 752, doi: [10.1093/mnras/stt2243](https://doi.org/10.1093/mnras/stt2243)
- Harrison, F. A., Bloom, J. S., Frail, D. A., et al. 1999, ApJL, 523, L121, doi: [10.1086/312282](https://doi.org/10.1086/312282)
- Hjorth, J., Sollerman, J., Møller, P., et al. 2003, Nature, 423, 847
- Holland, S. T., & Swift Science Team. 2006, in American Institute of Physics Conference Series, Vol. 836, Gamma-Ray Bursts in the Swift Era, ed. S. S. Holt, N. Gehrels, & J. A. Nousek, 436–439
- Holland, S. T., Weidinger, M., Fynbo, J. P. U., et al. 2003, AJ, 125, 2291, doi: [10.1086/374235](https://doi.org/10.1086/374235)
- Holland, S. T., De Pasquale, M., Mao, J., et al. 2012, ApJ, 745, 41, doi: [10.1088/0004-637X/745/1/41](https://doi.org/10.1088/0004-637X/745/1/41)
- Huang, Y. F., & Cheng, K. S. 2003, MNRAS, 341, 263, doi: [10.1046/j.1365-8711.2003.06430.x](https://doi.org/10.1046/j.1365-8711.2003.06430.x)
- Huang, Y. F., Cheng, K. S., & Gao, T. T. 2006, ApJ, 637, 873, doi: [10.1086/498423](https://doi.org/10.1086/498423)
- Israel, G. L., Marconi, G., Covino, S., et al. 1999, A&A, 348, L5
- Jakobsson, P., Fynbo, J. P. U., Ledoux, C., et al. 2006, Astronomy and Astrophysics, 460, L13
- Jensen, B. L., Fynbo, J. U., Gorosabel, J., et al. 2001, A&A, 370, 909, doi: [10.1051/0004-6361:20010291](https://doi.org/10.1051/0004-6361:20010291)
- Jordi, K., Grebel, E. K., & Ammon, K. 2006, A&A, 460, 339, doi: [10.1051/0004-6361:20066082](https://doi.org/10.1051/0004-6361:20066082)
- Kann, D. A., Klose, S., & Zeh, A. 2006, ApJ, 641, 993, doi: [10.1086/500652](https://doi.org/10.1086/500652)
- Kann, D. A., Klose, S., Zhang, B., et al. 2010, ApJ, 720, 1513, doi: [10.1088/0004-637X/720/2/1513](https://doi.org/10.1088/0004-637X/720/2/1513)
- . 2011, ApJ, 734, 96, doi: [10.1088/0004-637X/734/2/96](https://doi.org/10.1088/0004-637X/734/2/96)
- Kann, D. A., Schady, P., Olivares E, F., et al. 2016, arXiv.org, arXiv:1606.06791
- Kelly, P. L., Filippenko, A. V., Fox, O. D., Zheng, W., & Clubb, K. I. 2013, The Astrophysical Journal Letters, 775, L5
- Klose, S., Greiner, J., Rau, A., et al. 2004, AJ, 128, 1942, doi: [10.1086/424539](https://doi.org/10.1086/424539)
- Klotz, A., Boér, M., Atteia, J. L., et al. 2005, A&A, 439, L35, doi: [10.1051/0004-6361:200500153](https://doi.org/10.1051/0004-6361:200500153)
- Kobayashi, S., & Zhang, B. 2003, ApJ, 597, 455, doi: [10.1086/378283](https://doi.org/10.1086/378283)

- Kröhler, T., Greiner, J., McBreen, S., et al. 2009a, *ApJ*, 697, 758, doi: [10.1088/0004-637X/697/1/758](https://doi.org/10.1088/0004-637X/697/1/758)
- Kröhler, T., Greiner, J., Afonso, P., et al. 2009b, *A&A*, 508, 593, doi: [10.1051/0004-6361/200912649](https://doi.org/10.1051/0004-6361/200912649)
- Kröhler, T., Ledoux, C., Fynbo, J. P. U., et al. 2013, *A&A*, 557, A18, doi: [10.1051/0004-6361/201321772](https://doi.org/10.1051/0004-6361/201321772)
- Kuroda, D., Yanagisawa, K., Shimizu, Y., et al. 2011, GRB Coordinates Network, 1719, 1
- Lazzati, D., & Perna, R. 2003, *MNRAS*, 340, 694, doi: [10.1046/j.1365-8711.2003.06334.x](https://doi.org/10.1046/j.1365-8711.2003.06334.x)
- Levan, A. J., Tanvir, N. R., Starling, R. L. C., et al. 2014, *ApJ*, 781, 13, doi: [10.1088/0004-637X/781/1/13](https://doi.org/10.1088/0004-637X/781/1/13)
- Levesque, E. M., Bloom, J. S., Butler, N. R., et al. 2010, *MNRAS*, 401, 963, doi: [10.1111/j.1365-2966.2009.15733.x](https://doi.org/10.1111/j.1365-2966.2009.15733.x)
- Li, L., Liang, E.-W., Tang, Q.-W., et al. 2012, *ApJ*, 758, 27, doi: [10.1088/0004-637X/758/1/27](https://doi.org/10.1088/0004-637X/758/1/27)
- Li, L., Wu, X.-F., Huang, Y.-F., et al. 2015, *The Astrophysical Journal*, 805, 13
- Li, W., Jha, S., Filippenko, A. V., et al. 2005, GRB Coordinates Network, 4095, 1
- Liang, E.-W., Racusin, J. L., Zhang, B., Zhang, B.-B., & Burrows, D. N. 2008, *The Astrophysical Journal*, 675, 528
- Liang, E.-W., Zhang, B.-B., & Zhang, B. 2007, *ApJ*, 670, 565, doi: [10.1086/521870](https://doi.org/10.1086/521870)
- Liang, E. W., Zhang, B., O'Brien, P. T., et al. 2006, *ApJ*, 646, 351, doi: [10.1086/504684](https://doi.org/10.1086/504684)
- Liang, E.-W., Li, L., Gao, H., et al. 2013, *The Astrophysical Journal*, 774, 13
- Littlejohns, O. M., Willingale, R., O'Brien, P. T., et al. 2012, *MNRAS*, 421, 2692, doi: [10.1111/j.1365-2966.2012.20499.x](https://doi.org/10.1111/j.1365-2966.2012.20499.x)
- Maiorano, E., Masetti, N., Palazzi, E., et al. 2006, *A&A*, 455, 423, doi: [10.1051/0004-6361:20054728](https://doi.org/10.1051/0004-6361:20054728)
- Mangano, V., Holland, S. T., Malesani, D., et al. 2007, *A&A*, 470, 105, doi: [10.1051/0004-6361:20077232](https://doi.org/10.1051/0004-6361:20077232)
- Markwardt, C. B. 2009, *Astronomical Data Analysis Software and Systems XVIII ASP Conference Series*, 411, 251
- Martin-Carrillo, A., Hanlon, L., Topinka, M., et al. 2014, *Astronomy & Astrophysics*, 567, A84
- Maselli, A., Melandri, A., Nava, L., et al. 2014, *Science*, 343, 48, doi: [10.1126/science.1242279](https://doi.org/10.1126/science.1242279)
- Masetti, N., Bartolini, C., Bernabei, S., et al. 2000, *A&A*, 359, L23
- McBreen, S., Kröhler, T., Rau, A., et al. 2010, *Astronomy and Astrophysics*, 516, A71
- McKenzie, E. H., & Schaefer, B. E. 1999, *PASP*, 111, 964, doi: [10.1086/316404](https://doi.org/10.1086/316404)
- Melandri, A., Pian, E., Ferrero, P., et al. 2012, *A&A*, 547, A82, doi: [10.1051/0004-6361/201219879](https://doi.org/10.1051/0004-6361/201219879)
- Melandri, A., Covino, S., Zaninoni, E., et al. 2017, arXiv.org
- Mészáros, P., & Rees, M. J. 1997, *The Astrophysical Journal*, 476, 232
- Milvang-Jensen, B., Goldoni, P., Tanvir, N. R., et al. 2010, GRB Coordinates Network, 1087, 1
- Mirabal, N., Halpern, J. P., An, D., Thorstensen, J. R., & Terndrup, D. M. 2006, *ApJL*, 643, L99, doi: [10.1086/505177](https://doi.org/10.1086/505177)
- Mirabal, N., Halpern, J. P., Chornock, R., et al. 2003, *ApJ*, 595, 935, doi: [10.1086/377471](https://doi.org/10.1086/377471)
- Modjaz, M., Li, W., Butler, N., et al. 2009, *ApJ*, 702, 226, doi: [10.1088/0004-637X/702/1/226](https://doi.org/10.1088/0004-637X/702/1/226)
- Molinari, E., Vergani, S. D., Malesani, D., et al. 2007, *A&A*, 469, L13, doi: [10.1051/0004-6361:20077388](https://doi.org/10.1051/0004-6361:20077388)
- Morgan, A. N., Perley, D. A., Cenko, S. B., et al. 2014, *MNRAS*, 440, 1810, doi: [10.1093/mnras/stu344](https://doi.org/10.1093/mnras/stu344)
- Mu, H.-J., Lin, D.-B., Xi, S.-Q., et al. 2016, *ApJ*, 831, 111, doi: [10.3847/0004-637X/831/1/111](https://doi.org/10.3847/0004-637X/831/1/111)
- Mundell, C. G., Melandri, A., Guidorzi, C., et al. 2007, *ApJ*, 660, 489, doi: [10.1086/512605](https://doi.org/10.1086/512605)
- Nardini, M., Ghisellini, G., Ghirlanda, G., et al. 2006, *A&A*, 451, 821, doi: [10.1051/0004-6361:20054085](https://doi.org/10.1051/0004-6361:20054085)
- Nardini, M., Greiner, J., Kröhler, T., et al. 2011, *A&A*, 531, A39, doi: [10.1051/0004-6361/201116814](https://doi.org/10.1051/0004-6361/201116814)
- Nardini, M., Elliott, J., Filgas, R., et al. 2014, *Astronomy & Astrophysics*, 562, A29
- Nicuesa Guelbenzu, A., Klose, S., Rossi, A., et al. 2011, *A&A*, 531, L6, doi: [10.1051/0004-6361/201116657](https://doi.org/10.1051/0004-6361/201116657)
- Nicuesa Guelbenzu, A., Klose, S., Kröhler, T., et al. 2012, *A&A*, 538, L7, doi: [10.1051/0004-6361/201118416](https://doi.org/10.1051/0004-6361/201118416)
- Nysewander, M., Reichart, D. E., Crain, J. A., et al. 2009, *ApJ*, 693, 1417, doi: [10.1088/0004-637X/693/2/1417](https://doi.org/10.1088/0004-637X/693/2/1417)

- Oke, J. B., & Sandage, A. 1968, *Astrophysical Journal*, 154, 21
- Olivares E., F., Greiner, J., Schady, P., et al. 2012, *A&A*, 539, A76, doi: [10.1051/0004-6361/201117929](https://doi.org/10.1051/0004-6361/201117929)
- . 2015, *A&A*, 577, A44, doi: [10.1051/0004-6361/201321936](https://doi.org/10.1051/0004-6361/201321936)
- O'Meara, J., Chen, H. W., & Prochaska, J. X. 2010, GRB Coordinates Network, 1108, 1
- Page, K. L., Willingale, R., Bissaldi, E., et al. 2009, *MNRAS*, 400, 134, doi: [10.1111/j.1365-2966.2009.15462.x](https://doi.org/10.1111/j.1365-2966.2009.15462.x)
- Page, K. L., Starling, R. L. C., Fitzpatrick, G., et al. 2011, *MNRAS*, 416, 2078, doi: [10.1111/j.1365-2966.2011.19183.x](https://doi.org/10.1111/j.1365-2966.2011.19183.x)
- Panaitescu, A., & Kumar, P. 2002, *The Astrophysical Journal*, 571, 779
- Panaitescu, A., & Vestrand, W. T. 2008, *MNRAS*, 387, 497, doi: [10.1111/j.1365-2966.2008.13231.x](https://doi.org/10.1111/j.1365-2966.2008.13231.x)
- . 2011, *MNRAS*, 414, 3537, doi: [10.1111/j.1365-2966.2011.18653.x](https://doi.org/10.1111/j.1365-2966.2011.18653.x)
- Pandey, S. B., Sagar, R., Anupama, G. C., et al. 2004, *A&A*, 417, 919, doi: [10.1051/0004-6361:20034515](https://doi.org/10.1051/0004-6361:20034515)
- Pandey, S. B., Sahu, D. K., Resmi, L., et al. 2003, *Bulletin of the Astronomical Society of India*, 31, 19
- Pandey, S. B., Castro-Tirado, A. J., Jelínek, M., et al. 2009, *A&A*, 504, 45, doi: [10.1051/0004-6361/200811135](https://doi.org/10.1051/0004-6361/200811135)
- Pei, Y. C. 1992, *ApJ*, 395, 130, doi: [10.1086/171637](https://doi.org/10.1086/171637)
- Penprase, B. E., Berger, E., Fox, D. B., et al. 2006, *ApJ*, 646, 358, doi: [10.1086/504678](https://doi.org/10.1086/504678)
- Perley, D. A., Bloom, J. S., Butler, N. R., et al. 2008, *ApJ*, 672, 449, doi: [10.1086/523929](https://doi.org/10.1086/523929)
- Perley, D. A., Bloom, J. S., Klein, C. R., et al. 2010, *MNRAS*, 406, 2473, doi: [10.1111/j.1365-2966.2010.16772.x](https://doi.org/10.1111/j.1365-2966.2010.16772.x)
- Perley, D. A., Morgan, A. N., Updike, A., et al. 2011, *AJ*, 141, 36, doi: [10.1088/0004-6256/141/2/36](https://doi.org/10.1088/0004-6256/141/2/36)
- Perley, D. A., Cenko, S. B., Corsi, A., et al. 2014, *ApJ*, 781, 37, doi: [10.1088/0004-637X/781/1/37](https://doi.org/10.1088/0004-637X/781/1/37)
- Perna, R., & Lazzati, D. 2002, *ApJ*, 580, 261, doi: [10.1086/343081](https://doi.org/10.1086/343081)
- Perna, R., Lazzati, D., & Fiore, F. 2003, *ApJ*, 585, 775, doi: [10.1086/346109](https://doi.org/10.1086/346109)
- Peterson, B. M. 1997, *An Introduction to Active Galactic Nuclei*
- Pian, E., Mazzali, P. A., Masetti, N., et al. 2006, *Nature*, 442, 1011, doi: [10.1038/nature05082](https://doi.org/10.1038/nature05082)
- Piran, T. 2004, *Reviews of Modern Physics*, 76, 1143, doi: [10.1103/RevModPhys.76.1143](https://doi.org/10.1103/RevModPhys.76.1143)
- Piranomonte, S., Ward, P. A., Fiore, F., et al. 2008, *Astronomy and Astrophysics*, 492, 775
- Price, P. A., Harrison, F. A., Galama, T. J., et al. 2001, *ApJL*, 549, L7, doi: [10.1086/319152](https://doi.org/10.1086/319152)
- Prochaska, J. X., Shiode, J., Bloom, J. S., et al. 2008, GRB Coordinates Network, 7849, 1
- Rau, A., Savaglio, S., Krühler, T., et al. 2010, *The Astrophysical Journal*, 720, 862
- Resmi, L., Ishwara-Chandra, C. H., Castro-Tirado, A. J., et al. 2005, *A&A*, 440, 477, doi: [10.1051/0004-6361:20041642](https://doi.org/10.1051/0004-6361:20041642)
- Resmi, L., Misra, K., Jóhannesson, G., et al. 2012, *MNRAS*, 427, 288, doi: [10.1111/j.1365-2966.2012.21713.x](https://doi.org/10.1111/j.1365-2966.2012.21713.x)
- Rhoads, J. E., & Fruchter, A. S. 2001, *ApJ*, 546, 117, doi: [10.1086/318246](https://doi.org/10.1086/318246)
- Roming, P. W. A., Koch, T. S., Oates, S. R., et al. 2017, ArXiv e-prints. <https://arxiv.org/abs/1701.03713>
- Rykoff, E. S., Mangano, V., Yost, S. A., et al. 2006, *ApJL*, 638, L5, doi: [10.1086/501007](https://doi.org/10.1086/501007)
- Rykoff, E. S., Aharonian, F., Akerlof, C. W., et al. 2009, *ApJ*, 702, 489, doi: [10.1088/0004-637X/702/1/489](https://doi.org/10.1088/0004-637X/702/1/489)
- Sagar, R., Mohan, V., Pandey, S. B., et al. 2000, *Bulletin of the Astronomical Society of India*, 28, 499
- Sahu, K. C., Vreeswijk, P., Bakos, G., et al. 2000, *ApJ*, 540, 74, doi: [10.1086/309340](https://doi.org/10.1086/309340)
- Sari, R., Piran, T., & Narayan, R. 1998, *The Astrophysical Journal*, 497, L17
- Schady, P., Krühler, T., Greiner, J., et al. 2015, *Astronomy & Astrophysics*, 579, A126
- Schlafly, E. F., & Finkbeiner, D. P. 2011, *ApJ*, 737, 103, doi: [10.1088/0004-637X/737/2/103](https://doi.org/10.1088/0004-637X/737/2/103)
- Schulze, S., Malesani, D., Cucchiara, A., et al. 2014, *A&A*, 566, A102, doi: [10.1051/0004-6361/201423387](https://doi.org/10.1051/0004-6361/201423387)
- Shen, R., Kumar, P., & Robinson, E. L. 2006, *Monthly Notices of the Royal Astronomical Society*, 371, 1441
- Shin, M.-S., Berger, E., Penprase, B. E., et al. 2006, ArXiv Astrophysics e-prints

- Šimon, V., Pizzichini, G., & Hudec, R. 2013, Gamma-ray Bursts: 15 Years of GRB Afterglows. Edited by A. J. Castro-Tirado, 61, 271
- Sokolov, V. V., Kopylov, A. I., Zharikov, S. V., et al. 1998, *A&A*, 334, 117
- Sokolov, V. V., Zharikov, S. V., Baryshev, Y. V., et al. 1999, *A&A*, 344, 43
- Sollerman, J., Jaunsen, A. O., Fynbo, J. P. U., et al. 2006, *A&A*, 454, 503, doi: [10.1051/0004-6361:20065226](https://doi.org/10.1051/0004-6361:20065226)
- Sparre, M., Sollerman, J., Fynbo, J. P. U., et al. 2011, *ApJL*, 735, L24, doi: [10.1088/2041-8205/735/1/L24](https://doi.org/10.1088/2041-8205/735/1/L24)
- Starling, R. L. C., Wijers, R. A. M. J., Wiersema, K., et al. 2007, *ApJ*, 661, 787, doi: [10.1086/511953](https://doi.org/10.1086/511953)
- Stratta, G., Fiore, F., Antonelli, L. A., Piro, L., & De Pasquale, M. 2004, *ApJ*, 608, 846, doi: [10.1086/420836](https://doi.org/10.1086/420836)
- Stratta, G., Gendre, B., Atteia, J. L., et al. 2013, *ApJ*, 779, 66, doi: [10.1088/0004-637X/779/1/66](https://doi.org/10.1088/0004-637X/779/1/66)
- Tanvir, N. R., & Ball, J. 2012, GRB Coordinates Network, 3532, 1
- Tanvir, N. R., Wiersema, K., Levan, A. J., et al. 2012, GRB Coordinates Network, 3441, 1
- Thöne, C. C., Greiner, J., Savaglio, S., & Jehin, E. 2007, *ApJ*, 671, 628, doi: [10.1086/522558](https://doi.org/10.1086/522558)
- Thöne, C. C., Kann, D. A., Jóhannesson, G., et al. 2010, *A&A*, 523, A70, doi: [10.1051/0004-6361/200810340](https://doi.org/10.1051/0004-6361/200810340)
- Thöne, C. C., Campana, S., Lazzati, D., et al. 2011, *MNRAS*, 414, 479, doi: [10.1111/j.1365-2966.2011.18408.x](https://doi.org/10.1111/j.1365-2966.2011.18408.x)
- Torii, K., Kato, T., Yamaoka, H., et al. 2003, *ApJL*, 597, L101, doi: [10.1086/379846](https://doi.org/10.1086/379846)
- Toy, V. L., Cenko, S. B., Silverman, J. M., et al. 2016, *ApJ*, 818, 79, doi: [10.3847/0004-637X/818/1/79](https://doi.org/10.3847/0004-637X/818/1/79)
- Uemura, M., Kato, T., Ishioka, R., & Yamaoka, H. 2003, *PASJ*, 55, L31, doi: [10.1093/pasj/55.3.L31](https://doi.org/10.1093/pasj/55.3.L31)
- Uhm, Z. L., & Zhang, B. 2014, *ApJ*, 780, 82, doi: [10.1088/0004-637X/780/1/82](https://doi.org/10.1088/0004-637X/780/1/82)
- Ukwatta, T. N., Sonbas, E., Gehrels, N., et al. 2011, GRB Coordinates Network, 1715, 1
- Updike, A. C., Haislip, J. B., Nysewander, M. C., et al. 2008, *ApJ*, 685, 361, doi: [10.1086/590236](https://doi.org/10.1086/590236)
- Šimon, V., Hudec, R., & Pizzichini, G. 2004, *A&A*, 427, 901, doi: [10.1051/0004-6361:20041548](https://doi.org/10.1051/0004-6361:20041548)
- Šimon, V., Hudec, R., Pizzichini, G., & Masetti, N. 2001, *A&A*, 377, 450, doi: [10.1051/0004-6361:20011158](https://doi.org/10.1051/0004-6361:20011158)
- van Paradijs, J., Groot, P. J., Galama, T., et al. 1997, *Nature*, 386, 686, doi: [10.1038/386686a0](https://doi.org/10.1038/386686a0)
- Varela, K., van Eerten, H., Greiner, J., et al. 2016, *Astronomy & Astrophysics*, 589, A37
- Vergani, S. D., Flores, H., Covino, S., et al. 2011, *Astronomy & Astrophysics*, 535, A127
- Vestrand, W. T., Wren, J. A., Panaiteescu, A., et al. 2014, *Science*, 343, 38
- Virgili, F. J., Mundell, C. G., Pal'shin, V., et al. 2013, *ApJ*, 778, 54, doi: [10.1088/0004-637X/778/1/54](https://doi.org/10.1088/0004-637X/778/1/54)
- Volnova, A., Pozanenko, A., Korobtsev, I., & Elunko, E. 2011, GRB Coordinates Network, 1742, 1
- Volnova, A. A., Pruzhinskaya, M. V., Pozanenko, A. S., et al. 2017, *MNRAS*, 467, 3500, doi: [10.1093/mnras/stw3297](https://doi.org/10.1093/mnras/stw3297)
- Vreeswijk, P., Fynbo, J., & Melandri, A. 2011, GRB Coordinates Network, 2648, 1
- Vreeswijk, P. M., Fruchter, A., Kaper, L., et al. 2001, *ApJ*, 546, 672, doi: [10.1086/318308](https://doi.org/10.1086/318308)
- Vreeswijk, P. M., Ledoux, C., Smette, A., et al. 2007, *A&A*, 468, 83, doi: [10.1051/0004-6361:20066780](https://doi.org/10.1051/0004-6361:20066780)
- Vreeswijk, P. M., Ledoux, C., Raassen, A. J. J., et al. 2013, *A&A*, 549, A22, doi: [10.1051/0004-6361/201219652](https://doi.org/10.1051/0004-6361/201219652)
- Wang, X.-G., Zhang, B., Liang, E.-W., et al. 2015, *ApJS*, 219, 9, doi: [10.1088/0067-0049/219/1/9](https://doi.org/10.1088/0067-0049/219/1/9)
- Waxman, E., & Draine, B. T. 2000, *The Astrophysical Journal*, 537, 796
- Wiersema, K., Curran, P. A., Krühler, T., et al. 2012, *Monthly Notices of the Royal Astronomical Society*, 426, 2
- Woosley, S. E., & Bloom, J. S. 2006, *ARA&A*, 44, 507, doi: [10.1146/annurev.astro.43.072103.150558](https://doi.org/10.1146/annurev.astro.43.072103.150558)
- Woźniak, P. R., Vestrand, W. T., Panaiteescu, A. D., et al. 2009, *ApJ*, 691, 495, doi: [10.1088/0004-637X/691/1/495](https://doi.org/10.1088/0004-637X/691/1/495)
- Woźniak, P. R., Vestrand, W. T., Panaiteescu, A. D., et al. 2009, *The Astrophysical Journal*, 691, 495
- Wren, J., Vestrand, W. T., Woźniak, P., & Davis, H. 2010, in *Proc. SPIE*, Vol. 7737, Observatory Operations: Strategies, Processes, and Systems III, 773723

- Wu, X. F., Dai, Z. G., Huang, Y. F., & Lu, T. 2003, Monthly Notice of the Royal Astronomical Society, 342, 1131
- Xin, L.-P., Liang, E.-W., Wei, J.-Y., et al. 2011, MNRAS, 410, 27, doi: [10.1111/j.1365-2966.2010.17419.x](https://doi.org/10.1111/j.1365-2966.2010.17419.x)
- Xu, D., Starling, R. L. C., Fynbo, J. P. U., et al. 2009, ApJ, 696, 971, doi: [10.1088/0004-637X/696/1/971](https://doi.org/10.1088/0004-637X/696/1/971)
- Xu, D., de Ugarte Postigo, A., Leloudas, G., et al. 2013, ApJ, 776, 98, doi: [10.1088/0004-637X/776/2/98](https://doi.org/10.1088/0004-637X/776/2/98)
- Yang, B., Jin, Z.-P., Li, X., et al. 2015, Nature Communications, 6, 7323, doi: [10.1038/ncomms8323](https://doi.org/10.1038/ncomms8323)
- Yost, S. A., Swan, H. F., Rykoff, E. S., et al. 2007, ApJ, 657, 925, doi: [10.1086/510896](https://doi.org/10.1086/510896)
- Yuan, F., Schady, P., Racusin, J. L., et al. 2010, The Astrophysical Journal, 711, 870
- Zafar, T., Watson, D., Fynbo, J. P. U., et al. 2011, A&A, 532, A143, doi: [10.1051/0004-6361/201116663](https://doi.org/10.1051/0004-6361/201116663)
- Zeh, A., Klose, S., & Kann, D. A. 2006, ApJ, 637, 889, doi: [10.1086/498442](https://doi.org/10.1086/498442)
- Zhang, B. 2007, Chinese Journal of Astronomy and Astrophysics, 7, 1
- Zhang, B., Fan, Y. Z., Dyks, J., et al. 2006, ApJ, 642, 354, doi: [10.1086/500723](https://doi.org/10.1086/500723)
- Zhang, B., Kobayashi, S., & Mészáros, P. 2003, ApJ, 595, 950, doi: [10.1086/377363](https://doi.org/10.1086/377363)
- Zhang, B., & Mészáros, P. 2004, International Journal of Modern Physics A, 19, 2385
- Zhao, X. H., Bai, J. M., & Mao, J. 2011, GRB Coordinates Network, 1733, 1
- Zharikov, S. V., Sokolov, V. V., & Baryshev, Y. V. 1998, A&A, 337, 356
- Ziaeepour, H., Holland, S. T., Boyd, P. T., et al. 2008, MNRAS, 385, 453, doi: [10.1111/j.1365-2966.2008.12859.x](https://doi.org/10.1111/j.1365-2966.2008.12859.x)

APPENDIX

Table 7. Color Indices and Their Relation Spectral Indices for the Golden Sample

GRB	Time (ks)	$g-r$	β_o^{CI} (g-r)	Time (ks)	$r-i$	β_o^{CI} (r-i)	Time (ks)	$i-z$	β_o^{CI} (i-z)	Time (ks)	$J-H$	β_o^{CI} (J-H)	Time (ks)	$H-K_s$	β_o^{CI} (H-K _s)
071025	0.175	-0.38±0.89	-1.27±2.97	0.175	1.29±0.87	4.02±2.73
071025	0.210	-0.06±0.25	-0.19±0.83	0.210	0.60±0.28	1.87±0.87
071025	0.246	0.29±0.22	0.96±0.72	0.246	0.64±0.20	2.01±0.62
071025	0.282	0.39±0.17	1.31±0.58	0.282	0.49±0.16	1.54±0.49
071025	0.318	0.40±0.19	1.34±0.63	0.318	0.45±0.18	1.42±0.56
071025	0.355	0.22±0.17	0.73±0.56	0.355	0.53±0.18	1.67±0.55
071025	0.391	0.23±0.16	0.78±0.54	0.391	0.52±0.16	1.64±0.49
071025	0.427	0.39±0.17	1.28±0.58	0.427	0.66±0.16	2.07±0.51
071025	0.463	0.20±0.13	0.66±0.42	0.463	0.43±0.13	1.36±0.41
071025	0.499	0.18±0.12	0.59±0.39	0.499	0.73±0.11	2.28±0.36
071025	0.554	0.22±0.09	0.73±0.30	0.554	0.60±0.09	1.86±0.28
071025	0.626	0.31±0.11	1.03±0.36	0.626	0.42±0.11	1.30±0.33
071025	0.698	0.24±0.10	0.79±0.33	0.698	0.51±0.10	1.58±0.31
071025	0.771	0.20±0.08	0.66±0.27	0.771	0.32±0.09	0.99±0.29
071025	0.844	0.21±0.12	0.71±0.40	0.844	0.55±0.13	1.73±0.39
071025	0.917	0.08±0.12	0.28±0.39	0.917	0.57±0.12	1.77±0.38
071025	0.989	0.27±0.11	0.91±0.38	0.989	0.44±0.12	1.38±0.38
071025	1.08	0.28±0.13	0.95±0.44	1.08	0.50±0.13	1.57±0.40
071025	1.19	0.41±0.10	1.37±0.33	1.19	0.45±0.10	1.41±0.30
071025	1.30	0.17±0.11	0.56±0.37	1.30	0.51±0.12	1.58±0.37
071025	1.41	0.20±0.09	0.65±0.30	1.41	0.58±0.10	1.83±0.31
071025	1.52	0.22±0.08	0.74±0.25	1.52	0.41±0.09	1.29±0.27
071025	1.62	0.11±0.08	0.35±0.27	1.62	0.34±0.10	1.06±0.30
071025	1.73	0.16±0.08	0.54±0.25	1.73	0.42±0.09	1.32±0.29
071025	1.84	0.13±0.07	0.44±0.25	1.84	0.38±0.09	1.18±0.28
071025	1.95	0.09±0.08	0.31±0.27	1.95	0.42±0.10	1.33±0.32
071025	2.06	0.13±0.09	0.43±0.30	2.06	0.49±0.11	1.53±0.33
071025	2.17	0.25±0.09	0.84±0.30	2.17	0.29±0.11	0.89±0.35
071025	2.28	0.23±0.10	0.78±0.34	2.28	0.38±0.12	1.18±0.37
071025	2.39	0.27±0.09	0.89±0.31	2.39	0.50±0.11	1.57±0.34
071025	2.49	0.11±0.11	0.36±0.35	2.49	0.49±0.13	1.54±0.40
071025	2.60	0.04±0.12	0.12±0.40	2.60	0.30±0.15	0.94±0.47
071025	2.71	0.20±0.12	0.67±0.41	2.71	0.48±0.15	1.52±0.46
071025	2.86	0.28±0.13	0.92±0.42	2.86	0.47±0.14	1.47±0.45
071025	3.08	0.19±0.10	0.62±0.33	3.08	0.58±0.11	1.83±0.36
071025	3.35	0.11±0.11	0.35±0.38	3.35	0.50±0.14	1.57±0.43
071025	3.66	0.29±0.11	0.95±0.37	3.66	0.46±0.13	1.43±0.41
071025	10.8	-0.12±0.27	-0.41±0.91	10.8	0.57±0.32	1.79±1.00
071025	14.9	0.27±0.34	0.91±1.12	14.9	0.35±0.41	1.09±1.27
071025	0.286	0.18±0.07	0.61±0.25	0.286	0.36±0.09	1.12±0.29
071031	0.396	0.66±0.02	2.20±0.08	0.396	1.16±0.12	0.24±0.02	0.396	0.11±0.05	0.59±0.25	0.396	0.23±0.06	0.75±0.20	0.334	0.31±0.08	0.96±0.26
071031	0.621	0.72±0.03	2.41±0.09	0.507	0.21±0.01	0.99±0.06	0.396	0.10±0.04	0.55±0.20	0.396	0.23±0.06	0.75±0.20	0.334	0.31±0.08	0.96±0.26

Table 7 continued on next page

Table 7 (continued)

GRB	Time	$g-r$	β_o^{CI}	Time	$r-i$	β_o^{CI}	Time	$i-z$	β_o^{CI}	Time	$J-H$	β_o^{CI}	Time	$H-K_s$	β_o^{CI}
	(ks)	(g-r)	(ks)		(r-i)	(ks)		(i-z)	(ks)		(J-H)	(ks)		(H-K _s)	(H-K _s)
071031	0.821	0.67±0.02	2.23±0.06	0.621	0.15±0.03	0.70±0.15	0.507	0.12±0.02	0.64±0.10	0.415	0.21±0.04	0.69±0.12	0.415	0.31±0.06	0.98±0.18
071031	1.02	0.68±0.02	2.26±0.08	0.821	0.23±0.02	1.12±0.12	0.621	0.11±0.02	0.59±0.10	0.448	0.27±0.05	0.90±0.16	0.448	0.38±0.07	1.17±0.22
071031	1.23	0.67±0.02	2.23±0.06	1.02	0.23±0.02	1.08±0.12	0.821	0.14±0.02	0.73±0.13	0.499	0.19±0.05	0.64±0.16	0.499	0.35±0.08	1.09±0.24
071031	1.84	0.63±0.02	2.12±0.08	1.23	0.22±0.02	1.04±0.09	1.02	0.12±0.02	0.64±0.13	0.531	0.23±0.07	0.78±0.22	0.531	0.33±0.06	1.04±0.18
071031	2.02	0.65±0.02	2.17±0.08	1.43	0.23±0.01	1.08±0.06	1.23	0.17±0.02	0.92±0.13	0.557	0.17±0.06	0.58±0.21	0.557	0.28±0.06	0.87±0.20
071031	2.21	0.63±0.02	2.09±0.06	1.84	0.21±0.02	0.99±0.12	1.43	0.14±0.01	0.73±0.06	0.759	0.23±0.08	0.78±0.27	0.611	0.35±0.07	1.09±0.21
071031	2.43	0.64±0.02	2.14±0.08	2.02	0.18±0.02	0.87±0.09	1.84	0.15±0.04	0.78±0.20	0.795	0.12±0.06	0.40±0.19	0.640	0.35±0.07	1.09±0.23
071031	2.63	0.65±0.05	2.17±0.17	2.21	0.22±0.02	1.04±0.09	2.02	0.10±0.02	0.56±0.10	0.887	0.27±0.04	0.90±0.14	0.671	0.30±0.07	0.93±0.23
071031	2.97	0.64±0.05	2.14±0.16	2.43	0.20±0.02	0.95±0.12	2.21	0.11±0.04	0.59±0.23	0.929	0.17±0.06	0.58±0.20	0.795	0.34±0.06	1.07±0.19
071031	3.21	0.59±0.03	1.97±0.10	2.63	0.18±0.07	0.87±0.32	2.43	0.13±0.02	0.69±0.13	0.958	0.21±0.04	0.69±0.13	0.833	0.35±0.06	1.09±0.17
071031	3.31	0.62±0.05	2.06±0.16	2.97	0.20±0.06	0.95±0.27	2.63	0.13±0.08	0.63±0.42	1.00	0.24±0.04	0.81±0.14	0.860	0.39±0.06	1.23±0.19
071031	3.42	0.62±0.09	2.06±0.29	3.12	0.15±0.03	0.70±0.15	2.75	0.09±0.02	0.44±0.13	1.04	0.19±0.04	0.64±0.14	0.887	0.30±0.06	0.93±0.20
071031	3.64	0.63±0.03	2.12±0.10	3.21	0.17±0.02	0.83±0.12	2.84	0.07±0.04	0.37±0.23	1.07	0.16±0.04	0.55±0.14	0.929	0.38±0.06	1.17±0.19
071031	3.81	0.63±0.03	2.12±0.10	3.31	0.20±0.03	0.95±0.15	2.97	0.17±0.07	0.87±0.39	1.08	0.31±0.04	1.04±0.13	1.00	0.39±0.05	1.23±0.15
071031	4.25	0.62±0.08	2.06±0.27	3.42	0.17±0.06	0.83±0.30	3.12	0.12±0.07	0.64±0.38	1.12	0.22±0.04	0.72±0.13	1.04	0.31±0.06	0.96±0.20
071031	4.45	0.66±0.02	2.20±0.06	3.64	0.15±0.02	0.70±0.12	3.21	0.11±0.03	0.59±0.17	1.17	0.21±0.04	0.69±0.13	1.08	0.31±0.06	0.96±0.17
071031	4.66	0.63±0.03	2.09±0.10	3.81	0.14±0.02	0.66±0.12	3.31	0.09±0.04	0.46±0.23	1.21	0.15±0.06	0.49±0.21	1.12	0.25±0.06	0.77±0.20
071031	4.81	0.63±0.02	2.22±0.08	4.25	0.17±0.02	0.79±0.12	3.42	0.14±0.10	0.73±0.54	1.27	0.21±0.04	0.69±0.14	1.17	0.29±0.06	0.90±0.17
071031	5.04	0.61±0.02	2.03±0.08	4.45	0.11±0.04	0.54±0.19	3.64	0.13±0.04	0.69±0.20	1.29	0.12±0.06	0.40±0.20	1.23	0.39±0.07	1.23±0.21
071031	5.28	0.58±0.02	1.94±0.08	4.66	0.17±0.03	0.83±0.15	3.81	0.09±0.02	0.46±0.13	1.33	0.26±0.06	0.87±0.19	1.27	0.22±0.06	0.68±0.20
071031	5.45	0.61±0.02	2.03±0.06	4.81	0.15±0.02	0.70±0.12	3.99	0.17±0.03	0.87±0.17	1.37	0.26±0.04	0.87±0.13	1.29	0.39±0.06	1.23±0.19
071031	5.62	0.60±0.02	2.00±0.06	5.04	0.21±0.02	0.99±0.12	4.25	0.08±0.03	0.41±0.17	1.39	0.12±0.04	0.40±0.14	1.33	0.33±0.06	1.04±0.17
071031	5.88	0.62±0.02	2.06±0.08	5.28	0.17±0.02	0.79±0.12	4.45	0.14±0.06	0.73±0.33	1.43	0.16±0.06	0.52±0.19	1.37	0.33±0.06	1.04±0.20
071031	6.26	0.58±0.02	1.94±0.08	5.45	0.17±0.02	0.79±0.09	4.66	0.08±0.04	0.41±0.20	1.53	0.23±0.04	0.78±0.14	1.39	0.28±0.06	0.87±0.20
071031	6.46	0.62±0.02	2.06±0.06	5.62	0.17±0.02	0.79±0.09	4.81	0.10±0.04	0.50±0.20	1.78	0.20±0.04	0.66±0.14	1.43	0.43±0.06	1.34±0.20
071031	6.66	0.58±0.02	1.94±0.08	5.88	0.13±0.02	0.62±0.12	5.04	0.06±0.04	0.32±0.20	1.87	0.20±0.05	0.66±0.17	1.53	0.34±0.06	1.07±0.20
071031	6.87	0.57±0.02	1.88±0.06	6.26	0.16±0.02	0.75±0.12	5.28	0.06±0.04	0.32±0.20	2.05	0.25±0.03	0.84±0.10	1.78	0.26±0.07	0.82±0.22
071031	7.20	0.59±0.02	1.97±0.08	6.66	0.17±0.03	0.79±0.15	5.45	0.10±0.03	0.50±0.17	2.25	0.27±0.04	0.90±0.14	1.87	0.23±0.04	0.71±0.13
071031	7.43	0.63±0.02	2.12±0.06	6.87	0.16±0.03	0.75±0.15	5.62	0.06±0.02	0.32±0.13	2.47	0.14±0.04	0.46±0.13	2.05	0.30±0.04	0.93±0.12
071031	7.78	0.57±0.02	1.91±0.08	7.20	0.10±0.03	0.50±0.15	5.88	0.13±0.03	0.69±0.17	2.75	0.29±0.04	0.95±0.13	2.25	0.27±0.05	0.85±0.16
071031	8.15	0.59±0.02	1.97±0.08	7.43	0.13±0.02	0.62±0.09	6.26	0.13±0.02	0.69±0.13	2.88	0.27±0.05	0.90±0.17	2.47	0.40±0.06	1.26±0.17
071031	8.41	0.61±0.02	2.03±0.08	7.54	0.17±0.02	0.79±0.12	6.66	0.10±0.03	0.55±0.17	2.97	0.32±0.06	1.07±0.19	2.75	0.08±0.07	0.25±0.22
071031	8.54	0.60±0.02	2.00±0.08	7.78	0.16±0.02	0.75±0.12	6.87	0.14±0.04	0.73±0.19	3.21	0.23±0.06	0.78±0.18	2.97	0.15±0.11	0.47±0.34
071031	8.81	0.59±0.03	1.97±0.10	8.15	0.19±0.02	0.91±0.12	7.20	0.17±0.04	0.87±0.23	3.47	0.14±0.05	0.46±0.16	3.12	0.11±0.08	0.36±0.26
071031	8.95	0.62±0.02	2.06±0.08	8.41	0.10±0.02	0.50±0.12	7.43	0.14±0.03	0.73±0.17	3.64	0.16±0.06	0.55±0.19	3.21	0.31±0.07	0.96±0.21
071031	9.23	0.56±0.02	1.86±0.08	8.54	0.14±0.02	0.66±0.12	7.54	0.10±0.03	0.50±0.17	3.87	0.16±0.05	0.52±0.16	3.31	0.23±0.08	0.71±0.26
071031	9.37	0.55±0.02	1.77±0.06	8.81	0.17±0.03	0.79±0.15	7.78	0.10±0.03	0.55±0.17	4.06	0.21±0.05	0.69±0.16	3.64	0.31±0.07	0.96±0.23
071031	9.82	0.57±0.03	1.88±0.10	8.95	0.17±0.03	0.79±0.15	8.15	0.08±0.05	0.41±0.25	4.25	0.28±0.06	0.93±0.19	3.87	0.25±0.07	0.77±0.23
071031	10.3	0.57±0.02	1.88±0.06	9.37	0.22±0.02	1.04±0.12	8.41	0.14±0.03	0.73±0.17	4.45	0.30±0.06	0.98±0.19	4.06	0.27±0.07	0.85±0.22
071031	10.4	0.56±0.03	1.86±0.09	9.82	0.14±0.03	0.66±0.15	8.54	0.18±0.03	0.96±0.17	4.66	0.26±0.05	0.87±0.17	4.25	0.32±0.08	1.01±0.24
071031	10.8	0.59±0.02	1.97±0.06	10.4	0.20±0.03	0.95±0.15	8.81	0.13±0.02	0.69±0.13	5.04	0.19±0.06	0.64±0.20	4.45	0.13±0.07	0.41±0.21
071031	11.3	0.63±0.02	2.12±0.08	10.8	0.17±0.02	0.79±0.09	8.95	0.14±0.04	0.73±0.23	5.28	0.10±0.07	0.32±0.23	4.66	0.15±0.10	0.47±0.31
071031	11.8	0.59±0.02	1.97±0.06	11.3	0.14±0.02	0.66±0.12	9.37	0.10±0.04	0.50±0.20	5.45	0.26±0.06	0.87±0.19	5.04	0.31±0.13	0.96±0.40

Table 7 continued on next page

Table 7 (continued)

GRB	Time (ks)	$g-r$	β_o^{CI} (g-r)	Time (ks)	$r-i$	β_o^{CI} (r-i)	Time (ks)	$i-z$	β_o^{CI} (i-z)	Time (ks)	$J-H$	β_o^{CI} (J-H)	Time (ks)	$H-K_s$	β_o^{CI} (H-K _s)
071031	12.2	0.58±0.02	1.94±0.08	11.8	0.15±0.02	0.70±0.12	9.82	0.19±0.04	1.01±0.23	5.70	0.21±0.05	0.69±0.17	5.28	0.31±0.07	0.98±0.21
071031	13.6	0.63±0.03	2.09±0.10	12.2	0.17±0.02	0.79±0.12	10.1	0.11±0.04	0.59±0.20	5.88	0.14±0.09	0.46±0.30	5.45	0.28±0.06	0.87±0.17
071031	14.0	0.58±0.02	1.94±0.08	14.0	0.20±0.02	0.95±0.12	10.4	0.14±0.03	0.73±0.17	8.54	0.16±0.05	0.52±0.16	5.70	0.28±0.07	0.87±0.21
071031	14.5	0.60±0.02	2.00±0.08	15.9	0.17±0.02	0.83±0.12	10.8	0.14±0.03	0.73±0.17	13.8	0.16±0.05	0.52±0.16	5.88	0.30±0.09	0.93±0.29
071031	14.9	0.58±0.03	1.94±0.10	17.4	0.21±0.04	0.99±0.21	11.3	0.17±0.02	0.92±0.13	15.9	0.15±0.06	0.49±0.19	6.66	0.16±0.06	0.49±0.17
071031	15.4	0.63±0.03	2.09±0.10	18.0	0.18±0.04	0.87±0.21	11.8	0.17±0.02	0.92±0.13	17.7	0.11±0.07	0.37±0.22	7.54	0.18±0.06	0.58±0.19
071031	15.9	0.63±0.02	2.12±0.08	19.4	0.19±0.05	0.91±0.23	12.2	0.16±0.02	0.82±0.13	19.7	0.19±0.08	0.64±0.26	9.37	0.14±0.07	0.44±0.21
071031	16.4	0.64±0.04	2.14±0.14	20.4	0.23±0.04	1.12±0.21	15.9	0.16±0.02	0.82±0.13	21.7	0.18±0.09	0.61±0.30	10.1	0.18±0.06	0.55±0.18
071031	17.4	0.64±0.05	2.14±0.16	21.7	0.14±0.06	0.66±0.21	21.7	0.22±0.06	1.14±0.32	23.4	0.14±0.11	0.46±0.36	13.8	0.21±0.06	0.66±0.20
071031	18.0	0.57±0.04	1.88±0.14	23.8	0.11±0.05	0.54±0.23	23.8	0.21±0.06	1.10±0.33	25.7	0.26±0.12	0.87±0.40	15.9	0.19±0.07	0.60±0.21
071031	18.5	0.60±0.03	2.00±0.10	25.7	0.05±0.07	0.25±0.32	25.7	0.30±0.07	1.56±0.35	17.7	0.24±0.08	0.74±0.25
071031	19.4	0.70±0.06	2.32±0.19	19.7	0.16±0.10	0.49±0.31
071031	20.0	0.61±0.04	2.03±0.13	21.7	0.23±0.11	0.71±0.35
071031	20.4	0.58±0.05	1.94±0.17	25.7	0.18±0.14	0.55±0.43
071031	21.7	0.63±0.06	2.09±0.19
071031	23.8	0.59±0.06	1.97±0.21
071031	25.7	0.62±0.05	2.06±0.17
080413B	0.342	0.16±0.06	0.43±0.19	0.342	0.04±0.05	0.19±0.24	0.342	0.14±0.06	0.12±0.06	0.63±0.30
080413B	0.444	0.14±0.05	0.47±0.17	0.444	0.04±0.05	0.19±0.24	0.444	0.17±0.05	0.544	0.17±0.05	0.85±0.26
080413B	0.544	0.15±0.05	0.50±0.17	0.544	-0.02±0.04	-0.10±0.20	0.544	0.17±0.05	0.646	0.17±0.06	0.86±0.30
080413B	0.646	0.14±0.05	0.47±0.17	0.646	0.02±0.05	0.10±0.24	0.646	0.17±0.06	0.765	0.18±0.06	0.95±0.34
080413B	0.765	0.11±0.06	0.37±0.19	0.765	-0.01±0.06	-0.05±0.27	0.765	0.18±0.06	0.866	0.18±0.06	0.95±0.30
080413B	0.866	0.14±0.05	0.47±0.17	0.866	0.03±0.05	0.14±0.24	0.866	0.18±0.06	0.968	0.18±0.06	0.95±0.30
080413B	0.968	0.12±0.04	0.40±0.14	0.968	0.02±0.05	0.10±0.24	0.968	0.19±0.06	1.07	0.19±0.06	1.06±0.30
080413B	1.07	0.16±0.05	0.53±0.17	1.07	-0.03±0.05	-0.14±0.24	1.07	0.19±0.06	1.24	0.17±0.06	0.85±0.34
080413B	1.24	0.16±0.06	0.53±0.19	1.24	0.01±0.06	0.05±0.27	1.24	0.12±0.06	1.34	0.12±0.06	0.63±0.30
080413B	1.34	0.15±0.05	0.50±0.17	1.34	0.06±0.05	0.29±0.24	1.34	0.10±0.06	1.44	0.23±0.06	1.21±0.30
080413B	1.44	0.14±0.05	0.47±0.17	1.44	-0.02±0.05	-0.10±0.24	1.44	0.17±0.06	1.54	0.17±0.06	0.86±0.30
080413B	1.54	0.18±0.05	0.60±0.17	1.54	-0.01±0.05	-0.05±0.24	1.54	0.13±0.07	1.68	0.13±0.07	0.68±0.37
080413B	1.68	0.14±0.06	0.47±0.19	1.68	0.0±0.06	0.0±0.30	1.68	0.10±0.06	0.53±0.30
080413B	1.78	0.16±0.04	0.53±0.14	1.78	0.04±0.05	0.19±0.24	1.78	0.10±0.06	0.75±0.30
080413B	1.88	0.16±0.05	0.53±0.17	1.88	0.0±0.05	0.0±0.24	1.88	0.15±0.06	0.99	0.14±0.06	0.74±0.30
080413B	1.99	0.16±0.04	0.43±0.14	1.99	-0.01±0.05	-0.05±0.24	1.99	0.14±0.06	1.20	0.21±0.06	1.11±0.34
080413B	2.10	0.13±0.06	0.43±0.19	2.10	0.02±0.06	0.10±0.27	2.10	0.17±0.06	2.20	0.17±0.06	0.85±0.30
080413B	2.20	0.17±0.05	0.57±0.17	2.20	0.0±0.05	0.0±0.24	2.20	0.16±0.06	2.30	0.16±0.06	0.84±0.30
080413B	2.30	0.19±0.06	0.63±0.19	2.30	0.0±0.06	0.0±0.27	2.30	0.13±0.06	2.41	0.13±0.06	0.66±0.30
080413B	2.41	0.13±0.06	0.43±0.19	2.41	0.01±0.06	0.05±0.27	2.41	0.16±0.06	2.52	0.09±0.07	0.47±0.38
080413B	2.52	0.15±0.06	0.50±0.19	2.52	0.08±0.06	0.38±0.27	2.52	0.15±0.06	2.62	0.15±0.06	0.79±0.30
080413B	2.62	0.15±0.05	0.50±0.17	2.62	0.04±0.05	0.19±0.24	2.62	0.16±0.06	2.72	0.25±0.06	1.32±0.30
080413B	2.72	0.14±0.05	0.47±0.17	2.72	0.0±0.05	0.0±0.24	2.72	0.17±0.06	2.83	0.17±0.06	0.89±0.30
080413B	2.83	0.15±0.06	0.50±0.19	2.83	0.03±0.06	0.14±0.27	2.83	0.17±0.06	2.94	0.21±0.07	1.11±0.37
080413B	2.94	0.18±0.06	0.60±0.19	2.94	-0.03±0.06	-0.14±0.30	2.94	0.19±0.06	3.04	0.19±0.06	1.00±0.30
080413B	3.04	0.17±0.04	0.57±0.14	3.04	-0.04±0.05	-0.19±0.24	3.04	0.17±0.06	3.14	0.18±0.06	0.98±0.30

Table 7 continued on next page

Table 7 (*continued*)

GRB	Time (ks)	$g-r$	β_o^{CI} (g-r)	Time (ks)	$r-i$	β_o^{CI} (r-i)	Time (ks)	$i-z$	β_o^{CI} (i-z)	Time (ks)	$J-H$	β_o^{CI} (J-H)	Time (ks)	$H-K_s$	β_o^{CI} (H-K _s)
080413B	3.14	0.18±0.04	0.60±0.14	3.14	0.02±0.05	0.10±0.24	3.14	0.11±0.06	0.55±0.34
080413B	3.24	0.15±0.06	0.50±0.19	3.24	0.05±0.06	0.24±0.27	3.24	0.14±0.06	0.74±0.34
080413B	3.36	0.16±0.06	0.53±0.19	3.36	0.03±0.06	0.14±0.30	3.36	0.14±0.08	0.74±0.41
080413B	3.46	0.15±0.05	0.50±0.17	3.46	-0.02±0.05	-0.10±0.24	3.46	0.22±0.06	1.16±0.34
080413B	3.56	0.16±0.05	0.53±0.17	3.56	0.03±0.05	0.14±0.24	3.56	0.14±0.06	0.74±0.34
080413B	3.66	0.20±0.06	0.67±0.19	3.66	-0.03±0.06	-0.14±0.27	3.66	0.14±0.06	0.74±0.34
080413B	3.77	0.13±0.06	0.43±0.21	3.77	0.02±0.06	0.10±0.30	3.77	0.15±0.08	0.73±0.41
080413B	3.87	0.21±0.06	0.70±0.21	3.87	-0.10±0.06	-0.48±0.30	3.87	0.22±0.07	1.16±0.37
080413B	3.97	0.15±0.06	0.50±0.19	3.97	-0.05±0.06	-0.24±0.27	3.97	0.26±0.06	1.37±0.30
080413B	4.08	0.13±0.06	0.43±0.19	4.08	0.03±0.06	0.14±0.30	4.08	0.22±0.07	1.16±0.37
080413B	4.19	0.16±0.06	0.53±0.21	4.19	0.06±0.06	0.29±0.30	4.19	0.11±0.08	0.55±0.41
080413B	4.29	0.24±0.06	0.80±0.19	4.29	-0.02±0.06	-0.10±0.27	4.29	0.16±0.06	0.84±0.34
080413B	4.39	0.13±0.06	0.43±0.21	4.39	0.11±0.06	0.52±0.27	4.39	0.10±0.06	0.53±0.34
080413B	4.50	0.14±0.06	0.47±0.19	4.50	0.06±0.06	0.0±0.30	4.50	0.25±0.06	1.32±0.34
080413B	4.62	0.16±0.10	0.53±0.34	4.62	0.10±0.08	0.48±0.37	4.62	0.17±0.10	0.89±0.53
080413B	4.71	0.05±0.07	0.17±0.24	4.71	0.06±0.06	0.29±0.30	4.71	0.23±0.07	1.21±0.37
080413B	4.82	0.06±0.07	0.20±0.24	4.82	0.05±0.07	0.24±0.34	4.82	0.21±0.09	1.11±0.49
080413B	4.92	0.27±0.09	0.90±0.29	4.92	-0.05±0.09	-0.24±0.45	4.92	0.20±0.10	1.05±0.53
080413B	90.3	0.28±0.06	0.93±0.19	90.3	0.10±0.06	0.48±0.30	90.3	0.16±0.06	0.84±0.34
080413B	176	0.37±0.06	1.23±0.21	176	0.17±0.06	0.81±0.30	176	0.11±0.07	0.58±0.37
080413B	262	0.36±0.06	1.20±0.19	262	0.21±0.06	1.00±0.27	262	0.22±0.06	1.16±0.34
080413B	435	0.25±0.06	0.83±0.21	435	0.19±0.07	0.90±0.34	435	0.31±0.08	1.63±0.45
080413B	522	0.37±0.14	1.23±0.46	522	0.29±0.13	1.38±0.62	522	-0.05±0.16	-0.26±0.82
080413B	781	0.38±0.34	1.27±1.12	781	0.30±0.23	1.43±1.12	781	-0.29±0.31	-1.53±1.62
080710	0.417	0.44±0.04	1.48±0.13	0.417	0.28±0.04	1.31±0.18	0.417	0.23±0.04	1.19±0.20
080710	0.575	0.44±0.03	1.46±0.10	0.575	0.25±0.03	1.17±0.12	0.575	0.28±0.03	1.46±0.14
080710	0.746	0.43±0.02	1.45±0.06	0.746	0.22±0.02	1.04±0.09	0.746	0.25±0.02	1.33±0.12
080710	0.933	0.42±0.02	1.41±0.05	0.933	0.21±0.01	1.00±0.07	0.933	0.27±0.02	1.43±0.10
080710	1.07	0.42±0.01	1.41±0.03	1.07	0.25±0.01	1.19±0.05	1.07	0.24±0.01	1.25±0.07
080710	1.20	0.44±0.01	1.45±0.03	1.20	0.23±0.01	1.09±0.05	1.20	0.26±0.01	1.35±0.06
080710	1.34	0.39±0.01	1.30±0.03	1.34	0.25±0.01	1.19±0.04	1.34	0.25±0.01	1.31±0.06
080710	1.46	0.42±0.01	1.39±0.03	1.46	0.26±0.01	1.23±0.04	1.46	0.23±0.01	1.19±0.05
080710	1.56	0.41±0.01	1.36±0.03	1.56	0.24±0.01	1.16±0.04	1.56	0.26±0.01	1.35±0.05
080710	1.68	0.45±0.01	1.49±0.03	1.68	0.24±0.01	1.15±0.04	1.68	0.24±0.01	1.27±0.05
080710	1.79	0.42±0.01	1.42±0.03	1.79	0.26±0.01	1.24±0.04	1.79	0.24±0.01	1.26±0.06
080710	1.90	0.43±0.01	1.43±0.03	1.90	0.25±0.01	1.18±0.04	1.90	0.24±0.01	1.25±0.05
080710	2.01	0.41±0.01	1.37±0.03	2.01	0.25±0.01	1.19±0.04	2.01	0.25±0.01	1.31±0.04
080710	2.19	0.42±0.01	1.41±0.02	2.19	0.24±0.01	1.14±0.03	2.19	0.24±0.01	1.27±0.03
080710	2.38	0.44±0.01	1.47±0.02	2.38	0.24±0.01	1.13±0.03	2.38	0.24±0.01	1.25±0.03
080710	2.54	0.41±0.01	1.37±0.02	2.54	0.23±0.01	1.11±0.04	2.54	0.24±0.01	1.27±0.05
080710	2.64	0.42±0.01	1.42±0.03	2.64	0.23±0.01	1.10±0.04	2.64	0.25±0.01	1.32±0.05
080710	2.76	0.43±0.01	1.42±0.03	2.76	0.23±0.01	1.10±0.04	2.76	0.24±0.01	1.28±0.05
080710	2.83	0.43±0.01	1.42±0.03	2.83	0.23±0.01	1.11±0.04	2.83	0.24±0.01	1.27±0.05

Table 7 continued on next page

Table 7 (continued)

GRB	Time (ks)	$g-r$	β_o^{CI} (g-r)	Time (ks)	$r-i$	β_o^{CI} (r-i)	Time (ks)	$i-z$	β_o^{CI} (i-z)	Time (ks)	$J-H$	β_o^{CI} (J-H)	Time (ks)	$H-K_s$	β_o^{CI} (H-K _s)
080710	2.91	0.42±0.01	1.41±0.03	2.91	0.24±0.01	1.16±0.04	2.91	0.23±0.01	1.23±0.05
080710	2.99	0.41±0.01	1.37±0.03	2.99	0.24±0.01	1.14±0.04	2.99	0.23±0.01	1.23±0.05
080710	3.06	0.41±0.01	1.38±0.03	3.06	0.23±0.01	1.11±0.04	3.06	0.23±0.01	1.19±0.05
080710	3.13	0.41±0.01	1.36±0.03	3.13	0.23±0.01	1.12±0.04	3.13	0.23±0.01	1.24±0.06
080710	3.20	0.43±0.01	1.42±0.03	3.20	0.23±0.01	1.10±0.04	3.20	0.23±0.01	1.25±0.06
080710	3.32	0.42±0.01	1.40±0.03	3.32	0.23±0.01	1.10±0.04	3.32	0.24±0.01	1.26±0.06
080710	3.41	0.41±0.01	1.37±0.03	3.41	0.22±0.01	1.03±0.04	3.41	0.25±0.01	1.28±0.06
080710	4.16	0.40±0.01	1.35±0.02	4.16	0.23±0.01	1.08±0.03	4.16	0.23±0.01	1.18±0.04
080710	4.45	0.40±0.01	1.35±0.02	4.45	0.22±0.01	1.06±0.03	4.45	0.24±0.01	1.25±0.04
080710	4.66	0.40±0.01	1.32±0.02	4.66	0.23±0.01	1.09±0.03	4.66	0.23±0.01	1.26±0.04
080710	5.60	0.39±0.01	1.30±0.02	5.60	0.24±0.01	1.13±0.03	5.60	0.23±0.01	1.21±0.04
080710	5.80	0.41±0.01	1.36±0.02	5.80	0.21±0.01	1.01±0.03	5.80	0.24±0.01	1.28±0.04
080710	6.03	0.39±0.01	1.30±0.02	6.03	0.23±0.01	1.10±0.03	6.03	0.23±0.01	1.24±0.04
080710	6.22	0.39±0.01	1.31±0.02	6.22	0.22±0.01	1.06±0.03	6.22	0.24±0.01	1.27±0.04
080710	6.59	0.39±0.01	1.31±0.02	6.59	0.22±0.01	1.05±0.03	6.59	0.23±0.01	1.22±0.04
080710	6.79	0.38±0.01	1.26±0.02	6.79	0.23±0.01	1.12±0.03	6.79	0.23±0.01	1.19±0.04
080710	6.98	0.39±0.01	1.30±0.02	6.98	0.23±0.01	1.08±0.03	6.98	0.24±0.01	1.26±0.05
080710	7.28	0.39±0.01	1.30±0.02	7.28	0.23±0.01	1.08±0.03	7.28	0.23±0.01	1.23±0.05
080710	7.47	0.39±0.01	1.30±0.02	7.47	0.24±0.01	1.12±0.03	7.47	0.23±0.01	1.22±0.04
080710	7.66	0.42±0.01	1.39±0.02	7.66	0.24±0.01	1.15±0.03	7.66	0.23±0.01	1.19±0.04
080710	7.85	0.41±0.01	1.38±0.02	7.85	0.23±0.01	1.07±0.03	7.85	0.21±0.01	1.12±0.04
080710	8.04	0.41±0.01	1.36±0.02	8.04	0.22±0.01	1.05±0.03	8.04	0.23±0.01	1.22±0.04
080710	8.24	0.39±0.01	1.30±0.02	8.24	0.23±0.01	1.08±0.04	8.24	0.24±0.01	1.27±0.05
080710	8.43	0.39±0.01	1.30±0.02	8.43	0.23±0.01	1.08±0.03	8.43	0.21±0.01	1.28±0.04
080710	8.62	0.39±0.01	1.31±0.02	8.62	0.21±0.01	0.98±0.03	8.62	0.20±0.01	1.05±0.04
080710	8.81	0.38±0.01	1.25±0.03	8.81	0.21±0.01	1.02±0.03	8.81	0.24±0.01	1.25±0.04
080710	9.08	0.38±0.01	1.26±0.03	9.08	0.22±0.01	1.07±0.04	9.08	0.23±0.01	1.29±0.07
080710	9.27	0.37±0.01	1.24±0.02	9.27	0.22±0.01	1.06±0.03	9.27	0.22±0.01	1.15±0.05
080710	9.46	0.40±0.01	1.32±0.02	9.46	0.21±0.01	1.00±0.03	9.46	0.20±0.01	1.06±0.05
080710	9.65	0.39±0.01	1.30±0.02	9.65	0.24±0.01	1.13±0.03	9.65	0.22±0.01	1.14±0.04
080710	9.85	0.39±0.01	1.30±0.03	9.85	0.23±0.01	1.11±0.04	9.85	0.23±0.01	1.23±0.06
080710	10.0	0.39±0.01	1.31±0.02	10.0	0.22±0.01	1.04±0.03	10.0	0.22±0.01	1.16±0.04
080710	10.2	0.39±0.01	1.30±0.02	10.2	0.22±0.01	1.03±0.03	10.2	0.21±0.01	1.12±0.05
080710	10.4	0.40±0.01	1.33±0.03	10.4	0.24±0.01	1.13±0.03	10.4	0.22±0.01	1.16±0.05
080710	10.6	0.40±0.01	1.33±0.03	10.6	0.23±0.01	1.09±0.04	10.6	0.24±0.01	1.28±0.06
080710	10.8	0.40±0.01	1.33±0.02	10.8	0.23±0.01	1.07±0.03	10.8	0.20±0.01	1.06±0.04
080710	11.0	0.40±0.01	1.32±0.02	11.0	0.22±0.01	1.07±0.03	11.0	0.21±0.01	1.12±0.04
080710	11.2	0.39±0.01	1.30±0.03	11.2	0.23±0.01	1.10±0.04	11.2	0.23±0.01	1.23±0.04
080710	11.3	0.40±0.01	1.33±0.02	11.3	0.23±0.01	1.09±0.04	11.3	0.25±0.01	1.29±0.06
080710	11.6	0.40±0.01	1.34±0.02	11.6	0.23±0.01	1.10±0.04	11.6	0.20±0.01	1.06±0.05
080710	11.8	0.40±0.01	1.33±0.02	11.8	0.21±0.01	1.00±0.04	11.8	0.22±0.01	1.17±0.05
080710	12.0	0.40±0.01	1.34±0.04	12.0	0.22±0.01	1.06±0.06	12.0	0.23±0.01	1.23±0.06
080710	12.1	0.39±0.01	1.30±0.04	12.1	0.22±0.01	1.05±0.06	12.1	0.26±0.01	1.37±0.07

Table 7 continued on next page

Table 7 (*continued*)

GRB	Time	$g-r$	β_o^{CI}	Time	$r-i$	β_o^{CI}	Time	$i-z$	β_o^{CI}	Time	$J-H$	β_o^{CI}	Time	$H-K_s$	β_o^{CI}
	(ks)	(g-r)	(ks)		(r-i)	(ks)		(i-z)	(ks)		(J-H)	(ks)		(H-K _s)	(H-K _s)
080710	12.3	0.41±0.01	1.35±0.03	12.3	0.22±0.01	1.07±0.04	12.3	0.26±0.01	1.35±0.06
080710	12.4	0.41±0.01	1.35±0.04	12.4	0.24±0.01	1.16±0.05	12.4	0.21±0.01	1.10±0.07
080710	12.6	0.40±0.02	1.33±0.05	12.6	0.23±0.01	1.11±0.06	12.6	0.27±0.02	1.43±0.09
080710	26.7	0.45±0.08	1.50±0.26	26.7	0.23±0.09	1.10±0.41	26.7	0.20±0.13	1.05±0.69
080710	35.3	0.53±0.09	1.77±0.31	35.3	0.28±0.13	1.33±0.64	35.3	0.31±0.19	1.63±1.01
081007	1.12	-0.15±0.19	-0.49±0.65	1.12	0.05±0.14	0.26±0.68	1.12	0.03±0.12	0.16±0.63	1.12	0.42±0.06	1.40±0.19	1.12	0.18±0.06	0.57±0.18
081007	1.56	-0.14±0.19	-0.45±0.65	1.56	0.07±0.14	0.25±0.68	1.56	0.01±0.12	0.05±0.63	1.64	0.43±0.06	1.44±0.19	1.64	0.22±0.05	0.70±0.16
081007	2.16	-0.13±0.19	-0.42±0.65	2.16	0.05±0.14	0.26±0.68	2.16	0.02±0.11	0.11±0.60	2.25	0.45±0.06	1.50±0.19	2.25	0.21±0.05	0.67±0.16
081007	3.02	-0.05±0.19	-0.15±0.65	3.02	-0.02±0.14	-0.08±0.68	3.02	1E-3±0.12	0.01±0.63	3.02	0.50±0.07	1.67±0.24	3.02	0.16±0.06	0.51±0.20
081007	4.32	-0.02±0.19	-0.05±0.65	4.32	-0.02±0.14	-0.08±0.68	4.32	0.06±0.11	0.32±0.60	4.32	0.42±0.06	1.40±0.19	4.32	0.17±0.05	0.54±0.16
081007	6.13	-0.09±0.19	-0.29±0.65	6.13	0.05±0.14	0.26±0.68	6.13	1E-3±0.11	0.01±0.60	6.13	0.41±0.06	1.37±0.21	6.13	0.18±0.06	0.57±0.18
081007	7.95	-0.11±0.19	-0.35±0.65	7.95	0.01±0.14	0.07±0.68	7.95	-0.02±0.11	-0.10±0.60	7.95	0.44±0.06	1.47±0.21	7.95	0.18±0.06	0.57±0.20
081007	78.8	0.01±0.21	0.05±0.69	78.8	0.05±0.16	0.26±0.78	78.8	0.03±0.13	0.16±0.67	79.2	0.57±0.12	1.90±0.39	79.2	0.03±0.14	0.11±0.44
081007	329	-0.21±0.43	-0.69±1.45	329	0.01±0.39	0.07±1.85	329	0.02±0.40	0.11±2.08
081007	937	0.24±0.28	1.16±1.31	937	-0.27±0.34	-1.42±1.79
081007	1.37E3	-0.12±0.40	-0.55±1.92	1.63E3	0.12±0.45	0.64±2.35
081007	1.63E3	0.21±0.44	1.02±2.09	1.98E3	0.21±0.52	1.11±2.75
081007	1.98E3	-0.03±0.46	-0.12±2.17
081008	13.7	0.18±0.04	0.60±0.14	13.7	0.35±0.04	1.66±0.19	13.7	0.23±0.05	1.19±0.26	13.8	0.13±0.04	0.44±0.14	13.8	0.03±0.05	0.10±0.17
081008	13.8	0.17±0.03	0.56±0.10	13.8	0.34±0.03	1.61±0.13	13.8	0.21±0.04	1.12±0.18	14.4	0.14±0.04	0.47±0.14	14.4	0.01±0.05	0.03±0.15
081008	13.9	0.20±0.03	0.68±0.11	13.9	0.34±0.03	1.63±0.13	13.9	0.19±0.04	1.03±0.18	15.0	0.13±0.04	0.44±0.13	15.0	-0.03±0.05	-0.09±0.16
081008	14.0	0.17±0.03	0.58±0.10	14.0	0.33±0.03	1.59±0.14	14.0	0.19±0.04	1.00±0.18	15.7	0.20±0.04	0.66±0.12	15.7	0.01±0.05	0.04±0.14
081008	14.2	0.18±0.04	0.61±0.14	14.2	0.33±0.04	1.56±0.19	14.2	0.17±0.04	0.92±0.24	17.0	0.16±0.04	0.52±0.14	17.0	0.01±0.05	0.04±0.14
081008	14.3	0.14±0.03	0.45±0.10	14.3	0.32±0.03	1.50±0.16	14.3	0.19±0.04	0.99±0.21	18.8	0.18±0.04	0.62±0.12	18.8	0.02±0.04	0.05±0.13
081008	14.4	0.17±0.03	0.58±0.10	14.4	0.28±0.03	1.34±0.13	14.4	0.18±0.03	0.97±0.16	29.5	0.12±0.06	0.39±0.19	29.5	-0.03±0.07	-0.10±0.22
081008	14.5	0.16±0.03	0.52±0.10	14.5	0.33±0.03	1.56±0.14	14.5	0.19±0.03	1.02±0.16
081008	14.7	0.16±0.03	0.53±0.11	14.7	0.33±0.03	1.57±0.16	14.7	0.20±0.04	1.04±0.19
081008	14.9	0.13±0.03	0.43±0.11	14.9	0.35±0.03	1.67±0.14	14.9	0.20±0.03	1.04±0.16
081008	15.0	0.19±0.03	0.65±0.09	15.0	0.33±0.02	1.56±0.11	15.0	0.18±0.02	0.96±0.13
081008	15.2	0.19±0.02	0.63±0.08	15.2	0.31±0.03	1.47±0.13	15.2	0.19±0.03	1.02±0.14
081008	15.4	0.17±0.03	0.56±0.09	15.4	0.29±0.04	1.40±0.17	15.4	0.19±0.04	1.02±0.21
081008	15.6	0.18±0.02	0.61±0.08	15.6	0.32±0.03	1.53±0.13	15.6	0.19±0.03	0.99±0.15
081008	15.8	0.17±0.03	0.56±0.09	15.8	0.32±0.03	1.53±0.13	15.8	0.24±0.02	1.26±0.12
081008	16.0	0.21±0.02	0.70±0.08	16.0	0.28±0.03	1.31±0.12	16.0	0.20±0.03	1.05±0.13
081008	16.3	0.18±0.02	0.61±0.07	16.3	0.27±0.02	1.27±0.11	16.3	0.19±0.03	1.00±0.14
081008	16.7	0.22±0.02	0.73±0.07	16.7	0.29±0.02	1.38±0.10	16.7	0.25±0.02	1.29±0.12
081008	17.2	0.20±0.02	0.66±0.07	17.2	0.32±0.02	1.54±0.10	17.2	0.20±0.02	1.05±0.12
081008	17.6	0.20±0.02	0.66±0.08	17.6	0.31±0.02	1.48±0.10	17.6	0.21±0.02	1.08±0.12
081008	18.1	0.20±0.03	0.65±0.09	18.1	0.31±0.02	1.47±0.10	18.1	0.22±0.03	1.17±0.14
081008	18.5	0.18±0.02	0.62±0.07	18.5	0.31±0.02	1.48±0.10	18.5	0.18±0.02	0.94±0.12
081008	19.0	0.17±0.02	0.57±0.07	19.0	0.33±0.02	1.57±0.10	19.0	0.18±0.02	0.94±0.12
081008	19.4	0.19±0.02	0.65±0.07	19.4	0.34±0.02	1.60±0.10	19.4	0.17±0.02	0.87±0.12
081008	28.8	0.22±0.05	0.74±0.16	28.8	0.30±0.04	1.44±0.18	28.8	0.21±0.04	1.12±0.24

Table 7 continued on next page

Table 7 (continued)

GRB	Time	$g-r$	β_o^{CI}	Time	$r-i$	β_o^{CI}	Time	$i-z$	β_o^{CI}	Time	$J-H$	β_o^{CI}	Time	$H-K_s$	β_o^{CI}
	(ks)	(g-r)	(ks)		(r-i)	(ks)		(i-z)	(ks)		(J-H)	(ks)		(H-K _s)	(H-K _s)
081008	29.3	0.23±0.04	0.78±0.12	29.3	0.28±0.04	1.31±0.17	29.3	0.23±0.04	1.22±0.19
081008	29.7	0.22±0.04	0.73±0.13	29.7	0.34±0.03	1.63±0.14	29.7	0.22±0.03	1.18±0.17
081008	30.2	0.24±0.04	0.80±0.12	30.2	0.35±0.03	1.66±0.15	30.2	0.21±0.03	1.09±0.18
081008	1.88	0.41±0.30	1.98±1.41	1.88	0.13±0.29	0.71±1.51
081029	0.521	1.15±0.02	3.84±0.08	0.521	0.38±0.03	1.80±0.13	0.521	0.29±0.03	1.55±0.18	0.531	0.28±0.10	1.09±0.32	0.531	0.10±0.10	0.31±0.31
081029	0.629	1.14±0.03	3.81±0.09	0.629	0.38±0.03	1.80±0.15	0.629	0.26±0.03	1.35±0.16	0.636	0.18±0.11	0.76±0.37	0.636	0.02±0.13	0.06±0.39
081029	0.739	1.15±0.03	3.83±0.09	0.739	0.37±0.03	1.76±0.14	0.739	0.28±0.03	1.48±0.18	0.747	0.14±0.10	0.60±0.34	0.747	0.13±0.11	0.39±0.33
081029	0.849	1.16±0.02	3.85±0.06	0.849	0.36±0.03	1.71±0.12	0.972	0.28±0.04	1.45±0.20	0.857	0.17±0.07	0.71±0.22	0.857	0.18±0.09	0.57±0.27
081029	0.972	1.14±0.03	3.80±0.09	0.972	0.37±0.03	1.77±0.16	1.08	0.27±0.04	1.43±0.19	0.979	0.20±0.08	0.82±0.28	0.979	0.09±0.09	0.27±0.27
081029	1.08	1.13±0.03	3.76±0.09	1.08	0.38±0.03	1.81±0.15	1.19	0.29±0.03	1.54±0.18	1.08	0.23±0.10	0.91±0.33	1.08	0.20±0.10	0.62±0.30
081029	1.19	1.14±0.03	3.79±0.09	1.19	0.36±0.03	1.72±0.14	1.29	0.28±0.04	1.48±0.20	1.19	0.29±0.10	1.12±0.33	1.19	0.11±0.11	0.34±0.35
081029	1.29	1.15±0.02	3.84±0.08	1.29	0.37±0.03	1.75±0.15	1.44	0.27±0.03	1.41±0.15	1.30	0.29±0.08	1.11±0.27	1.30	0.10±0.10	0.32±0.31
081029	1.44	1.11±0.02	3.71±0.08	1.44	0.37±0.02	1.74±0.11	1.62	0.27±0.03	1.42±0.18	1.47	0.27±0.11	1.05±0.37	1.47	0.11±0.11	0.34±0.36
081029	1.62	1.14±0.02	3.78±0.08	1.62	0.36±0.03	1.73±0.13	1.81	0.26±0.02	1.36±0.13	1.65	0.29±0.10	1.11±0.33	1.65	0.05±0.11	0.15±0.33
081029	1.81	1.11±0.02	3.71±0.07	1.81	0.36±0.02	1.73±0.11	2.00	0.30±0.03	1.56±0.13	1.84	0.24±0.11	0.93±0.36	1.84	0.18±0.11	0.56±0.34
081029	2.00	1.12±0.02	3.74±0.07	2.00	0.35±0.02	1.65±0.10	2.21	0.28±0.03	1.46±0.17	2.02	0.06±0.08	0.35±0.27	2.02	0.24±0.09	0.74±0.28
081029	2.21	1.12±0.03	3.73±0.08	2.21	0.35±0.03	1.67±0.12	2.39	0.26±0.03	1.38±0.15	2.23	0.23±0.09	0.90±0.29	2.23	0.03±0.09	0.10±0.28
081029	2.39	1.13±0.02	3.78±0.06	2.39	0.37±0.02	1.78±0.10	2.58	0.25±0.03	1.32±0.17	2.41	0.20±0.08	0.81±0.28	2.41	0.14±0.09	0.44±0.27
081029	2.58	1.13±0.02	3.76±0.08	2.58	0.36±0.02	1.72±0.11	2.78	0.25±0.06	1.33±0.29	2.61	0.20±0.08	0.80±0.26	2.61	0.20±0.09	0.63±0.27
081029	2.78	1.13±0.02	3.76±0.08	2.78	0.35±0.02	1.67±0.11	3.55	0.27±0.04	1.43±0.20	2.81	0.16±0.08	0.68±0.26	2.81	0.23±0.08	0.73±0.24
081029	3.55	1.14±0.03	3.81±0.11	3.55	0.35±0.03	1.65±0.15	3.68	0.24±0.04	1.28±0.19	3.55	0.25±0.09	0.99±0.29	3.55	-0.02±0.10	-0.07±0.30
081029	3.68	1.13±0.03	3.76±0.10	3.68	0.39±0.03	1.85±0.15	3.79	0.26±0.03	1.38±0.18	3.69	0.09±0.07	0.45±0.22	3.69	0.30±0.11	0.93±0.34
081029	3.79	1.15±0.03	3.82±0.09	3.79	0.39±0.03	1.86±0.16	4.03	0.27±0.04	1.44±0.19	3.80	0.29±0.07	1.12±0.23	3.80	0.03±0.08	0.08±0.25
081029	4.03	1.15±0.03	3.84±0.09	4.03	0.38±0.03	1.83±0.15	4.14	0.26±0.04	1.36±0.19	4.04	0.25±0.13	0.97±0.42	4.04	0.38±0.14	1.20±0.42
081029	4.14	1.14±0.03	3.79±0.09	4.14	0.40±0.03	1.89±0.14	4.25	0.28±0.04	1.50±0.23	4.15	0.14±0.11	0.59±0.37	4.15	0.36±0.12	1.14±0.38
081029	4.25	1.17±0.02	3.91±0.08	4.25	0.39±0.03	1.86±0.16	4.37	0.29±0.05	1.54±0.24	4.26	0.21±0.10	0.85±0.32	4.26	-0.12±0.11	-0.38±0.35
081029	4.37	1.17±0.03	3.91±0.10	4.37	0.39±0.03	1.87±0.15	4.50	0.27±0.04	1.39±0.18	4.38	0.29±0.08	1.10±0.26	4.38	0.07±0.08	0.21±0.26
081029	4.50	1.15±0.03	3.83±0.09	4.50	0.41±0.03	1.94±0.13	4.61	0.29±0.04	1.54±0.21	4.51	0.27±0.11	1.06±0.35	4.51	0.17±0.12	0.54±0.36
081029	4.61	1.14±0.02	3.79±0.08	4.61	0.41±0.03	1.98±0.14	4.73	0.30±0.05	1.53±0.25	4.74	0.25±0.08	0.98±0.26	4.74	0.08±0.10	0.25±0.32
081029	4.73	1.19±0.02	3.96±0.08	4.73	0.41±0.03	1.94±0.15	4.85	0.30±0.04	1.56±0.23	4.85	0.33±0.06	1.24±0.19	4.85	0.14±0.09	0.44±0.28
081029	4.85	1.16±0.02	3.88±0.08	4.85	0.41±0.03	1.96±0.16	4.98	0.30±0.04	1.61±0.22	4.99	0.35±0.07	1.31±0.24	4.99	0.20±0.08	0.63±0.24
081029	5.09	1.17±0.03	3.90±0.10	5.09	0.42±0.03	2.00±0.15	5.09	0.28±0.04	1.48±0.19	5.10	0.30±0.08	1.14±0.28	5.10	0.25±0.09	0.79±0.29
081029	5.21	1.21±0.02	4.02±0.08	5.21	0.41±0.03	1.98±0.14	5.21	0.31±0.04	1.64±0.23	5.21	0.37±0.08	1.36±0.26	5.21	-0.01±0.09	-0.02±0.29
081029	5.65	1.19±0.03	3.96±0.11	5.74	0.44±0.03	2.08±0.15	5.30	0.30±0.04	1.61±0.22	5.31	0.34±0.08	1.27±0.27	5.31	0.05±0.09	0.16±0.28
081029	5.74	1.16±0.03	3.87±0.10	5.84	0.43±0.03	2.05±0.14	5.74	0.29±0.03	1.55±0.17	5.65	0.34±0.07	1.27±0.22	5.65	0.05±0.11	0.14±0.33
081029	5.94	1.20±0.03	4.00±0.09	5.94	0.41±0.03	1.95±0.15	5.84	0.31±0.04	1.61±0.22	5.75	0.27±0.05	1.04±0.18	5.75	0.33±0.08	1.02±0.25
081029	6.58	1.17±0.03	3.91±0.10	6.58	0.43±0.03	2.06±0.14	5.94	0.33±0.04	1.75±0.23	5.85	0.35±0.06	1.32±0.20	5.85	0.19±0.12	0.59±0.37
081029	6.69	1.18±0.03	3.93±0.09	6.69	0.43±0.03	2.06±0.14	6.58	0.31±0.04	1.62±0.20	5.94	0.32±0.06	1.22±0.20	5.94	0.12±0.09	0.37±0.27
081029	6.79	1.20±0.03	3.98±0.09	6.79	0.41±0.03	1.98±0.13	6.69	0.32±0.03	1.71±0.18	6.58	0.32±0.10	1.22±0.35	6.58	0.22±0.11	0.69±0.34
081029	6.91	1.19±0.03	3.95±0.10	6.91	0.42±0.03	2.01±0.14	6.79	0.33±0.03	1.72±0.18	6.70	0.20±0.13	0.81±0.42	6.70	0.35±0.13	1.10±0.39
081029	7.02	1.19±0.03	3.96±0.09	7.02	0.42±0.03	2.00±0.13	6.91	0.31±0.04	1.64±0.21	6.80	0.32±0.07	1.22±0.25	6.80	0.17±0.08	0.53±0.26
081029	7.12	1.19±0.03	3.97±0.09	7.12	0.42±0.03	2.02±0.14	7.02	0.28±0.04	1.46±0.19	6.91	0.35±0.08	1.33±0.27	6.91	0.16±0.09	0.49±0.27
081029	7.24	1.19±0.03	3.95±0.09	7.24	0.41±0.03	1.96±0.12	7.12	0.30±0.04	1.57±0.22	7.02	0.33±0.10	1.24±0.33	7.02	0.07±0.10	0.22±0.31

Table 7 continued on next page

Table 7 (*continued*)

GRB	Time	$g-r$	β_o^{CI}	Time	$r-i$	β_o^{CI}	Time	$i-z$	β_o^{CI}	Time	$J-H$	β_o^{CI}	Time	$H-K_s$	β_o^{CI}
	(ks)	(g-r)	(ks)		(r-i)	(ks)		(i-z)	(ks)		(J-H)	(ks)		(H-K _s)	(H-K _s)
081029	7.34	1.20±0.03	4.01±0.10	7.34	0.42±0.03	2.00±0.14	7.24	0.32±0.03	1.69±0.15	7.13	0.27±0.12	1.04±0.38	7.13	0.27±0.11	0.83±0.34
081029	8.06	1.20±0.02	3.98±0.06	8.06	0.41±0.02	1.96±0.10	7.34	0.31±0.04	1.62±0.23	7.24	0.32±0.12	1.20±0.40	7.24	0.13±0.11	0.39±0.35
081029	8.50	1.20±0.02	3.98±0.07	8.50	0.43±0.02	2.06±0.09	7.62	0.29±0.03	1.54±0.14	7.35	0.32±0.08	1.19±0.26	7.35	0.20±0.08	0.64±0.24
081029	8.94	1.16±0.02	3.87±0.05	8.94	0.43±0.02	2.06±0.09	8.06	0.31±0.02	1.62±0.12	7.63	0.29±0.06	1.11±0.19	7.63	0.19±0.06	0.58±0.20
081029	9.38	1.18±0.02	3.95±0.07	9.38	0.42±0.02	2.00±0.10	8.50	0.30±0.02	1.66±0.11	8.06	0.26±0.06	1.02±0.19	8.06	0.26±0.07	0.82±0.21
081029	9.82	1.18±0.02	3.93±0.07	9.82	0.41±0.02	1.97±0.11	8.94	0.30±0.03	1.55±0.14	8.51	0.27±0.06	1.06±0.21	8.51	0.19±0.06	0.60±0.18
081029	10.3	1.17±0.02	3.99±0.07	10.3	0.43±0.02	2.03±0.11	9.38	0.30±0.02	1.56±0.12	8.95	0.32±0.06	1.20±0.20	8.95	0.17±0.06	0.54±0.20
081029	10.7	1.16±0.02	3.87±0.07	10.7	0.42±0.02	2.00±0.10	9.82	0.30±0.02	1.59±0.12	9.39	0.32±0.06	1.20±0.20	9.39	0.17±0.07	0.53±0.21
081029	11.1	1.18±0.02	3.93±0.05	11.1	0.42±0.02	1.99±0.10	10.3	0.31±0.02	1.63±0.13	9.83	0.32±0.05	1.22±0.18	9.83	0.16±0.06	0.50±0.18
081029	11.6	1.17±0.02	3.88±0.07	11.6	0.43±0.02	2.04±0.10	10.7	0.31±0.03	1.63±0.14	10.3	0.27±0.06	1.06±0.19	10.3	0.15±0.07	0.47±0.21
081029	12.0	1.18±0.02	3.92±0.08	12.0	0.41±0.02	1.93±0.12	11.1	0.32±0.03	1.67±0.17	10.7	0.33±0.05	1.25±0.16	10.7	0.12±0.06	0.38±0.19
081029	12.5	1.17±0.02	3.90±0.08	12.5	0.42±0.02	1.98±0.11	11.6	0.30±0.03	1.53±0.14	11.1	0.30±0.05	1.16±0.17	11.1	0.13±0.06	0.41±0.18
081029	12.9	1.18±0.02	3.94±0.07	12.9	0.41±0.02	1.97±0.10	12.0	0.30±0.03	1.60±0.15	11.6	0.27±0.06	1.04±0.19	11.6	0.20±0.07	0.63±0.22
081029	13.4	1.16±0.02	3.87±0.07	13.4	0.41±0.02	1.98±0.10	12.5	0.30±0.03	1.55±0.14	12.0	0.26±0.06	1.00±0.19	12.0	0.16±0.07	0.51±0.22
081029	14.3	1.18±0.02	3.93±0.07	14.3	0.42±0.02	2.00±0.11	12.9	0.29±0.03	1.52±0.13	12.5	0.32±0.05	1.20±0.18	12.5	0.08±0.07	0.24±0.21
081029	14.7	1.17±0.02	3.89±0.07	14.7	0.40±0.02	1.91±0.10	13.4	0.31±0.03	1.63±0.15	12.9	0.28±0.06	1.09±0.21	12.9	0.15±0.07	0.46±0.21
081029	15.3	1.18±0.05	3.92±0.16	15.3	0.41±0.04	1.95±0.19	14.3	0.29±0.02	1.55±0.12	13.4	0.30±0.06	1.13±0.21	13.4	0.27±0.06	0.83±0.18
081029	16.3	1.18±0.02	3.92±0.06	16.3	0.42±0.02	2.01±0.11	14.7	0.30±0.03	1.57±0.15	14.3	0.32±0.06	1.21±0.19	14.3	0.11±0.07	0.35±0.23
081029	16.8	1.18±0.02	3.92±0.07	16.8	0.42±0.02	2.00±0.12	15.3	0.29±0.03	1.51±0.13	14.7	0.29±0.05	1.20±0.18	12.5	0.08±0.07	0.24±0.21
081029	17.2	1.17±0.02	3.89±0.07	17.2	0.42±0.03	2.01±0.13	16.3	0.30±0.03	1.59±0.17	15.3	0.33±0.08	1.24±0.26	15.3	0.15±0.10	0.48±0.30
081029	17.8	1.16±0.02	3.85±0.07	17.8	0.42±0.02	1.99±0.11	16.8	0.30±0.03	1.59±0.15	16.3	0.27±0.05	1.06±0.18	16.3	0.24±0.05	0.74±0.17
081029	18.3	1.18±0.02	3.92±0.07	18.3	0.43±0.02	2.06±0.11	17.2	0.29±0.03	1.53±0.17	16.8	0.24±0.06	0.94±0.20	16.8	0.18±0.08	0.56±0.24
081029	18.8	1.15±0.02	3.82±0.07	18.8	0.42±0.03	2.00±0.12	17.8	0.27±0.03	1.44±0.15	17.2	0.25±0.07	0.96±0.24	17.2	0.17±0.08	0.55±0.24
081029	19.3	1.17±0.02	3.89±0.06	19.3	0.41±0.03	1.95±0.13	18.3	0.28±0.03	1.47±0.16	17.8	0.34±0.07	1.29±0.25	17.8	0.11±0.08	0.59±0.23
081029	19.7	1.19±0.02	3.95±0.08	19.7	0.41±0.03	1.95±0.13	18.8	0.31±0.03	1.64±0.18	18.3	0.26±0.06	1.00±0.21	18.3	0.26±0.07	0.81±0.21
081029	20.3	1.13±0.02	3.78±0.06	20.3	0.43±0.02	2.04±0.11	19.3	0.28±0.04	1.45±0.19	18.8	0.23±0.09	0.92±0.29	18.8	0.26±0.09	0.81±0.29
081029	21.0	1.18±0.03	3.93±0.08	21.0	0.41±0.03	1.98±0.16	19.7	0.29±0.03	1.52±0.17	19.3	0.29±0.07	1.12±0.23	19.3	0.10±0.07	0.31±0.22
081029	82.3	1.20±0.09	4.01±0.29	82.3	0.33±0.07	1.55±0.33	20.3	0.29±0.03	1.52±0.18	19.7	0.29±0.07	1.12±0.23	19.7	0.20±0.07	0.61±0.23
081029	83.1	1.16±0.08	3.85±0.27	83.1	0.41±0.07	1.93±0.35	21.0	0.28±0.04	1.50±0.19	20.3	0.26±0.06	1.00±0.19	20.3	0.16±0.07	0.49±0.21
081029	92.0	1.29±0.11	4.29±0.36	92.0	0.41±0.07	1.93±0.35	82.3	0.26±0.10	1.37±0.50	21.0	0.29±0.07	1.10±0.24	21.0	0.13±0.08	0.40±0.25
081029	92.7	1.25±0.11	4.17±0.38	92.7	0.47±0.09	2.24±0.42	83.1	0.18±0.11	0.96±0.56	82.4	0.17±0.25	0.71±0.84
081029	108	1.01±0.18	3.37±0.60	108	0.17±0.19	0.81±0.90	92.0	0.04±0.11	0.19±0.59	83.1	-0.06±0.25	-0.07±0.82
081029	109	1.06±0.20	3.53±0.67	109	0.31±0.17	1.48±0.81	92.0	0.01±0.31	0.19±1.04
081029	168	0.07±0.20	0.33±0.94
090426	44.7	0.40±0.09	1.33±0.31	44.7	0.04±0.11	0.19±0.54	44.7	0.16±0.11	0.84±0.60
090426	45.5	0.41±0.08	1.37±0.28	45.5	-0.02±0.10	-0.10±0.48	45.5	0.09±0.22	0.47±1.18
090426	46.3	0.36±0.06	1.20±0.21	46.3	0.08±0.10	0.38±0.49	46.3	0.18±0.14	0.95±0.75
090426	47.0	0.18±0.07	0.60±0.24	47.0	0.27±0.09	1.29±0.45	47.0	0.08±0.16	0.42±0.85
090426	47.8	0.25±0.06	0.83±0.21	47.8	0.19±0.09	0.90±0.43	47.8	0.35±0.17	1.84±0.89
090426	49.1	0.33±0.04	1.10±0.14	49.1	0.17±0.06	0.81±0.28	49.1	0.17±0.09	0.89±0.45
090426	50.9	0.32±0.04	1.07±0.14	50.9	0.17±0.07	0.81±0.32	50.9	0.27±0.09	1.42±0.49
090426	52.8	0.24±0.05	0.80±0.17	52.8	0.23±0.06	1.10±0.30	52.8	0.16±0.10	0.84±0.54
090426	54.6	0.24±0.05	0.80±0.17	54.6	0.24±0.08	1.14±0.36	54.6	0.10±0.09	0.53±0.45

Table 7 continued on next page

Table 7 (continued)

GRB	Time (ks)	$g-r$	β_o^{CI} (g-r)	Time (ks)	$r-i$	β_o^{CI} (r-i)	Time (ks)	$i-z$	β_o^{CI} (i-z)	Time (ks)	$J-H$	β_o^{CI} (J-H)	Time (ks)	$H-K_s$	β_o^{CI} (H-K _s)
090426	56.4	0.29±0.06	0.97±0.19	56.4	0.22±0.07	1.05±0.34	56.4	0.14±0.13	0.74±0.66
090426	140	0.23±0.15	0.77±0.50	140	0.17±0.20	0.81±0.96	140	0.25±0.25	1.32±1.30
090426	223	-0.01±0.16	-0.03±0.54	223	0.40±0.19	1.90±0.91
090510	26.8	1.07±0.56	3.58±1.85	23.3	1.04±0.63	4.98±3.00	22.6	0.39±0.57	2.03±2.98
090510	23.1	0.07±0.76	0.25±2.52	23.1	0.81±0.62	3.88±2.95	23.6	0.21±0.45	1.08±2.35
090510	25.9	0.22±0.38	0.75±1.25	22.9	0.68±0.69	3.21±3.26	29.0	0.53±0.35	2.77±1.86
090510	25.0	-0.06±0.45	-0.19±1.51	24.1	0.80±0.35	3.79±1.68	24.1	-0.27±0.49	-1.44±2.59
090510	27.2	0.41±0.49	1.38±1.49	27.2	0.50±0.32	2.36±1.52	25.0	-0.02±0.49	-0.13±2.57
090510	26.3	0.28±0.54	0.95±1.79	25.0	0.28±0.45	1.31±2.16	27.2	-0.10±0.35	-0.55±1.85
090510	29.5	0.18±0.40	0.61±1.33	27.7	0.63±0.28	2.98±1.32	31.7	0.47±0.30	2.45±1.61
090510	28.1	0.30±0.41	1.01±1.38	28.6	0.26±0.36	1.21±1.72	28.6	0.08±0.41	0.40±2.16
090510	27.7	0.07±0.34	0.25±1.14	24.5	-0.35±0.49	-1.69±2.34	29.5	0.15±0.49	0.77±2.60
090510	29.0	0.14±0.47	0.48±1.56	28.1	0.36±0.36	1.74±1.72	28.1	-0.12±0.45	-0.65±2.38
090510	34.4	0.87±0.63	2.91±2.09	29.0	0.41±0.41	1.93±1.93	25.9	-0.02±0.61	-0.13±3.21
090510	35.3	0.08±0.45	0.28±1.49	25.4	-0.29±0.45	-1.40±2.16	30.8	-0.10±0.55	-0.55±2.89
090510	34.8	0.04±0.56	0.15±1.85	30.8	0.04±0.36	0.21±1.72	30.4	-0.00±0.49	-0.02±2.60
090510	29.5	0.14±0.38	0.69±1.82	33.1	0.20±0.41	1.03±2.16
090510	25.9	-0.27±0.47	-1.26±2.26	35.7	0.74±0.70	3.87±3.69
090510	29.9	0.14±0.40	0.69±1.91	32.6	-0.22±0.54	-1.18±2.84
090510	33.5	0.47±0.31	2.26±1.47	35.3	-0.26±0.52	-1.39±2.73
090510	32.6	0.32±0.38	1.50±1.79
090510	30.4	0.03±0.36	0.12±1.70
090510	31.7	0.12±0.30	0.55±1.45
090510	26.8	-0.48±0.36	-2.31±1.72
090510	35.3	0.46±0.43	2.17±2.06
090510	31.3	-0.10±0.32	-0.45±1.51
090510	33.1	0.35±0.42	1.69±1.99
090510	32.2	-0.16±0.50	-0.74±2.39
090510	34.4	-0.38±0.58	-1.79±2.77
090926A	73.2	1.30±0.04	4.33±0.12	73.2	1.16±0.04	5.52±0.17	73.2	1.21±0.04	6.37±0.22
090926A	73.3	1.28±0.03	4.27±0.09	73.3	1.17±0.03	5.57±0.13	73.3	1.18±0.04	6.21±0.19
090926A	73.4	1.28±0.03	4.27±0.09	73.4	1.17±0.03	5.57±0.13	73.4	1.16±0.04	6.11±0.19
090926A	73.5	1.30±0.03	4.33±0.09	73.5	1.13±0.03	5.38±0.13	73.5	1.20±0.04	6.32±0.19
090926A	73.9	1.26±0.04	4.20±0.12	73.9	1.14±0.04	5.43±0.17	73.9	1.18±0.04	6.21±0.22
090926A	74.1	1.25±0.03	4.17±0.09	74.1	1.19±0.03	5.67±0.13	74.1	1.15±0.04	6.05±0.19
090926A	74.3	1.25±0.03	4.17±0.09	74.3	1.18±0.03	5.62±0.13	74.3	1.17±0.04	6.16±0.19
090926A	74.5	1.28±0.03	4.27±0.09	74.5	1.17±0.03	5.57±0.13	74.5	1.17±0.03	6.16±0.15
090926A	74.8	1.27±0.03	4.23±0.09	74.8	1.18±0.03	5.62±0.13	74.8	1.18±0.04	6.21±0.19
090926A	75.3	1.25±0.03	4.17±0.09	75.3	1.19±0.03	5.67±0.13	75.3	1.16±0.03	6.11±0.15
090926A	75.7	1.25±0.03	4.17±0.09	75.7	1.18±0.03	5.62±0.13	75.7	1.17±0.03	6.16±0.15
090926A	76.2	1.25±0.03	4.17±0.09	76.2	1.17±0.03	5.57±0.13	76.2	1.17±0.03	6.16±0.15
090926A	76.8	1.24±0.03	4.13±0.09	76.8	1.16±0.03	5.52±0.13	76.8	1.22±0.04	6.42±0.19
090926A	76.8	1.26±0.03	4.20±0.09	76.8	1.18±0.03	5.62±0.13	76.8	1.20±0.04	6.32±0.22

Table 7 continued on next page

Table 7 (*continued*)

GRB	Time (ks)	$g-r$	β_o^{CI} (g-r)	Time (ks)	$r-i$	β_o^{CI} (r-i)	Time (ks)	$i-z$	β_o^{CI} (i-z)	Time (ks)	$J-H$	β_o^{CI} (J-H)	Time (ks)	$H-K_s$	β_o^{CI} (H-K _s)
090926A	76.8	1.22±0.03	4.07±0.09	76.8	1.18±0.04	5.62±0.17	76.8	1.20±0.04	6.32±0.19
090926A	76.8	1.24±0.03	4.13±0.09	76.8	1.20±0.04	5.71±0.17	76.8	1.18±0.04	6.21±0.22
090926A	76.9	1.26±0.03	4.20±0.09	76.9	1.17±0.03	5.47±0.13	76.9	1.18±0.04	6.21±0.19
090926A	77.1	1.29±0.03	4.30±0.09	77.1	1.14±0.03	5.43±0.13	77.1	1.21±0.04	6.37±0.19
090926A	83.2	1.24±0.03	4.13±0.09	83.2	1.14±0.03	5.43±0.13	83.2	1.16±0.04	6.11±0.19
090926A	83.4	1.24±0.03	4.13±0.09	83.4	1.18±0.03	5.62±0.13	83.4	1.12±0.03	5.86±0.15
090926A	83.6	1.25±0.03	4.17±0.09	83.6	1.16±0.03	5.52±0.13	83.6	1.18±0.03	6.21±0.15
090926A	83.8	1.29±0.03	4.30±0.09	83.8	1.13±0.03	5.38±0.13	83.8	1.15±0.03	6.05±0.15
090926A	84.0	1.22±0.03	4.07±0.09	84.0	1.15±0.03	5.48±0.13	84.0	1.17±0.04	6.16±0.19
090926A	84.1	1.22±0.03	4.07±0.09	84.1	1.17±0.03	5.57±0.13	84.1	1.12±0.03	5.89±0.15
090926A	84.3	1.21±0.03	4.03±0.09	84.3	1.17±0.03	5.57±0.13	84.3	1.18±0.03	6.21±0.15
090926A	84.5	1.22±0.03	4.07±0.09	84.5	1.12±0.03	5.33±0.13	84.5	1.22±0.03	6.42±0.15
090926A	84.7	1.21±0.03	4.03±0.09	84.7	1.13±0.03	5.38±0.13	84.7	1.18±0.04	6.21±0.19
090926A	84.9	1.26±0.03	4.20±0.09	84.9	1.14±0.03	5.43±0.13	84.9	1.16±0.03	6.11±0.15
090926A	85.1	1.22±0.03	4.07±0.09	85.1	1.15±0.03	5.48±0.13	85.1	1.17±0.03	6.16±0.15
090926A	85.3	1.24±0.03	4.13±0.09	85.3	1.14±0.03	5.43±0.13	85.3	1.17±0.03	6.16±0.15
090926A	91.6	1.21±0.03	4.03±0.09	91.6	1.19±0.03	5.67±0.13	91.6	1.12±0.04	5.89±0.19
090926A	91.8	1.26±0.03	4.20±0.09	91.8	1.15±0.03	5.48±0.13	91.8	1.15±0.03	6.05±0.15
090926A	92.0	1.18±0.03	3.93±0.09	92.0	1.16±0.03	5.52±0.13	92.0	1.13±0.04	5.95±0.19
090926A	92.2	1.20±0.03	4.00±0.09	92.2	1.18±0.03	5.62±0.13	92.2	1.18±0.04	6.21±0.19
090926A	92.3	1.21±0.04	4.03±0.12	92.3	1.18±0.04	5.62±0.17	92.3	1.14±0.04	6.00±0.22
090926A	92.5	1.22±0.03	4.07±0.09	92.5	1.15±0.03	5.48±0.13	92.5	1.17±0.04	6.16±0.19
090926A	92.7	1.23±0.03	4.10±0.09	92.7	1.15±0.03	5.48±0.13	92.7	1.18±0.04	6.21±0.19
090926A	92.9	1.25±0.04	4.17±0.12	92.9	1.17±0.04	5.57±0.17	92.9	1.16±0.04	6.11±0.22
090926A	93.1	1.23±0.04	4.10±0.14	93.1	1.21±0.05	5.76±0.24	93.1	1.17±0.06	6.16±0.30
090926A	93.3	1.27±0.04	4.23±0.12	93.3	1.17±0.04	5.57±0.20	93.3	1.17±0.04	6.16±0.22
090926A	93.5	1.17±0.04	3.90±0.12	93.5	1.20±0.04	5.71±0.20	93.5	1.15±0.05	6.05±0.26
090926A	93.7	1.22±0.04	4.07±0.12	93.7	1.19±0.04	5.67±0.17	93.7	1.13±0.04	5.95±0.22
090926A	102	1.18±0.04	3.93±0.14	102	1.22±0.05	5.81±0.24	102	1.18±0.07	6.21±0.38
090926A	102	1.28±0.03	4.27±0.09	102	1.15±0.04	5.48±0.17	102	1.16±0.05	6.11±0.26
090926A	103	1.23±0.03	4.10±0.09	103	1.18±0.04	5.62±0.17	103	1.11±0.06	5.84±0.31
090926A	103	1.24±0.03	4.13±0.09	103	1.15±0.03	5.48±0.13	103	1.17±0.04	6.16±0.19
090926A	103	1.21±0.03	4.03±0.09	103	1.19±0.04	5.67±0.17	103	1.18±0.05	6.21±0.26
090926A	103	1.27±0.03	4.23±0.09	103	1.12±0.04	5.33±0.17	103	1.23±0.05	6.47±0.26
090926A	103	1.22±0.03	4.07±0.09	103	1.19±0.03	5.67±0.13	103	1.22±0.04	6.42±0.19
090926A	104	1.23±0.03	4.10±0.09	104	1.15±0.03	5.48±0.13	104	1.22±0.04	6.42±0.19
090926A	104	1.26±0.03	4.20±0.09	104	1.17±0.04	5.57±0.17	104	1.16±0.05	6.11±0.26
090926A	104	1.28±0.03	4.27±0.09	104	1.17±0.04	5.57±0.17	104	1.17±0.05	6.16±0.26
090926A	104	1.25±0.03	4.17±0.09	104	1.15±0.03	5.48±0.13	104	1.16±0.04	6.11±0.19
090926A	104	1.26±0.03	4.20±0.09	104	1.12±0.03	5.33±0.13	104	1.21±0.04	6.37±0.19
090926A	166	1.16±0.07	3.87±0.24	166	1.22±0.07	5.81±0.34	166	1.07±0.08	5.63±0.45
090926A	167	1.24±0.06	4.13±0.21	167	1.09±0.06	5.19±0.30	167	1.18±0.09	6.21±0.45
090926A	167	1.23±0.06	4.10±0.19	167	1.14±0.05	5.43±0.24	167	1.15±0.07	6.05±0.38

Table 7 continued on next page

Table 7 (continued)

GRB	Time (ks)	$g-r$	β_o^{CI} (g-r)	Time (ks)	$r-i$	β_o^{CI} (r-i)	Time (ks)	$i-z$	β_o^{CI} (i-z)	Time (ks)	$J-H$	β_o^{CI} (J-H)	Time (ks)	$H-K_s$	β_o^{CI} (H-K _s)
090926A	167	1.27±0.05	4.23±0.17	167	1.13±0.05	5.38±0.24	167	1.12±0.06	5.89±0.34
090926A	167	1.12±0.08	3.73±0.26	167	1.24±0.08	5.90±0.37	167	1.16±0.07	6.11±0.38
090926A	167	1.24±0.08	4.13±0.27	167	1.15±0.06	4.88±0.30	167	1.18±0.09	6.21±0.45
090926A	168	1.17±0.06	3.90±0.19	168	1.13±0.04	5.38±0.20	168	1.23±0.05	6.47±0.26
090926A	168	1.17±0.05	3.90±0.17	168	1.22±0.06	5.81±0.28	168	1.10±0.07	5.73±0.37
090926A	174	1.28±0.06	4.27±0.19	174	1.23±0.05	5.86±0.24	174	1.20±0.07	6.32±0.38
090926A	174	1.28±0.04	4.27±0.12	174	1.10±0.04	5.24±0.21	174	1.24±0.06	6.53±0.30
090926A	174	1.28±0.04	4.27±0.14	174	1.18±0.04	5.62±0.20	174	1.21±0.04	6.37±0.22
090926A	174	1.31±0.05	4.37±0.17	174	1.20±0.06	5.71±0.28	174	1.13±0.07	5.95±0.37
090926A	175	1.28±0.06	4.27±0.21	175	1.17±0.06	5.57±0.27	175	1.20±0.07	6.32±0.38
090926A	175	1.25±0.04	4.17±0.14	175	1.17±0.04	5.57±0.20	175	1.24±0.06	6.53±0.31
090926A	175	1.30±0.05	4.33±0.17	175	1.19±0.04	5.67±0.20	175	1.19±0.05	6.24±0.26
090926A	175	1.36±0.04	4.53±0.12	175	1.17±0.04	5.57±0.17	175	1.14±0.05	6.00±0.26
090926A	265	1.27±0.06	4.23±0.19	265	1.13±0.05	5.38±0.24	265	1.23±0.06	6.47±0.34
090926A	265	1.26±0.05	4.20±0.17	265	1.13±0.04	5.38±0.20	265	1.27±0.04	6.68±0.22
090926A	266	1.26±0.04	4.20±0.15	266	1.21±0.04	5.76±0.17	266	1.19±0.05	6.26±0.26
090926A	266	1.27±0.05	4.23±0.17	266	1.25±0.04	5.95±0.20	266	1.25±0.04	6.58±0.22
090926A	331	1.31±0.09	4.37±0.31	331	1.22±0.07	5.81±0.34	331	1.20±0.09	6.32±0.45
090926A	332	1.28±0.06	4.27±0.19	332	1.29±0.04	6.14±0.20	332	1.19±0.05	6.26±0.26
090926A	332	1.32±0.06	4.40±0.19	332	1.17±0.05	5.57±0.24	332	1.21±0.06	6.37±0.30
090926A	333	1.32±0.05	4.40±0.17	333	1.25±0.05	5.95±0.24	333	1.20±0.06	6.32±0.30
090926A	356	1.25±0.08	4.17±0.26	356	1.26±0.07	6.00±0.34	356	1.20±0.08	6.32±0.41
090926A	356	1.28±0.06	4.27±0.21	356	1.25±0.06	5.95±0.30	356	1.29±0.07	6.79±0.37
090926A	356	1.39±0.05	4.63±0.17	356	1.19±0.05	5.67±0.24	356	1.26±0.06	6.63±0.34
090926A	357	1.25±0.07	4.17±0.22	357	1.28±0.05	6.10±0.24	357	1.16±0.08	6.11±0.42
090926A	419	1.27±0.12	4.23±0.39	419	1.27±0.09	6.05±0.44	419	1.16±0.11	6.11±0.56
091018	11.0	0.19±0.05	0.63±0.17	11.0	0.16±0.05	0.76±0.24	11.0	0.12±0.06	0.63±0.34	11.3	0.06±0.06	0.19±0.19	11.3	0.18±0.09	0.57±0.27
091018	11.2	0.19±0.04	0.63±0.12	11.2	0.15±0.04	0.71±0.17	11.2	0.13±0.06	0.65±0.31	12.0	0.11±0.05	0.35±0.17	12.0	0.06±0.08	0.19±0.25
091018	11.3	0.23±0.03	0.77±0.09	11.3	0.13±0.03	0.62±0.13	11.3	0.14±0.04	0.74±0.19	12.8	0.07±0.05	0.22±0.17	12.8	0.22±0.07	0.69±0.22
091018	11.5	0.19±0.03	0.63±0.09	11.5	0.12±0.04	0.57±0.17	11.5	0.16±0.04	0.84±0.22	13.6	0.09±0.04	0.29±0.14	13.6	0.11±0.07	0.35±0.21
091018	11.7	0.18±0.03	0.60±0.09	11.7	0.12±0.04	0.57±0.17	11.7	0.15±0.04	0.79±0.22	14.3	0.07±0.05	0.22±0.17	14.3	0.08±0.07	0.26±0.22
091018	11.9	0.16±0.03	0.53±0.09	11.9	0.12±0.03	0.57±0.13	11.9	0.14±0.04	0.74±0.19	15.1	0.12±0.04	0.39±0.14	15.1	0.08±0.07	0.26±0.21
091018	12.1	0.17±0.02	0.57±0.07	12.1	0.12±0.03	0.57±0.13	12.1	0.16±0.04	0.84±0.19	15.9	0.15±0.04	0.49±0.14	15.9	0.03±0.07	0.10±0.21
091018	12.3	0.17±0.02	0.57±0.07	12.3	0.14±0.03	0.67±0.13	12.3	0.13±0.04	0.68±0.19	16.6	0.11±0.04	0.35±0.14	16.6	0.11±0.07	0.35±0.21
091018	12.5	0.18±0.03	0.60±0.09	12.5	0.12±0.04	0.57±0.17	12.5	0.17±0.04	0.89±0.22	17.4	0.08±0.04	0.25±0.14	17.4	0.08±0.07	0.26±0.21
091018	12.7	0.19±0.03	0.63±0.09	12.7	0.13±0.03	0.62±0.13	12.7	0.14±0.04	0.74±0.19	18.2	0.11±0.05	0.35±0.17	18.2	0.15±0.07	0.47±0.22
091018	12.9	0.20±0.03	0.67±0.09	12.9	0.12±0.03	0.57±0.13	12.9	0.12±0.04	0.63±0.19	18.9	0.13±0.05	0.42±0.17	18.9	0.19±0.07	0.60±0.22
091018	13.1	0.18±0.03	0.60±0.09	13.1	0.14±0.03	0.67±0.13	13.1	0.09±0.04	0.47±0.19	19.7	0.13±0.05	0.42±0.17	19.7	0.17±0.07	0.54±0.22
091018	13.2	0.21±0.03	0.70±0.09	13.2	0.10±0.04	0.48±0.17	13.2	0.14±0.04	0.74±0.22	20.5	0.13±0.04	0.42±0.14	20.5	0.09±0.07	0.29±0.21
091018	13.4	0.19±0.03	0.63±0.09	13.4	0.12±0.03	0.57±0.13	13.4	0.16±0.04	0.84±0.19	30.1	0.04±0.10	0.12±0.32	30.1	0.15±0.11	0.47±0.36
091018	13.6	0.17±0.03	0.57±0.09	13.6	0.13±0.03	0.62±0.13	13.6	0.13±0.04	0.68±0.19	38.8	0.06±0.10	0.19±0.33	38.8	0.09±0.12	0.29±0.38
091018	13.8	0.17±0.03	0.57±0.09	13.8	0.14±0.03	0.67±0.13	13.8	0.13±0.04	0.68±0.19
091018	14.0	0.18±0.03	0.60±0.09	14.0	0.13±0.03	0.62±0.13	14.0	0.17±0.04	0.89±0.19

Table 7 continued on next page

Table 7 (*continued*)

GRB	Time	$g-r$	β_o^{CI} (g-r)	Time	$r-i$	β_o^{CI} (r-i)	Time	$i-z$	β_o^{CI} (i-z)	Time	$J-H$	β_o^{CI} (J-H)	Time	$H-K_s$	β_o^{CI} (H-Ks)
091018	14.2	0.18±0.03	0.60±0.09	14.2	0.15±0.03	0.71±0.13	14.2	0.17±0.04	0.89±0.19
091018	14.4	0.19±0.03	0.63±0.09	14.4	0.14±0.03	0.67±0.13	14.4	0.15±0.04	0.78±0.19
091018	14.6	0.19±0.03	0.63±0.09	14.6	0.15±0.03	0.71±0.13	14.6	0.14±0.04	0.74±0.19
091018	14.8	0.18±0.03	0.60±0.09	14.8	0.15±0.03	0.71±0.13	14.8	0.14±0.04	0.74±0.19
091018	15.0	0.19±0.03	0.63±0.09	15.0	0.15±0.03	0.71±0.13	15.0	0.14±0.04	0.74±0.19
091018	15.2	0.17±0.03	0.57±0.09	15.2	0.15±0.03	0.71±0.13	15.2	0.11±0.04	0.58±0.19
091018	15.3	0.18±0.03	0.60±0.09	15.3	0.13±0.03	0.62±0.13	15.3	0.13±0.04	0.68±0.19
091018	15.6	0.21±0.03	0.70±0.09	15.6	0.14±0.03	0.67±0.13	15.6	0.15±0.04	0.79±0.19
091018	15.7	0.19±0.03	0.63±0.09	15.7	0.13±0.03	0.62±0.13	15.7	0.14±0.04	0.74±0.19
091018	15.9	0.19±0.03	0.63±0.09	15.9	0.12±0.03	0.57±0.13	15.9	0.13±0.04	0.68±0.19
091018	16.1	0.17±0.03	0.57±0.09	16.1	0.15±0.03	0.71±0.13	16.1	0.15±0.04	0.75±0.19
091018	16.3	0.20±0.03	0.67±0.09	16.3	0.12±0.03	0.57±0.13	16.3	0.14±0.04	0.74±0.19
091018	16.5	0.17±0.03	0.57±0.09	16.5	0.15±0.03	0.71±0.13	16.5	0.14±0.04	0.74±0.19
091018	16.7	0.19±0.03	0.63±0.09	16.7	0.15±0.03	0.71±0.13	16.7	0.14±0.04	0.74±0.19
091018	16.9	0.20±0.03	0.67±0.09	16.9	0.16±0.03	0.76±0.13	16.9	0.13±0.03	0.68±0.15
091018	17.1	0.18±0.03	0.60±0.09	17.1	0.14±0.03	0.67±0.13	17.1	0.17±0.04	0.89±0.19
091018	17.3	0.18±0.03	0.60±0.09	17.3	0.15±0.03	0.71±0.13	17.3	0.18±0.04	0.95±0.19
091018	17.5	0.21±0.03	0.70±0.09	17.5	0.13±0.03	0.62±0.13	17.5	0.18±0.04	0.95±0.19
091018	17.7	0.20±0.03	0.67±0.09	17.7	0.14±0.03	0.67±0.13	17.7	0.20±0.04	1.05±0.19
091018	17.9	0.18±0.03	0.60±0.09	17.9	0.15±0.03	0.71±0.13	17.9	0.16±0.04	0.84±0.19
091018	18.0	0.16±0.03	0.53±0.09	18.0	0.17±0.03	0.81±0.13	18.0	0.12±0.04	0.63±0.19
091018	18.2	0.18±0.03	0.60±0.09	18.2	0.17±0.03	0.81±0.13	18.2	0.12±0.04	0.63±0.19
091018	18.4	0.21±0.03	0.70±0.09	18.4	0.15±0.03	0.71±0.13	18.4	0.17±0.04	0.89±0.19
091018	18.6	0.17±0.03	0.57±0.09	18.6	0.17±0.03	0.81±0.13	18.6	0.14±0.04	0.74±0.19
091018	18.8	0.17±0.03	0.57±0.09	18.8	0.15±0.03	0.71±0.13	18.8	0.16±0.04	0.84±0.19
091018	19.0	0.17±0.03	0.57±0.09	19.0	0.16±0.03	0.76±0.13	19.0	0.13±0.04	0.68±0.19
091018	19.2	0.18±0.03	0.60±0.09	19.2	0.18±0.03	0.86±0.13	19.2	0.09±0.04	0.47±0.19
091018	19.4	0.20±0.03	0.67±0.09	19.4	0.12±0.03	0.57±0.13	19.4	0.14±0.04	0.74±0.19
091018	19.6	0.17±0.03	0.57±0.09	19.6	0.14±0.03	0.67±0.13	19.6	0.12±0.04	0.63±0.19
091018	19.8	0.17±0.03	0.57±0.09	19.8	0.14±0.03	0.67±0.13	19.8	0.11±0.04	0.58±0.19
091018	19.9	0.19±0.03	0.63±0.09	19.9	0.14±0.03	0.67±0.13	19.9	0.09±0.04	0.47±0.19
091018	20.1	0.20±0.03	0.67±0.09	20.1	0.10±0.04	0.48±0.17	20.1	0.18±0.04	0.95±0.22
091018	20.3	0.19±0.03	0.63±0.09	20.3	0.12±0.03	0.57±0.13	20.3	0.18±0.04	0.95±0.19
091018	20.5	0.19±0.03	0.63±0.09	20.5	0.14±0.04	0.67±0.17	20.5	0.14±0.04	0.74±0.22
091018	20.7	0.17±0.03	0.57±0.09	20.7	0.16±0.04	0.76±0.17	20.7	0.14±0.04	0.74±0.22
091018	30.1	0.19±0.03	0.63±0.09	30.1	0.15±0.03	0.71±0.13	30.1	0.16±0.03	0.84±0.15
091018	38.8	0.20±0.03	0.67±0.09	38.8	0.16±0.03	0.76±0.13	38.8	0.15±0.04	0.79±0.19
091018	104	0.17±0.05	0.57±0.17	104	0.12±0.07	0.57±0.32	104	0.23±0.09	1.21±0.49
091018	113	0.14±0.05	0.47±0.17	113	0.17±0.07	0.81±0.32	113	0.19±0.10	1.00±0.53
091018	129	0.14±0.07	0.47±0.24	129	0.24±0.11	1.14±0.53	129	0.03±0.16	0.16±0.82
091018	192	0.19±0.06	0.63±0.19	192	0.31±0.09	1.48±0.43	192	0.03±0.12	0.16±0.63
091018	273	0.13±0.12	0.43±0.41	273	0.28±0.16	1.33±0.78	273	-0.11±0.24	-0.58±1.26
091029	0.307	0.35±0.04	1.17±0.15	0.307	0.06±0.04	0.29±0.17	0.307	0.19±0.09	1.00±0.45

Table 7 continued on next page

Table 7 (continued)

GRB	Time (ks)	$g-r$	β_o^{CI} (g-r)	Time (ks)	$r-i$	β_o^{CI} (r-i)	Time (ks)	$i-z$	β_o^{CI} (i-z)	Time (ks)	$J-H$	β_o^{CI} (J-H)	Time (ks)	$H-K_s$	β_o^{CI} (H-K _s)
091029	0.410	0.31±0.04	1.03±0.15	0.410	0.09±0.03	0.43±0.13	0.410	0.22±0.04	1.16±0.24
091029	0.515	0.33±0.04	1.10±0.12	0.515	0.10±0.04	0.48±0.17	0.515	0.17±0.06	0.85±0.31
091029	0.729	0.30±0.04	1.00±0.12	0.729	0.05±0.04	0.24±0.21	0.729	0.23±0.06	1.21±0.34
091029	0.826	0.33±0.04	1.10±0.12	0.826	0.04±0.04	0.19±0.17	0.826	0.18±0.07	0.95±0.35
091029	0.924	0.32±0.04	1.07±0.12	0.924	0.05±0.04	0.24±0.17	0.924	0.18±0.06	0.95±0.31
091029	1.02	0.33±0.04	1.10±0.15	1.02	0.05±0.04	0.24±0.17	1.02	0.17±0.08	0.85±0.40
091029	1.15	0.29±0.04	0.97±0.12	1.15	0.05±0.04	0.24±0.21	1.15	0.14±0.06	0.74±0.34
091029	1.34	0.27±0.04	0.90±0.14	1.34	0.05±0.03	0.24±0.15	1.34	0.14±0.06	0.74±0.31
091029	1.52	0.28±0.04	0.93±0.12	1.52	0.03±0.03	0.14±0.13	1.52	0.17±0.05	0.85±0.28
091029	1.92	0.27±0.03	0.80±0.11	1.92	0.03±0.03	0.14±0.15	1.92	0.18±0.06	0.95±0.31
091029	2.11	0.25±0.04	0.83±0.12	2.11	0.02±0.03	0.10±0.13	2.11	0.12±0.04	0.63±0.24
091029	2.31	0.26±0.03	0.87±0.11	2.31	0.01±0.03	0.05±0.15	2.31	0.20±0.06	1.05±0.31
091029	2.50	0.26±0.03	0.87±0.11	2.50	0.04±0.02	0.19±0.11	2.50	0.15±0.05	0.75±0.28
091029	2.84	0.27±0.02	0.90±0.07	2.84	0.01±0.02	0.05±0.11	2.84	0.18±0.04	0.95±0.19
091029	3.29	0.24±0.02	0.80±0.07	3.29	0.03±0.01	0.14±0.07	3.29	0.12±0.03	0.63±0.17
091029	3.74	0.25±0.02	0.83±0.07	3.74	0.02±0.02	0.10±0.11	3.74	0.12±0.04	0.63±0.19
091029	4.19	0.25±0.02	0.83±0.07	4.19	0.02±0.02	0.10±0.11	4.19	0.14±0.04	0.74±0.24
091029	4.66	0.25±0.02	0.83±0.07	4.66	0.02±0.02	0.10±0.11	4.66	0.16±0.04	0.84±0.19
091029	5.10	0.24±0.02	0.80±0.07	5.10	0.02±0.02	0.10±0.11	5.10	0.11±0.04	0.55±0.24
091029	5.55	0.24±0.01	0.80±0.05	5.55	0.03±0.02	0.14±0.11	5.55	0.13±0.04	0.68±0.19
091029	6.01	0.24±0.02	0.80±0.07	6.01	0.01±0.02	0.05±0.11	6.01	0.12±0.04	0.63±0.24
091029	6.47	0.23±0.02	0.77±0.07	6.47	0.02±0.02	0.10±0.11	6.47	0.14±0.04	0.74±0.19
091029	6.91	0.23±0.02	0.77±0.07	6.91	0.01±0.02	0.05±0.11	6.91	0.13±0.04	0.68±0.19
091029	7.36	0.24±0.01	0.80±0.05	7.36	0.01±0.02	0.05±0.11	7.36	0.11±0.04	0.58±0.19
091029	7.81	0.24±0.01	0.80±0.05	7.81	0.03±0.02	0.14±0.11	7.81	0.13±0.04	0.68±0.19
091029	8.27	0.25±0.02	0.83±0.07	8.27	0.01±0.02	0.05±0.11	8.27	0.13±0.04	0.68±0.24
091029	8.72	0.24±0.02	0.80±0.07	8.72	0.01±0.02	0.05±0.11	8.72	0.14±0.04	0.74±0.19
091029	9.17	0.23±0.02	0.77±0.07	9.17	0.01±0.02	0.05±0.11	9.17	0.16±0.04	0.84±0.24
091029	9.62	0.24±0.01	0.80±0.05	9.62	0.0±0.02	0.05±0.11	9.62	0.15±0.04	0.75±0.19
091029	10.4	0.23±0.01	0.77±0.05	14.4	0.04±0.02	0.19±0.11	14.4	0.13±0.04	0.68±0.24
091029	15.4	0.25±0.01	0.83±0.05	15.4	0.02±0.02	0.10±0.11	15.4	0.16±0.05	0.84±0.28
091029	15.8	0.25±0.01	0.83±0.05	15.8	0.02±0.02	0.10±0.11	15.8	0.13±0.04	0.68±0.19
091029	16.3	0.24±0.01	0.87±0.05	16.3	0.02±0.02	0.10±0.11	16.3	0.13±0.04	0.68±0.24
091029	16.7	0.24±0.01	0.80±0.05	16.7	0.07±0.02	0.33±0.11	16.7	0.14±0.04	0.74±0.24
091029	17.4	0.26±0.02	0.87±0.07	17.4	0.03±0.02	0.14±0.11	17.4	0.14±0.04	0.74±0.24
091029	17.8	0.27±0.02	0.90±0.07	17.8	0.02±0.02	0.10±0.11	17.8	0.16±0.04	0.84±0.24
091029	18.3	0.33±0.03	1.07±0.11	18.3	0.08±0.04	0.38±0.20	18.3	0.09±0.06	0.47±0.34
091029	104	0.31±0.06	1.03±0.19	104	0.07±0.07	0.33±0.32	104	0.19±0.11	1.00±0.57
091029	171	0.33±0.11	1.10±0.36	171	-0.05±0.11	-0.24±0.52	171	0.24±0.14	1.26±0.75
091029	189	0.28±0.04	0.93±0.14	189	-0.09±0.07	-0.43±0.32	189	0.31±0.11	1.63±0.57
091029	345	0.07±0.25	0.23±0.83	345	0.09±0.21	0.43±1.01	345	-0.17±0.23	-0.89±1.19
091127	3.30	0.04±0.01	0.13±0.05	3.30	0.05±0.01	0.24±0.07	3.30	0.07±0.01	0.37±0.07
091127	3.40	0.06±0.01	0.20±0.05	3.40	0.05±0.01	0.24±0.07	3.40	0.07±0.01	0.37±0.07

Table 7 continued on next page

Table 7 (*continued*)

GRB	Time (ks)	$g-r$	β_o^{CI} (g-r)	Time (ks)	$r-i$	β_o^{CI} (r-i)	Time (ks)	$i-z$	β_o^{CI} (i-z)	Time (ks)	$J-H$	β_o^{CI} (J-H)	Time (ks)	$H-K_s$	β_o^{CI} (H-K _s)
091127	3.52	0.07±0.01	0.23±0.05	3.52	0.05±0.01	0.24±0.07	3.52	0.06±0.01	0.32±0.07
091127	3.62	0.07±0.01	0.23±0.05	3.62	0.06±0.01	0.29±0.07	3.62	0.05±0.01	0.24±0.07
091127	3.72	0.08±0.01	0.27±0.05	3.72	0.06±0.01	0.29±0.07	3.72	0.06±0.01	0.32±0.07
091127	3.82	0.06±0.01	0.20±0.05	3.82	0.06±0.01	0.29±0.07	3.82	0.06±0.01	0.32±0.07
091127	3.99	0.07±0.01	0.23±0.05	3.99	0.07±0.01	0.33±0.07	3.99	0.04±0.01	0.21±0.07
091127	4.18	0.08±0.01	0.27±0.05	4.18	0.06±0.01	0.29±0.07	4.18	0.05±0.01	0.26±0.07
091127	4.36	0.08±0.01	0.27±0.05	4.36	0.07±0.01	0.33±0.07	4.36	0.05±0.01	0.26±0.07
091127	4.55	0.07±0.01	0.23±0.05	4.55	0.08±0.01	0.38±0.07	4.55	0.06±0.01	0.32±0.07
091127	4.77	0.08±0.01	0.27±0.05	4.77	0.06±0.01	0.29±0.07	4.77	0.05±0.01	0.26±0.07
091127	4.96	0.09±0.01	0.30±0.05	4.96	0.06±0.01	0.29±0.07	4.96	0.06±0.01	0.32±0.07
091127	5.15	0.08±0.01	0.27±0.05	5.15	0.05±0.01	0.24±0.07	5.15	0.08±0.01	0.42±0.07
091127	5.35	0.08±0.01	0.27±0.05	5.35	0.07±0.01	0.33±0.07	5.35	0.07±0.01	0.37±0.07
091127	5.53	0.10±0.01	0.33±0.05	5.53	0.05±0.01	0.24±0.07	5.53	0.06±0.01	0.32±0.07
091127	5.63	0.07±0.01	0.23±0.05	5.63	0.08±0.01	0.38±0.07	5.63	0.05±0.01	0.26±0.07
091127	5.73	0.10±0.01	0.33±0.05	5.73	0.06±0.01	0.29±0.07	5.73	0.07±0.01	0.37±0.07
091127	5.84	0.08±0.01	0.27±0.05	5.84	0.05±0.01	0.24±0.07	5.84	0.09±0.01	0.47±0.07
091127	5.97	0.10±0.01	0.33±0.05	5.97	0.07±0.01	0.33±0.07	5.97	0.07±0.01	0.37±0.07
091127	6.07	0.08±0.01	0.27±0.05	6.07	0.08±0.01	0.38±0.07	6.07	0.04±0.01	0.21±0.07
091127	6.17	0.08±0.01	0.27±0.05	6.17	0.08±0.01	0.38±0.07	6.17	0.05±0.01	0.24±0.07
091127	6.28	0.08±0.01	0.27±0.05	6.28	0.08±0.01	0.38±0.07	6.28	0.07±0.01	0.37±0.07
091127	6.40	0.08±0.01	0.27±0.05	6.40	0.06±0.01	0.29±0.07	6.40	0.08±0.01	0.42±0.07
091127	6.50	0.09±0.01	0.30±0.05	6.50	0.07±0.01	0.33±0.07	6.50	0.07±0.01	0.37±0.07
091127	6.60	0.08±0.01	0.27±0.05	6.60	0.08±0.01	0.38±0.07	6.60	0.05±0.01	0.26±0.07
091127	6.71	0.10±0.01	0.33±0.05	6.71	0.07±0.01	0.33±0.07	6.71	0.07±0.01	0.37±0.07
091127	6.83	0.08±0.01	0.27±0.05	6.83	0.07±0.01	0.33±0.07	6.83	0.08±0.01	0.42±0.07
091127	6.93	0.09±0.01	0.30±0.05	6.93	0.08±0.01	0.38±0.07	6.93	0.07±0.01	0.37±0.07
091127	7.03	0.08±0.01	0.27±0.05	7.03	0.09±0.01	0.43±0.07	7.03	0.06±0.01	0.32±0.07
091127	7.14	0.09±0.01	0.30±0.05	7.14	0.08±0.01	0.38±0.07	7.14	0.07±0.01	0.37±0.07
091127	7.26	0.09±0.01	0.30±0.05	7.26	0.09±0.01	0.43±0.07	7.26	0.06±0.01	0.32±0.07
091127	7.36	0.09±0.01	0.30±0.05	7.36	0.08±0.01	0.38±0.07	7.36	0.07±0.01	0.37±0.07
091127	7.46	0.09±0.01	0.30±0.05	7.46	0.07±0.01	0.33±0.07	7.46	0.08±0.01	0.42±0.07
091127	7.56	0.09±0.01	0.30±0.05	7.56	0.09±0.01	0.43±0.07	7.56	0.06±0.01	0.32±0.07
091127	7.68	0.09±0.01	0.30±0.05	7.68	0.08±0.01	0.38±0.07	7.68	0.09±0.01	0.47±0.07
091127	7.78	0.10±0.01	0.33±0.05	7.78	0.08±0.01	0.38±0.07	7.78	0.06±0.01	0.32±0.07
091127	7.88	0.10±0.01	0.33±0.05	7.88	0.06±0.01	0.29±0.07	7.88	0.07±0.01	0.37±0.07
091127	7.99	0.08±0.01	0.27±0.05	7.99	0.10±0.01	0.48±0.07	7.99	0.06±0.01	0.32±0.07
091127	8.10	0.08±0.01	0.27±0.05	8.10	0.07±0.01	0.33±0.07	8.10	0.07±0.01	0.37±0.07
091127	8.20	0.09±0.01	0.30±0.05	8.20	0.09±0.01	0.43±0.07	8.20	0.06±0.01	0.32±0.07
091127	8.31	0.09±0.01	0.30±0.05	8.31	0.09±0.01	0.43±0.07	8.31	0.07±0.01	0.37±0.07
091127	8.41	0.09±0.01	0.30±0.05	8.41	0.08±0.01	0.38±0.07	8.41	0.06±0.01	0.32±0.07
091127	8.55	0.11±0.01	0.37±0.05	8.55	0.09±0.01	0.43±0.07	8.55	0.06±0.01	0.32±0.07
091127	8.66	0.09±0.01	0.30±0.05	8.66	0.10±0.01	0.48±0.07	8.66	0.06±0.01	0.32±0.07
091127	8.76	0.11±0.01	0.37±0.05	8.76	0.07±0.01	0.33±0.07	8.76	0.09±0.01	0.47±0.07

Table 7 continued on next page

Table 7 (continued)

GRB	Time (ks)	$g-r$	β_o^{CI} (g-r)	Time (ks)	$r-i$	β_o^{CI} (r-i)	Time (ks)	$i-z$	β_o^{CI} (i-z)	Time (ks)	$J-H$	β_o^{CI} (J-H)	Time (ks)	$H-K_s$	β_o^{CI} (H-K _s)
091127	8.86	0.11±0.01	0.37±0.05	8.86	0.07±0.01	0.33±0.07	8.86	0.07±0.01	0.37±0.07
091127	8.98	0.11±0.01	0.37±0.05	8.98	0.09±0.01	0.43±0.07	8.98	0.06±0.01	0.32±0.07
091127	9.08	0.12±0.01	0.40±0.05	9.08	0.08±0.01	0.38±0.07	9.08	0.05±0.01	0.26±0.07
091127	9.18	0.11±0.01	0.37±0.05	9.18	0.09±0.01	0.43±0.07	9.18	0.06±0.01	0.32±0.07
091127	9.28	0.10±0.01	0.33±0.05	9.28	0.10±0.01	0.48±0.07	9.28	0.06±0.01	0.32±0.07
091127	9.40	0.10±0.01	0.33±0.05	9.40	0.08±0.01	0.38±0.07	9.40	0.07±0.01	0.32±0.07
091127	9.50	0.09±0.01	0.39±0.05	9.50	0.09±0.01	0.43±0.07	9.50	0.08±0.01	0.42±0.07
091127	9.60	0.10±0.01	0.33±0.05	9.60	0.08±0.01	0.38±0.07	9.60	0.06±0.01	0.32±0.07
091127	9.70	0.10±0.01	0.33±0.05	9.70	0.08±0.01	0.38±0.07	9.70	0.06±0.01	0.32±0.07
091127	9.82	0.11±0.01	0.37±0.05	9.82	0.08±0.01	0.38±0.07	9.82	0.06±0.01	0.32±0.07
091127	9.92	0.10±0.01	0.33±0.05	9.92	0.09±0.01	0.43±0.07	9.92	0.06±0.01	0.32±0.07
091127	10.0	0.10±0.01	0.33±0.05	10.0	0.09±0.01	0.43±0.07	10.0	0.07±0.01	0.37±0.07
091127	10.1	0.10±0.01	0.33±0.05	10.1	0.09±0.01	0.43±0.07	10.1	0.06±0.01	0.32±0.07
091127	10.3	0.10±0.01	0.33±0.05	10.3	0.11±0.01	0.52±0.07	10.3	0.06±0.01	0.32±0.07
091127	10.4	0.10±0.01	0.33±0.05	10.4	0.08±0.01	0.38±0.07	10.4	0.09±0.01	0.47±0.07
091127	10.5	0.10±0.01	0.33±0.05	10.5	0.07±0.01	0.33±0.07	10.5	0.09±0.01	0.47±0.07
091127	10.6	0.10±0.01	0.33±0.05	10.6	0.09±0.01	0.43±0.07	10.6	0.07±0.01	0.37±0.07
091127	10.7	0.11±0.01	0.37±0.05	10.7	0.07±0.01	0.33±0.07	10.7	0.06±0.01	0.32±0.07
091127	10.8	0.10±0.01	0.33±0.05	10.8	0.10±0.01	0.48±0.07	10.8	0.06±0.01	0.32±0.07
091127	10.9	0.09±0.01	0.33±0.05	10.9	0.07±0.01	0.33±0.07	10.9	0.08±0.01	0.42±0.07
091127	11.0	0.12±0.01	0.40±0.05	11.0	0.09±0.01	0.43±0.07	11.0	0.08±0.01	0.42±0.07
091127	11.1	0.12±0.01	0.40±0.05	11.1	0.06±0.01	0.29±0.07	11.1	0.07±0.01	0.37±0.07
091127	11.2	0.11±0.01	0.37±0.05	11.2	0.07±0.01	0.33±0.07	11.2	0.09±0.01	0.47±0.07
091127	11.3	0.11±0.01	0.37±0.05	11.3	0.07±0.01	0.33±0.07	11.3	0.08±0.01	0.42±0.07
091127	11.4	0.10±0.01	0.33±0.05	11.4	0.08±0.01	0.38±0.07	11.4	0.08±0.01	0.42±0.07
091127	11.5	0.10±0.01	0.33±0.05	11.5	0.10±0.01	0.48±0.07	11.5	0.07±0.01	0.37±0.07
091127	11.6	0.11±0.01	0.37±0.05	11.6	0.08±0.01	0.38±0.07	11.6	0.07±0.01	0.37±0.07
091127	11.7	0.11±0.01	0.37±0.05	11.7	0.08±0.01	0.38±0.07	11.7	0.08±0.01	0.42±0.07
091127	11.8	0.11±0.01	0.37±0.05	11.8	0.08±0.01	0.38±0.07	11.8	0.07±0.01	0.37±0.07
091127	12.0	0.11±0.01	0.37±0.05	12.0	0.09±0.01	0.43±0.07	12.0	0.06±0.01	0.32±0.07
091127	12.1	0.11±0.01	0.37±0.05	12.1	0.09±0.01	0.43±0.07	12.1	0.07±0.01	0.37±0.07
091127	12.2	0.11±0.01	0.37±0.05	12.2	0.09±0.01	0.43±0.07	12.2	0.07±0.01	0.37±0.07
091127	12.3	0.13±0.01	0.43±0.05	12.3	0.09±0.01	0.43±0.07	12.3	0.07±0.01	0.37±0.07
091127	12.4	0.10±0.01	0.33±0.05	12.4	0.09±0.01	0.43±0.07	12.4	0.08±0.01	0.42±0.07
091127	12.5	0.12±0.01	0.40±0.05	12.5	0.09±0.01	0.43±0.07	12.5	0.07±0.01	0.37±0.07
091127	12.6	0.11±0.01	0.37±0.05	12.6	0.11±0.01	0.52±0.07	12.6	0.05±0.01	0.26±0.07
091127	12.7	0.11±0.01	0.37±0.05	12.7	0.09±0.01	0.43±0.07	12.7	0.08±0.01	0.42±0.07
091127	12.8	0.10±0.01	0.33±0.05	12.8	0.11±0.01	0.52±0.07	12.8	0.06±0.01	0.32±0.07
091127	12.9	0.11±0.01	0.37±0.05	12.9	0.08±0.01	0.38±0.07	12.9	0.07±0.01	0.37±0.07
091127	13.0	0.10±0.01	0.33±0.05	13.0	0.10±0.01	0.48±0.07	13.0	0.08±0.01	0.42±0.07
091127	13.1	0.11±0.01	0.37±0.05	13.1	0.10±0.01	0.48±0.07	13.1	0.07±0.01	0.37±0.07
091127	13.2	0.10±0.01	0.33±0.05	13.2	0.08±0.01	0.38±0.07	13.2	0.09±0.01	0.47±0.07
091127	13.4	0.11±0.01	0.37±0.05	13.4	0.10±0.01	0.48±0.07	13.4	0.07±0.01	0.37±0.07

Table 7 continued on next page

Table 7 (*continued*)

GRB	Time (ks)	$g-r$	β_o^{CI} (g-r)	Time (ks)	$r-i$	β_o^{CI} (r-i)	Time (ks)	$i-z$	β_o^{CI} (i-z)	Time (ks)	$J-H$	β_o^{CI} (J-H)	Time (ks)	$H-K_s$	β_o^{CI} (H-K _s)
091127	13.5	0.12±0.01	0.40±0.05	13.5	0.08±0.01	0.38±0.07	13.5	0.07±0.01	0.37±0.07
091127	13.6	0.10±0.01	0.33±0.05	13.6	0.09±0.01	0.43±0.07	13.6	0.07±0.01	0.37±0.07
091127	13.7	0.12±0.01	0.40±0.05	13.7	0.09±0.01	0.43±0.07	13.7	0.08±0.01	0.42±0.07
091127	13.8	0.11±0.01	0.37±0.05	13.8	0.08±0.01	0.38±0.07	13.8	0.08±0.01	0.42±0.07
091127	13.9	0.12±0.01	0.40±0.05	13.9	0.06±0.01	0.29±0.07	13.9	0.10±0.01	0.53±0.07
091127	14.0	0.10±0.01	0.33±0.05	14.0	0.09±0.01	0.43±0.07	14.0	0.10±0.01	0.53±0.07
091127	14.1	0.12±0.01	0.49±0.05	14.1	0.08±0.01	0.38±0.07	14.1	0.09±0.01	0.47±0.07
091127	14.2	0.12±0.01	0.40±0.05	14.2	0.09±0.01	0.43±0.07	14.2	0.07±0.01	0.37±0.07
091127	14.3	0.13±0.01	0.43±0.05	14.3	0.09±0.01	0.43±0.07	14.3	0.09±0.01	0.47±0.07
091127	14.4	0.11±0.01	0.37±0.05	14.4	0.10±0.01	0.48±0.07	14.4	0.07±0.01	0.37±0.07
091127	14.5	0.12±0.01	0.40±0.05	14.5	0.09±0.01	0.43±0.07	14.5	0.08±0.01	0.42±0.07
091127	14.6	0.11±0.01	0.37±0.05	14.6	0.09±0.01	0.43±0.07	14.6	0.08±0.01	0.42±0.07
091127	14.7	0.11±0.01	0.37±0.05	14.7	0.09±0.01	0.43±0.07	14.7	0.07±0.01	0.37±0.07
091127	14.8	0.11±0.01	0.37±0.05	14.8	0.09±0.01	0.43±0.07	14.8	0.06±0.01	0.33±0.07
091127	15.0	0.11±0.01	0.37±0.05	15.0	0.07±0.01	0.33±0.07	15.0	0.10±0.01	0.53±0.07
091127	15.1	0.11±0.01	0.37±0.05	15.1	0.10±0.01	0.48±0.07	15.1	0.07±0.01	0.37±0.07
091127	15.2	0.11±0.01	0.37±0.05	15.2	0.10±0.01	0.48±0.07	15.2	0.08±0.01	0.42±0.07
091127	15.3	0.10±0.01	0.33±0.05	15.3	0.10±0.01	0.43±0.07	15.3	0.07±0.01	0.33±0.07
091127	15.4	0.12±0.01	0.40±0.05	15.4	0.08±0.01	0.38±0.07	15.4	0.09±0.01	0.47±0.07
091127	15.5	0.12±0.01	0.40±0.05	15.5	0.12±0.01	0.57±0.07	15.5	0.07±0.01	0.37±0.07
091127	15.6	0.10±0.01	0.33±0.05	15.6	0.13±0.01	0.62±0.07	15.6	0.07±0.01	0.42±0.07
091127	15.7	0.11±0.01	0.37±0.05	15.7	0.09±0.01	0.43±0.07	15.7	0.08±0.01	0.42±0.07
091127	15.8	0.12±0.01	0.40±0.05	15.8	0.08±0.01	0.38±0.07	15.8	0.09±0.01	0.47±0.07
091127	15.9	0.11±0.01	0.37±0.05	15.9	0.11±0.01	0.52±0.07	15.9	0.06±0.01	0.32±0.07
091127	16.0	0.12±0.01	0.40±0.05	16.0	0.09±0.01	0.43±0.07	16.0	0.09±0.01	0.47±0.07
091127	16.1	0.10±0.01	0.33±0.05	16.1	0.10±0.01	0.48±0.07	16.1	0.08±0.01	0.42±0.07
091127	16.2	0.13±0.01	0.43±0.05	16.2	0.12±0.01	0.57±0.07	16.2	0.05±0.01	0.29±0.07
091127	16.3	0.12±0.01	0.40±0.05	16.3	0.12±0.01	0.57±0.07	16.3	0.04±0.01	0.21±0.07
091127	16.4	0.11±0.01	0.37±0.05	16.4	0.11±0.01	0.52±0.07	16.4	0.04±0.01	0.21±0.07
091127	16.5	0.11±0.01	0.37±0.05	16.5	0.10±0.01	0.48±0.07	16.5	0.04±0.01	0.21±0.07
091127	16.6	0.12±0.01	0.40±0.05	16.6	0.08±0.01	0.38±0.07	16.6	0.09±0.01	0.47±0.07
091127	16.7	0.13±0.01	0.43±0.05	16.7	0.12±0.01	0.57±0.07	16.7	0.04±0.01	0.21±0.07
091127	16.8	0.12±0.01	0.40±0.05	16.8	0.08±0.01	0.38±0.07	16.8	0.09±0.01	0.47±0.07
091127	16.9	0.13±0.01	0.43±0.05	16.9	0.14±0.01	0.44±0.01	16.9	0.10±0.01	0.26±0.07	-1.37±0.07
091127	17.1	0.12±0.01	0.40±0.05	17.1	0.10±0.01	0.50±0.07	17.1	0.08±0.01	0.42±0.07
091127	17.3	0.12±0.01	0.40±0.05	17.3	0.10±0.01	0.48±0.07	17.3	0.08±0.01	0.42±0.07
091127	17.5	0.11±0.01	0.37±0.05	17.5	0.10±0.01	0.48±0.07	17.5	0.09±0.01	0.47±0.07
091127	17.7	0.09±0.01	0.30±0.05	17.7	0.11±0.01	0.52±0.07	17.7	0.08±0.01	0.42±0.07
091127	17.9	0.10±0.01	0.33±0.05	17.9	0.11±0.01	0.52±0.07	17.9	0.08±0.01	0.42±0.07
091127	18.1	0.11±0.01	0.37±0.05	18.1	0.09±0.01	0.43±0.07	18.1	0.09±0.01	0.47±0.07
091127	18.3	0.10±0.01	0.33±0.05	18.3	0.12±0.01	0.57±0.07	18.3	0.05±0.01	0.26±0.07
091127	18.5	0.11±0.01	0.37±0.05	18.5	0.09±0.01	0.43±0.07	18.5	0.09±0.01	0.47±0.07
091127	18.7	0.11±0.01	0.37±0.05	18.7	0.14±0.01	0.67±0.07	18.7	0.05±0.01	0.26±0.07
091127	18.9	0.11±0.01	0.37±0.05	18.9	0.11±0.01	0.52±0.07	18.9	0.07±0.01	0.37±0.07
091127	19.1	0.10±0.01	0.33±0.05	19.1	0.12±0.01	0.57±0.07	19.1	0.05±0.01	0.26±0.07
091127	19.3	0.12±0.01	0.40±0.05	19.3	0.09±0.01	0.43±0.07	19.3	0.10±0.01	0.53±0.07

Table 7 continued on next page

Table 7 (continued)

GRB	Time (ks)	$g-r$	β_o^{CI} (g-r)	Time (ks)	$r-i$	β_o^{CI} (r-i)	Time (ks)	$i-z$	β_o^{CI} (i-z)	Time (ks)	$J-H$	β_o^{CI} (J-H)	Time (ks)	$H-K_s$	β_o^{CI} (H-K _s)
091127	19.5	0.10±0.01	0.33±0.05	19.5	0.09±0.01	0.43±0.07	19.5	0.08±0.01	0.42±0.07
091127	19.7	0.13±0.01	0.43±0.05	19.7	0.10±0.01	0.48±0.07	19.7	0.08±0.01	0.42±0.07
091127	19.9	0.13±0.01	0.43±0.05	19.9	0.10±0.01	0.48±0.07	19.9	0.09±0.01	0.47±0.07
091127	20.1	0.11±0.01	0.37±0.05	20.1	0.10±0.01	0.48±0.07	20.1	0.05±0.01	0.26±0.07
091127	20.3	0.12±0.01	0.40±0.05	20.3	0.12±0.01	0.57±0.07	20.3	0.05±0.01	0.26±0.07
091127	20.5	0.12±0.01	0.40±0.05	20.5	0.12±0.01	0.57±0.07	20.5	0.06±0.01	0.32±0.07
091127	20.7	0.12±0.01	0.49±0.05	20.7	0.12±0.02	0.57±0.11	20.7	0.04±0.02	0.21±0.12
091127	20.9	0.11±0.01	0.37±0.05	20.9	0.12±0.02	0.57±0.11	20.9	0.06±0.03	0.32±0.15
091127	21.1	0.08±0.01	0.27±0.05	21.1	0.13±0.01	0.62±0.07	21.1	0.06±0.01	0.32±0.07
091127	21.3	0.12±0.01	0.40±0.05	21.3	0.11±0.01	0.52±0.07	21.3	0.08±0.01	0.42±0.07
091127	21.5	0.12±0.01	0.40±0.05	21.5	0.11±0.01	0.52±0.07	21.5	0.09±0.01	0.47±0.07
091127	92.4	0.18±0.03	0.60±0.09	92.4	0.19±0.03	0.90±0.13	92.4	0.07±0.04	0.37±0.19
091127	93.3	0.21±0.02	0.70±0.07	93.3	0.17±0.02	0.81±0.11	93.3	0.10±0.04	0.53±0.19
091127	109	0.20±0.02	0.67±0.07	109	0.14±0.02	0.67±0.11	109	0.11±0.03	0.55±0.15
091127	180	0.25±0.03	0.83±0.09	180	0.22±0.03	1.05±0.13	180	0.01±0.04	0.05±0.19
091127	190	0.25±0.04	0.83±0.12	190	0.18±0.03	0.86±0.13	190	0.07±0.04	0.37±0.19
091127	277	0.33±0.06	1.10±0.21	277	0.18±0.06	0.86±0.27	277	0.03±0.07	0.16±0.38
091127	364	0.29±0.10	0.97±0.34	364	0.19±0.08	0.90±0.37	364	0.09±0.08	0.47±0.45
091127	534	0.36±0.10	1.20±0.33	534	0.16±0.08	0.76±0.40	534	-0.03±0.10	-0.16±0.53
091127	959	0.92±0.06	3.07±0.19	959	0.40±0.07	1.90±0.32	959	-0.50±0.16	-2.63±0.85
091127	961	0.94±0.06	3.13±0.31	961	0.35±0.06	1.67±0.28	961	-0.37±0.13	-1.95±0.68
091127	3.99E3	0.95±0.09	3.17±0.31	3.99E3	0.50±0.08	2.38±0.37	3.99E3	-0.25±0.11	-1.32±0.57
091127	4.24E3	0.77±0.13	2.57±0.42	4.24E3	0.45±0.10	2.14±0.48	4.24E3	-0.03±0.19	-0.16±0.99
091127	4.67E3	0.74±0.22	2.47±0.75	4.67E3	0.40±0.18	1.90±0.84	4.67E3	-0.02±0.23	-0.14±1.21
091127	2.92E4	0.84±0.09	2.80±0.31	2.92E4	0.40±0.09	1.90±0.41	2.92E4	-0.50±0.19	-2.63±1.02
100316D	42.5	-0.19±0.06	-0.66±0.19	42.5	-0.01±0.06	-0.04±0.30	42.5	0.06±0.09	0.320±0.45	1.28	-0.27±0.40	-0.90±1.32
100316D	50.2	-0.15±0.04	-0.49±0.14	50.2	-0.07±0.05	-0.32±0.24	50.2	0.14±0.06	0.740±0.30	3.04	-0.27±0.27	-0.90±0.90
100316D	128	-0.20±0.06	-0.66±0.19	128	0.27±0.06	1.30±0.30	128	0.04±0.07	0.220±0.37	3.87	-0.27±0.30	-0.90±0.99
100316D	147	0.10±0.05	0.34±0.17	147	0.04±0.06	0.20±0.28	147	1E-3±0.08	0.010±0.41	4.72	-0.04±0.30	-0.13±0.99
100316D	216	0.07±0.06	0.24±0.19	216	0.04±0.06	0.20±0.30	216	0.26±0.06	1.370±0.34	6.46	-0.56±0.34	-1.86±1.13
100316D	304	0.22±0.04	0.74±0.14	304	0.12±0.04	0.58±0.20	304	0.26±0.04	1.370±0.22	9.05	-0.37±0.29	-1.23±0.96
100316D	387	0.17±0.05	0.57±0.17	387	0.02±0.05	0.10±0.24	387	0.33±0.06	1.740±0.30	992	-0.50±0.23	-1.66±0.76
100316D	472	0.17±0.06	0.57±0.19	472	0.03±0.06	0.15±0.27	472	0.39±0.06	2.060±0.30	1.25E3	-0.21±0.25	-0.70±0.84
100316D	646	0.25±0.07	0.84±0.24	646	0.05±0.07	0.25±0.34	646	0.25±0.08	1.320±0.45	1.34E3	-0.31±0.23	-1.03±0.77
100316D	905	0.52±0.04	1.41±0.14	905	-0.11±0.05	-0.51±0.24	905	0.57±0.05	3.010±0.26	1.86E3	-0.36±0.23	-1.20±0.77
100316D	992	0.44±0.04	1.47±0.14	992	-0.02±0.05	-0.09±0.24	992	0.62±0.05	3.210±0.26	2.20E3	-0.68±0.25	-2.26±0.82
100316D	1.25E3	0.59±0.05	1.97±0.17	1.25E3	-0.05±0.04	-0.23±0.20	1.25E3	0.66±0.04	3.480±0.22
100316D	1.34E3	0.60±0.06	2.01±0.21	1.34E3	-0.13±0.06	-0.61±0.30	1.34E3	0.80±0.06	4.220±0.34
100316D	1.69E3	0.92±0.11	3.07±0.37	1.69E3	-0.07±0.09	-0.32±0.41	1.69E3	0.84±0.09	4.430±0.45
100316D	1.86E3	0.99±0.07	3.31±0.24	1.86E3	-0.04±0.06	-0.18±0.27	1.86E3	0.79±0.05	4.160±0.26
100316D	2.20E3	1.08±0.06	3.61±0.19	2.20E3	0.08±0.04	0.39±0.20	2.20E3	0.75±0.04	3.950±0.22
100316D	2.81E3	1.31±0.11	4.37±0.36	2.81E3	0.10±0.06	0.49±0.30	2.81E3	0.85±0.06	4.480±0.34
100316D	3.50E3	0.05±0.09	0.25±0.44	3.50E3	0.89±0.09	4.690±0.45

Table 7 continued on next page

Table 7 (continued)

GRB	Time	g-r	β_o^{CI}	Time	r-i	β_o^{CI}	Time	i-z	β_o^{CI}	Time	J-H	β_o^{CI}	Time	H-K _s	β_o^{CI}
	(ks)	(g-r)	(ks)		(r-i)	(ks)		(i-z)	(ks)		(J-H)	(ks)		(H-K _s)	(H-Ks)
100621A	1.04	0.98±0.21	3.26±0.70	0.257	0.72±0.21	3.45±1.01	0.257	1.01±0.13	5.33±0.69	0.229	0.89±0.15	2.97±0.51	0.221	0.66±0.13	2.08±0.41
100621A	1.63	1.01±0.28	3.38±0.94	0.348	0.98±0.15	4.65±0.73	0.348	0.90±0.15	4.76±0.81	0.257	0.45±0.10	1.50±0.34	0.267	0.56±0.10	1.74±0.32
100621A	2.38	1.30±0.38	4.34±1.26	0.470	1.09±0.13	5.17±0.62	0.547	0.90±0.10	4.76±0.54	0.361	0.69±0.13	2.30±0.44	0.288	0.48±0.15	1.49±0.48
100621A	3.75	1.16±0.21	3.86±0.70	1.63	1.05±0.24	5.00±1.16	0.686	1.01±0.13	5.33±0.69	0.453	0.58±0.15	1.93±0.51	0.361	0.40±0.13	1.24±0.41
100621A	5.47	1.67±0.21	5.55±0.70	2.38	0.90±0.15	4.31±0.73	3.89	0.80±0.13	4.19±0.69	0.860	0.58±0.18	1.92±0.60	0.453	0.36±0.13	1.13±0.41
100621A	10.4	1.05±0.15	3.50±0.51	5.47	1.16±0.13	5.52±0.62	4.36	0.83±0.13	4.38±0.69	1.00	0.57±0.18	1.91±0.60	1.00	0.44±0.16	1.38±0.51
100621A	8.60	1.12±0.18	5.34±0.86	5.26	1.05±0.13	5.53±0.69	1.08	0.42±0.16	1.40±0.54	1.21	0.53±0.15	1.64±0.48	
100621A	9.63	1.01±0.18	4.83±0.86	7.68	0.94±0.13	4.95±0.69	1.57	0.48±0.15	1.61±0.51	2.29	0.43±0.10	1.34±0.32	
100621A	10.4	1.09±0.18	5.17±0.86	8.93	0.98±0.18	5.14±0.95	1.76	0.52±0.13	1.72±0.44	4.20	0.23±0.08	0.73±0.25	
100621A	9.63	0.94±0.20	4.95±1.08	1.90	0.55±0.15	1.84±0.51	4.20	0.45±0.10	1.41±0.32	
100621A	10.8	0.98±0.18	5.14±0.95	2.13	0.47±0.15	1.56±0.51	4.36	0.66±0.10	2.06±0.32	
100621A	100	-0.18±0.15	-0.95±0.81	3.75	0.41±0.18	1.36±0.60	4.70	0.51±0.13	1.59±0.41	
100621A	100	-0.43±0.15	-2.29±0.81	4.04	0.55±0.13	1.82±0.44	5.07	0.50±0.15	1.57±0.48	
100621A	361	-0.33±0.10	-1.71±0.54	4.04	0.29±0.13	0.95±0.44	28.8	0.90±0.23	2.80±0.72	
100621A	4.36	0.61±0.10	2.03±0.34	100	3.00±0.15	9.37±0.48	
100621A	5.07	0.58±0.18	1.94±0.60	
100621A	10.8	0.50±0.18	1.65±0.60	
100621A	
100814A	0.670	0.16±0.03	0.53±0.09	0.617	0.10±0.05	0.47±0.24	0.617	0.10±0.06	0.51±0.34	0.526	0.28±0.08	0.93±0.28	0.624	0.19±0.10	0.58±0.30
100814A	1.08	0.08±0.03	0.26±0.09	0.820	0.10±0.05	0.47±0.23	0.927	0.03±0.07	0.13±0.37	0.624	0.26±0.07	0.85±0.23	0.677	0.25±0.06	0.78±0.20
100814A	1.33	0.05±0.03	0.15±0.10	0.927	0.18±0.05	0.87±0.26	1.08	-0.04±0.04	-0.23±0.22	0.677	0.17±0.06	0.58±0.20	0.827	0.15±0.12	0.48±0.38
100814A	1.44	0.06±0.03	0.20±0.10	1.08	0.13±0.03	0.62±0.16	1.33	-0.04±0.05	-0.19±0.29	0.726	0.19±0.10	0.62±0.33	1.03	-0.07±0.16	-0.20±0.51
100814A	1.49	0.05±0.02	0.18±0.07	1.13	0.13±0.05	0.61±0.23	1.44	0.03±0.05	0.13±0.26	0.827	0.18±0.09	0.59±0.29	1.08	-0.04±0.08	-0.13±0.26
100814A	1.54	0.03±0.03	0.09±0.09	1.33	0.09±0.04	0.43±0.20	1.49	0.02±0.05	0.12±0.24	0.936	0.21±0.10	0.69±0.32	1.23	-0.32±0.19	-1.00±0.59
100814A	1.64	0.04±0.02	0.15±0.08	1.44	0.07±0.04	0.31±0.20	1.84	-0.07±0.05	-0.35±0.24	1.03	0.18±0.09	0.61±0.30	1.44	0.13±0.15	0.41±0.47
100814A	1.89	0.03±0.02	0.10±0.07	1.49	0.11±0.03	0.50±0.14	1.89	-0.01±0.04	-0.05±0.21	1.08	0.24±0.06	0.80±0.21	1.49	0.05±0.10	0.15±0.31
100814A	2.04	-0.01±0.02	-0.04±0.08	1.84	0.12±0.03	0.58±0.16	1.94	-0.02±0.05	-0.13±0.28	1.13	0.15±0.09	0.49±0.31	1.64	-0.13±0.18	-0.40±0.55
100814A	2.32	0.10±0.02	0.34±0.06	1.89	0.12±0.03	0.58±0.15	2.04	0.08±0.06	0.41±0.32	1.23	0.27±0.10	0.90±0.33	1.90	0.04±0.11	0.13±0.35
100814A	2.48	0.03±0.02	0.10±0.08	1.94	0.07±0.04	0.34±0.18	2.32	0.04±0.04	0.22±0.22	1.34	0.10±0.10	0.33±0.34	2.05	-0.05±0.19	-0.14±0.58
100814A	2.59	0.01±0.03	0.04±0.10	2.04	0.12±0.04	0.57±0.20	2.48	0.07±0.05	0.38±0.25	1.44	-0.07±0.10	-0.22±0.33	2.32	0.23±0.10	0.72±0.32
100814A	2.69	0.06±0.03	0.20±0.10	2.25	0.04±0.04	0.20±0.19	2.59	0.01±0.06	0.03±0.30	1.49	0.04±0.07	0.12±0.23	2.75	0.03±0.12	0.09±0.39
100814A	2.74	0.03±0.02	0.10±0.07	2.32	0.06±0.03	0.27±0.12	2.69	-0.02±0.06	-0.08±0.30	1.54	0.05±0.10	0.18±0.32	3.15	-0.07±0.12	-0.21±0.37
100814A	2.89	0.01±0.02	0.03±0.08	2.48	0.09±0.04	0.41±0.19	2.74	-0.06±0.04	-0.02±0.24	1.64	0.17±0.11	0.58±0.35	3.57	0.09±0.13	0.29±0.39
100814A	3.00	0.04±0.03	0.14±0.10	2.59	0.11±0.04	0.53±0.20	2.79	0.03±0.06	0.14±0.34	1.85	0.07±0.11	0.23±0.36	3.97	-0.15±0.15	-0.46±0.47
100814A	3.10	0.04±0.03	0.13±0.09	2.69	0.14±0.05	0.66±0.23	2.89	-0.04±0.05	-0.24±0.26	1.90	0.14±0.08	0.48±0.26	4.38	-0.10±0.13	-0.30±0.41
100814A	3.15	0.05±0.02	0.15±0.06	2.74	0.13±0.03	0.62±0.14	3.00	0.03±0.05	0.15±0.28	1.95	0.16±0.12	0.54±0.40	4.79	0.02±0.14	0.06±0.43
100814A	3.20	0.06±0.02	0.20±0.08	2.79	0.17±0.04	0.83±0.20	3.10	0.04±0.06	0.20±0.34	2.05	0.13±0.12	0.44±0.40	5.20	-0.16±0.15	-0.51±0.47
100814A	3.30	0.01±0.03	0.02±0.10	2.89	0.10±0.03	0.45±0.15	3.15	0.03±0.04	0.13±0.20	2.16	0.05±0.13	0.17±0.42	5.61	0.21±0.14	0.66±0.42
100814A	3.41	0.01±0.03	0.03±0.11	3.00	0.06±0.04	0.29±0.20	3.20	0.01±0.06	0.07±0.33	2.26	0.19±0.11	0.62±0.38	6.01	0.13±0.16	0.39±0.50
100814A	3.56	0.05±0.02	0.17±0.06	3.10	0.10±0.04	0.46±0.19	3.30	0.04±0.06	0.20±0.32	2.32	0.12±0.08	0.40±0.27	6.42	-0.12±0.16	-0.36±0.49
100814A	3.61	-0.02±0.03	-0.05±0.10	3.15	0.07±0.02	0.34±0.11	3.41	-0.05±0.06	-0.25±0.30	2.49	0.07±0.14	0.23±0.46	6.83	-0.42±0.21	-1.32±0.64
100814A	3.82	0.04±0.03	0.14±0.10	3.20	0.03±0.04	0.15±0.17	3.51	0.02±0.05	0.10±0.29	2.60	0.19±0.12	0.63±0.40	7.41	0.11±0.18	0.35±0.55
100814A	3.92	0.03±0.03	0.09±0.10	3.30	0.13±0.03	0.61±0.15	3.56	0.02±0.05	0.11±0.25	2.70	-0.04±0.13	-0.12±0.44	7.81	-0.13±0.22	-0.42±0.68

Table 7 continued on next page

Table 7 (continued)

GRB	Time (ks)	$g-r$	β_o^{CI} (g-r)	Time (ks)	$r-i$	β_o^{CI} (r-i)	Time (ks)	$i-z$	β_o^{CI} (i-z)	Time (ks)	$J-H$	β_o^{CI} (J-H)	Time (ks)	$H-K_s$	β_o^{CI} (H-K _s)
100814A	3.97	0.01±0.02	0.03±0.08	3.41	0.11±0.04	0.54±0.21	3.61	-0.03±0.07	-0.18±0.35	2.75	0.09±0.07	0.30±0.25	8.22	-0.41±0.22	-1.29±0.68
100814A	4.02	0.01±0.03	0.04±0.10	3.51	0.07±0.04	0.33±0.19	3.71	-0.01±0.06	-0.07±0.31	2.90	-0.00±0.13	-0.01±0.42	12.7	-0.31±0.14	-0.96±0.44
100814A	4.12	0.02±0.02	0.07±0.08	3.56	0.11±0.03	0.53±0.14	3.82	-0.03±0.06	-0.14±0.33	3.00	0.19±0.13	0.62±0.43	18.0	0.02±0.11	0.07±0.35
100814A	4.22	0.06±0.03	0.20±0.10	3.61	0.15±0.04	0.70±0.19	3.92	-0.04±0.06	-0.19±0.30	3.10	0.03±0.11	0.11±0.36	19.9	-0.05±0.12	-0.15±0.38
100814A	4.32	-0.01±0.03	-0.02±0.10	3.71	0.09±0.03	0.43±0.15	3.97	0.01±0.04	0.04±0.23	3.15	0.18±0.07	0.60±0.23	21.8	-0.10±0.13	-0.32±0.41
100814A	4.37	0.05±0.02	0.18±0.06	3.82	0.11±0.04	0.52±0.19	4.12	-0.01±0.05	-0.08±0.25	3.20	0.29±0.12	0.96±0.39	90.0	0.45±0.14	1.42±0.44
100814A	4.52	0.03±0.03	0.10±0.04	3.92	0.13±0.04	0.62±0.21	4.22	0.08±0.06	0.45±0.34	3.30	0.05±0.10	0.16±0.34	93.4	-0.12±0.16	-0.37±0.51
100814A	4.63	-0.01±0.03	-0.03±0.10	3.97	0.13±0.03	0.60±0.13	4.32	0.01±0.06	0.05±0.31	3.52	0.19±0.12	0.63±0.41	93.8	-0.39±0.16	-1.23±0.50
100814A	4.78	0.02±0.02	0.06±0.06	4.12	0.11±0.02	0.51±0.11	4.37	0.01±0.04	0.06±0.20	3.57	0.14±0.09	0.45±0.28	105	-0.08±0.11	-0.24±0.34
100814A	4.83	0.03±0.03	0.09±0.10	4.22	0.02±0.04	0.11±0.20	4.42	-0.01±0.05	-0.07±0.26	3.97	0.04±0.09	0.13±0.29	105	0.06±0.12	0.20±0.36
100814A	4.93	0.04±0.03	0.13±0.09	4.32	0.13±0.03	0.63±0.16	4.52	-0.07±0.05	-0.34±0.28	4.38	0.23±0.08	0.77±0.26	279	0.06±0.10	0.20±0.31
100814A	5.04	0.04±0.03	0.14±0.10	4.37	0.07±0.02	0.35±0.12	4.73	0.02±0.05	0.09±0.28	4.79	0.07±0.08	0.24±0.26	281	0.14±0.11	0.43±0.33
100814A	5.14	0.09±0.02	0.30±0.07	4.42	0.05±0.04	0.25±0.18	4.78	0.01±0.04	0.04±0.20	5.20	0.19±0.08	0.63±0.27	282	0.34±0.17	1.07±0.53
100814A	5.19	0.07±0.02	0.22±0.05	4.52	0.14±0.03	0.69±0.16	4.83	0.01±0.05	0.03±0.24	5.61	0.09±0.09	0.29±0.31	363	0.15±0.13	0.46±0.39
100814A	5.24	0.07±0.02	0.23±0.06	4.73	0.12±0.03	0.58±0.16	4.93	0.01±0.06	0.04±0.32	6.01	-0.04±0.10	-0.13±0.32	450	0.18±0.18	0.57±0.56
100814A	5.34	0.05±0.03	0.18±0.09	4.78	0.10±0.03	0.47±0.12	5.14	-0.03±0.06	-0.13±0.31	6.42	0.14±0.10	0.48±0.32	533	0.17±0.24	0.52±0.75
100814A	5.45	0.01±0.03	0.05±0.11	4.83	0.06±0.04	0.30±0.19	5.19	0.00±0.04	0.02±0.23	6.83	0.09±0.10	0.30±0.32	535	0.04±0.30	0.13±0.94
100814A	5.55	0.08±0.03	0.28±0.10	4.93	0.07±0.04	0.32±0.18	5.24	0.05±0.06	0.27±0.31	7.41	0.10±0.10	0.35±0.34	621	0.38±0.31	1.20±0.96
100814A	5.60	0.04±0.02	0.13±0.07	5.14	0.10±0.03	0.46±0.16	5.34	0.03±0.05	0.16±0.24	7.81	0.01±0.11	0.03±0.36	622	0.18±0.27	0.57±0.84
100814A	5.65	0.04±0.03	0.14±0.10	5.19	0.09±0.03	0.41±0.12	5.45	-0.06±0.07	-0.29±0.36	8.22	0.22±0.09	0.72±0.29	708	0.37±0.52	1.14±1.63
100814A	5.75	0.01±0.03	0.05±0.10	5.24	0.09±0.03	0.43±0.14	5.60	0.03±0.04	0.17±0.20	12.7	0.18±0.07	0.60±0.23
100814A	5.86	0.04±0.03	0.14±0.10	5.34	0.13±0.03	0.61±0.14	5.75	0.08±0.06	0.42±0.31	18.0	0.23±0.07	0.77±0.22
100814A	5.96	0.01±0.03	0.04±0.09	5.45	0.18±0.04	0.86±0.21	5.86	-0.08±0.07	-0.41±0.35	19.9	0.24±0.08	0.80±0.27
100814A	6.01	0.06±0.02	0.20±0.05	5.60	0.10±0.02	0.49±0.12	5.96	0.03±0.06	0.18±0.32	21.8	0.23±0.07	0.77±0.25
100814A	6.16	0.11±0.03	0.35±0.11	5.75	0.10±0.04	0.47±0.19	6.01	-0.01±0.04	-0.04±0.21	90.0	0.08±0.12	0.26±0.38
100814A	6.27	-0.02±0.03	-0.08±0.11	5.86	0.11±0.04	0.52±0.20	6.16	0.01±0.07	0.06±0.35	93.4	1E-3±0.10	0.00±0.34
100814A	6.36	0.06±0.03	0.18±0.10	5.96	0.08±0.04	0.38±0.19	6.36	0.07±0.06	0.36±0.31	93.8	0.24±0.09	0.80±0.31
100814A	6.42	-0.01±0.02	-0.03±0.07	6.01	0.07±0.02	0.32±0.12	6.42	0.04±0.04	0.19±0.23	105	0.16±0.08	0.54±0.27
100814A	6.56	0.03±0.02	0.11±0.08	6.05	0.11±0.03	0.52±0.17	6.46	-0.01±0.06	-0.06±0.33	105	0.08±0.09	0.26±0.28
100814A	6.68	0.02±0.03	0.07±0.10	6.16	0.04±0.04	0.20±0.21	6.68	-0.04±0.07	-0.18±0.35	279	0.37±0.07	1.23±0.23
100814A	6.77	0.01±0.03	0.05±0.09	6.36	0.09±0.04	0.42±0.20	6.77	-0.01±0.07	-0.07±0.35	281	0.27±0.08	0.88±0.25
100814A	6.82	0.03±0.02	0.11±0.06	6.42	0.11±0.03	0.53±0.13	6.82	0.00±0.04	0.01±0.22	282	0.08±0.12	0.25±0.40
100814A	6.87	0.07±0.03	0.23±0.10	6.46	0.12±0.04	0.58±0.20	6.97	0.01±0.07	0.08±0.35	363	0.32±0.09	1.05±0.29
100814A	6.97	0.06±0.02	0.19±0.08	6.56	0.05±0.03	0.24±0.14	7.25	-0.02±0.06	-0.10±0.31	450	0.37±0.13	1.23±0.43
100814A	7.25	0.02±0.03	0.06±0.10	6.68	0.14±0.04	0.65±0.20	7.35	0.04±0.06	0.19±0.31	535	0.49±0.17	1.64±0.56
100814A	7.35	0.04±0.03	0.14±0.10	6.77	0.08±0.04	0.37±0.19	7.40	0.01±0.04	0.03±0.22	708	0.15±0.30	0.50±1.02
100814A	7.40	0.02±0.02	0.08±0.06	6.82	0.08±0.03	0.36±0.12	7.45	0.00±0.06	0.01±0.34
100814A	7.55	0.01±0.03	0.04±0.10	6.87	0.04±0.04	0.19±0.19	7.55	0.05±0.06	0.25±0.33
100814A	7.66	0.03±0.03	0.10±0.10	6.97	0.02±0.04	0.09±0.19	7.66	-0.07±0.06	-0.39±0.32
100814A	7.76	0.03±0.03	0.09±0.09	7.25	0.09±0.04	0.44±0.21	7.76	0.09±0.06	0.49±0.29
100814A	7.81	0.04±0.02	0.13±0.07	7.35	0.08±0.04	0.38±0.17	7.81	-0.01±0.04	-0.05±0.21
100814A	7.86	0.03±0.03	0.11±0.09	7.40	0.10±0.02	0.48±0.11	7.96	0.03±0.07	0.13±0.36
100814A	7.96	0.00±0.03	0.01±0.10	7.45	0.09±0.04	0.42±0.17	8.06	0.05±0.06	0.27±0.30

Table 7 continued on next page

Table 7 (*continued*)

GRB	Time (ks)	$g-r$	β_o^{CI} (g-r)	Time (ks)	$r-i$	β_o^{CI} (r-i)	Time (ks)	$i-z$	β_o^{CI} (i-z)	Time (ks)	$J-H$	β_o^{CI} (J-H)	Time (ks)	$H-K_s$	β_o^{CI} (H-K _s)
100814A	8.06	0.05±0.03	0.15±0.10	7.55	0.09±0.04	0.41±0.20	8.16	-0.01±0.05	-0.03±0.28
100814A	8.16	0.06±0.03	0.21±0.10	7.66	0.09±0.04	0.44±0.19	8.21	-0.03±0.03	-0.13±0.17
100814A	8.21	0.06±0.02	0.21±0.05	7.76	0.07±0.04	0.32±0.20	12.0	-0.02±0.03	-0.11±0.13
100814A	8.26	0.08±0.03	0.27±0.09	7.81	0.07±0.03	0.34±0.13	12.7	-0.02±0.01	-0.10±0.07
100814A	8.36	0.06±0.03	0.21±0.09	7.86	0.08±0.04	0.38±0.19	12.9	-0.01±0.03	-0.05±0.13
100814A	12.0	0.02±0.01	0.06±0.04	7.96	0.10±0.04	0.50±0.20	13.3	-0.02±0.02	-0.09±0.12
100814A	12.4	0.04±0.01	0.12±0.04	8.06	0.06±0.04	0.30±0.18	17.3	-0.00±0.03	-0.04±0.15
100814A	12.7	0.03±0.01	0.09±0.02	8.16	0.10±0.04	0.50±0.18	17.7	-1E-3±0.02	-0.01±0.11
100814A	12.9	0.03±0.01	0.10±0.03	8.21	0.08±0.02	0.39±0.10	17.9	0±0.01	0±0.07
100814A	13.3	0.03±0.01	0.08±0.03	8.36	0.06±0.04	0.30±0.17	19.8	0.01±0.02	0.08±0.09
100814A	17.3	0.03±0.01	0.11±0.04	12.0	0.11±0.02	0.51±0.07	20.5	-0.01±0.03	-0.03±0.14
100814A	17.7	0.03±0.01	0.10±0.04	12.4	0.10±0.02	0.50±0.08	21.8	0.00±0.02	0.02±0.09
100814A	17.9	0.03±0.01	0.10±0.02	12.7	0.11±0.01	0.51±0.04	22.0	-0.03±0.03	-0.14±0.15
100814A	18.2	0.03±0.01	0.10±0.03	12.9	0.10±0.02	0.49±0.08	23.2	-0.01±0.03	-0.07±0.15
100814A	18.6	0.04±0.01	0.14±0.04	13.3	0.09±0.02	0.44±0.08	90.0	0.06±0.05	0.29±0.28
100814A	19.2	0.02±0.01	0.07±0.03	17.3	0.10±0.02	0.46±0.09	93.2	-0.01±0.06	-0.03±0.34
100814A	19.8	0.03±0.01	0.10±0.02	17.7	0.11±0.01	0.50±0.07	93.3	0.00±0.04	0.01±0.23
100814A	20.1	0.02±0.01	0.08±0.03	17.9	0.11±0.01	0.50±0.05	93.8	0.01±0.05	0.07±0.25
100814A	20.5	0.03±0.01	0.10±0.03	18.6	0.09±0.02	0.42±0.08	93.8	0.04±0.07	0.23±0.35
100814A	21.1	0.04±0.01	0.15±0.03	19.6	0.10±0.02	0.48±0.08	105	-0.04±0.06	-0.23±0.33
100814A	21.5	0.02±0.01	0.07±0.04	19.8	0.12±0.01	0.56±0.05	105	0.07±0.06	0.35±0.34
100814A	21.8	0.03±0.01	0.11±0.02	20.5	0.12±0.01	0.59±0.06	105	0.04±0.04	0.22±0.20
100814A	22.0	0.03±0.01	0.11±0.04	21.8	0.10±0.01	0.48±0.06	105	0.05±0.06	0.26±0.32
100814A	22.4	0.03±0.01	0.10±0.04	22.0	0.08±0.02	0.40±0.09	105	0.08±0.05	0.44±0.26
100814A	23.0	0.02±0.01	0.07±0.04	22.4	0.10±0.02	0.46±0.09	105	0.12±0.06	0.61±0.33
100814A	23.2	0.04±0.01	0.12±0.04	23.0	0.09±0.02	0.44±0.10	105	0.10±0.04	0.50±0.19
100814A	90.0	0.09±0.02	0.29±0.08	23.2	0.10±0.02	0.49±0.09	106	0.06±0.07	0.33±0.34
100814A	93.3	0.12±0.02	0.41±0.08	90.0	0.20±0.04	0.94±0.18	106	0.12±0.06	0.63±0.33
100814A	93.7	0.18±0.04	0.60±0.12	93.2	0.07±0.05	0.34±0.23	279	0.07±0.03	0.35±0.14
100814A	93.8	0.12±0.02	0.41±0.07	93.3	0.15±0.03	0.71±0.17	279	0.09±0.02	0.46±0.10
100814A	93.9	0.08±0.03	0.26±0.09	93.4	0.14±0.06	0.67±0.27	280	0.10±0.03	0.54±0.14
100814A	105	0.13±0.03	0.44±0.09	93.6	0.15±0.06	0.70±0.27	280	0.10±0.03	0.54±0.17
100814A	105	0.11±0.01	0.38±0.04	93.8	0.15±0.03	0.71±0.15	281	0.10±0.03	0.51±0.16
100814A	105	0.10±0.03	0.35±0.09	93.8	0.19±0.05	0.90±0.22	281	0.10±0.03	0.53±0.17
100814A	105	0.14±0.03	0.48±0.10	105	0.16±0.04	0.76±0.19	281	0.09±0.02	0.49±0.10
100814A	105	0.17±0.02	0.57±0.08	105	0.14±0.03	0.65±0.17	281	0.09±0.03	0.48±0.18
100814A	105	0.12±0.02	0.38±0.05	105	0.17±0.02	0.80±0.10	282	0.05±0.09	0.27±0.47
100814A	106	0.11±0.03	0.37±0.10	105	0.19±0.04	0.91±0.18	282	0.13±0.09	0.68±0.45
100814A	106	0.05±0.03	0.16±0.09	105	0.16±0.04	0.78±0.18	282	0.03±0.06	0.14±0.33
100814A	279	0.23±0.01	0.76±0.04	105	0.09±0.04	0.43±0.19	283	0.05±0.09	0.24±0.49
100814A	279	0.22±0.01	0.74±0.04	106	0.15±0.02	0.72±0.11	363	0.10±0.03	0.54±0.17
100814A	279	0.22±0.01	0.74±0.02	106	0.15±0.03	0.72±0.16	363	0.11±0.04	0.57±0.19
100814A	280	0.22±0.01	0.73±0.05	106	0.22±0.04	1.04±0.20	363	0.12±0.02	0.61±0.11

Table 7 continued on next page

Table 7 (continued)

GRB	Time (ks)	$g-r$	β_o^{CI} (g-r)	Time (ks)	$r-i$	β_o^{CI} (r-i)	Time (ks)	$i-z$	β_o^{CI} (i-z)	Time (ks)	$J-H$	β_o^{CI} (J-H)	Time (ks)	$H-K_s$	β_o^{CI} (H-K _s)
100814A	280	0.20±0.01	0.67±0.03	279	0.24±0.02	1.16±0.09	449	0.17±0.06	0.87±0.29
100814A	281	0.22±0.01	0.72±0.05	279	0.22±0.02	1.02±0.10	450	0.12±0.03	0.65±0.18
100814A	281	0.24±0.01	0.79±0.05	279	0.23±0.01	1.12±0.06	450	0.09±0.06	0.48±0.32
100814A	281	0.22±0.01	0.74±0.03	280	0.24±0.02	1.16±0.10	533	0.06±0.07	0.31±0.35
100814A	281	0.21±0.01	0.69±0.04	280	0.23±0.02	1.10±0.10	533	0.12±0.04	0.64±0.21
100814A	282	0.20±0.02	0.65±0.07	281	0.25±0.02	1.18±0.09	533	0.15±0.06	0.78±0.32
100814A	282	0.22±0.04	0.73±0.13	281	0.22±0.02	1.03±0.10	534	0.20±0.07	1.03±0.37
100814A	363	0.23±0.01	0.78±0.05	281	0.23±0.01	1.11±0.06	534	0.11±0.09	0.57±0.45
100814A	363	0.22±0.01	0.72±0.05	281	0.23±0.02	1.11±0.09	535	0.10±0.04	0.52±0.24
100814A	363	0.23±0.01	0.76±0.03	282	0.30±0.07	1.44±0.36	536	0.13±0.08	0.67±0.40
100814A	364	0.24±0.02	0.79±0.05	282	0.22±0.06	1.03±0.28	620	0.06±0.08	0.33±0.43
100814A	364	0.21±0.01	0.69±0.05	282	0.27±0.04	1.28±0.21	620	0.20±0.06	1.03±0.31
100814A	449	0.24±0.02	0.80±0.07	283	0.21±0.08	1.02±0.36	621	0.16±0.05	0.82±0.26
100814A	450	0.22±0.02	0.74±0.08	363	0.24±0.02	1.12±0.10	621	0.15±0.08	0.78±0.42
100814A	450	0.23±0.01	0.76±0.05	363	0.23±0.02	1.09±0.11	621	0.16±0.08	0.86±0.43
100814A	450	0.20±0.02	0.68±0.06	363	0.24±0.01	1.16±0.07	622	0.11±0.08	0.57±0.40
100814A	450	0.21±0.02	0.70±0.07	364	0.26±0.02	1.22±0.10	622	0.16±0.07	0.85±0.35
100814A	533	0.22±0.05	0.74±0.16	449	0.25±0.04	1.19±0.17	622	0.13±0.05	0.70±0.25
100814A	533	0.32±0.05	1.06±0.17	450	0.27±0.02	1.26±0.10	623	0.16±0.08	0.83±0.43
100814A	533	0.28±0.03	0.92±0.09	450	0.29±0.03	1.37±0.16	708	0.15±0.16	0.73±0.85
100814A	533	0.25±0.04	0.84±0.14	450	0.29±0.04	1.38±0.17	708	0.19±0.09	1.01±0.49
100814A	534	0.27±0.05	0.90±0.15	533	0.27±0.05	1.30±0.24	709	0.05±0.16	0.26±0.83
100814A	534	0.24±0.04	0.81±0.14	533	0.25±0.04	1.20±0.20	709	0.19±0.15	1.01±0.81
100814A	535	0.24±0.03	0.80±0.11	533	0.26±0.03	1.22±0.13	961	0.08±0.16	0.44±0.86
100814A	535	0.23±0.02	0.76±0.07	533	0.25±0.05	1.18±0.22	1.31E3	-0.35±0.27	-1.83±1.43
100814A	535	0.22±0.03	0.75±0.11	534	0.21±0.05	1.01±0.25	5.45E3	-0.25±0.35	-1.31±1.82
100814A	536	0.21±0.03	0.70±0.11	534	0.24±0.05	1.14±0.25
100814A	620	0.20±0.05	0.66±0.16	535	0.27±0.04	1.28±0.18
100814A	620	0.27±0.04	0.90±0.14	535	0.29±0.03	1.38±0.13
100814A	621	0.24±0.03	0.79±0.10	536	0.29±0.05	1.40±0.24
100814A	621	0.19±0.05	0.63±0.16	620	0.24±0.05	1.15±0.24
100814A	621	0.24±0.06	0.80±0.18	620	0.24±0.04	1.15±0.20
100814A	622	0.26±0.05	0.84±0.18	621	0.26±0.04	1.26±0.17
100814A	622	0.26±0.05	0.88±0.16	621	0.27±0.06	1.27±0.27
100814A	622	0.25±0.03	0.84±0.10	621	0.33±0.06	1.55±0.28
100814A	623	0.22±0.04	0.72±0.14	622	0.20±0.05	0.95±0.26
100814A	623	0.26±0.04	0.87±0.15	622	0.18±0.05	0.87±0.23
100814A	708	0.36±0.15	1.20±0.49	622	0.22±0.04	1.03±0.18
100814A	708	0.33±0.14	1.11±0.45	623	0.25±0.05	1.20±0.23
100814A	708	0.23±0.07	0.75±0.24	623	0.17±0.06	0.80±0.28
100814A	961	0.41±0.28	1.36±0.92	708	0.23±0.13	1.09±0.62
100814A	1.31E3	0.29±0.16	0.97±0.54	708	0.18±0.10	0.84±0.46
100814A	1.31E3	0.10±0.16	0.34±0.54	708	0.22±0.07	1.06±0.33

Table 7 continued on next page

Table 7 (continued)

GRB	Time (ks)	$g-r$	β_o^{CI} (g-r)	Time (ks)	$r-i$	β_o^{CI} (r-i)	Time (ks)	$i-z$	β_o^{CI} (i-z)	Time (ks)	$J-H$	β_o^{CI} (J-H)	Time (ks)	$H-K_s$	β_o^{CI} (H-K _s)
100814A	2.26E3	-0.02±0.13	-0.07±0.45	709	0.25±0.11	1.18±0.54
100814A	5.45E3	0.05±0.19	0.16±0.62	709	0.23±0.11	1.08±0.53
100814A	1.25E4	-0.08±0.26	-0.26±0.85	961	0.40±0.16	1.88±0.77
100814A	1.25E4	-0.13±0.27	-0.42±0.89	1.31E3	0.28±0.19	1.32±0.89
100814A	1.31E3	0.16±0.19	0.75±0.90
100814A	1.31E3	0.07±0.24	0.31±1.12
100814A	2.26E3	0.35±0.20	1.68±0.95
100814A	5.45E3	0.19±0.23	0.91±1.11
101219B	29.5	0.02±0.07	0.05±0.24	29.5	-0.04±0.08	-0.20±0.37	29.5	0.20±0.09	1.04±0.48	29.5	0.05±0.15	0.17±0.50	29.5	0.28±0.26	0.87±0.81
101219B	30.8	-0.04±0.06	-0.15±0.19	30.8	0.10±0.04	0.47±0.20	30.8	-0.02±0.05	-0.12±0.26	30.8	0.15±0.14	0.51±0.45	30.8	0.23±0.23	0.71±0.71
101219B	32.5	-0.05±0.06	-0.18±0.21	32.5	0.08±0.04	0.38±0.17	32.5	0.01±0.04	0.04±0.22	32.5	0.32±0.12	1.07±0.41	32.5	-0.10±0.28	-0.32±0.87
101219B	38.5	0.01±0.07	0.02±0.24	38.5	0.11±0.05	0.52±0.24	38.5	-0.08±0.05	-0.44±0.26	38.6	0.27±0.16	0.91±0.52	38.6	0.56±0.26	1.74±0.81
101219B	117	-0.05±0.10	-0.18±0.33	117	0.06±0.06	0.28±0.30	117	-0.07±0.09	-0.38±0.45	117	0.39±0.25	1.31±0.84	117	0.75±0.39	2.33±1.22
101219B	206	-0.00±0.18	-0.01±0.61	206	-0.11±0.11	-0.53±0.54	206	-0.20±0.17	-1.07±0.92	557	0.35±0.59	1.17±1.96
101219B	293	0.22±0.07	0.72±0.23	293	-0.06±0.12	-0.29±0.58	293	-0.29±0.16	-1.54±0.86
101219B	466	0.29±0.07	0.95±0.24	466	-0.07±0.08	-0.34±0.37	466	-0.31±0.17	-1.65±0.90
101219B	557	0.41±0.14	1.35±0.45	557	-0.03±0.14	-0.15±0.64	557	-0.37±0.30	-1.96±1.56
101219B	812	0.67±0.07	2.22±0.24	812	0.12±0.09	0.57±0.42	812	-0.75±0.19	-3.96±0.99
101219B	897	0.49±0.14	1.62±0.46	897	0.09±0.13	0.42±0.62	897	-0.54±0.20	-2.86±1.06
101219B	1.07E3	0.75±0.09	2.49±0.31	1.07E3	0.14±0.11	0.66±0.51	1.07E3	-0.53±0.19	-3.12±1.01
101219B	1.24E3	0.61±0.23	2.02±0.76	1.24E3	-0.16±0.23	-0.77±1.08	1.24E3	-0.19±0.33	-1.02±1.73
101219B	1.42E3	0.75±0.20	2.49±0.65	1.42E3	0.31±0.17	1.47±0.80	1.42E3	-0.44±0.29	-2.33±1.52
101219B	2.11E3	0.45±0.23	2.14±1.11	2.11E3	-0.33±0.27	-1.75±1.42
101219B	2.28E3	0.89±0.21	4.23±0.98	2.28E3	-0.12±0.23	-0.65±1.21
101219B	3.06E3	0.41±0.18	1.95±0.85	3.06E3	-0.37±0.37	-1.96±1.94
110918A	194	0.26±0.04	0.88±0.15	194	0.22±0.04	1.05±0.21	194	0.11±0.08	0.55±0.42	126	0.16±0.11	0.53±0.38	194	-0.20±0.19	-0.63±0.60
110918A	194	0.21±0.05	0.71±0.17	194	0.22±0.04	1.05±0.20	194	0.19±0.09	1.02±0.45	194	0.23±0.15	0.78±0.50	205	-0.32±0.20	-1.01±0.63
110918A	195	0.22±0.04	0.75±0.12	195	0.25±0.04	1.19±0.21	195	0.11±0.07	0.55±0.38	205	0.36±0.14	1.21±0.48	215	0.03±0.19	0.11±0.60
110918A	204	0.21±0.04	0.71±0.12	204	0.19±0.04	0.90±0.17	204	0.17±0.07	0.91±0.35	215	0.26±0.16	0.86±0.52	291	0.34±0.20	1.07±0.63
110918A	205	0.21±0.04	0.71±0.12	205	0.22±0.04	1.05±0.17	205	0.17±0.07	0.91±0.35	291	0.13±0.15	0.43±0.50	381	0.16±0.23	0.50±0.71
110918A	205	0.21±0.04	0.71±0.12	205	0.25±0.04	1.19±0.17	205	0.12±0.07	0.65±0.35	381	0.84±0.19	2.79±0.63	553	0.31±0.26	0.96±0.80
110918A	215	0.21±0.04	0.71±0.12	215	0.23±0.04	1.10±0.21	215	0.10±0.07	0.54±0.38	553	0.98±0.22	3.25±0.73
110918A	215	0.21±0.04	0.71±0.15	215	0.21±0.04	1.00±0.17	215	0.20±0.08	1.07±0.40
110918A	216	0.22±0.06	0.75±0.19	216	0.19±0.05	0.90±0.24	216	0.20±0.08	1.07±0.42
110918A	290	0.26±0.03	0.88±0.09	290	0.14±0.04	0.67±0.17	290	0.25±0.07	1.33±0.35
110918A	291	0.21±0.04	0.71±0.14	291	0.22±0.05	1.05±0.24	291	0.20±0.07	1.07±0.38
110918A	291	0.24±0.04	0.81±0.12	291	0.20±0.04	0.95±0.17	291	0.17±0.06	0.91±0.31
110918A	381	0.28±0.03	0.95±0.09	381	0.23±0.04	1.10±0.17	381	0.09±0.06	0.49±0.31
110918A	553	0.21±0.05	0.71±0.17	553	0.36±0.07	1.71±0.32	553	0.28±0.09	1.49±0.49
110918A	726	0.14±0.07	0.48±0.24	726	0.43±0.10	2.05±0.49	726	0.47±0.13	2.49±0.71
110918A	982	0.11±0.09	0.38±0.31	982	0.73±0.11	3.48±0.54	982	0.41±0.13	2.47±0.67
110918A	1.51E3	0.23±0.11	0.78±0.35	1.51E3	0.71±0.51	1.51E3	0.29±0.11	1.54±0.60
111209A	64.5	-0.11±0.07	-0.33±0.23	64.5	-0.10±0.06	-0.50±0.27	64.5	-0.11±0.07	-0.53±0.36	64.5	0.20±0.20	0.68±0.67	64.5	0.00±0.29	0.01±0.90

Table 7 continued on next page

Table 7 (continued)

GRB	Time (ks)	$g-r$	β_o^{CI} (g-r)	Time (ks)	$r-i$	β_o^{CI} (r-i)	Time (ks)	$i-z$	β_o^{CI} (i-z)	Time (ks)	$J-H$	β_o^{CI} (J-H)	Time (ks)	$H-K_s$	β_o^{CI} (H-K _s)	
111209A	64.9	-0.07±0.06	-0.22±0.20	64.9	-0.10±0.06	-0.48±0.30	64.9	-0.14±0.07	-0.73±0.39	65.0	0.18±0.21	0.59±0.69	65.0	0.50±0.24	1.57±0.76	
111209A	65.4	-0.09±0.07	-0.29±0.25	65.4	-0.03±0.06	-0.17±0.28	65.4	-0.17±0.07	-0.89±0.38	65.4	0.20±0.22	0.68±0.73	65.4	0.18±0.30	0.55±0.95	
111209A	65.8	-0.05±0.07	-0.18±0.24	65.8	-0.10±0.05	-0.48±0.25	65.8	-0.13±0.07	-0.67±0.38	65.8	0.23±0.23	0.78±0.77	65.8	0.32±0.26	1.01±0.80	
111209A	66.3	-0.09±0.07	-0.31±0.23	66.3	-0.09±0.05	-0.44±0.26	66.3	-0.10±0.06	-0.51±0.33	66.3	0.22±0.23	0.72±0.78	66.3	0.04±0.29	0.11±0.92	
111209A	66.7	-0.08±0.07	-0.26±0.24	66.7	-0.08±0.05	-0.39±0.22	66.7	-0.14±0.06	-0.72±0.34	66.7	0.06±0.22	0.37±0.26	66.7	0.37±0.25	1.16±0.83	
111209A	67.1	-0.08±0.07	-0.28±0.22	67.1	-0.08±0.06	-0.37±0.29	67.1	-0.18±0.07	-0.97±0.37	67.2	0.26±0.24	0.87±0.80	67.2	0.04±0.33	0.13±1.04	
111209A	67.6	-0.10±0.07	-0.35±0.23	67.6	-0.08±0.05	-0.38±0.24	67.6	-0.09±0.06	-0.45±0.29	67.6	0.04±0.19	0.13±0.65	67.6	0.46±0.27	1.44±0.83	
111209A	68.0	-0.06±0.06	-0.18±0.20	68.0	-0.09±0.05	-0.42±0.23	68.0	-0.12±0.06	-0.62±0.32	68.0	0.20±0.19	0.65±0.65	68.0	0.30±0.27	0.93±0.86	
111209A	68.5	-0.04±0.06	-0.13±0.20	68.5	-0.10±0.05	-0.49±0.23	68.5	-0.15±0.06	-0.78±0.31	68.5	0.22±0.20	0.74±0.66	68.5	0.37±0.25	1.15±0.77	
111209A	69.2	-0.09±0.06	-0.32±0.20	69.2	-0.10±0.04	-0.45±0.21	69.2	-0.06±0.03	-0.33±0.17	69.2	0.17±0.19	0.57±0.63	69.2	0.28±0.26	0.86±0.80	
111209A	70.0	-0.09±0.06	-0.29±0.19	70.0	-0.08±0.04	-0.38±0.18	70.0	-0.07±0.06	-0.36±0.29	70.0	0.22±0.21	0.72±0.70	70.0	0.20±0.25	0.63±0.78	
111209A	70.8	-0.13±0.06	-0.42±0.19	70.8	-0.08±0.04	-0.37±0.21	70.8	-0.08±0.05	-0.41±0.26	70.8	0.01±0.22	0.02±0.74	70.8	0.21±0.25	0.65±0.79	
111209A	71.6	-0.09±0.06	-0.31±0.19	71.6	-0.09±0.03	-0.45±0.13	71.6	-0.09±0.06	-0.48±0.31	71.6	0.17±0.22	0.57±0.72	71.6	0.38±0.22	1.19±0.68	
111209A	72.4	-0.08±0.06	-0.26±0.20	72.4	-0.11±0.03	-0.50±0.15	72.4	-0.07±0.06	-0.35±0.30	72.4	0.34±0.20	1.14±0.66	72.4	0.37±0.20	1.16±0.64	
111209A	73.2	-0.08±0.05	-0.28±0.16	73.2	-0.05±0.03	-0.25±0.15	73.2	-0.08±0.06	-0.44±0.31	73.2	0.22±0.19	0.72±0.63	73.2	0.27±0.21	0.84±0.66	
111209A	74.0	-0.02±0.06	-0.07±0.20	74.0	-0.11±0.03	-0.54±0.15	74.0	-0.01±0.05	-0.05±0.26	74.0	0.19±0.15	0.62±0.49	74.0	0.34±0.20	1.06±0.63	
111209A	74.8	-0.05±0.05	-0.16±0.18	74.8	-0.09±0.03	-0.43±0.15	74.8	-0.07±0.04	-0.35±0.22	74.8	0.08±0.19	0.25±0.64	74.8	0.38±0.21	1.19±0.65	
111209A	75.6	-0.02±0.08	-0.07±0.28	75.6	-0.09±0.04	-0.45±0.17	75.6	-0.09±0.07	-0.49±0.36	75.6	0.17±0.16	0.57±0.54	75.6	0.31±0.22	0.96±0.69	
111209A	76.3	-0.03±0.07	-0.11±0.23	76.3	-0.05±0.03	-0.24±0.13	76.3	-0.07±0.05	-0.36±0.25	76.4	0.09±0.17	0.31±0.57	76.4	0.28±0.20	0.89±0.63	
111209A	77.1	5.54E-4±0.07	0.00±0.20	77.1	-0.11±0.03	-0.54±0.15	77.1	-0.07±0.04	-0.36±0.21	77.2	0.08±0.17	0.26±0.55	77.2	0.40±0.22	1.23±0.69	
111209A	78.0	0.00±0.08	0.01±0.25	78.0	-0.05±0.03	-0.24±0.15	78.0	-0.05±0.03	-0.27±0.18	78.0	0.30±0.16	1.02±0.54	78.0	0.66±0.21	1.18±0.66	
111209A	78.8	-0.05±0.09	-0.17±0.28	78.8	-0.05±0.04	-0.22±0.18	78.8	-0.05±0.05	-0.26±0.26	78.8	0.21±0.15	0.70±0.50	78.8	0.25±0.22	0.78±0.67	
111209A	79.6	-0.01±0.08	-0.04±0.28	79.6	-0.01±0.04	-0.04±0.17	79.6	-0.08±0.05	-0.44±0.28	79.6	0.21±0.16	0.70±0.52	79.6	0.46±0.21	1.42±0.67	
111209A	80.4	0.03±0.09	0.11±0.29	80.4	-0.01±0.04	-0.03±0.17	80.4	-0.06±0.04	-0.33±0.18	80.4	0.32±0.13	1.07±0.44	80.4	0.38±0.18	1.19±0.55	
111209A	81.2	-0.01±0.07	-0.03±0.22	81.2	-0.06±0.06	-0.28±0.28	81.2	-0.03±0.04	-0.14±0.23	81.2	0.15±0.15	0.52±0.50	81.2	0.47±0.20	1.47±0.62	
111209A	82.0	-0.03±0.06	-0.18±0.20	82.0	-0.08±0.04	-0.37±0.18	82.0	-0.06±0.04	-0.02±0.23	82.0	0.22±0.14	0.72±0.47	82.0	0.39±0.23	1.22±0.73	
111209A	82.8	-0.05±0.06	-0.15±0.18	82.8	-0.00±0.03	-0.01±0.16	82.8	-0.08±0.03	-0.41±0.18	82.8	0.28±0.17	0.94±0.57	82.8	0.40±0.19	1.26±0.59	
111209A	84.0	0.02±0.06	0.08±0.21	84.0	-0.08±0.04	-0.36±0.19	84.0	-0.04±0.04	-0.22±0.21	84.0	0.34±0.14	1.15±0.46	84.0	0.39±0.19	1.20±0.58	
111209A	84.8	-0.04±0.04	-0.13±0.14	84.8	-0.01±0.03	-0.04±0.12	84.8	-0.06±0.03	-0.50±0.17	85.0	0.27±0.15	0.88±0.49	85.0	0.28±0.19	0.86±0.61	
111209A	85.6	-0.02±0.06	-0.15±0.18	85.6	-0.00±0.03	-0.01±0.16	85.6	-0.08±0.05	-0.42±0.28	85.6	0.22±0.16	0.72±0.54	85.6	0.25±0.21	0.77±0.67	
111209A	86.4	-0.04±0.04	-0.11±0.14	86.4	-0.01±0.03	-0.02±0.20	86.4	-0.08±0.05	-0.32±0.27	86.4	0.53±0.19	1.76±0.64	86.4	0.23±0.22	0.73±0.69	
111209A	87.2	-0.05±0.06	-0.16±0.21	87.2	-0.02±0.04	-0.25±0.18	87.2	-0.10±0.06	-0.50±0.31	87.2	0.42±0.16	1.41±0.55	87.2	0.06±0.24	0.18±0.75	
111209A	88.0	-0.02±0.06	-0.23±0.20	88.0	-0.05±0.04	-0.30±0.12	88.0	-0.07±0.04	-0.36±0.21	88.0	0.08±0.17	0.26±0.55	88.0	0.40±0.22	1.23±0.69	
111209A	88.8	-0.03±0.06	-0.17±0.28	88.8	-0.05±0.04	-0.22±0.18	88.8	-0.05±0.05	-0.26±0.26	88.8	0.21±0.15	0.70±0.50	88.8	0.25±0.22	0.78±0.67	
111209A	89.6	-0.01±0.08	-0.04±0.28	89.6	-0.01±0.04	-0.04±0.17	89.6	-0.08±0.05	-0.44±0.28	89.6	0.21±0.16	0.70±0.52	89.6	0.46±0.21	1.42±0.67	
111209A	90.4	0.03±0.09	0.11±0.29	90.4	-0.01±0.04	-0.03±0.17	90.4	-0.06±0.04	-0.33±0.18	90.4	0.32±0.13	1.07±0.44	90.4	0.38±0.18	1.19±0.55	
111209A	91.2	-0.01±0.07	-0.03±0.22	91.2	-0.06±0.06	-0.28±0.28	91.2	-0.03±0.04	-0.14±0.23	91.2	0.15±0.15	0.52±0.50	91.2	0.47±0.20	1.47±0.62	
111209A	92.0	-0.03±0.06	-0.18±0.20	92.0	-0.08±0.04	-0.37±0.18	92.0	-0.06±0.04	-0.02±0.23	92.0	0.22±0.14	0.72±0.47	92.0	0.39±0.23	1.22±0.73	
111209A	92.8	-0.05±0.06	-0.15±0.18	92.8	-0.00±0.03	-0.01±0.16	92.8	-0.08±0.03	-0.41±0.18	92.8	0.28±0.17	0.94±0.57	92.8	0.40±0.19	1.26±0.59	
111209A	93.6	-0.02±0.06	-0.08±0.21	93.6	-0.08±0.04	-0.36±0.19	93.6	-0.04±0.04	-0.22±0.21	93.6	0.34±0.14	1.15±0.46	93.6	0.39±0.19	1.20±0.58	
111209A	94.4	-0.04±0.04	-0.13±0.14	94.4	-0.01±0.03	-0.02±0.20	94.4	-0.06±0.03	-0.50±0.17	94.4	0.27±0.15	0.88±0.49	94.4	0.28±0.19	0.86±0.61	
111209A	95.2	-0.03±0.06	-0.11±0.13	95.2	0.01±0.03	0.05±0.15	95.2	-0.13±0.04	-0.71±0.22	95.2	0.16±0.19	0.72±0.54	95.2	0.25±0.21	0.77±0.67	
111209A	96.0	-0.05±0.06	-0.17±0.20	96.0	0.01±0.05	0.06±0.22	96.0	-0.09±0.07	-0.47±0.35	96.0	0.29±0.25	0.96±0.83	96.0	0.52±0.33	1.62±1.04	
111209A	96.8	-0.08±0.09	-0.20±0.31	96.8	0.01±0.12	0.06±0.56	96.8	-0.11±0.12	-0.60±0.62	96.8	0.25±0.37	0.82±1.23	96.8	0.44±0.46	1.38±1.43	
111209A	97.6	-0.06±0.04	-0.21±0.13	97.6	0.02±0.05	0.07±0.24	97.6	-0.17±0.08	-0.88±0.41	97.6	0.46±0.46	1.54±1.52	97.6	0.16±0.61	0.51±1.91	
111209A	98.4	-0.06±0.04	-0.02±0.07	98.4	0.02±0.08	0.10±0.37	98.4	-0.21±0.11	-1.14±0.57	98.4	0.34±0.34	1.10E3	98.4	0.18±0.57	0.57±1.79	
111209A	99.2	0.14±0.10	0.48±0.34	99.2	0.10±0.09	0.50±0.41	99.2	1.88E3	-0.31±0.11	1.64±0.60	99.2	0.04±0.36	1.88E3	99.2	0.14±1.21	3.13±2.49
111209A	100.0	-0.01±0.21	-0.04±0.69	100.0	0.19±0.67	2.40E3	100.0	-0.15±0.17	-0.77±0.91	2.40E3	0.37±0.48	1.25±1.60	100.0	
111209A	100.8	0.309E3	0.28±0.14	100.8	0.94±0.48	...	100.8	100.8	100.8	
111209A	101.6	4.26E3	0.26±0.27	101.6	0.85±0.91	...	101.6	101.6	101.6	

Table 7 continued on next page

Table 7 (continued)

GRB	Time	$g-r$	β_o^{CI} (g-r)	Time	$r-i$	β_o^{CI} (r-i)	Time	$i-z$	β_o^{CI} (i-z)	Time	$J-H$	β_o^{CI} (J-H)	Time	$H-K_s$	β_o^{CI} (H-K _s)			
111209A	4.73E3	0.06±0.38	0.21±1.27	...	0.59±0.08	2.81±0.37	21.2	0.33±0.08	1.74±0.45	21.2	0.35±0.17	1.18±0.57	21.2	0.48±0.19	1.50±0.60			
120711A	21.2	0.67±0.12	2.23±0.40	21.2	0.50±0.08	2.38±0.38	21.6	0.45±0.09	2.37±0.45	21.6	0.38±0.16	1.25±0.52	21.6	0.17±0.18	0.53±0.57			
120711A	21.6	0.68±0.15	2.27±0.49	21.6	0.57±0.07	2.71±0.34	21.9	0.38±0.08	2.00±0.41	22.3	0.34±0.15	1.12±0.50	22.3	0.12±0.19	0.38±0.60			
120711A	21.9	0.70±0.10	2.33±0.34	21.9	0.55±0.06	2.71±0.27	22.1	0.24±0.07	1.26±0.38	22.9	0.28±0.18	0.95±0.60	22.9	0.24±0.22	0.75±0.68			
120711A	22.1	0.66±0.11	2.20±0.36	22.1	0.64±0.07	3.05±0.34	22.3	0.28±0.06	1.47±0.34	23.4	0.44±0.19	1.45±0.62	23.4	0.35±0.19	1.09±0.60			
120711A	22.3	0.68±0.10	2.27±0.34	22.3	0.61±0.06	2.90±0.27	22.5	0.34±0.06	1.79±0.30	23.8	0.55±0.18	1.82±0.59	23.8	0.04±0.21	0.13±0.67			
120711A	22.5	0.69±0.10	2.30±0.33	22.5	0.67±0.07	3.19±0.34	22.9	0.29±0.07	1.53±0.37	24.2	0.34±0.16	1.12±0.53	24.2	0.07±0.21	0.22±0.67			
120711A	22.9	0.64±0.10	2.13±0.34	22.9	0.66±0.08	3.14±0.37	23.3	0.29±0.10	1.53±0.54	24.7	0.54±0.16	1.78±0.52	25.1	0.25±0.20	0.78±0.64			
120711A	23.3	0.58±0.14	1.93±0.48	23.3	0.62±0.10	2.95±0.48	23.8	0.30±0.10	1.58±0.53	25.1	0.28±0.18	0.92±0.59	25.5	0.30±0.23	0.94±0.73			
120711A	23.8	0.70±0.14	2.33±0.45	23.8	0.62±0.07	3.10±0.34	24.2	0.30±0.07	1.58±0.37	25.5	0.38±0.16	1.25±0.52	26.0	0.48±0.21	1.50±0.67			
120711A	24.2	0.65±0.10	2.17±0.34	24.2	0.65±0.07	3.03±0.30	24.6	0.71±0.06	3.38±0.30	24.6	0.22±0.08	1.16±0.41	26.0	0.39±0.16	1.28±0.55			
120711A	24.6	0.69±0.09	2.30±0.30	24.6	0.60±0.06	2.86±0.30	25.1	0.32±0.07	1.68±0.37	26.4	0.51±0.16	1.68±0.55	26.8	0.36±0.21	1.13±0.67			
120711A	25.1	0.87±0.10	2.90±0.33	25.1	0.56±0.06	2.67±0.30	25.5	0.37±0.07	1.95±0.37	26.8	0.35±0.17	1.18±0.57	27.3	0.47±0.23	1.47±0.71			
120711A	25.5	0.67±0.10	2.23±0.33	25.5	0.53±0.06	2.52±0.30	25.9	0.37±0.07	1.95±0.37	27.3	0.34±0.17	1.15±0.57	27.7	0.40±0.24	1.25±0.76			
120711A	25.9	0.67±0.09	2.23±0.30	25.9	0.55±0.06	2.62±0.30	26.4	0.42±0.07	2.21±0.37	27.7	0.40±0.19	1.32±0.64	28.1	0.45±0.23	1.41±0.71			
120711A	26.4	0.66±0.08	2.20±0.27	26.4	0.55±0.06	2.48±0.30	26.8	0.37±0.08	1.95±0.41	28.1	0.36±0.19	1.22±0.62	28.5	0.42±0.23	1.31±0.73			
120711A	26.8	0.66±0.08	2.20±0.27	26.8	0.52±0.06	2.90±0.24	27.3	0.27±0.06	1.42±0.34	28.5	0.50±0.20	1.65±0.66	28.9	0.36±0.26	1.13±0.81			
120711A	27.3	0.70±0.08	2.33±0.25	27.3	0.61±0.05	2.86±0.34	27.7	0.33±0.07	1.74±0.37	28.9	0.46±0.20	1.52±0.66	29.3	0.33±0.26	1.03±0.82			
120711A	27.7	0.74±0.10	2.47±0.34	27.7	0.60±0.07	2.86±0.34	28.1	0.33±0.07	1.74±0.38	29.3	0.28±0.20	1.92±0.66	29.7	0.18±0.24	0.56±0.76			
120711A	28.1	0.66±0.11	2.20±0.36	28.1	0.64±0.06	3.05±0.27	28.1	0.33±0.07	1.74±0.38	29.3	0.21±0.35	2.18±0.61	29.7	0.35±0.18	0.84±0.67			
120711A	108	0.85±0.44	2.83±1.47	108	0.59±0.22	2.81±1.04	108	0.04±0.35	0.21±1.86	108	0.30±0.17	1.63±0.90	30.1	0.27±0.22	0.84±0.67			
120711A	110	0.63±0.17	2.10±0.57	110	0.60±0.15	2.86±0.73	110	0.31±0.15	2.11±1.01	110	0.40±0.19	2.11±1.01	108	0.54±0.40	1.78±1.32	108	0.46±0.41	1.44±1.28
120711A	111	0.66±0.15	2.20±0.51	111	0.54±0.12	2.57±0.57	111	0.21±0.13	1.11±0.67	113	0.21±0.13	1.11±0.67	110	0.67±0.32	2.22±1.07	
120711A	113	0.64±0.12	2.13±0.39	113	0.59±0.11	2.81±0.52	113	0.32±0.31	1.68±1.64	115	0.32±0.31	1.68±1.64	115	0.28±0.23	1.31±0.73	
120711A	115	0.40±0.59	1.33±1.97	115	0.61±0.32	2.90±1.52	115	1.57±0.77	3.70	0.88±0.18	4.63±0.97	
120711A	370	0.84±0.19	2.80±0.63	370	0.33±0.16	1.95±0.11	0.169	0.28±0.03	1.47±0.15	
120815A	0.169	0.89±0.03	2.97±0.11	0.169	0.43±0.02	2.05±0.11	0.273	0.27±0.03	1.42±0.15	
120815A	0.273	0.90±0.03	3.00±0.11	0.273	0.43±0.02	2.05±0.11	0.375	0.29±0.03	1.53±0.15	
120815A	0.375	0.88±0.03	2.93±0.11	0.375	0.42±0.02	2.00±0.11	1.95±0.13	0.482	0.28±0.03	1.47±0.15	
120815A	1.482	0.87±0.03	2.90±0.09	0.482	0.41±0.03	2.00±0.07	0.698	0.26±0.02	1.37±0.12	
120815A	0.698	0.84±0.02	2.80±0.07	0.698	0.41±0.02	1.95±0.11	0.884	0.27±0.03	1.42±0.15	
120815A	0.884	0.86±0.02	2.87±0.07	0.884	0.41±0.02	1.83	0.43±0.02	2.05±0.11	1.83	0.28±0.03	1.47±0.15	
120815A	1.07	0.87±0.01	2.90±0.05	1.07	0.42±0.01	2.00±0.07	1.07	0.25±0.02	1.32±0.12	
120815A	1.26	0.85±0.01	2.83±0.05	1.26	0.41±0.02	1.95±0.11	1.26	0.29±0.03	1.53±0.15	
120815A	1.45	0.87±0.01	2.90±0.05	1.45	0.40±0.02	1.90±0.11	1.45	0.28±0.03	1.47±0.15	
120815A	1.64	0.88±0.01	2.93±0.05	1.64	0.42±0.01	2.00±0.07	1.64	0.28±0.02	1.47±0.12	
120815A	1.83	0.84±0.01	2.89±0.05	1.83	0.43±0.02	2.05±0.11	1.83	0.28±0.03	1.47±0.15	
120815A	2.03	0.87±0.01	2.90±0.05	2.03	0.43±0.02	2.05±0.11	2.03	0.27±0.03	1.42±0.15	
120815A	2.36	0.87±0.01	2.90±0.05	2.36	0.42±0.01	2.00±0.07	2.36	0.27±0.02	1.42±0.12	
120815A	2.81	0.86±0.01	2.87±0.05	2.81	0.46±0.02	2.19±0.11	2.81	0.25±0.03	1.32±0.15	
120815A	3.26	0.88±0.02	2.83±0.07	3.26	0.44±0.02	2.10±0.11	3.26	0.29±0.03	1.53±0.15	
120815A	3.71	0.89±0.01	2.97±0.05	3.71	0.41±0.03	1.95±0.15	3.71	0.29±0.04	1.53±0.19	
120815A	4.17	0.86±0.01	2.87±0.05	4.17	0.44±0.02	2.10±0.11	4.17	0.27±0.03	1.42±0.15	

Table 7 continued on next page

Table 7 (continued)

GRB	Time (ks)	$g-r$	β_o^{CI} (g-r)	Time (ks)	$r-i$	β_o^{CI} (r-i)	Time (ks)	$i-z$	β_o^{CI} (i-z)	Time (ks)	$J-H$	β_o^{CI} (J-H)	Time (ks)	$H-K_s$	β_o^{CI} (H-K _s)
120815A	4.61	0.86±0.02	2.87±0.07	4.61	0.44±0.02	2.10±0.11	4.61	0.28±0.03	1.47±0.15
120815A	5.05	0.92±0.03	3.07±0.09	5.05	0.40±0.03	1.90±0.13	5.05	0.31±0.04	1.63±0.19
120815A	5.50	0.89±0.03	2.97±0.11	5.50	0.38±0.02	1.81±0.11	5.50	0.35±0.03	1.84±0.15
120815A	6.04	0.92±0.04	3.07±0.12	6.04	0.42±0.04	2.00±0.20	6.04	0.28±0.04	1.47±0.22
120815A	6.46	0.89±0.05	2.97±0.17	6.46	0.50±0.05	2.38±0.24	6.46	0.16±0.06	0.84±0.30
120815A	6.89	0.88±0.05	2.93±0.18	6.89	0.46±0.04	2.19±0.17	6.89	0.22±0.04	1.16±0.22
120815A	7.33	0.83±0.04	2.73±0.12	7.33	0.47±0.04	2.24±0.17	7.33	0.26±0.05	1.37±0.26
120815A	7.76	0.82±0.05	2.73±0.17	7.76	0.43±0.04	2.05±0.20	7.76	0.20±0.05	1.05±0.26
120815A	8.20	0.82±0.05	2.73±0.18	8.20	0.44±0.04	2.10±0.17	8.20	0.25±0.05	1.32±0.26
120815A	8.63	0.87±0.04	2.90±0.15	8.63	0.40±0.04	1.90±0.17	8.63	0.24±0.04	1.24±0.22
120815A	9.06	0.89±0.04	2.97±0.15	9.06	0.44±0.04	2.10±0.17	9.06	0.24±0.04	1.24±0.22
120815A	9.50	0.88±0.04	2.93±0.15	9.50	0.48±0.04	2.29±0.17	9.50	0.14±0.05	0.74±0.26
120815A	9.93	0.81±0.04	2.70±0.15	9.93	0.45±0.04	2.14±0.17	9.93	0.24±0.04	1.26±0.22
120815A	10.4	0.92±0.04	3.07±0.14	10.4	0.44±0.04	2.10±0.20	10.4	0.21±0.05	1.11±0.26
120815A	10.6	0.93±0.04	3.10±0.15	10.6	0.43±0.04	2.05±0.17	10.6	0.19±0.05	1.00±0.26
120815A	11.1	0.90±0.07	3.00±0.22	11.1	0.43±0.05	2.05±0.24	11.1	0.26±0.06	1.37±0.30
121024A	11.1	0.74±0.10	2.47±0.33	11.1	0.17±0.08	0.81±0.40	11.1	0.19±0.08	0.98±0.41	11.1	0.32±0.15	1.06±0.50	11.1	0.37±0.17	1.16±0.53
121024A	15.5	0.73±0.07	2.44±0.24	15.5	0.24±0.07	1.14±0.34	15.5	0.11±0.06	0.56±0.34	15.5	0.33±0.14	1.09±0.47	15.5	0.30±0.16	0.94±0.49
121024A	17.0	0.72±0.07	2.41±0.24	17.0	0.26±0.07	1.24±0.34	17.0	0.16±0.06	0.83±0.34	17.0	0.35±0.13	1.16±0.45	17.0	0.11±0.16	0.35±0.49
121024A	21.4	0.75±0.28	2.51±0.92	21.4	0.22±0.08	1.05±0.40	21.4	0.15±0.11	0.77±0.57	21.4	0.49±0.16	1.62±0.52	21.4	0.05±0.19	0.16±0.60
121024A	88.0	0.67±0.26	2.24±0.85	88.0	0.17±0.13	0.81±0.64	88.0	0.15±0.17	0.77±0.91	88.0	0.20±0.40	0.66±1.35	88.0	0.32±0.44	1.01±1.37
121024A	107	0.68±0.14	2.27±0.48	107	0.29±0.12	1.38±0.57	107	0.18±0.16	0.93±0.83	107	0.38±0.45	1.26±1.51	107	0.54±0.47	1.69±1.48
121217A	1.12	0.92±0.06	3.07±0.19	1.12	0.37±0.06	1.76±0.27	1.12	0.29±0.06	1.53±0.30
121217A	1.23	1.03±0.26	3.43±0.26	1.23	0.33±0.08	1.57±0.37	1.23	0.37±0.08	1.95±0.41
121217A	1.34	0.93±0.06	3.10±0.19	1.34	0.49±0.06	2.33±0.27	1.34	0.18±0.06	0.95±0.34
121217A	1.45	1.10±0.08	3.67±0.27	1.45	0.39±0.06	1.86±0.30	1.45	0.26±0.07	1.37±0.37
121217A	1.59	0.95±0.04	3.17±0.15	1.59	0.38±0.04	1.81±0.17	1.59	0.30±0.05	1.58±0.26
121217A	1.79	1.03±0.03	3.43±0.11	1.79	0.37±0.03	1.76±0.15	1.79	0.31±0.04	1.63±0.22
121217A	1.98	0.94±0.03	3.13±0.09	1.98	0.41±0.04	1.95±0.17	1.98	0.26±0.04	1.37±0.22
121217A	2.17	0.94±0.04	3.13±0.15	2.17	0.41±0.04	1.95±0.17	2.17	0.22±0.05	1.16±0.26
121217A	2.37	0.98±0.04	3.27±0.15	2.37	0.39±0.04	1.86±0.17	2.37	0.29±0.04	1.53±0.22
121217A	2.57	0.97±0.04	3.23±0.15	2.57	0.40±0.04	1.90±0.17	2.57	0.24±0.04	1.26±0.22
121217A	2.76	0.98±0.04	3.27±0.12	2.76	0.38±0.04	1.81±0.17	2.76	0.30±0.04	1.58±0.22
121217A	2.95	0.93±0.04	3.10±0.12	2.95	0.38±0.04	1.81±0.17	2.95	0.26±0.04	1.37±0.22
121217A	3.15	0.99±0.04	3.30±0.12	3.15	0.39±0.04	1.86±0.21	3.15	0.24±0.05	1.26±0.26
121217A	3.35	0.94±0.04	3.13±0.12	3.35	0.37±0.04	1.76±0.17	3.35	0.30±0.04	1.58±0.22
121217A	3.54	0.94±0.04	3.13±0.12	3.54	0.42±0.04	2.00±0.17	3.54	0.24±0.04	1.26±0.22
121217A	3.74	0.97±0.04	3.23±0.15	3.74	0.34±0.04	1.62±0.17	3.74	0.29±0.04	1.53±0.22
121217A	3.94	0.99±0.06	3.30±0.19	3.94	0.37±0.05	1.76±0.24	3.94	0.24±0.06	1.26±0.30
121217A	4.13	0.93±0.06	3.10±0.19	4.13	0.42±0.05	2.00±0.24	4.13	0.22±0.06	1.16±0.30
121217A	4.32	0.96±0.07	3.20±0.24	4.32	0.42±0.04	2.00±0.17	4.32	0.24±0.05	1.26±0.26
121217A	4.52	1.01±0.08	3.37±0.25	4.52	0.34±0.04	1.62±0.20	4.52	0.25±0.04	1.32±0.22
121217A	4.74	1.03±0.12	3.43±0.39	4.74	0.35±0.06	1.67±0.30	4.74	0.27±0.08	1.42±0.41

Table 7 continued on next page

Table 7 (continued)

GRB	Time (ks)	$g-r$	β_o^{CI} (g-r)	Time (ks)	$r-i$	β_o^{CI} (r-i)	Time (ks)	$i-z$	β_o^{CI} (i-z)	Time (ks)	$J-H$	β_o^{CI} (J-H)	Time (ks)	$H-K_s$	β_o^{CI} (H-K _s)
121217A	4.74	0.98±0.16	3.27±0.52	4.74	0.36±0.07	1.71±0.34	4.74	0.27±0.08	1.42±0.45
121217A	4.74	1.02±0.12	3.40±0.40	4.74	0.35±0.07	1.67±0.34	4.74	0.37±0.09	1.95±0.45
121217A	4.74	0.97±0.16	3.23±0.53	4.74	0.36±0.08	1.71±0.37	4.74	0.37±0.09	1.95±0.49
121217A	74.7	0.98±0.09	3.27±0.31	74.7	0.36±0.08	1.71±0.37	74.7	0.08±0.11	0.42±0.57
121217A	86.4	1.25±0.13	4.17±0.43	86.4	0.27±0.08	1.29±0.37	86.4	0.0±0.12	0.0±0.61
121217A	88.2	1.07±0.10	3.57±0.33	88.2	0.34±0.08	1.62±0.38	88.2	0.16±0.11	0.84±0.56
121217A	174	0.52±0.16	2.48±0.75	174	-0.31±0.23	-1.63±1.21
121217A	347	0.10±0.22	0.48±1.03	347	-0.23±0.35	-1.21±1.84
130427A	0.138	0.28±0.02	0.92±0.07	0.138	0.16±0.02	0.75±0.08	0.138	0.17±0.03	0.84±0.15
130427A	0.150	0.28±0.02	0.95±0.07	0.150	0.18±0.02	0.85±0.08	0.150	0.15±0.03	0.79±0.15
130427A	0.161	0.30±0.02	0.99±0.07	0.161	0.13±0.02	0.64±0.08	0.161	0.13±0.03	0.66±0.15
130427A	0.172	0.30±0.02	1.01±0.07	0.172	0.12±0.02	0.55±0.08	0.172	0.14±0.03	0.75±0.15
130427A	0.184	0.26±0.02	0.85±0.07	0.184	0.11±0.02	0.52±0.08	0.184	0.12±0.03	0.63±0.15
130427A	0.196	0.26±0.02	0.86±0.07	0.196	0.13±0.02	0.60±0.08	0.196	0.17±0.03	0.84±0.15
130427A	0.208	0.23±0.02	0.76±0.07	0.208	0.14±0.02	0.65±0.08	0.208	0.10±0.03	0.51±0.15
130427A	0.219	0.29±0.02	0.96±0.07	0.219	0.12±0.02	0.58±0.08	0.219	0.14±0.03	0.71±0.15
130427A	0.231	0.28±0.02	0.93±0.07	0.231	0.09±0.02	0.40±0.08	0.231	0.20±0.03	1.03±0.15
130427A	0.247	0.29±0.02	0.98±0.07	0.247	0.11±0.02	0.53±0.08	0.247	0.19±0.03	1.01±0.15
130427A	0.261	0.27±0.02	0.89±0.07	0.261	0.14±0.02	0.67±0.08	0.261	0.15±0.03	0.75±0.14
130427A	0.274	0.27±0.02	0.91±0.07	0.274	0.12±0.02	0.58±0.08	0.274	0.11±0.03	0.58±0.14
130427A	0.287	0.28±0.02	0.94±0.07	0.287	0.12±0.02	0.55±0.08	0.287	0.15±0.03	0.75±0.14
130427A	0.300	0.28±0.02	0.93±0.07	0.300	0.13±0.02	0.62±0.08	0.300	0.14±0.03	0.72±0.15
130427A	0.313	0.30±0.02	1.01±0.07	0.313	0.11±0.02	0.50±0.08	0.313	0.18±0.03	0.93±0.15
130427A	0.326	0.31±0.02	1.04±0.07	0.326	0.10±0.02	0.47±0.08	0.326	0.16±0.03	0.82±0.15
130427A	0.339	0.30±0.02	1.01±0.07	0.339	0.11±0.02	0.52±0.08	0.339	0.13±0.03	0.69±0.15
130427A	0.352	0.26±0.02	0.87±0.07	0.352	0.13±0.02	0.60±0.08	0.352	0.16±0.03	0.82±0.15
130427A	0.366	0.32±0.02	1.08±0.07	0.366	0.11±0.02	0.50±0.08	0.366	0.17±0.03	0.84±0.15
130427A	0.379	0.29±0.02	0.98±0.07	0.379	0.15±0.02	0.71±0.08	0.379	0.15±0.03	0.75±0.15
130427A	0.392	0.29±0.02	0.96±0.07	0.392	0.13±0.02	0.64±0.08	0.392	0.14±0.03	0.74±0.15
130427A	0.406	0.29±0.02	0.98±0.07	0.406	0.13±0.02	0.60±0.08	0.406	0.14±0.03	0.76±0.15
130427A	0.419	0.29±0.02	0.98±0.07	0.419	0.14±0.02	0.68±0.08	0.419	0.10±0.03	0.52±0.15
130427A	0.432	0.29±0.02	0.96±0.07	0.432	0.12±0.02	0.58±0.08	0.432	0.20±0.03	1.04±0.15
130427A	0.445	0.30±0.02	1.01±0.07	0.445	0.13±0.02	0.63±0.08	0.445	0.15±0.03	0.81±0.15
130427A	0.459	0.31±0.02	1.03±0.07	0.459	0.10±0.02	0.50±0.08	0.459	0.14±0.03	0.74±0.16
130427A	0.472	0.27±0.02	0.91±0.07	0.472	0.14±0.02	0.69±0.08	0.472	0.17±0.03	0.87±0.16
130427A	0.485	0.28±0.02	0.95±0.07	0.485	0.13±0.02	0.63±0.08	0.485	0.17±0.03	0.88±0.16
130427A	0.498	0.30±0.02	0.99±0.07	0.498	0.14±0.02	0.67±0.08	0.498	0.18±0.03	0.95±0.16
130427A	0.525	0.30±0.02	1.02±0.07	0.525	0.14±0.02	0.65±0.08	0.525	0.15±0.03	0.80±0.14
130427A	0.567	0.27±0.02	0.90±0.07	0.567	0.14±0.02	0.66±0.08	0.567	0.17±0.03	0.88±0.16
130427A	0.608	0.29±0.02	0.95±0.07	0.608	0.14±0.02	0.65±0.08	0.608	0.15±0.03	0.85±0.16
130427A	0.650	0.29±0.02	0.96±0.07	0.650	0.14±0.02	0.65±0.08	0.650	0.15±0.03	0.81±0.15
130427A	0.692	0.30±0.02	1.00±0.07	0.692	0.13±0.02	0.61±0.08	0.692	0.16±0.03	0.82±0.16
130427A	0.733	0.29±0.02	0.98±0.07	0.733	0.13±0.02	0.63±0.08	0.733	0.17±0.03	0.83±0.17

Table 7 continued on next page

Table 7 (continued)

GRB	Time (ks)	$g-r$	β_o^{CI} (g-r)	Time (ks)	$r-i$	β_o^{CI} (r-i)	Time (ks)	$i-z$	β_o^{CI} (i-z)	Time (ks)	$J-H$	β_o^{CI} (J-H)	Time (ks)	$H-K_s$	β_o^{CI} (H-K _s)
130427A	0.775	0.30±0.02	1.00±0.07	0.775	0.11±0.02	0.51±0.08
130427A	0.816	0.28±0.02	0.93±0.07	0.816	0.14±0.02	0.67±0.08
130427A	0.858	0.27±0.02	0.91±0.07	0.858	0.17±0.02	0.81±0.08
130427A	0.899	0.27±0.02	0.91±0.07	0.899	0.14±0.02	0.67±0.08
130427A	0.941	0.28±0.02	0.92±0.07	0.941	0.16±0.02	0.78±0.08
130427A	0.982	0.30±0.02	1.00±0.07	0.982	0.16±0.02	0.77±0.08
130427A	1.02	0.28±0.02	0.95±0.07	1.02	0.12±0.02	0.59±0.08
130427A	1.07	0.30±0.02	1.01±0.07	1.07	0.16±0.02	0.77±0.08
130427A	1.11	0.29±0.02	0.95±0.07	1.11	0.13±0.02	0.60±0.08
130427A	1.15	0.31±0.02	1.04±0.07	1.15	0.11±0.02	0.53±0.08
130427A	1.19	0.29±0.02	0.96±0.07	1.19	0.15±0.02	0.70±0.08
130427A	1.23	0.30±0.02	1.02±0.08	1.23	0.12±0.02	0.56±0.08
130427A	1.27	0.30±0.02	1.00±0.08	1.27	0.13±0.02	0.60±0.09
130427A	1.32	0.30±0.02	1.01±0.08	1.32	0.12±0.02	0.56±0.09
130427A	1.36	0.28±0.02	0.93±0.08	1.36	0.12±0.02	0.56±0.09
130427A	1.40	0.27±0.02	0.88±0.08	1.40	0.15±0.02	0.70±0.09
130427A	1.44	0.28±0.02	0.92±0.08	1.44	0.14±0.02	0.66±0.09
130427A	1.48	0.27±0.02	0.91±0.08	1.48	0.14±0.02	0.68±0.09
130427A	1.53	0.27±0.02	0.90±0.08	1.53	0.14±0.02	0.67±0.09
130427A	1.57	0.29±0.02	0.96±0.08	1.57	0.12±0.02	0.55±0.09
130427A	1.61	0.26±0.02	0.88±0.08	1.61	0.16±0.02	0.74±0.09
130427A	1.65	0.29±0.02	0.97±0.08	1.65	0.13±0.02	0.60±0.09
130427A	1.69	0.29±0.02	0.98±0.08	1.69	0.13±0.02	0.60±0.10
130427A	1.73	0.29±0.02	0.95±0.08	1.73	0.14±0.02	0.67±0.10
130427A	1.78	0.31±0.02	1.03±0.08	1.78	0.14±0.02	0.69±0.10
130427A	1.82	0.28±0.03	0.93±0.08	1.82	0.13±0.02	0.62±0.10
130427A	1.86	0.28±0.03	0.92±0.08	1.86	0.13±0.02	0.61±0.10
130427A	1.90	0.28±0.03	0.94±0.08	1.90	0.11±0.02	0.51±0.10
130427A	1.94	0.28±0.03	0.94±0.09	1.94	0.13±0.02	0.60±0.11
130427A	1.98	0.26±0.03	0.88±0.09	1.98	0.12±0.02	0.58±0.11
130427A	2.02	0.26±0.03	0.88±0.09	2.02	0.13±0.02	0.61±0.11
130427A	2.07	0.28±0.03	0.94±0.09	2.07	0.13±0.02	0.60±0.11
130427A	2.11	0.28±0.03	0.92±0.09	2.11	0.10±0.02	0.47±0.11
130427A	2.15	0.27±0.03	0.89±0.09	2.15	0.16±0.02	0.76±0.11
130427A	2.19	0.26±0.03	0.88±0.09	2.19	0.14±0.02	0.69±0.11
130427A	2.23	0.27±0.03	0.89±0.09	2.23	0.14±0.02	0.66±0.11
130427A	2.28	0.27±0.03	0.90±0.09	2.28	0.11±0.02	0.50±0.11
130427A	2.32	0.26±0.03	0.86±0.09	2.32	0.13±0.02	0.63±0.11
130427A	2.36	0.27±0.03	0.91±0.09	2.36	0.11±0.02	0.54±0.11
130427A	2.40	0.28±0.03	0.93±0.09	2.40	0.14±0.02	0.66±0.11
130427A	2.44	0.29±0.03	0.96±0.09	2.44	0.15±0.02	0.73±0.11
130427A	2.48	0.28±0.03	0.92±0.09	2.48	0.11±0.03	0.52±0.12
130427A	2.53	0.28±0.03	0.93±0.09	2.53	0.16±0.03	0.75±0.12

Table 7 continued on next page

Table 7 (continued)

GRB	Time (ks)	$g-r$	β_o^{CI} (g-r)	Time (ks)	$r-i$	β_o^{CI} (r-i)	Time (ks)	$i-z$	β_o^{CI} (i-z)	Time (ks)	$J-H$	β_o^{CI} (J-H)	Time (ks)	$H-K_s$	β_o^{CI} (H-K _s)
130427A	2.57	0.29±0.03	0.96±0.09	2.57	0.12±0.03	0.55±0.12
130427A	2.61	0.22±0.03	0.74±0.09	2.61	0.12±0.03	0.57±0.12
130427A	2.65	0.30±0.03	1.01±0.09	2.65	0.09±0.03	0.43±0.12
130427A	2.69	0.26±0.03	0.85±0.10	2.69	0.13±0.03	0.60±0.13
130427A	2.73	0.28±0.03	0.94±0.10	2.73	0.14±0.03	0.69±0.13
130427A	2.78	0.24±0.03	0.79±0.10	2.78	0.14±0.03	0.65±0.13
130427A	2.82	0.30±0.03	0.99±0.10	2.82	0.10±0.03	0.49±0.13
130427A	2.86	0.28±0.03	0.94±0.10	2.86	0.12±0.03	0.58±0.13
130427A	2.90	0.27±0.03	0.89±0.10	2.90	0.20±0.03	0.94±0.13
130427A	2.94	0.24±0.03	0.87±0.10	2.94	0.16±0.03	0.75±0.13
130427A	2.98	0.31±0.03	1.04±0.10	2.98	0.10±0.03	0.50±0.13
130427A	3.03	0.30±0.03	1.00±0.10	3.03	0.13±0.03	0.63±0.13
130427A	3.07	0.26±0.03	0.88±0.10	3.07	0.11±0.03	0.54±0.14
130427A	3.11	0.30±0.03	1.00±0.10	3.11	0.10±0.03	0.48±0.14
130427A	3.15	0.27±0.03	0.89±0.10	3.15	1E-3±0.03	0.00±0.14
130427A	3.19	0.22±0.03	0.73±0.11	3.19	0.17±0.03	0.82±0.14
130427A	3.23	0.23±0.03	0.78±0.10	3.23	0.12±0.03	0.59±0.14
130427A	3.28	0.26±0.03	0.86±0.11	3.28	0.11±0.03	0.50±0.14
130427A	3.32	0.28±0.03	0.94±0.11	3.32	0.15±0.03	0.71±0.14
130427A	3.36	0.27±0.03	0.89±0.11	3.36	0.08±0.03	0.39±0.15
130427A	3.40	0.28±0.03	0.92±0.11	3.40	0.12±0.03	0.59±0.14
130427A	3.44	0.21±0.03	0.69±0.11	3.44	0.01±0.03	0.06±0.15
130427A	3.48	0.26±0.03	0.88±0.11	3.48	0.13±0.03	0.61±0.14
130427A	3.53	0.29±0.03	0.96±0.11	3.53	0.11±0.03	0.50±0.15
130427A	3.57	0.24±0.03	0.97±0.11	3.57	0.00±0.03	0.01±0.16
130427A	3.61	0.24±0.03	0.79±0.11	3.61	0.11±0.03	0.50±0.15
130427A	3.65	0.25±0.03	0.83±0.11
130427A	3.69	0.32±0.03	1.06±0.12
130427A	3.74	0.26±0.03	0.87±0.11
130427A	3.78	0.26±0.03	0.85±0.11
130427A	3.82	0.25±0.03	0.83±0.11
130427A	3.86	0.24±0.03	0.79±0.11
130427A	3.90	0.25±0.03	0.72±0.12
130427A	3.94	0.23±0.03	0.76±0.11
130427A	3.99	0.26±0.04	0.86±0.12
130427A	4.03	0.28±0.04	0.92±0.12
130427A	4.07	0.28±0.04	0.93±0.12
130427A	4.11	0.28±0.04	0.95±0.12
130427A	4.15	0.27±0.04	0.89±0.12
130427A	4.19	0.25±0.04	0.84±0.12
130427A	4.24	0.27±0.04	0.90±0.12
130427A	4.28	0.23±0.04	0.77±0.12
130427A	4.32	0.22±0.04	0.72±0.12

Table 7 continued on next page

Table 7 (continued)

GRB	Time (ks)	$g-r$	β_o^{CI} (g-r)	Time (ks)	$r-i$	β_o^{CI} (r-i)	Time (ks)	$i-z$	β_o^{CI} (i-z)	Time (ks)	$J-H$	β_o^{CI} (J-H)	Time (ks)	$H-K_s$	β_o^{CI} (H-K _s)
130427A	4.36	0.29±0.04	0.98±0.12
130427A	4.40	0.32±0.04	1.05±0.13
130427A	4.45	0.24±0.04	0.79±0.12
130427A	4.49	0.26±0.04	0.85±0.13
130427A	4.53	0.21±0.04	0.69±0.12
130427A	4.57	0.26±0.04	0.86±0.13
130427A	4.61	0.28±0.04	0.93±0.13
130427A	4.65	0.30±0.04	0.99±0.13
130427A	4.70	0.26±0.04	0.88±0.13
130427A	4.74	0.27±0.04	0.89±0.13
130427A	4.78	0.25±0.04	0.82±0.13
130427A	4.82	0.21±0.04	0.70±0.13
130427A	4.86	0.20±0.04	0.85±0.13
130427A	4.90	0.23±0.04	0.75±0.14
130427A	4.94	0.28±0.04	0.94±0.14
130427A	4.99	0.23±0.04	0.77±0.14
130427A	5.03	0.23±0.04	0.76±0.14
130427A	5.07	0.22±0.04	0.73±0.14
130427A	5.11	0.21±0.04	0.70±0.14
130427A	5.15	0.24±0.04	0.80±0.15
130427A	5.20	0.27±0.04	0.90±0.14
130427A	5.24	0.25±0.04	0.84±0.14
130427A	5.28	0.20±0.04	0.65±0.15
130427A	5.32	0.22±0.04	0.73±0.14
130427A	5.36	0.27±0.04	0.91±0.15
130427A	5.40	0.16±0.04	0.54±0.15
130427A	5.45	0.24±0.05	0.79±0.15
130427A	5.49	0.22±0.05	0.74±0.15
130427A	5.53	0.30±0.05	0.99±0.16
130427A	5.57	0.23±0.05	0.78±0.15
130427A	5.61	0.20±0.04	0.67±0.15
130427A	5.65	0.27±0.05	0.90±0.16
130427A	5.70	0.28±0.05	0.95±0.16
130427A	5.74	0.28±0.05	0.95±0.16
130427A	5.78	0.26±0.05	0.86±0.16
130427A	5.82	0.27±0.05	0.88±0.16
130427A	5.86	0.25±0.05	0.84±0.16
130427A	5.90	0.30±0.05	1.01±0.16
130427A	5.95	0.25±0.05	0.84±0.17
130427A	5.99	0.21±0.05	0.69±0.17
130427A	6.03	0.27±0.05	0.89±0.17
130427A	6.07	0.20±0.05	0.66±0.17
130427A	6.11	0.14±0.05	0.46±0.16

Table 7 continued on next page

Table 7 (continued)

GRB	Time (ks)	$g-r$	β_o^{CI} (g-r)	Time (ks)	$r-i$	β_o^{CI} (r-i)	Time (ks)	$i-z$	β_o^{CI} (i-z)	Time (ks)	$J-H$	β_o^{CI} (J-H)	Time (ks)	$H-K_s$	β_o^{CI} (H-Ks)
130427A	6.15	0.25±0.05	0.82±0.17
130427A	6.20	0.22±0.05	0.74±0.17
130427A	6.24	0.23±0.05	0.78±0.17
130427A	6.28	0.27±0.05	0.91±0.17
130427A	6.32	0.27±0.05	0.90±0.18
130427A	6.36	0.22±0.05	0.74±0.18
130427A	6.40	0.29±0.05	0.67±0.17
130427A	6.45	0.27±0.05	0.91±0.18
130427A	6.49	0.18±0.05	0.60±0.17
130427A	6.53	0.36±0.06	1.22±0.19
130427A	6.57	0.21±0.05	0.71±0.18
130427A	6.61	0.27±0.06	0.91±0.20
130427A	6.65	0.16±0.06	0.54±0.18
130427A	6.70	0.19±0.05	0.62±0.18
130427A	6.74	0.27±0.06	0.88±0.19
130427A	6.78	0.26±0.06	0.86±0.19
130427A	6.82	0.29±0.06	0.96±0.19
130427A	6.86	0.24±0.06	0.81±0.18
130427A	6.90	0.21±0.06	0.71±0.19
130427A	6.94	0.27±0.06	0.90±0.19
130427A	6.99	0.11±0.06	0.36±0.19
130427A	7.03	0.21±0.06	0.69±0.20
130427A	7.07	0.31±0.06	1.02±0.20
130427A	7.11	0.22±0.06	0.72±0.20
130427A	7.15	0.24±0.06	0.80±0.20
130427A	7.19	0.21±0.06	0.89±0.19
130427A	7.24	0.25±0.06	0.83±0.21
130427A	7.28	0.23±0.06	0.77±0.21
130427A	7.32	0.26±0.06	0.88±0.21
130427A	7.36	0.21±0.06	0.71±0.22
130427A	7.40	0.18±0.06	0.61±0.21
130427A	7.45	0.27±0.07	0.91±0.22
130427A	7.49	0.32±0.07	1.07±0.22
130427A	7.53	0.17±0.06	0.57±0.21
130427A	7.57	0.30±0.07	1.01±0.23	...	0.938	0.06±2.29	0.27±10.90	2.64	0.15±0.50	0.86±2.61	1.57	0.55±0.18	1.82±0.59	0.656	0.38±0.22
130925A	19.1	-1.01±2.05	-4.83±9.77	2.83	0.29±0.61	1.54±3.21	1.97	0.80±0.15	2.65±0.51	0.861	0.67±0.23	1.20±0.67
130925A	3.03	-0.23±0.38	-1.23±1.98	2.27	0.61±0.16	2.04±0.54	1.07	0.67±0.20	2.10±0.61
130925A	3.23	0.30±0.58	1.59±3.04	2.47	0.64±0.16	2.12±0.54	1.27	0.60±0.19	1.87±0.58
130925A	19.1	-0.80±1.82	-4.21±9.57	2.66	0.42±0.15	1.41±0.49	1.57	0.29±0.15	0.91±0.47
130925A	2.86	0.54±0.13	1.79±0.42	1.97	0.38±0.12	1.19±0.37
130925A	3.06	0.64±0.12	2.12±0.40	2.27	0.20±0.14	0.63±0.45
130925A	3.25	0.59±0.16	1.98±0.54	2.47	0.52±0.13	1.62±0.42

Table 7 continued on next page

Table 7 (*continued*)

GRB	Time (ks)	$g-r$	β_o^{CI} (g-r)	Time (ks)	$r-i$	β_o^{CI} (r-i)	Time (ks)	$i-z$	β_o^{CI} (i-z)	Time (ks)	$J-H$	β_o^{CI} (J-H)	Time (ks)	$H-K_s$	β_o^{CI} (H-K _s)
130925A	3.45	0.69±0.25	2.31±0.83	2.66	0.34±0.13	1.07±0.42
130925A	3.64	0.48±0.26	1.59±0.85	2.86	0.64±0.11	2.01±0.36
130925A	3.94	0.65±0.22	2.17±0.73	3.06	0.73±0.11	2.27±0.35
130925A	4.33	0.34±0.23	1.13±0.77	3.25	0.63±0.17	1.95±0.52
130925A	4.76	0.65±0.30	2.16±1.02	3.45	0.42±0.20	1.31±0.64
130925A	5.21	0.37±0.31	1.24±1.04	3.64	0.81±0.25	2.52±0.79
130925A	5.67	0.48±0.39	1.58±1.29	3.94	0.47±0.18	1.47±0.55
130925A	6.11	0.92±0.66	3.07±2.21	4.33	0.35±0.23	1.10±0.72
130925A	7.04	0.76±0.33	2.53±1.09	7.04	0.34±0.19	1.06±0.60
130925A	8.30	0.71±0.30	2.35±1.00	8.30	-0.02±0.21	-0.05±0.67
130925A	9.55	0.98±0.45	3.26±1.51	9.55	0.06±0.25	0.17±0.78
130925A	10.4	0.60±1.98	1.99±6.60	19.5	0.03±0.42	0.10±1.30
130925A	357	-0.20±2.91	-0.65±9.71	104	0.37±0.71	1.15±2.21
130925A	184	0.13±1.02	0.41±3.20